

UNIWERSYTET MIKOŁAJA KOPERNIKA W TORUNIU
WYDZIAŁ CHEMII
KATEDRA CHEMII ŚRODOWISKA I BIOANALITYKI
INTERDYSCYPLINARNE CENTRUM NOWOCZESNYCH TECHNOLOGII

mgr Agnieszka Anna Rodzik

*Badanie mechanizmów tworzenia nanokompozytów metal-białko
jako potencjalnych środków przeciwdrobnoustrojowych*

Rozprawa doktorska

Praca wykonana pod kierunkiem
prof. zw. dr hab., dr h.c. multi. Bogusława Buszewskiego, czł. rzecz. PAN
z Katedry Chemii Środowiska i Bioanalitiky, Wydział Chemii UMK w Toruniu
oraz dra hab. Pawła Piotra Pomastowskiego, prof. UMK jako promotora pomocniczego
z Interdyscyplinarnego Centrum Nowoczesnych Technologii UMK w Toruniu



**UNIWERSYTET
MIKOŁAJA KOPERNIKA
W TORUNIU**
Wydział Chemii

Toruń 2023

*The study of the mechanisms for the formation metal-protein nanocomposites
as potential antimicrobial agents*

Podziękowania

Pragnę wyrazić serdeczne podziękowania:

Panu prof. dr. hab. Bogusławowi Buszewskiemu za opiekę promotorską, możliwość wykonania badań w Pańskim zespole, możliwość konsultacji i okazaną pomoc, cenne uwagi, które wpłynęły na ostateczny kształt niniejszej rozprawy oraz za serce i czas;

Panu dr. hab. Pawłowi Pomastowskiemu prof. UMK za możliwość realizacji doktoratu w ramach projektu, opiekę i wszelkie wskazówki;

Pani dr. Viorice Railean za wszelką pomoc podczas wykonywania badań eksperymentalnych, przekazaną wiedzę, każdy rozwiązany „problem” i liczne dyskusje, a także za motywację do krytycznego spojrzenia na problematykę badawczą. Ponadto dziękuję za wyrozumiałość, bezinteresowność, ogromną cierpliwość, za każde dobre słowo i wsparcie nie tylko naukowe;

Panu dr. hab. inż. Myroslavovi Sprynskiemu prof. UMK za okazane wsparcie, cenne wskazówki i liczne rozmowy dotyczące kinetyki;

Współpracownikom za pomoc i życzliwość;

Rodzinie, Rodzeństwu i Przyjaciołom za wsparcie duchowe oraz wiarę w moje możliwości, a w sposób szczególny Rodzicom za wsparcie na całej drodze edukacji i motywację;

dziękuję również mojemu Narzeczonemu za anielską cierpliwość i wyrozumiałość.

Praca powstała w wyniku realizacji projektów Opus 14 o nr 2017/27/B/ST4/02628 i Preludium 19 o nr 2020/37/N/ST4/04082 finansowanych z Narodowego Centrum Nauki.



Część badań współfinansowana była w ramach Grantów Młodych o nr 2092/2019, 492/2020 oraz PDB/granty wydziałowe pochodzących ze środków Wydziału Chemii Uniwersytetu Mikołaja Kopernika w Toruniu.

Spis treści

Wykaz skrótów.....	6
1. Wprowadzenie	8
2. Cel badawczy	11
3. Problem badawczy.....	13
3.1. Białka	13
3.1.1. <i>Białka mleka i serwatki</i>	15
3.2. Wiązanie białek z metalami	23
3.2.1. <i>Immobilizacja jonów metali do białek i charakterystyka wiązania</i>	27
3.2.2. <i>Charakterystyka nanokompozytów</i>	33
3.2.3. <i>Mechanizm formowania się nanokompozytów</i>	38
3.3. Innowacyjne rozwiązanie w walce z lekoopornością	41
3.4. Bibliografia	44
4. Publikacje naukowe.....	54
4.1. Hybrydowe układy metal-białko w ujęciu serwatkowym.....	54
4.2. A study of zinc ions immobilization by β -lactoglobulin.....	64
4.3. The study of zinc ions binding to α_{S1} -, β -, κ -casein	79
4.4. Study on zinc ions binding to the individual casein fractions α_{S1} , β - and κ -casein....	98
4.5. Immobilized enzyme microreactors for efficient analysis of tryptic peptides in β - casein and β -lactoglobulin.....	119
4.6. Study on silver ions binding to β -lactoglobulin	144
4.7. The influence of zinc ions concentration on β -lactoglobulin structure – physicochemical properties of Zn- β -lactoglobulin complexes.....	158
4.8. Metal-protein action for the wound healing process using murine model C57BL/6J mouse	169
5. Podsumowanie i wnioski	189
6. Streszczenie	192
7. Abstract	194
8. Dorobek naukowy.....	196
9. Oświadczenia.....	202

Wykaz skrótów

α_{S1} - i α_{S2} CN	α_{S1} - i α_{S2} -kazeina
α LA	α -laktoalbumina
β CN	β -kazeina
β LG	β -laktoglobulina
ΔG°	Energia swobodna Gibbsa (ang. <i>Gibbs Free Energy</i>)
κ CN	κ -kazeina
AgNPs	Nanocząstki srebra (ang. <i>Silver Nanoparticle</i>)
BSA	Albumina surowicy bydłej (ang. <i>Bovine Serum Albumin</i>)
BSE	Elektrony wstecznie rozproszone (ang. <i>Back Scattered Electrons</i>)
CE	Elektroforeza kapilarna (ang. <i>Capillary Electrophoresis</i>)
CFU	Jednostka tworząca kolonie (ang. <i>Colony Forming Unit</i>)
DFT	Teoria funkcjonałów gęstości (ang. <i>Density Functional Theory</i>)
EDX	Spektroskopia rentgenowska z dyspersją energii (ang. <i>Energy Dispersive X-ray analysis</i>)
FTIR	Spektroskopia w podczerwieni z transformacją Fouriera (ang. <i>Fourier Transform Infrared Spectroscopy</i>)
HRTEM	Wysokorozdzielcza transmisyjna mikroskopia elektronowa (ang. <i>High-Resolution Transmission Electron Microscopy</i>)
ICP-MS	Spektrometria mas sprzężona z plazmą wzbudzaną indukcyjnie (ang. <i>Inductively Coupled Plasma Mass Spectrometry</i>)
IEC	Chromatografia jonowymienna (ang. <i>Ion-Exchange Chromatography</i>)
IG	Immunoglobulina (ang. <i>Immunoglobulin</i>)
μ -IMER	Mikroprzepływowy immobilizowany reaktor enzymatyczny (ang. <i>Microfluidic Immobilized Enzyme Reactor</i>)
JCR	Baza Journal Citation Reports
IP	Model kinetyki dyfuzji wewnątrzcząsteczkowej (ang. <i>Intra-Particle Diffusion model</i>)
LTF	Laktoferyna (ang. <i>Lactoferrin</i>)
MALDI-TOF MS	Spektrometria mas z laserową jonizacją/desorpcją próbki wspomaganą matrycą z analizatorem czasu przelotu (ang. <i>Matrix Assisted Laser Desorption/Ionization with Time-of-Flight Analyzer Mass Spectrometry</i>)

MD	Dokowanie molekularne (ang. <i>Molecular Docking</i>)
MDs	Analiza molekularna (ang. <i>Molecular Dynamics</i>)
MIC	Minimalne stężenie hamujące (ang. <i>Minimal Inhibitory Concentration</i>)
pI	Punkt izoelektryczny (ang. <i>Isoelectric Point</i>)
PFO	Model kinetyki pseudo-pierwszego rzędu (ang. <i>Pseudo-First Order model</i>)
PMF	Peptydowy odcisk palca (ang. <i>Peptide Mass Fingerprint</i>)
PTMs	Modyfikacje potranslacyjne (ang. <i>Post-translational Modifications</i>)
PSO	Model kinetyki pseudo-drugiego rzędu (ang. <i>Pseudo-Second Order model</i>)
QM	Obliczenia mechaniki kwantowej (ang. <i>Quantum Mechanics</i>)
RP-HPLC	Wysokosprawną chromatografię cieczową w układzie odwróconych faz (ang. <i>Reversed Phase – High Performance Liquid Chromatography</i>)
SAED	Obraz dyfrakcyjny z wybranego obszaru próbki (ang. <i>Selected Area Electron Diffraction</i>)
SC	Pokrycie sekwencji (ang. <i>Sequence Coverage</i>)
SE	Elektrony wtórne (ang. <i>Secondary Electrons</i>)
SEC	Chromatografia wykluczania (ang. <i>Size-Exclusion Chromatography</i>)
SEM	Skaningowa mikroskopia elektronowa (ang. <i>Scanning Electron Microscope</i>)
TEM	Transmisyjna mikroskopia elektronowa (ang. <i>Transmission Electron Microscope</i>)
UV-Vis	Spektroskopia w nadfiolecie i świetle widzialnym (ang. <i>Ultraviolet-Visible Spectroscopy</i>)
WPC	Koncentrat białka serwatkowego (ang. <i>Whey Protein Concentration</i>)
WPI	Izolat białka serwatkowego (ang. <i>Whey Protein Isolate</i>)
XRD	Dyfrakcja rentgenowska (ang. <i>X-ray Diffraction</i>)
ZP	Potencjał zeta (ang. <i>Zeta Potential</i>)

1. Wprowadzenie

Podstawowym budulcem wszystkich organizmów żywych są białka. Stanowią one podstawowe strukturalne i funkcjonalne składniki komórek obecnych w naszym organizmie. Są one niezbędne w prawidłowym procesie wzrostu, podczas regeneracji komórek, tkanek czy całych narządów. Wykorzystanie metod proteomicznych do badań klinicznych otwiera możliwość identyfikacji nowych biomarkerów i nowych celów terapeutycznych w diagnostyce oraz w leczeniu chorób cywilizacyjnych w tym nowotworowych [1].

Szeroki zakres aktywności odżywczych, funkcjonalnych oraz biologicznych wykazują białka mleka. Wśród nich białka kazeiny (CN) stanowią około 80% frakcji, które uzupełniają białka serwatkowe (około 20% frakcji). Ze względu na strukturę i pełnione funkcje wśród kazein można wyróżnić trzy frakcje: α_{S1} - i α_{S2} , β -, κ -CN [2]. Kazeina jest podstawowym materiałem budulcowym do tworzenia hemoglobiny i białek osocza krwi. Ponadto stymuluje proliferację limfocytów i aktywuje makrofagi. Specyfiką tych białek jest obecność wiązania z grupą fosforanową, która ma istotny wpływ na możliwość tworzenia wiązań z metalami. Z kolei wśród białek serwatkowych, dominującym białkiem stanowiącym około 50–60% jest β -laktoglobulina (β LG). Jej biologiczna rola nie jest do końca poznana, jednak uważa się, że pełni ona rolę transportową, zwłaszcza odporności biernej u noworodka, a także w regulacji metabolizmu fosforu w gruczole mlekowym [3]. Należy nadmienić, iż białka serwatkowe uzyskiwane są jako odpad przy produkcji serów. Jednak zarówno serwatka jak i mleko są bogatym źródłem biologicznie aktywnych białek.

Znaczącą kwestią badawczą jest fakt, iż wprowadzenie centrum metalicznego, m.in. na zasadach teorii Lewisa (jonu metalu) do białka może poprawić różnorodność chemiczną, a tym samym specyficzność i biodostępność. Obecnie, badanie i zrozumienie oddziaływań pomiędzy metalami, a biomolekułami takimi jak białka stanowi jedno z najważniejszych zagadnień, które budzi coraz większe zainteresowanie. Jony metali są niezwykle ważnym składnikiem wielu układów biologicznych i odgrywają fundamentalną rolę w funkcji wielu białek.

Pierwiastkiem często wykorzystywanym w medycynie jest cynk. Odgrywa on fundamentalną rolę w ogólnym funkcjonowaniu wielu funkcji organizmu. Magazynowany jest głównie w erytrocytach i leukocytach, jednak znajduje się także w mięśniach, kościach i skórze. Jest on uznany za główny pierwiastek śladowy w procesie gojenia się ran z uwagi na jego udział w wielu różnych procesach komórkowych. Stąd też, bardzo ważne jest uzupełnianie niedoborów cynku. Główną formą, jaką przybiera cynk w środowisku komórkowym jest jego udział w metaloenzymach oraz jego zaangażowanie w stymulację wielu szlaków

enzymatycznych [4]. Najczęściej wykorzystywanym metalem o właściwościach terapeutycznych jest również srebro. Jego antybakteryjne właściwości są znane od wielu lat. Srebro wykazuje skuteczne działanie wobec szerokiego spektrum Gram dodatnich i Gram ujemnych bakterii czy grzybów [5]. Ponadto, dzięki rozwijającej się nanotechnologii możliwe jest wykorzystanie nanocząstek metali (np. nanocząstek srebra, AgNPs) jako środka przeciwdrobnoustrojowego. Właściwości nanocząstek srebra pozwalają na ich zastosowanie w medycynie i służbie zdrowia, gdzie mogą stanowić świetny preparat w leczeniu infekcji. W nanoskali materiał ten charakteryzuje się unikalnymi właściwościami elektrycznymi, optycznymi i katalitycznymi, co stało się inspiracją do diagnozowania, wykrywania i obrazowania oraz ukierunkowania badań na bezpośrednie podawanie leków [6].

Okazuje się, że wolne jony metali cynku i srebra mogą wykazywać właściwości toksyczne, jednakże w połączeniu z układami takimi jak białka efekt cytotoksyczności zostaje wyeliminowany. Natura wiązania jonów metali z białkami nadal nie jest do końca poznana i wymaga wdrażania szczegółowych badań poznania mechanizmu działania. Dzięki właściwościom przeciwdrobnoustrojowym takich nanokompozytów, badania tego typu stwarzają możliwość pogłębienia badań aplikacyjnych nad suplementacją czy też regeneracją trudno gojących się ran. Ten drugi efekt stanowi bardzo poważny problem terapeutyczny.

Biorąc pod uwagę wyżej przedstawione problemy badawcze przedmiotem niniejszej rozprawy doktorskiej było zbadanie mechanizmów wiązania jonów cynku i srebra do układów biokoloidalnych takich jak białka. Wynikiem takiego połączenia było uzyskanie metalokompleksów, a także w przypadku immobilizacji jonów srebra powstanie nanocząstek srebra. Połączenia typu metalokompleks wraz z jednoczesnym otrzymaniem nanocząstek określane jest mianem nanokompleksu/nanokompozytu. Źródłem biologicznie aktywnych białek było mleko (białka frakcji kazeinowych (CN) – α_{SI} -, β -, κ -CN) oraz serwatka (białko β -laktoglobulina, β LG). Za podstawę powstającej pracy doktorskiej przyjęto interdyscyplinarne podejście oparte na chemii, biochemii, mikrobiologii i nanotechnologii. Zastosowanie metod instrumentalnych umożliwiło opisanie procesu wiązania jonów metali do aktywnych grup funkcyjnych białek oraz mechanizmu tworzenia się nanokompozytów, uwzględniając zmiany na poziomie strukturalnym oraz morfologicznym badanych układów. Dodatkowo, wykorzystano modelowanie molekularne oraz obliczenia kwantowo-mechaniczne, które wzbogaciły i ułatwiły interpretację zachodzących zjawisk w badanych układach metal-białko. Stanowiąc to może podstawę uzyskania potencjalnego preparatu przeciwbakteryjnego w leczeniu trudno gojących się ran. Ponadto, zbadane zostały właściwości przeciwdrobnoustrojowe uzyskanych kompleksów. Zwieńczeniem badań były studia

aplikacyjne z wykorzystaniem modelu zwierzęcego (myszy) mające określić wpływ działania kompleksów na proces terapeutyczny (gojenie się ran).

Dysertacja oparta jest na publikacjach naukowych opublikowanych w specjalistycznych czasopismach indeksowanych w bazie Journal Citation Reports (JCR):

- [P1] **A. Rodzik**, P. Pomastowski, V. Railean-Plugaru, B. Buszewski, *Hybrydowe układy metal-białko w ujęciu serwatkowym*, *Analityka: nauka i praktyka*, 2021, 2, 4-12. **PM = 20**
- [P2] B. Buszewski, **A. Rodzik**, V. Railean-Plugaru, M. Sprynskyy, P. Pomastowski, *A study of zinc ions immobilization by β -lactoglobulin*, *Colloids and Surfaces A*, 2020, 591, 1-13, doi: 10.1016/j.colsurfa.2020.124443. **IF = 5,518; PM = 70**
- [P3] **A. Rodzik**, P. Pomastowski, V. Railean-Plugaru, M. Sprynskyy, B. Buszewski, *The study of zinc ions binding to α_{S1} -, β -, κ -casein*, *International Journal of Molecular Sciences*, 2020, 21(21), 1-18, doi: 10.3390/ijms21218096. **IF = 6,208; PM = 140**
- [P4] **A. Rodzik**, A. Król-Górniak, V. Railean, M. Sugajski, A. Gołębiowski, D. S. Horne, B. Michalke, M. Sprynskyy, P. Pomastowski, B. Buszewski, *Study on zinc ions binding to the individual casein fractions α_{S1} -, β - and κ -casein*, *Journal of Molecular Structure*, 2023, 1272, doi: 10.1016/j.molstruc.2022.134251. **IF = 3,841; PM = 70**
- [P5] **A. Rodzik**, V. Railean, P. Pomastowski, B. Buszewski, M. Szumski, *Immobilized enzyme microreactors for efficient analysis of tryptic peptides in β -casein and β -lactoglobulin*, *Scientific Reports*, Submission ID 5d953fac-cd31-4150-9da3-e4e688f203eb. **IF = 4,996; PM = 140**
- [P6] **A. Rodzik**, V. Railean, P. Pomastowski, P. Žuvela, M. W. Wong, M. Sprynskyy, B. Buszewski *Study on silver ions binding to β -lactoglobulin*, *Biophysical Chemistry*, 2022, 291, doi: 10.1016/j.bpc.2022.106897. **IF = 3,628; PM = 70**
- [P7] **A. Rodzik**, V. Railean, P. Pomastowski, P. Žuvela, M. W. Wong, B. Buszewski, *The influence of zinc ions concentration on β -lactoglobulin structure – physicochemical properties of Zn- β -lactoglobulin complexes*, *Journal of Molecular Structure*, 2022, 1268, 1-10, doi: 10.1016/j.molstruc.2022.133745. **IF = 3,841; PM = 70**
- [P8] **A. Rodzik**, P. Pomastowski, M. Buszewska-Forajta, V. Railean, A. Gołębiowski, B. Buszewski, K. Niedojadło, K. Rafińska, *Metal-protein action for the wound healing process using murine model C57BL/6J mouse*, *Scientific Reports*, Submission ID 15404681-edaf-4c74-885f-ae8688b6dbd7. **IF = 4,996; PM = 140**

IF – impact factor, **PM** – punkty ministerialne

2. Cel badawczy

Nadrzędnym celem prowadzonych badań w ramach rozprawy doktorskiej było poznanie mechanizmów tworzenia się nanokompozytów metali w wyniku przeprowadzenia syntezy jonów cynku oraz srebra z białkiem serwatkowym β -laktoglobuliną (β LG) oraz jonów cynku z białkami mleka – α_{S1} -, β -, κ -kazeinami (α_{S1} CN, β CN, κ -CN). Uzyskane nanokompozyty poddane zostały fizykochemicznej charakterystyce wykorzystując bogate instrumentarium badawcze. Określona została także aktywność biologiczna nanokompozytów wobec patogennych szczepów opornych na antybiotyki. Ponadto przeprowadzone zostały badania aplikacyjne wykorzystując model zwierzęcy (myszy).

Cele szczegółowe zrealizowano poprzez:

1. Syntezę/immobilizację jonów cynku oraz srebra przez białka mleka i białka serwatkowe:
 - i. Kinetyczne i izotermiczne badania immobilizacji jonów cynku i srebra w oparciu o metodę sorpcji wsadowej.
2. Fizykochemiczną charakterystykę powstałych indywiduów przy wykorzystaniu całego spektrum technik instrumentalnych.
3. Opis mechanizmu immobilizacji jonów cynku i srebra do badanych białek oraz tworzenie nanocząstek srebra tworzących układ hybrydowy Ag β LG/AgNPs β LG:
 - i. Modelowanie molekularne pozwalające na modelowanie otrzymanych struktur;
 - ii. Obliczenia teorii funkcjonałów gęstości wskazujące miejsca wiązania.
4. Określenie aktywności biologicznej otrzymanych nanokompozytów:
 - i. Pilotażowe badanie aktywności przeciwdrobnoustrojowej otrzymanych preparatów wobec szczepów o znaczeniu klinicznym;
 - ii. Oznaczenie jednostek tworzących kolonie (CFU) i określenie ich dla wszystkich komórek bakteryjnych jako procentu żywych komórek w porównaniu z próbą kontrolną (hodowla bez obróbki).
5. Badania aplikacyjne/farmakologiczne otrzymanych nanokompozytów:
 - i. Proces gojenia się rany przy wykorzystaniu modelu zwierzęcego (myszy).

Powyższe zadania zrealizowane zostały poprzez zastosowanie następujących technik fizykochemicznych:

- Spektroskopia w podczerwieni z transformacją Fouriera (FTIR);

- Spektroskopia Ramana;
- Spektroskopia UV-Vis;
- Spektrofluorymetria;
- Skaningowa i transmisyjna mikroskopia elektronowa (SEM, TEM);
- Dyfrakcja rentgenowska (XRD);
- Spektrometria emisyjna ze wzbudzeniem w plazmie indukcyjnie sprzężonej (ICP-MS);
- Spektrometria mas z jonizacją/desorpcją laserową wspomaganą matrycą oraz analizatorem czasu przelotu (MALDI-TOF MS);
- Elektroforetyczne techniki separacyjne.

3. Problem badawczy

3.1. Białka

Do najliczniejszych związków organicznych w systemach żywych należą białka. Są one bardzo zróżnicowane zarówno pod względem struktury, jak i funkcji w porównaniu do innych makrocząsteczek. Decydują one nie tylko o strukturze układu, prawidłowym funkcjonowaniu i rozwoju organizmów żywych, lecz również kontrolują każdy proces komórkowy, w tym procesy replikacji DNA i transkrypcji RNA, translacji i *splicingu* [7]. Ze względu na szeroki zakres właściwości biologicznych białek, powstała nowa dziedzina nauki jaką jest **proteomika**, która wykorzystuje je do opisu stanu organizmu. Nauka ta dotyczy badania białek, czasowej ekspresji i określania biologicznych struktur, funkcji i wzajemnych oddziaływań. Ze względu na modyfikacje jakim ulegają białka ich liczba jest znacznie większa niż liczba kodujących je genów. Stąd też, celem proteomiki jest generowanie profili białkowych, porównywanie ich i wykrywanie różnic między nimi [7], [8].

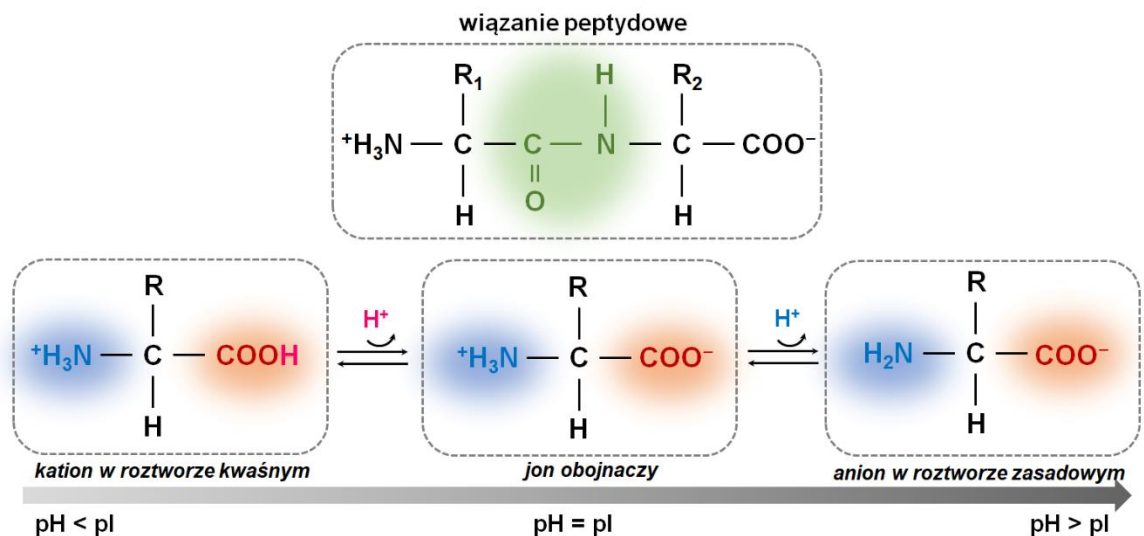
Badania białek wymuszają zastosowanie szeregu technik analitycznych o wysokiej selektywności, rozdzielczości i czułości. Zastosowanie analizy proteomicznej umożliwia relatywnie szybkie poszukiwanie nowych biomarkerów nowotworowych, których zastosowanie w przyszłości pozwoli na wykorzystanie ich zarówno do badań przesiewowych, jak i prognozowania choroby. Za sprawą proteomiki możliwe jest pełniejsze zrozumienie mechanizmów chorób, ułatwienie rozwoju nowych leków i szczepionek oraz szczegółowe badanie patogenów [8].

Z chemicznego punktu widzenia, białka są liniowymi polimerami/organicznymi makrocząsteczkami w układach żywych składającymi się z aminokwasów połączonych ze sobą wiązaniami peptydowymi (*Rys. 1*). Mogą przyjmować one ściśle określoną konformację przestrzenną, stąd też można wśród nich wyróżnić strukturę pierwszorzędową, drugorzędową, trzeciorzędową oraz czwartorzędową. Struktura pierwszorzędowa zawiera ściśle określoną sekwencję aminokwasową i jej oznaczenie jest bardzo ważne chociażby ze względu na wyjaśnienie mechanizmu działania białka np. mechanizm katalityczny enzymu czy też określenie zmiany sekwencji aminokwasowej będącej przyczyną nieprawidłowego funkcjonowania lub choroby organizmu np. Alzheimer [9], Parkinson [10], mukowiscydoza [11]. W związku z tym, iż utworzone łańcuchy polimerowe mogą zwiijać się w regularne struktury typu α -helisy i β -harmonijki powstaje struktura drugorzędowa. Indywidualne jednostki struktury drugorzędowej w przypadku silnego skręcenia lub wygięcia prowadzą do uzyskania struktury trzeciorzędowej. W skutek połączenia się kilku łańcuchów o konformacji

przestrzennej mamy do czynienia z uzyskaniem struktury supramolekularnej, która jest strukturą czwartorzędową. Powszechnie występuje dwadzieścia aminokwasów zbudowanych jedynie z izomerów L, których łańcuchy boczne różnią się wielkością, kształtem, ładunkiem elektrycznym, zdolnością do tworzenia wiązań wodorowych, hydrofobowych, hydrofilowych, jonowych, kowalencyjnych oraz reaktywnością chemiczną [12]. W roztworze o obojętnym pH aminokwasy funkcjonują w formie zjonizowanej jako tzw. jony obojnacze to znaczy, że aminokwas w tej postaci ma protonowaną grupę aminową ($-\text{NH}_3^+$) i zdeprotonowaną grupę karboksylową ($-\text{COO}^-$). Przy zmianie pH następuje również zmiana stanu jonizacji aminokwasu, tak więc w roztworze kwaśnym grupa aminowa będzie protonowana ($-\text{NH}_3^+$), natomiast grupa karboksylowa pozostanie niezjonizowana ($-\text{COOH}$). Podczas wzrostu pH grupa karboksylowa oddaje proton, a jej pK_a jest zbliżone do wartości 2. W warunkach zasadowych proton jest tracony przez grupę aminową i występuje jako $-\text{NH}_2$ (**Rys. 1**). Parametr pK_a definiowany jest według następującego równania:

$$\text{pK}_a = -\log K_a = \log \left(\frac{1}{K_a} \right) \quad (1)$$

Gdzie wartości pK_a są miarą siły kwasu w roztworze.



Rys. 1. Struktura wiązania peptydowego, stan jonizacji aminokwasów w funkcji pH oraz zależność pH od punktu izoelektrycznego (pI) białka; na podstawie [13].

Z uwagi na złożoną strukturę i rozkład ładunku elektrycznego białek, mogą być one uznane za (bio)koloidy, gdyż ich unikalny ładunek elektryczny jest mocno uwarunkowany wartością pH.

3.1.1. Białka mleka i serwatki

Mleko, którego skład i bogactwo oprócz powszechnie znanych faktów prozdrowotnych i odżywczych, nieustannie inspiruje do poszukiwania nowych, interesujących i ważnych wyzwań. Jest ono bowiem źródłem substancji biologicznie czynnych i zapasowych wpływających na procesy życiowe i prozdrowotne. Stanowi to kolejny argument za dokładnym poznaniem i opisaniem jego składu, właściwości oraz możliwości wykorzystania go jako surowca do otrzymywania nowych produktów i preparatów. Obejmuje ono całą gamę związków nieorganicznych (mikro- i makroelementy, sole itp.) oraz organicznych (substancje budulcowe i odżywcze, czyli: różnego rodzaju białka, tłuszcze, witaminy, cukry itp.). Wykorzystanie mleka jako źródła biologicznie aktywnych białek w sposób alternatywny doskonale wpisuje się także w ideę zrównoważonego rozwoju.

Głównymi białkami mleka (około 75–80% v/v) są kazeiny (CN). Stanowią one największy składnik białkowy w większości mlek o znaczeniu przemysłowym. Kompleks kazeinowy dzieli się na trzy frakcje: α_{S1} i α_{S2} (alfa), β (beta) i κ (kappa) [14], [15]. Pozostałą część (około 20%) stanowi serwatka, która przez długi okres czasu była uważana wyłącznie za odpad przy produkcji sera. Obecnie stała się ona punktem zainteresowania naukowców z powodu zawartych w niej składników, gdyż poza dostarczaniem substancji odżywczych, pozwala zapobiegać chorobom i ich skutkom lub je łagodzić [16]. Białko serwatkowe składa się z różnych białek, w tym β -laktoglobuliny (β LG), α -laktoalbuminy (α LA), laktoferyny (LTF), immunoglobulin (IG), albuminy surowicy bydlęcej (BSA) [17].

Kazeiny tworzą w połączeniu z fosforanem wapnia agregaty koloidalne zwane micelami. Kompleks micelarny stabilizowany jest przez siły van der Waalsa, oddziaływania hydrofobowe, wiązania wodorowe, stabilizację elektrostatyczną i steryczną [18]. Ponadto stabilizację miceli zapewniają właściwości fizykochemiczne, takie jak zdolność fosforylowanych reszt serynowych do wiązania się z jonami wapnia oraz amfifilowy charakter κ CN, czyli frakcji, która jest glikozylowana i odpowiada za stabilizację miceli na powierzchni [19]. Szczególną cechą dla kazein jest występowanie wiązania z grupą fosforanową, co więcej, wszystkie łańcuchy polipeptydowe posiadają w swojej strukturze przynajmniej jedną z tych grup – do fosforylacji prowadzi unikalna sekwencja aminokwasów [20]. We wspomnianej sekwencji najpierw występuje seryna (Ser), po niej dowolny aminokwas, po czym ponownie kwas glutaminowy (Glu^-) lub seryna. Ma to szczególnie istotny wpływ na możliwość tworzenia wiązań z metalami. Typowa micela składa się w 92% z α_{S1} -, α_{S2} -, β -, κ -kazeiny w stosunku 3: 1: 3: 1, 8% związków nieorganicznych takich jak: wapń (2,87%), fosforany (2,89%), cytryniany

(0,4%) oraz niewielkie ilości sodu, magnezu i potasu [19]. Stabilność dyspersyjna zależności miceli kazeinowych związana jest z ich strukturą. Wśród wielu proponowanych modeli miceli można wyróżnić trzy główne: (1) model submiceli Slattery'ego i Evarda [21]; (2) model nanoklastrów Holta [22] oraz (3) model podwójnego wiązania zaproponowany przez Horne'a [23]. Niemniej jednak, dokładna stabilność miceli jest nadal przedmiotem dyskusji i wymaga dalszych badań w tym zakresie.

Z kolei dominującym białkiem serwatkowym jest β -laktoglobulina (β LG) stanowiąca ponad 50% całkowitej zawartości białek serwatkowych, jednakże nie występuje w mleku ludzkim [24]. Jest ona niewielkim białkiem globularnym zaliczanym do rodziny lipokalin, składającym się ze 162 reszt aminokwasowych [25]. Stanowi źródło aminokwasów niezbędnych i rozgałęzionych, takich jak leucyna (Leu), izoleucyna (Ile) i walina (Val) [26]. Z uwagi na znaczną obecność cysteiny (Cys), tryptofanu (Trp) i aminokwasów rozgałęzionych, możliwość wiązania różnych ligandów hydrofobowych (witamina A, kwasy tłuszczowe) oraz bioaktywnych peptydów, β LG ma doskonałe właściwości odżywcze [27], [28], [29]. Dlatego też, została wybrana jako białko modelowe w niniejszej pracy. Możliwość wiązania kwasów tłuszczowych przez β LG związana jest z kielichowatą strukturą tego białka, która składa się z ośmioniciowego, antyrównoległego arkusza β otoczonego przez cztery ruchome pętle regulujące dostęp do wnętrza β -baryłki, czyli kielicha [30]. Niemniej jednak niezależnie od wielu zalet, białko to uznawane jest za główny alergen mleka odpowiedzialny za jego działanie alergizujące, zwłaszcza wśród małych dzieci. Jednakże liczne badania prowadzone nad zmianami konformacyjnymi β LG przyczyniają się do zmian w pojawiającej się alergenicności [31].

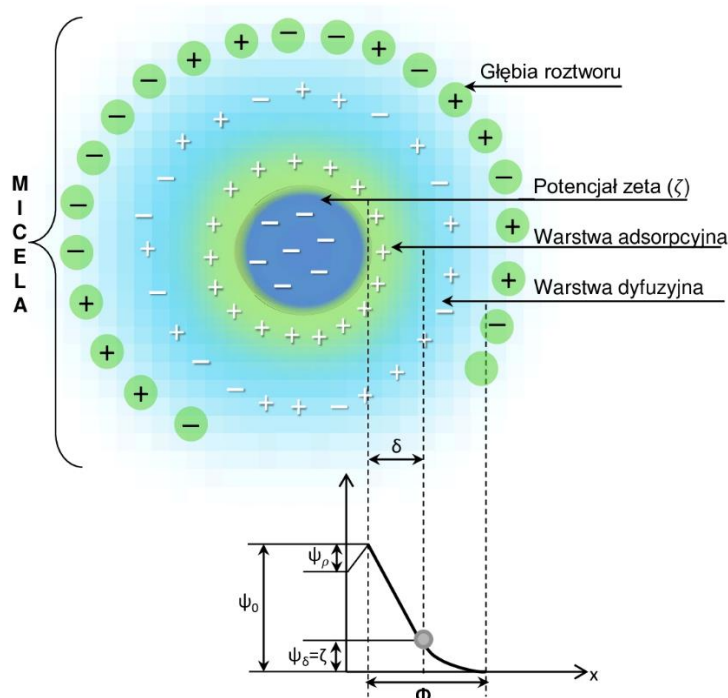
W metodach proteomicznych istnieje wiele różnych technik używanych do rozdzielania i charakteryzowania białek. W pracy przeglądowej pt.: *Hybrydowe układy metal-białko w ujęciu serwatkowym [P1]* skupiono się m.in. na omówieniu technik analitycznych stosowanych w badaniu białek. Techniki te oparte są na różnicach w rozpuszczalności, wielkości, ładunku, właściwościach adsorpcyjnych cząsteczek białek. Do najczęściej stosowanych technik rozdzielania białek należą metody membranowe, elektroforetyczne i chromatograficzne, które następnie mogą zostać zidentyfikowane za pomocą spektrometrii mas, a kolejno odpowiednio zinterpretowane. Wśród metod membranowych wyróżnić można mikrofiltrację, ultrafiltrację oraz nanofiltrację. Metody te różnią się między sobą i mogą być wykorzystywane do izolowania białek serwatkowych z rzeczywistych matryc w celu przygotowania koncentratu białek serwatkowych (WPC, ang. *Whey Protein Concentration*) i izolatu białek serwatkowych (WPI, ang. *Whey Protein Isolate*) oraz do rozdzielania przed

analizą. Druga grupa obejmuje zazwyczaj elektroforezę żelową w dwóch wariantach (postać natywna i denaturująca) oraz elektroforezę kapilarną (CE, ang. *Capillary Electrophoresis*). Do najbardziej zróżnicowanych technik należą techniki chromatograficzne, w których można wyróżnić chromatografię jonowymienną (IEC, ang. *Ion-Exchange Chromatography*), wykluczania (SEC, ang. *Size-Exclusion Chromatography*), cieczową w układzie odwróconych faz (RP-HPLC, ang. *Reversed Phase – High Performance Liquid Chromatography*). Przykładem wykorzystania sprzężonej techniki HPLC z detekcją spektrometryczną może być praca Pomastowskiego i in., w której opracowano szybką i selektywną metodę separacji frakcji kazeiny [32].

Jedną z kluczowych cech fizykochemicznych białek (biokoloidów) jest ich ładunek, który związany jest ze wspomnianą wcześniej stałą dysocjacji pK_a . Analiza wpływu pH na rozkład ładunków elektrycznych białek jest jednym z problemów badawczych. Dla białek i peptydów uwzględnia się siedem łańcuchów bocznych aminokwasów, które jonizują w zakresie pH od 1 do 14 – kwasów glutaminowego i asparaginowego (grupy karboksylowe), tyrozyny (grupa fenolowa), cysteiny (grupa tiolowa), histydyny (boczne łańcuchy imidazolowe), lizyny (grupa aminowa) oraz argininy (grupa guanidynowa) [33], [34]. Wartości pK_a wszystkich naładowanych grup mogą służyć do obliczenia całkowitego ładunku cząsteczki w dowolnym pH lub do oszacowania punktu izoelektrycznego (pI, ang. *Isoelectric Point*), czyli pH, dla którego istnieje równowaga ładunków dodatnich i ujemnych, stąd całkowity ładunek netto cząsteczki jest równy zeru. W pH poniżej swojego pI białka posiadają ładunek dodatni, a powyżej swojego pI ich ładunek jest ujemny (**Rys. 1**). Wartości pI uzyskuje się m.in. poprzez pomiar potencjału zeta (ζ , ZP, ang. *Zeta Potential*) w funkcji pH i określając pH dla których wartości ZP przekraczają wartość 0. Na podstawie teorii elektrokinetycznej opisaną równaniem Smoluchowskiego potencjał zeta definiuje się jako potencjał elektrokinetyczny, pojawiający się na granicy pomiędzy jonami warstwy adsorpcyjnej, a wolnymi przeciwjonami warstwy dyfuzyjnej. ZP jest proporcjonalny do gęstości ładunku na powierzchni (bio)koloidu, który zależy od pH [35], [36]. Zatem wartość potencjału zeta będzie różna w zależności od pH oraz stężenia elektrolitu (**Rys. 2**).

Przykładem wykorzystania pomiaru potencjału zeta oraz wyznaczenia punktu izoelektrycznego celem scharakteryzowania białek, mogą być prace *A study of zinc ions immobilization by β -lactoglobulin* [P2] oraz *The study of zinc ions binding to α_{S1} -, β - and κ -casein* [P3]. W niniejszych pracach potencjał zeta wyznaczono w funkcji różnego pH w czasie początkowym, po 1 h i po 5 h. Stwierdzono, że punkty izoelektryczne dla α_{S1} CN, β CN, κ CN i β LG wynoszą odpowiednio $4,80 \pm 0,72$, $4,55 \pm 2,15$, $4,40 \pm 0,28$ i $4,60 \pm 0,20$. Ładunki

powierzchniowe wszystkich badanych białek mieściły się w zakresie -35–32 mV. Ponadto zaobserwowano, że wraz ze wzrostem czasu zmienia się wartość potencjału zeta, a stabilność



Rys. 2. Budowa koloidu. Zmiana potencjału powierzchniowego w funkcji odległości od powierzchni miceli; na podstawie [13].

białek zauważalna jest po $t = 1$ h i $t = 5$ h. Przy niskich wartościach pH ładunek powierzchniowy białek był dodatni, a potencjały zeta stawały się bardziej ujemne wraz ze wzrostem pH. W pracy *Study on zinc ions binding to the individual casein fractions: α_{S1} -, β - and κ - casein [P4]* za pomocą potencjału zeta została zmierzona stabilność poszczególnych frakcji kazeinowych (α_{S1} -, β -, κ -CN) z jonami jonów cynku w zakresie stężeń 1–600 mg/l (**Rozdział 2.2.**) Wychodzi się z założenia, że dla standardowych układów koloidalnych, stabilizowanych oddziaływaniami elektrostatycznymi, wartości potencjału zeta pomiędzy -30 mV a +30 mV wskazują na układ niestabilny [35]. Potencjał zeta dla α_{S1} CN zarejestrowano w zakresie od $-31,8 \pm 2,8$ mV w wyniku dodania stężenia jonów cynku 1 mg/l do $17,3 \pm 1,7$ dla stężenia jonów cynku 600 mg/l mV. Potencjał zeta β CN był najbardziej stabilny podczas kompleksowania w zakresie od 40 do 180 mg/l jonów Zn_{aq}^{2+} ($-25,9 \pm 1,86$ do $-27,9 \pm 3,0$ mV), natomiast był niestabilny przy najniższym (1 mg/l) i najwyższym (600 mg/l) stężeniu cynku z ZP wynoszącymi odpowiednio $-5,1 \pm 0,6$ mV i $-5,9 \pm 3,8$ mV. Według wartości ZP mniejszą stabilność wykazywała forma κ CN, której ZP wahał się od $-12,5 \pm 1,1$ mV przy najniższym (1 mg/l) do $-1,3 \pm 0,2$ mV przy najwyższym stężeniu (600 mg/l) jonów Zn_{aq}^{2+} . Zjawisko to może być związane z właściwościami hydrofobowymi wszystkich trzech form kazeiny [37], [38].

Ponadto na podstawie wyników eksperymentalnych stwierdzono, że w przypadku α_1 CN i κ CN dodatek jonów cynku nie wpłynął na trwałość tego białka.

Kolejnym ważnym zagadnieniem w proteomice jest masa molekularna białek. Ze względu na to, że wiele białek może posiadać taką samą masę molekularną może nastąpić problem z prawidłową identyfikacją, co może być o wiele bardziej skomplikowane niż poznanie ludzkiego genomu i wymaga zastosowania współczesnych technik, które umożliwią poznanie ich składu. Rozwiązaniem może być pomiar mas molekularnych poszczególnych fragmentów danego białka, a nie jedynie całej sekwencji. Jedną z pierwszych metod identyfikacji białek była degradacja Edmana opracowana przez szwedzkiego naukowca w 1950 r. [39]. Metoda ta polegała na kolejnym odrywaniu aminokwasów z N-końca peptydu białka i określeniu typu oderwanego aminokwasu aż do momentu dotarcia do C-końca łańcucha polipeptydowego. Niestety wadą takiego postępowania jest ograniczenie analizy łańcucha posiadającego więcej niż 60 aminokwasów oraz długi czas analizy [40]. Znacznie szybszą metodą analizy białek jest wprowadzona w latach 90-tych laserowa jonizacja/desorpcja próbki wspomagana matrycą z analizatorem czasu przelotu (MALDI-TOF MS, ang. *Matrix Assisted Laser Desorption/Ionization with Time-of-Flight Analyzer Mass Spectrometry*). Jonizacja typu MALDI stosowana w spektrometrach spowodowała znaczną rewolucję w procesie identyfikacji białek. Główną jej zaletą jest analiza białek o dużej masie cząsteczkowej, wysoka przepustowość oraz czułość, dokładność masy, a także zautomatyzowana analiza wielu próbek w krótkim czasie. Niemniej jednak, mimo skuteczności tego podejścia, do wad można zaliczyć stosunkowo skomplikowane przygotowanie próbek; nieprawidłowe przygotowanie próbek do analizy może prowadzić do krystalizacji matrycy/analitu co z kolei będzie miało silny wpływ na m.in. procesy desorpcji. Zautomatyzowanie procesu identyfikacji i możliwość połączenia spektrometru masowego z rozdzielaniem białek wykorzystując elektroforezę w żelu przyczynił się do znacznego rozwoju badań proteomicznych.

W proteomice wykorzystuje się trzy główne strategie identyfikacji i charakterystyki białek metodami spektrometrycznymi. Są to strategie typu *top-down*, *bottom-up* i *shotgun*. Strategia *top down* polega na analizie białka natywnego (tzw. *intact*) bez przeprowadzania proteolizy za pomocą fragmentacji. Z kolei w podejściu typu *bottom-up* białka poddane są trawieniu proteolitycznemu (najczęściej trypsyną) do postaci peptydów przed analizą masy. Cały komplet mas peptydów tworzący sekwencję białka kształtuje jego unikalny identyfikator nazywany *odciskiem palca* (PMF, ang. *Peptide Mass Fingerprint*) będący wykorzystywany do prawidłowej identyfikacji. Za pomocą odpowiednich programów, na przykład ProFound czy MASCOT dokonuje się przeszukania baz danych białek, aby znaleźć białka, które trawione

tym samym enzymem ulegną rozpadowi na peptydy o tej samej masie cząsteczkowej. W przypadku strategii *shotgun* następuje bezpośrednie trawienie mieszaniny białek. Coraz lepsze rozpowszechnianie i udoskonalanie białkowych baz danych wpłynęło na dokładniejsze i głębsze analizy identyfikacji białek [40], [41].

Proteom mleka jest niezwykle złożony z powodu licznych modyfikacji potranslacyjnych (PTMs, ang. *Post-translational Modifications*) i procesów proteolitycznych. Kompozycja białek mleka charakteryzuje się dużą heterogennością z uwagi na liczne warianty genetyczne oraz izoformy o różnym stopniu modyfikacji potranslacyjnych, takich jak fosforylacja i glikozylacja głównie w kazeinach. Na przebieg fosforylacji wywierają wpływ różne czynniki, jak na przykład sekwencja białka, skuteczność enzymów kinazowych, ekspresja genu, dostępność substratu oraz dostęp do miejsca fosforylacji, które odpowiada za specyficzną konformację białka. Fosforylacja wpływa na stabilizację nano-klastrów fosforanu wapnia w micelach kazeiny. Micelarna struktura kazeiny daje mleku możliwość przenoszenia wapnia i fosforanów do organizmu noworodka. Identyfikacja i charakterystyka lokalizacji fosforylacji jest potrzebna do poznania sieci sygnalizacji białek mleka. Miejsca fosforylacji są źródłem informacji na temat funkcjonalnych zależności pomiędzy białkami sygnalizacyjnymi. Uwolnione podczas hydrolizy enzymatycznej peptydy wykazują specyficzne funkcje biologiczne, wynikające z ich działania i oddziaływań na poziomie komórkowym [42].

Do identyfikacji PTMs najlepszym sposobem jest zastosowanie metody, która byłaby skuteczna, pozbawiona detergentów, zautomatyzowana oraz pozwalałaby na uniknięcie utraty próbki i zanieczyszczeń. Tradycyjne procedury trawienia w roztworze charakteryzują się długim czasem inkubacji, autolizą proteazy, czy też niską wydajnością procesu trawienia. Rozwiązaniem ułatwiającym prowadzenie badań proteomicznych jest zastosowanie immobilizowanych mikroreaktorów enzymatycznych (μ -IMER, ang. *Microfluidic Immobilized Enzyme Reactor*), w których enzymy są osadzone na stałym nośniku. Dzięki zastosowaniu μ -IMER, można m.in. osiągnąć krótszy czas analizy, zwiększyć przepustowość próbek, a także wykorzystać μ -IMER ponownie. Ponadto metodą wzbogacania białek i peptydów specyficznych dla PTMs jest zastosowanie końcówek pipety ZipTip zawierających nośnik fazy C18. Analiza MS i MS/MS po takim przygotowaniu próbek pozwala na zwiększenie czułości podczas identyfikacji białek i wskazanie miejsc PTMs.

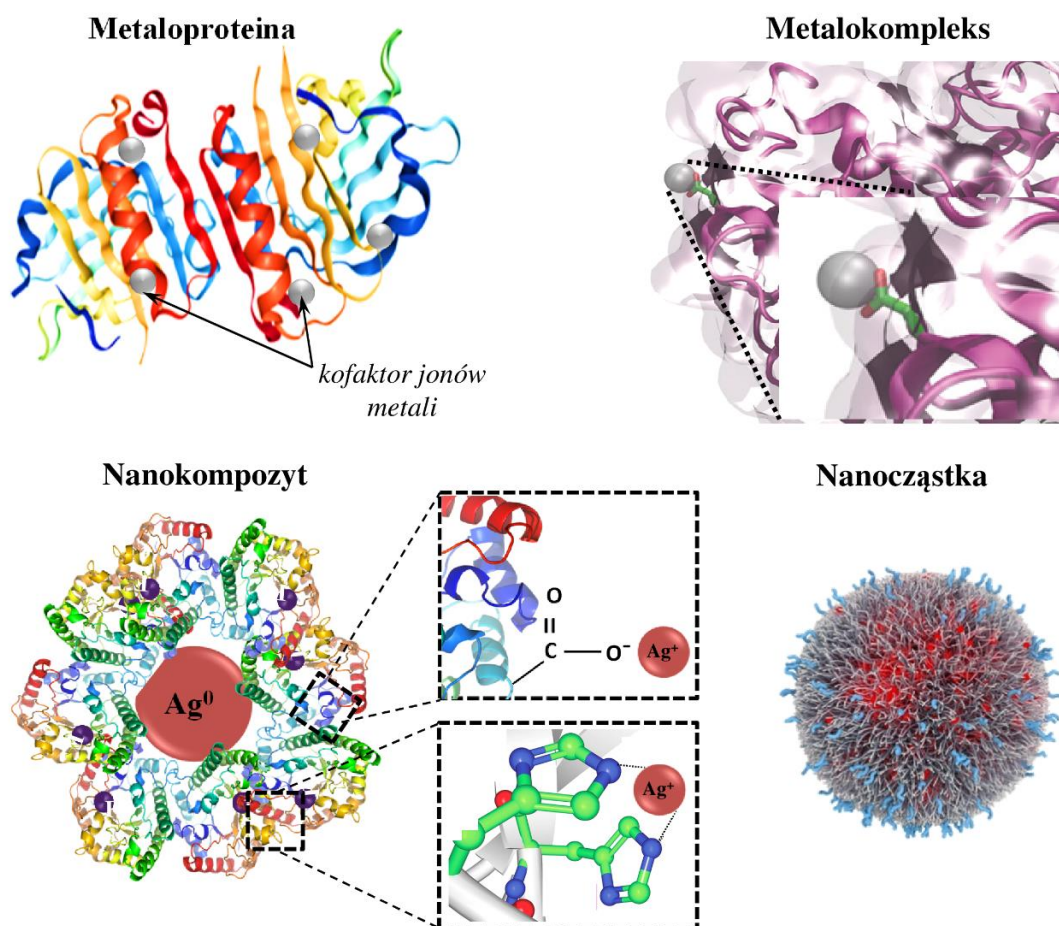
W pracach [P2, P4] analiza MALDI-TOF MS pozwoliła na określenie profili molekularnych uzyskanych natywnych białek. Badanie to pozwoliło na scharakteryzowanie białek w ramach wstępnej analizy fizykochemicznej. Stwierdzono, że masy nienaruszonych izoform kazeiny wynoszą m/z 23 985,874 \pm 0,326 i 19 032,393 \pm 0,326 odpowiednio dla β CN

i κ CN. Z kolei w przypadku α_{S1} CN zaobserwowano dwa nakładające się na siebie sygnały. Sygnały te odpowiadają wartościom m/z 23 530,363 \pm 0,326 i 23 604,819 \pm 0,326. Zgodnie z danymi literaturowymi, zarejestrowane sygnały mogą pochodzić od różnych form genetycznych α_{S1} CN. Masa β LG wyniosła 18 309 \pm 0,132 Da. Niewielkie różnice w masach β LG mogą być spowodowane obecnością modyfikacji potranslacyjnych [43] oraz zastosowaną metodą analityczną [44]. W badaniach własnych zaobserwowano, że β LG może występować w postaci dimerów $[2M-H]^+$ lub nawet trimerów $[3M-H]^+$, tetramerów $[4M-H]^+$ lub pentamerów $[5M-H]^+$, co jest zgodne z danymi literaturowymi [45], [46]. Ponadto w pracy *Immobilized enzyme microreactors for efficient analysis of tryptic peptides in β -casein and β -lactoglobulin* [P5] skupiono się na opracowaniu szybkiej metody analitycznej do badania peptydów trawionych trypsyną dwóch modelowych białek (β CN, β LG). Zastosowano dwa podejścia trawienia białek: klasyczne trawienie białek w żelu oraz w immobilizowanym mikroreaktorze enzymatycznym wraz z wykorzystaniem końcówek pipety ZipTip zawierających złożę chromatograficznej fazy stacjonarnej. Użycie końcówek oceniono pod względem poprawy lub pogorszenia wyniku pokrycia sekwencji oraz załadowania i oczyszczenia peptydów. Powstałe peptydy zostały zidentyfikowane poprzez zastosowanie oprogramowania BioTools z wykorzystaniem niestandardowych parametrów wyszukiwania: cysteina zmodyfikowana przez karbamidometylację, utlenianie i fosforylację. Dzięki porównaniu wyników otrzymanych z różnych metod trawienia i technik przygotowania próbek zostało określone najbardziej preferowane podejście do osiągnięcia najwyższego pokrycia sekwencji. Taki wybór ma kluczowe znaczenie dla dokładnej identyfikacji białek pozwalając na kompleksowe zrozumienie białek β CN i β LG. Stwierdzono, że lepsze pokrycie sekwencji dla utleniania zostało wykazane przez μ -IMER (33% β CN; 65% β LG) w porównaniu do klasycznego trawienia w roztworze (20% β CN; 49% β LG). Wynika z tego, że μ -IMER dostarcza bardziej wydajnego środowiska do trawienia białek, co prowadzi do lepszego zrozumienia ich sekwencji. Co więcej, po zastosowaniu końcówek pipety ZipTip nastąpiła poprawa pokrycia sekwencji zarówno w klasycznym trawieniu w roztworze (26% β CN; 60% β LG), jak i μ -IMER (41% β CN; 80% β LG). Zatem końcówki pipety ZipTip umożliwiają zwiększenie możliwości wykrywania i analizy procesu pokrycia sekwencji. Ponadto dla obu białek zidentyfikowano fosforylację – kluczowe modyfikacje potranslacyjne w funkcji białka. Nie wykryto fosforylacji w białku β CN przy zastosowaniu klasycznej metody trawienia w roztworze jednak po zastosowaniu końcówek pipety ZipTip pokrycie sekwencji wzrosło do 27%. Stosując μ -IMER pokrycie sekwencji było jeszcze wyższe (30%), a w układzie μ -IMER–ZipTip wyniosło 33%. Z kolei w przypadku β LG użycie ZipTip pozwoliło wykryć wyższy

odsetek zmodyfikowanych peptydów zarówno w przypadku trawienia klasycznego (79%) jak i μ -IMER (79%). Powyższe wyniki wskazują, że zastosowanie końcówek pipety ZipTip, szczególnie w połączeniu z μ -IMER zapewniają bardziej efektywną metodę pokrycia sekwencji białek i analizy modyfikacji potranslacyjnych.

3.2. Wiązanie białek z metalami

Białka będące biomolekułami nie istniałyby bez jonów metali, które nadają im całe spektrum nowych właściwości biologicznych [47]. Połączenia takie stwarzają nowe perspektywy ich zastosowania w przemyśle farmaceutycznym, kosmetycznym, medycynie czy technologii żywienia. Mogą zatem poprawić komfort i jakość życia człowieka. Z drugiej strony, dla chemików-analityków są prawdziwym wyzwaniem związanym ze zrozumieniem mechanizmów tworzenia oddziaływań tego typu. W pracy przeglądowej [P1] szerzej został opisany problem oddziaływania metali z białkami serwatkowymi. Otrzymanie biologicznie aktywnych kompleksów białko-metal pełni rolę doskonałego narzędzia do określenia ich wpływu na metabolizm badanego organizmu. Zmiany wywołane oddziaływaniami z metalami są wynikiem tworzenia nowych miejsc wiążących (decydują o oddziaływaniach białka z innymi ligandami), zmianami zachodzącymi w strukturze białka, grupami oddziałującymi umożliwiającymi badanie charakteru oraz siły oddziaływania, a także agregacji białka. Wynikiem oddziaływań metal-białko mogą być metaloproteiny, metalokompleksy, nanocząstki oraz nanokompozyty co zostało przedstawione na *Rys. 3*.



Rys. 3. Konsekwencje oddziaływań metal-białko; na podstawie [48].

Metaloproteiny powstają głównie poprzez tworzenie wiązań koordynacyjnych pomiędzy jonami metali, a grupami funkcyjnymi aminokwasów, chociażby grupami karboksylowymi, wpisując się tym samym w strukturę białka. Z kolei metalokompleks jest sztucznym układem zbudowanym ze słabych oddziaływań, takich jak oddziaływania elektrostatyczne, wiązanie wodorowe, siły Wan der Waalsa czy wiązania typu donor-akceptor. Oddziaływania pomiędzy białkami, a jonami metali mogą prowadzić do powstania nanocząstek, czyli struktur o wymiarach w zakresie 1–100 nm. Natomiast powstały układ składający się z utworzonego metalokompleksu i nanocząstek może tworzyć nanokompleks/nanokompozyt.

Wśród nieorganicznych kofaktorów w układach biologicznych, które ułatwiają różne funkcje białek i ich kompleksów, najbardziej rozpowszechnione są metale d-elektronowe [49]. Specyficzne miejsca wiązania metali znajdują się nie tylko w białkach, ale także w cząsteczkach DNA i RNA, które są ważne dla ich struktury i funkcji [50]. Zmiany w organizmie spowodowane brakiem pewnych jonów metali mogą prowadzić do chorób związanych m.in. z niedokrwistością złośliwą (niedobór żelaza), opóźnieniem wzrostu (niedobór cynku), chorobami serca (niedobór miedzi) [51].

Jednym z najobficiej występujących w organizmach żywych metali przejściowych jest cynk. Cynk to pierwiastek chemiczny usytuowany w IV okresie i XII grupie układu okresowego o liczbie atomowej 30. Ma on wypełnioną powłokę d-elektronową ($4s^23d^{10}$) i tym samym wykazuje brak energii stabilizacji pola ligandu i związanych z tym preferencji stereochemicznych. Stąd też liczba koordynacyjna i geometria kompleksów cynku określane są głównie przez promień jonu metalu i koordynujących atomów lub jonów liganda stąd jego *aquakompleksy* cechują się dość elastyczną geometrią koordynacji. W szeregu elektrochemicznym cynk występuje nad wodorem – jego wartość potencjału wynosi -76 V, stąd jego skłonność do utleniania [52].

Specjację cynku można najlepiej zrozumieć przy pomocy diagramu Pourbaix. Diagram ten pokazuje formy chemiczne jako funkcję wzorcowego potencjału redoks i wartości pH. Na podstawie diagramu wiemy, że w całym zakresie potencjałów redoks i wartości pH w biologii cynk jest obecny jako uwodniony na drugim stopniu utlenienia – $Zn(II)_{(aq)}$ wykazując właściwości obojętne. W środowisku kwaśnym występuje jako *aquakompleks*, natomiast w środowisku zasadowym pojawia się w postaci wodorotlenku w wyniku hydroksylacji [52]. Cynk jest konieczny do syntezy kwasu dezoksyrybonukleinowego (DNA) i replikacji, tym samym jest niezbędny do wzrostu. Bierze on także udział w homeostazie poprzez czynny udział w oddziaływaniu z płytkami krwi, jest także potrzebny do produkcji przeciwciał

i prawidłowego funkcjonowania komórek odpornościowych. Odgrywa główną rolę w proliferacji komórek zapalnych i moduluje zapalenie skóry, przyczynia się także do hamowania wzrostu bakterii [4].

Biologicznie aktywne cząsteczki, jak na przykład aminokwasy, peptydy, białka, węglowodany, nukleotydy, DNA, RNA czy witaminy posiadają atomy, które służą jako donory pary elektronowej dla koordynacji metali. Zatem są potencjalnymi ligandami do łączenia się z jonami metali. Według danych literaturowych, chemia koordynacyjna cynku w białkach i peptydach dotyczy donorów azotu, tlenu i siarki łańcuchów bocznych histydyny (His), kwasu glutaminowego (Glu^-), kwasu asparaginowego (Asp^-) oraz cysteiny (Cys) [52].

Innym metalem i jednym z najwcześniej poznanych jest srebro, które znalazło szerokie zastosowanie w medycynie. We wczesnych latach XIX wieku lekarze zszywali rany chirurgiczne srebrnymi drucikami, z kolei podczas I wojny światowej na rany żołnierzy nakładano opatrunki ze srebrem, aby zapobiec infekcjom i ułatwić gojenie. Srebro koloidalne znalazło szerokie zastosowanie na początku XX wieku w praktyce medycznej jako środek bakteriobójczy w szpitalach, niestety stracił na popularności w erze antybiotyków. Związki koordynacyjne Ag(I) ze względu na swoje niezwykle właściwości biologiczne zostały uznane za obiecujące terapeutyki, gdyż wykazują aktywność przeciwbakteryjną, przeciwgrzybiczną, przeciw pasożytniczą, przeciwnowotworową, co zostało potwierdzone w dużej liczbie badań.

Srebro jest metalem przejściowym należącym do grupy metali szlachetnych. W układzie okresowym jest ono umieszczone w V okresie i XI grupie. Jego liczba atomowa wynosi 47, a konfiguracja elektronowa to $[\text{Kr}] 4d^{10}5s^1$. Srebro jako metal nie jest rozpuszczalne w wodzie, natomiast rozpuszcza się w swojej formie kationowej. Jego forma metaliczna i większość jego związków nieorganicznych może jonizować i uwalniać biologicznie aktywne Ag_{aq}^+ w obecności wody i utleniacza. Standardowy potencjał redukcyjny dla pary Ag/Ag^+ wynosi 0,7994 V przy pH poniżej 6, lecz przy wyższym pH jest on nieco niższy, ponieważ zaczyna się tworzyć Ag_2O , [53]. Przyszłość metali w medycynie wydaje się być ściśle związana z ich formami nanometrycznymi [53]. Inną formą srebra są nanocząstki srebra, powszechnie stosowane w medycynie jako alternatywa dla standardowych antybiotyków. Nanotechnologia wykazuje bowiem niesamowity potencjał zarówno w zastosowaniach terapeutycznych, jak i diagnostycznych. Nanomateriały mogą być wykorzystywane jako leki, nośniki, sondy, środki kontrastowe do obrazowania, biosensory. Nie ma dowodów na to, że srebro jest trucizną dla człowieka, niemniej jego stężenie po dłuższym czasie ekspozycji może narastać w tkankach organizmu i tym samym prowadzić do niepożądanych skutków. Negatywne działanie jonów i nanocząstek srebra na zdrowie człowieka jest jednak stale oceniane i raportowane. Kiedy jony

srebra zostaną zgromadzone w tkankach ciała, szczególnie w skórze, mogą być one zredukowane do nanocząstek metalu poprzez procesy wynikające z działania światła słonecznego oraz innych reduktorów lub też wytrącić się w postaci nierozpuszczalnych ciemnych siarczków i selenków, tym samym barwiąc skórę w różnych odcieniach szaro-niebieskiego. Takie przebarwienia mogą być wywołane przez długotrwałe wdychanie i/lub spożycie związków srebra, jednak uważane są one za stan jedynie kosmetyczny, gdyż nie wywołują żadnych toksycznych skutków w organizmie. Jony srebra mają silne powinowactwo do białek eliminują tym samym działanie toksyczne [53], [54].

W pracach *A study of zinc ions immobilization by β -lactoglobulin [P2]*, *The study of zinc ions binding to α_{S1} -, β -, κ -casein [P3]*, *Study on zinc ions binding to the individual casein fractions α_{S1} -, β - and κ -casein [P4]*, *Study on silver ions binding to β -lactoglobulin [P6]*, *The influence of zinc ions concentration on β -lactoglobulin structure – physicochemical properties of Zn- β -lactoglobulin complexes [P7]* podjętym problemem naukowym było uzyskanie nanokompozytów na bazie β LG z jonami cynku i srebra oraz poszczególnych frakcji kazeinowych (α_{S1} -, β -, κ -CN) z jonami cynku.

3.2.1. Imobilizacja jonów metali do białek i charakterystyka wiązania

Do opisu natury procesów dotyczących mechanizmów wiązania jonów przez aktywne grupy funkcyjne biokoloidów (białek) stosuje się klasyczne założenia modeli kinetycznych. Adsorpcja jest procesem, w którym następuje przyleganie lub wiązanie jonów i cząsteczek na powierzchni materiału stałego. W tym przypadku materiał zgromadzony na interfejsie jest adsorbentem, a powierzchnia ciała stałego jest adsorbentem. Z kolei biosorpcja jest podkategorią adsorpcji, w której sorbentem jest matryca biologiczna [55]. Podczas adsorpcji biorą udział dwa główne procesy: fizyczny (sorpcja fizyczna) lub chemiczny (chemisorpcja). Adsorpcja fizyczna jest wynikiem słabych sił przyciągania (van der Waalsa), natomiast chemisorpcja obejmuje utworzenie silnego wiązania pomiędzy substancją rozpuszczoną, a adsorbentem, które polega na przeniesieniu elektronów [56]. Kinetyka adsorpcji jest jednym z głównych czynników, który musi być zrozumiany przed zastosowaniem jakiegokolwiek adsorbentu. W każdym procesie adsorpcji stosuje się liniową lub nieliniową analizę kinetyki [56]. Kinetyka adsorpcji zajmuje się badaniem szybkości procesu adsorpcji, która pozwala określić etap kontrolny i mechanizm procesu adsorpcji. Do badania szybkości i mechanizmu procesu adsorpcji najczęściej stosowane są modele kinetyki zerowego rzędu (równanie 2), pierwszego rzędu (równanie 3), pseudo-pierwszego rzędu (PFO, ang. *Pseudo-First Order*, (równanie 4)), pseudo-drugiego rzędu (PSO, ang. *Pseudo-Second Order*, (równanie 5)) oraz kinetyki dyfuzji wewnątrzcząsteczkowej (IP, ang. *Intra-Particle Diffusion model*, (równanie 6)) zaprezentowane poniżej:

$$C = C_0 - k_0 t \quad (2)$$

$$C = C_0 e^{-k_1 t} \quad (3)$$

$$q_t = q_e (1 - e^{-k_1 t}) \quad (4)$$

$$q_t = \frac{q_e^2 k_2 t}{1 + q_e k_2 t} \quad (5)$$

$$q_t = A + K_{ip} t^{0.5} \quad (6)$$

Gdzie: C – stężenie substancji rozpuszczonej w roztworze wodnym przez określony czas [mg/l]; C_0 – początkowe stężenie substancji rozpuszczonej w roztworze wodnym [mg/l]; k_0 – stała szybkości adsorpcji [(mg/l)/min], t – czas trwania adsorpcji [min]; k_1 – stała szybkości kinetyki sorpcji pierwszego/pseudo-pierwszego rzędu [1/min]; q_t – ilość adsorbentu zaadsorbowanego w czasie (mg/g); q_e – pojemność adsorpcyjna w stanie równowagi [mg/g]; k_2 – stała szybkości kinetyki sorpcji pseudo drugiego rzędu [(g/mg)/min]; A – stała określająca grubość dyfuzji warstwy granicznej lub adsorpcji na powierzchni zewnętrznej [mg/g]; K_{ip} – stała szybkości dyfuzji [mg/g min^{0.5}].

O wyborze modelu kinetycznego decyduje m.in. charakter biosorbentu, warunki doświadczenia i rodzaj sorbatu. Opis kinetyki adsorpcji ze względu na złożoność mechanizmów sorpcyjnych bywa skomplikowany. Uwzględniając to, z reguły analiza przebiegu adsorpcji polega na wyznaczeniu stałych kinetyki dla poszczególnych odcinków czasowych charakteryzujących jednorodny przebieg procesu. Bywa, że określony model kinetyki zostaje przypisany jedynie do fragmentu z całości procesu sorpcji. Kinetyka zerowego rzędu (równanie 2) umożliwia opis reakcji charakteryzujących się liniowym spadkiem stężenia sorbatu w czasie reakcji. Konfrontacja danych doświadczalnych z tym modelem stwarza możliwość określenia szybkości poszczególnych etapów procesu sorpcji wykazujących liniowy przebieg. W przypadku reakcji kinetycznej pierwszego rzędu (równanie 3) charakterystyczny jest liniowy spadek logarytmu naturalnego chwilowego stężenia substratu w czasie reakcji. Z kolei kinetyka PFO określana jest jako równanie szybkości Lagergrena (równanie 4). Zgodnie z tym modelem, różnica pomiędzy ilością zaadsorbowanych cząsteczek adsorbentu na adsorbencie w czasie równowagi adsorpcyjnej, a określonym czasem określa szybkość procesu adsorpcji [57]. Opisuje ona adsorpcję substancji rozpuszczonej na adsorbencie [56]. Kinetyka PSO znana jest jako równanie Ho i McKay (równanie 5). Z założenia, w modelu tym dzielenie się lub wymiana elektronów pomiędzy adsorbentem, a adsorbentem ma być etapem ograniczającym szybkość reakcji [57]. Szybkość adsorpcji substancji rozpuszczonej jest proporcjonalna do dostępnych miejsc na adsorbencie, a szybkość reakcji zależy od ilości substancji rozpuszczonej na powierzchni adsorbentu.

Niezależnie od tego, że na model PSO mogą wpływać pH, wielkość dawki, rozmiar cząstek i temperatura to model ocenia wpływ obserwowalnych parametrów szybkości [56]. Dopasowanie mechanizmu adsorpcji z każdym z modeli jest określana przez współczynnik determinacji (R^2). R^2 pokazuje stopień zmienności zmiennej zależnej, która zostaje wyjaśniona przez wszystkie niezależne zmienne. Waha się od 0 do 1, przy czym wartości bliskie zeru wskazują na idealne dopasowanie [56]. Pomimo, że modele kinetyczne PFO i PSO stanowią dwa efektywne modele służące do określenia mechanizmu procesu adsorpcji, to jednak nie wyjaśniają one mechanizmu dyfuzji cząsteczek adsorbentu na adsorbencie. Właściwym modelem do badania procesu adsorpcji jest model dyfuzji wewnątrzcząsteczkowej (równanie 6). Mechanizm dyfuzji adsorbentu na adsorbentach może być postrzegany przez model dyfuzji wewnątrzcząsteczkowej zaproponowany przez Webera i Morrisa [57]. Istnieją trzy etapy dyfuzji, które kontrolują przebieg kinetyki adsorpcji, są to mianowicie: (I) dyfuzja sorbatu z głębi roztworu do powierzchni sorbentu, (II) dyfuzja w warstwie granicznej oraz (III) dyfuzja w głąb struktury sorbentu (biokoloidu).

W pracach *A study of zinc ions immobilization by β -lactoglobulin [P2]*, *The study of zinc ions binding to α_{S1} -, β - and κ -casein [P3]* i *Study on silver ions binding to β -lactoglobulin [P6]* jednym z opisanych problemów naukowych było zastosowanie modeli kinetycznych: zerowego, pierwszego, pseudo-pierwszego, pseudo-drugiego rzędu oraz modelu wewnątrzcząsteczkowej dyfuzji Webera-Morrisa w celu określenia oddziaływań i procesów wiązania jonów cynku (Zn_{aq}^{2+}) i srebra (Ag_{aq}^{+}) do β LG oraz jonów Zn_{aq}^{2+} do poszczególnych frakcji kazeinowych (α_{S1} -, β -, κ -CN).

Wyniki badań wykazały, że proces adsorpcji zarówno jonów cynku jak i srebra do β LG jest procesem heterogenicznym składającym się z trzech głównych etapów: (I) szybkiej sorpcji początkowej; (II) stopniowej sorpcji (w przypadku wiązania jonów Zn_{aq}^{2+} do β LG wyróżniono dwa etapy stopniowej sorpcji); (III) równowagi sorpcyjnej. Dla etapu I prędkość sorpcji jonów Zn_{aq}^{2+} i Ag_{aq}^{+} była zdecydowanie najszybsza. Maksymalna skuteczność sorpcji i pojemność sorpcyjna wynosiły odpowiednio $69,55 \pm 0,37\%$ i $8,16 \pm 0,04$ mg/g dla jonów Zn_{aq}^{2+} oraz $48,24 \pm 3,73\%$ i $8,05 \pm 0,62$ mg/g dla jonów Ag_{aq}^{+} . W przypadku zastosowania modelu wewnątrzcząsteczkowego Webera-Morrisa wyróżniono dwa etapy. Etap I może być przypisany efektom dyfuzyjnym warstwy granicznej lub zewnętrznemu procesowi sorpcji powierzchniowej, natomiast etap II wynika z wewnątrzcząsteczkowej dyfuzji jonów Zn_{aq}^{2+} oraz jonów Ag_{aq}^{+} zakończony równowagą sorpcyjną. Etap I w przypadku sorpcji jonów Ag_{aq}^{+} dodatkowo może być związany z procesem redukcji stężenia jonów Ag_{aq}^{+} .

Kinetyka procesu wiązania jonów cynku do frakcji kazeinowych różni się w porównaniu do β LG. Mianowicie, etapy I i II związane są z szybką sorpcją oraz kolejno z wolniejszą stopniową sorpcją wraz z osiągnięciem równowagi sorpcyjnej (etap III) w przypadku β CN i κ CN. Inaczej proces adsorpcji wygląda w przypadku α_{S1} CN. W etapie I następuje szybka sorpcja początkowa, po czym występuje stopniowa sorpcja (etap II) oraz pojawia się etap III z jeszcze wolniejszą sorpcją w porównaniu z etapem II bez osiągnięcia stanu równowagi. Maksymalne efektywności sorpcji i pojemności sorpcyjne dla α_{S1} CN, β CN i κ CN wynoszą $58,31 \pm 1,31\%$ i $5,89 \pm 0,12$ mg/g (α_{S1} CN), $51,05 \pm 0,97\%$ i $5,16 \pm 0,11$ mg/g (β CN), $67,81 \pm 0,30\%$ i $6,85 \pm 0,05$ mg/g (κ CN). Następnie, stopniowa sorpcja jonów Zn_{aq}^{2+} powoduje ich dalszą dyfuzję wewnątrz struktury białka. Zastosowanie powyższych modeli w niniejszych pracach dostarczyło cennych informacji na temat mechanizmów biosorpcji i ujawniło złożony charakter procesu w każdym z badanych przypadków.

Cennych informacji do oceny pojemności adsorpcyjnej adsorbentu dowiedzieć się można również dzięki modelom izotermy równowagi adsorpcyjnej. Izotermę przedstawia się jako wykres stosunku ilości zaadsorbowanego adsorbentu na jednostkę masy adsorbentu od

stężenia równowagowego adsorbentu pozostającego w roztworze. Znanych jest wiele modeli izoterm pozwalających opisać równowagową relację pomiędzy adsorbentem, a adsorbentem, takich jak modele izoterm Temkina, Sipsa, Freundlicha i Langmuira. Izotermy Freundlicha (równanie 7) i Langmuira (równanie 8) są powszechnie stosowanymi modelami dostarczającymi cennych informacji pozwalających na określenie natury procesu biosorpcji; modele te charakteryzowały właściwości powierzchniowe i wskazywały na zdolność sorpcyjną adsorbentu:

$$q_e = K_F C_e^n \quad (7)$$

$$q_e = \frac{q_m K_L C_e}{1 + K_L C_e} \quad (8)$$

Gdzie: q_e – pojemność adsorpcyjna w stanie równowagi [mg/g]; K_F – stała podziału (l/g); C_e – stężenie substancji rozpuszczonej w stanie równowagi w roztworze wodnym (mg/l); n – stała empiryczna, charakteryzująca niejednorodność procesu adsorpcji; q_m – maksymalna pojemność adsorpcyjna (mg/g); K_L – stała podziału Langmuira (l/mg).

Korelacja danych równowagowych z każdym z równań wskazuje na jego zgodność z procesem adsorpcji i określa typ oddziaływań pomiędzy adsorbentem, a adsorbentem. Izoterma Freundlicha jest wprowadzona jako model empiryczny [58]. W modelu tym przyjmuje się, że adsorpcja zachodzi w miejscach, które są heterogeniczne pod względem energetycznym. Opisuje on sorpcję zachodzącą na granicy faz roztwór–ciało stałe, gdzie sorpcji ulegają zarówno cząsteczki substancji rozpuszczonej jak i rozpuszczalnika. Z kolei izoterma Langmuira opiera się na monowarstwowej adsorpcji na powierzchni o skończonej liczbie miejsc adsorpcyjnych o jednolitych strategiach, bez transmigracji adsorbentu w płaszczyźnie powierzchni. Po wypełnieniu miejsca, w tym miejscu nie może zachodzić dalsza sorpcja. Oznacza to, że powierzchnia osiąga punkt nasycenia, gdzie zostanie osiągnięta maksymalna adsorpcja powierzchni, wszystkie miejsca adsorpcji są równoważne energetycznie [58].

W pracach *A study of zinc ions immobilization by β -lactoglobulin* [P2], *Study on zinc ions binding to the individual casein fractions: α_{S1} -, β - and κ -casein* [P4] *Study on silver ions binding to β -lactoglobulin* [P6] opisanym problemem badawczym było wykorzystanie modeli izotermicznych w celu dokładniejszego zbadania mechanizmów związanych z wiązaniem jonów Zn_{aq}^{2+} i jonów Ag_{aq}^+ do β LG oraz jonów Zn_{aq}^{2+} do poszczególnych frakcji kazeinowych (α_{S1} -, β -, κ -CN). Wyniki izoterm adsorpcji przedstawione zostały w postaci wykresu zmiany pojemności sorpcyjnej w zależności od stężenia jonów cynku lub srebra w roztworze. Dodatkowo, uzyskane dane eksperymentalne porównano z wynikami uzyskanymi dla modeli Freundlicha i Langmuira. Stałe szybkości dla modeli Freundlicha i Langmuira w przypadku

jonów Zn_{aq}^{2+} do β LG wyniosły odpowiednio 6,18 l/g i 0,013 l/mg, 1,55 l/g i 0,0015 l/mg dla α SI CN, 0,66 l/g i 0,00745 l/mg dla β CN, 1,07 l/g i 0,0015 l/mg dla κ CN. Uzyskane stałe wskazują, że model Freundlicha zapewnia lepsze dopasowanie do uzyskanych danych eksperymentalnych dla każdego badanego przypadku. Można zatem przyjąć, że proces ma charakter powierzchniowy. Znacznie więcej informacji uzyskano prowadząc izotermę w funkcji C_e/C_0 (stężenie równowagowe/stężenie początkowe adsorbentu w roztworze). Uwzględnienie tego rodzaju zależności pozwoliło na zidentyfikowanie dwóch dominujących etapów sorpcji jonów Zn_{aq}^{2+} na β LG oraz wszystkie trzy frakcje kazeiny. W pierwszym etapie na powierzchni badanych białek zaobserwowano tworzenie się monowarstwy jonów Zn_{aq}^{2+} . Z kolei po etapie wstępnym powstała druga warstwa polegająca na wiązaniu jonów Zn_{aq}^{2+} z już zaadsorbowaną monowarstwą. Dla kazein, w przypadku β CN uzyskane krzywe zarówno dla izoterm Freundlicha i Langmuira, jak i w funkcji C_e/C_0 są nieco bardziej strome, co może świadczyć o tym, że białko to wykazuje znacznie silniejsze właściwości hydrofobowe niż α SI CN czy κ CN.

W przypadku wiązania jonów Ag_{aq}^+ do β LG, dodatkowo zastosowano model Henry'ego (równanie 9) dla początkowych niskich stężeń jonów srebra korzystając z następującego równania:

$$q_e = K_H C_e \quad (9)$$

Gdzie: K_H – stała równowagi adsorpcji Henry'ego [l/g].

Model ten posiada najprostsze równanie, w którym ilość adsorbentu powierzchniowego (jonów Ag_{aq}^+) jest proporcjonalna do stężenia równowagowego adsorbentu (jonów Ag_{aq}^+). Krzywa kształtu dla otrzymanej izoterm Langmuira wskazała, że im więcej miejsc w podłożu β LG jest wypełnionych przez jony Ag_{aq}^+ , tym trudniej jest wiążącym się jonom Ag_{aq}^+ znaleźć wolne miejsca. Krzywa izoterm Langmuira wskazuje, że jony Ag_{aq}^+ adsorbują się równomiernie na powierzchni β LG. Stałe szybkości dla zastosowanych modeli Freundlicha i Langmuira wyniosły odpowiednio 2,06 l/g i 0,0028 ml/g; można więc stwierdzić, że model Freundlicha, podobnie jak w przypadku wiązania jonów Zn_{aq}^{2+} zapewnia lepsze dopasowanie do uzyskanych danych eksperymentalnych. Zatem proces wiązania jonów srebra do β LG ma także charakter powierzchniowy. Wykorzystanie zależności C_e/C_0 pozwoliło na wskazanie dwóch etapów sorpcji jonów Ag_{aq}^+ . Pierwszy etap wskazał na małą pojemność sorpcyjną i monowarstwę jonów Ag_{aq}^+ na powierzchni β LG. Następnie, w drugim etapie, zastosowanie wyższych stężeń jonów Ag_{aq}^+ ok. 150–700 mg/l spowodowało rozluźnienie struktury β LG w wyniku zmian strukturalnych układu srebro- β LG spowodowanych wiązaniem $Ag^+ - Asp^-$

i $\text{Ag}^+\text{-Glu}^-$. Stopniowa penetracja wewnątrz struktury również wpływa na efekt relaksacji. Dodatkowo, zaobserwowano także redukcję jonów Ag_{aq}^+ do stężenia $C_e/C_0 > 0,79$ i uwolnienie metalicznego srebra (Ag^0) do postaci nanocząstek.

Istotne jest również zbadanie zachowania termodynamicznego adsorpcji jonów metali na białka. Parametry termodynamiczne takie jak zmiana entalpii/energii swobodnej Gibbsa (ΔG° , ang. *Gibbs Free Energy*) pozwalają określić spontaniczność danego procesu [59]. W pracach [P2, P3, P6, P7] została określona spontaniczność procesu sorpcji jonów Zn_{aq}^{2+} i Ag_{aq}^+ do αSI -, β -, $\kappa\text{-CN}$ i βLG . Ujemna wartość ΔG° wskazała na spontaniczny proces egzoergiczny.

3.2.2. Charakterystyka nanokompozytów

Z uwagi na unikalne właściwości nanokompozytów, istnieje szczególna potrzeba ich fizykochemicznej charakterystyki z wykorzystaniem komplementarnych technik instrumentalnych, które wpływają na zminimalizowanie problemów mogących pojawić się podczas ich interpretacji. Zastosowanie więcej niż jednego podejścia analitycznego w jednym badaniu pozwala na uzyskanie odpowiedzi na pytania, na które żadna pojedyncza technika nie jest w stanie odpowiedzieć samodzielnie. Wśród technik instrumentalnych można wyróżnić metody spektrometryczne (ICP-MS – ang. *Inductively Coupled Plasma Mass Spectrometry*, MALDI-TOF MS), spektroskopowe (FTIR – ang. *Fourier Transform Infrared Spectroscopy*, Raman, UV-Vis – ang. *Ultraviolet-Visible Spectroscopy*), mikroskopowe (SEM – ang. *Scanning Electron Microscope*, TEM – ang. *Transmission Electron Microscope*, EDX – ang. *Energy Dispersive X-Ray analysis*), dyfrakcyjne (XRD – ang. *X-ray Diffraction*), separacyjne (elektroforeza żelowa).

Spektrometria mas sprzężona z plazmą wzbudzaną indukcyjnie (ICP-MS) oraz wspomagana matrycą laserowa jonizacja/desorpcja próbki (MALDI) z analizatorem czasu przelotu (TOF) są technikami dostarczającymi zarówno informacji pierwiastkowych, jak i molekularnych dla nanomateriałów i innych substancji biologicznie aktywnych (np. białek, peptydów). W pracach [P2, P3, P4, P6, P7] ICP-MS umożliwiło detekcję stężeń jonów cynku i srebra celem zbadania mechanizmu wiązania się jonów cynku i srebra z β LG oraz poszczególnymi frakcjami kazeinowymi (α_{S1} -, β -, κ -CN). MALDI-TOF-MS pozwala z dużą dokładnością zobrazować obecność rdzenia organicznego, izotopów metali, połączeń metaloorganicznych oraz klastrów metali. W pracach Railean-Plugaru i in. [60], [61] wykorzystano podejście MALDI-TOF-MS do analizy związków metaloorganicznych opartych na jonach srebra oraz klastrów z peptydami zlokalizowanych na powierzchni biosyntezy nanocząstek srebra (AgNPs). Wyniki uzyskane w pracy *The study of zinc ions binding to α_{S1} -, β - and κ -casein* [P3] podczas analizy MALDI-TOF MS pozwoliły na precyzyjne określenie masy molekularnej użytej do wiązania białka. Dla kompleksu $Zn\alpha_{S1}CN$ zaobserwowano nowe sygnały ($m/z = 8\ 661,218$ i $m/z = 9\ 257,008$) spowodowane rozpadem białka na bardziej hydrofobowe fragmenty. Natomiast dla kompleksu $Zn\beta CN$ pojawił się nowy sygnał $m/z = 8\ 025,292$, który wskazał, że hydrofilowe jony cynku wiążą się z hydrofobowym białkiem poprzez pośrednie oddziaływanie z tlenem z wody. βCN wykazał większą hydrofobowość niż inne izoformy kazeiny, gdyż związane jest to z ujemnym ładunkiem na N-końcu z pięcioma fosfoserylowymi i hydrofobowymi resztami C-końcowymi [62].

W przypadku κ CN sygnał został stłumiony po związaniu z jonami cynku. Być może jest to efekt glikozylacji zachodzącej tylko w κ CN. Widma masowe otrzymane po związaniu białka z jonami cynku pozwalają na stwierdzenie, że w przypadku α_{S1} CN kluczową rolę odgrywają grupy karboksylowe Glu^- i Asp^- . W przypadku β CN wiązanie z jonami cynku odbywa się poprzez pośrednie oddziaływania z jonami tlenu, natomiast w κ CN wiązanie jonów cynku odbywa się prawdopodobnie poprzez słabe oddziaływania elektrostatyczne z deprotonowanymi grupami funkcyjnymi. Co więcej, w pracy [P4] monitorowano zmiany spowodowane dodatkiem różnych stężeń jonów cynku (120, 350 i 600 mg/L). Wraz ze wzrostem stężenia jonów cynku dla kompleksów $\text{Zn}\alpha_{S1}\text{CN}$ oraz $\text{Zn}\beta\text{CN}$ zaobserwowano zmniejszenie jego masy oraz spadek intensywności sygnałów. Z kolei dla kompleksów $\text{Zn}\kappa\text{CN}$ zauważono tłumienie sygnałów oraz pojawienie się dwóch nowych sygnałów ($m/z = \sim 7974$ i $m/z = \sim 8045$ m/z) i sześciu sygnałów w zakresie m/z 5000–7000 w porównaniu do jego formy natywnej.

Metodą doskonale uzupełniającą uzyskane wyniki kinetyczne oraz izotermiczne jest spektroskopia w podczerwieni z transformacją Fouriera (FTIR) pozwalająca na zlokalizowanie i opisanie grup funkcyjnych biorących udział w procesie wiązania metal-białko. Spektroskopia FTIR pozwala na analizę zarówno struktury (np. grup funkcyjnych) cząsteczek, jak i ich oddziaływania z otoczeniem. Zmiany w widmie świadczą o obecności konkretnych grup funkcyjnych, natomiast przesunięcia w kierunku innych długości fali niż dla widma próbki pierwotnej świadczą o oddziaływaniu danej grupy z inną grupą substancji dodanej. W pracy *A study of zinc ions immobilization by β -lactoglobulin* [P2] zastosowano metodę FTIR w celu monitorowania zmian w strukturze β LG po traktowaniu jonami Zn_{aq}^{2+} w różnych okresach czasu inkubacji (10 min, 6 h, 24 h). Uzyskane dane z tej analizy wskazały, że głównymi grupami zaangażowanymi w proces immobilizacji jonów Zn_{aq}^{2+} do β LG są grupy karboksylowe ($-\text{COO}^-$). Zaobserwowano także trend intensywności sygnałów w czasie inkubacji – wraz z wydłużaniem czasu inkubacji intensywność sygnałów wzrasta. Z kolei w pracy *The influence of zinc ions concentration on β -lactoglobulin structure – physicochemical properties of Zn- β -lactoglobulin complexes* [P7] zbadano β LG przed i po podaniu jonów Zn_{aq}^{2+} w różnych stężeniach jonów Zn_{aq}^{2+} (6, 60, 600 mg/l). Intensywność sygnałów spektralnych metalokompleksów zmniejszyła się w porównaniu z kontrolą (natywna β LG). Podobne rezultaty uzyskano dla tych samych stężeń jonów srebra [P6]. Ta sama technika została wykorzystana podczas syntezy jonów cynku do α_{S1} -, β -, κ -CN [P3, P4]. W przypadku kazein, oprócz grup karboksylowych zaangażowane w proces wiązania jonów cynku są również grupy fosforanowe ($-\text{PO}_3^{2-}/-\text{HPO}_3$). Dodatkowo, w pracy *Study on zinc ions binding to the individual casein fractions α_{S1} -, β - and κ -casein* [P4] widma FTIR zarejestrowane zostały

dla białek przed i po kompleksowaniu jonami cynku w trzech różnych stężeniach jonów cynku (120, 350 i 600 mg/l) wybranych na podstawie badań izotermicznych. W przypadku metalokompleksów $\alpha_{SI}CN$ o stężeniach jonów Zn_{aq}^{2+} wynoszących 120, 350 i 600 mg/l ($Zn\alpha_{SI}CN120/350/600$) obserwuje się, że wraz ze wzrostem stężenia jonów Zn_{aq}^{2+} intensywność sygnału maleje w całym zakresie spektralnym, natomiast dla kompleksów βCN i κCN ($Zn\beta CN120/350/600$, $Zn\kappa CN120/350/600$) intensywność sygnału wzrasta. Przyczyną obserwowanych zmian może być kinetyka wiązania jonów Zn_{aq}^{2+} z poszczególnymi frakcjami kazeiny, gdyż dla $\alpha_{SI}CN$ obserwowano trzy etapy: (I) szybką sorpcję początkową, (II) stopniową sorpcję i (III) coraz wolniejszą sorpcję bez osiągnięcia równowagi, w przypadku βCN i κCN równowaga została osiągnięta. Gdy stężenie jonów Zn_{aq}^{2+} jest wyższe, to znaczy, że związanych jonów Zn_{aq}^{2+} jest coraz więcej. Wynika to ze struktury samego białka i jego zdolności do wiązania jonów Zn_{aq}^{2+} .

Jako technikę uzupełniającą, w pracach [P2, P3, P4, P6, P7] wykorzystano spektroskopię Ramana (spektroskopia rozpraszania). FTIR jest wynikiem absorpcji energii przez wibrujące wiązania chemiczne, głównie ruchy rozciągające i zginające. Natomiast rozpraszanie Ramana wynika z tych samych typów przejść, jednakże obserwowalne słabe pasma w technice FTIR mogą być silne w spektroskopii Ramana i odwrotnie.

Metodą często wykorzystywaną w badaniach białek jest spektroskopia fluorescencyjna. Swoje właściwości fluorescencyjne białka zawdzięczają obecności w łańcuchu polipeptydowym aminokwasów aromatycznych takich jak tryptofan (Trp), tyrozyna (Tyr) i fenyloalanina (Phe). Ich fluorescencja mieści się w zakresie bliskiego ultrafioletu. W pracy *A study of zinc ions immobilization by β -lactoglobulin* [P2] zbadana została fluorescencja natywnego białka βLG oraz jego kompleksów z jonami Zn_{aq}^{2+} . W przypadku białka natywnego zauważono dwa główne pasma fluorescencji przy długości fali wzbudzenia (λ_{ex}) i emisji (λ_{em}) odpowiednio 238, 326 nm (I); 278, 328 nm (II), natomiast w przypadku kompleksu metalu pojawiło się nowe pasmo fluorescencji 270, 540 nm (III). Zjawisko to może być związane z ilością jonów cynku biorących udział w procesie wiązania z białkiem βLG , co prowadzi do ewentualnej zmiany konformacji wokół aminokwasów aromatycznych zawartych w strukturze białka. Ponadto zmiany $\lambda_{ex}/\lambda_{em}$ kompleksu $Zn\beta LG$ w porównaniu z fluorescencją natywnego białka mogą również wynikać z mechanizmu rezonansowego transferu energii lub energii rezonansu Förstera, spowodowanego oddziaływaniem d-elektronu jonów cynku z π -elektronem pierścieni aromatycznych lub Trp, Tyr i Phe [63]. Zmiany fluorescencji obserwowane po procesie immobilizacji mogły być również spowodowane oddziaływaniem jonów cynku z βLG poprzez wiązanie typu *sandwich*, charakterystyczne dla oddziaływania kation cynku- π Trp

[64]. Wyniki opisane w dwóch pracach Król i wsp. [65], [66] wskazały na amplifikację intensywności fluorescencji w obecności ZnO NPs – może być to wynikiem występowania zjawiska powierzchniowego rezonansu plazmonowego i stwarza to nowe możliwości wykorzystania nanomateriałów tlenku cynku jako np. biosensorów.

Dodatkowo, do poznania właściwości fizykochemicznych otrzymanego kompleksu Zn β LG posłużyła spektroskopia UV-Vis. Maksimum absorpcji dla β LG zaobserwowano przy długości fali 270–280 nm, co jest typowe dla białek i wynika z absorpcji aminokwasów aromatycznych wchodzących w skład struktury β LG, które stanowią 6,17% 162 aminokwasów – Trp (1,23%), Tyr (2,47%) i Phe (2,47%) [67], [68]. Po dodaniu jonów cynku do β LG zaobserwowano spadek intensywności absorbancji. Zjawisko to może wynikać z ekranowania chromoforów aromatycznych Tyr, Trp i Phe przez jony cynku [69]. Spadek intensywności sygnałów po dodaniu jonów cynku zaobserwowano także na widmie NMR co zostało przedstawione w pracy [P2].

Istotnym narzędziem w obrazowaniu i charakteryzowaniu nanokompozytów są techniki mikroskopowe. Do najczęściej powszechnie stosowanych technik należą skaningowa mikroskopia elektronowa (SEM) oraz transmisyjna mikroskopia elektronowa (TEM). W pracach [P2, P4, P6, P7] zostały określone właściwości morfologiczne i strukturalne przed procesem wiązania jonów cynku bądź srebra do białek (postać natywna białek) oraz po procesie wiązania (nanokompleks). Dodatkowo sprzężenie technik SEM/TEM z techniką spektroskopii rentgenowskiej z dyspersją energii (EDX) dostarczyło cennych informacji dotyczących rozmieszczenia pierwiastków na powierzchni (Zn, Ag). Analiza EDX dla metalokompleksów wykazała, że wraz ze wzrostem stężenia jonów Zn $_{aq}^{2+}$ /Ag $_{aq}^{+}$ pojawiły się intensywniejsze sygnały jonów Zn $_{aq}^{2+}$ /Ag $_{aq}^{+}$. Ponadto, technika SEM pozwala na obrazowanie powierzchni w dwóch trybach: elektronu wtórnego (SE, ang. *Secondary Electrons*) oraz elektronu wstecznie rozproszonego (BSE, ang. *Back Scattered Electrons*). Tryb SE umożliwia opisanie topografii powierzchni i rozmiarów badanych materiałów. Natomiast obrazy BSE SEM mogą być wykorzystane do potwierdzenia ich składu chemicznego, jak również rozmieszczenia poszczególnych pierwiastków w próbkach [70]. Dzięki temu, że obrazy BSE wykazują dużą czułość na różnice w liczbie atomowej (liczbie Z), możliwe jest uwidocznienie pierwiastków o wyższej liczbie atomowej jako jaśniejszych plam na obrazie SEM [71]. W pracy [P4] detekcja BSE stworzyła możliwość kontrastu obrazowania zdeponowanych jonów cynku na powierzchni frakcji kazeinowych. Zauważono, że zmiany morfologiczne powierzchni białka są zależne od stężenia jonów Zn $_{aq}^{2+}$ i Ag $_{aq}^{+}$. Wraz ze wzrostem ich stężenia morfologia powierzchni staje się bardziej porowata, wskazując na to, że pod wpływem wyższego stężenia

wiąże się więcej jonów Zn_{aq}^{2+}/Ag_{aq}^{+} . Paulson i wsp. [72] w swoich badaniach wyjaśniają, że wpływ jonów metali na agregację białka zależy od kilku czynników, np. pH, stężenia białka oraz stężenia metali, które przyczyniają się do hamowania lub przyspieszania agregacji. Badania te odgrywają ważną rolę we wszelkiego rodzaju patologiach w medycynie. Stwierdzono, że wraz ze wzrostem stężenia jonów metali w mózgu, znaczniejsza agregacja białek sprzyja postępowi choroby Alzheimera [72]. Bazując na danych eksperymentalnych można przypuszczać, że zastosowanie różnych stężeń d-elektronowych jonów metali i ich działanie na białko może wpłynąć na właściwości biologiczne i zastosowania otrzymanych metalokompleksów. Dodatkowo, analiza TEM po dodaniu jonów Ag_{aq}^{+} w najwyższym stężeniu (600 mg/L) wskazała na obecność sferycznych nanocząstek srebra (ok. 5 nm) homogenicznie rozproszonych, a także agregatów (ok. 1300 nm) umocowanych w strukturze białka. Tworzenie się nanocząstek srebra w wyniku oddziaływania metal-białko podczas analiz mikroskopowych, potwierdza obserwacje uzyskane z izotermy w funkcji C_e/C_0 poprzez redukcję jonów Ag^{+} do Ag^0 , koalescencję i nanokrystalizację [73]. Istnieją jednak również miejsca, gdzie pomiędzy nanocząstkami srebra tworzą się agregacje. Charakterystyczny obraz TEM wysokiej rozdzielczości (HRTEM, ang. *High-Resolution Transmission Electron Microscopy*) z wyraźnymi prążkami sieciowymi o odstępach 0,23 nm wskazał, że wzrost nanocząstek srebra zachodzi głównie w płaszczyźnie (111). Odległość międzypłaszczyznowa płaszczyzn Ag (111) jest zgodna z odstępem $d(111)$ masy Ag (0,2355 nm), a wzór dyfrakcji elektronów w wybranym obszarze (SAED, ang. *Selected Area Electron Diffraction*) z jasnymi pierścieniami kołowymi odnoszącymi się do płaszczyzn (111), (220), (222), (331) jednej z kulistych cząstek wskazuje, że mają one strukturę wysoko krystaliczną. Podobne wyniki uzyskano dla nanocząstek srebra w wyniku syntezy AgNPs z wykorzystaniem szczepów bakterii *Lactobacillus paracasei* LPC20 wyizolowanych z serwatki [74].

3.2.3. Mechanizm formowania się nanokompozytów

Obecnie, dogłębną analizę powierzchniowych procesów wiązania metal-białko można uzyskać opierając się na nowym podejściu stosowanym we współczesnych dyscyplinach naukowych, a mianowicie na metodach obliczeniowych, a dokładniej analizie molekularnej (MDs, ang. *Molecular Dynamics*) połączonej z obliczeniami mechaniki kwantowej (QM, ang. *Quantum Mechanics*) z wykorzystaniem teorii funkcjonałów gęstości (DFT, ang. *Density Functional Theory*). Metody te wykorzystują współczesną technologię, aby dostarczyć cenny wgląd w zrozumienie układów chemicznych wirtualnie, uzupełniając tym samym analizę eksperymentalną uzyskaną za pomocą metod instrumentalnych. Dynamika molekularna pozwala na przewidywanie/symulację struktury i dynamiki białek. Z kolei, obliczenia kwantowo mechaniczne znajdują szerokie zastosowanie w modelowaniu miejsc aktywnych białek oraz wyznaczeniu parametrów termodynamicznych i kinetycznych zachodzących procesów. Spełniają one doskonale swoje zadanie, ponieważ mogą uchwycić wszystkie efekty elektroniczne takie jak efekty polaryzacji i przeniesienia ładunku pomiędzy oddziałującymi jednostkami, które mają ogromne znaczenie dla prawidłowego opisu oddziaływań pomiędzy kationami metali i ligandami białkowymi [75]. Celem szczegółowego wyjaśnienia procesów wiązania jonów cynku oraz srebra do aktywnych grup funkcyjnych β LG w pracach *Study on silver ions binding to β -lactoglobulin* [P6] i *The influence of zinc ions concentration on β -lactoglobulin structure – physicochemical properties of Zn- β -lactoglobulin complexes* [P7] zastosowano modelowanie molekularne oraz obliczenia kwantowo mechaniczne. Otrzymane wyniki potwierdziły prawidłowość interpretacji wyników uzyskanych metodą spektroskopową na silną korelację pomiędzy liczbą miejsc wiążących $\text{Glu}^-/\text{Asp}^-$ jako dominujących aminokwasów oddziałujących z jonami Zn_{aq}^{2+} . Co więcej, wskazują one także na korelację ze stężeniem metalu – miejsca wiązania jonów cynku z wymienionymi aminokwasami zwiększają się wraz ze wzrostem stężenia jonów metali. Glu^- stanowił 65–85% wszystkich oddziaływań. Aminokwasy niepolarne Trp, Phe, Met nie brały udziału w oddziaływaniach z jonami cynku ze względu na ich wysokie wartości pK_a w okolicach 9,0. Podobna sytuacja występowała w przypadku aminokwasów zasadowych His, Arg i Lys [76]. Mimo że miejsca aktywne Zn-Lys pojawiają się dla Lys w wyższych stężeniach, to wartość pK_a około 8,95 dla Lys w warunkach analizy przeprowadzonej w pH 4,6 wskazuje, że nie może on oddziaływać z kationami cynku. Podobne obserwacje zaobserwowano dla aminokwasów polarnych, których wysokie wartości stałych pK_a wskazują, że podobnie jak aminokwasy niepolarne lub zasadowe nie mogą oddziaływać z jonami cynku, dla Cys ze względu na obecność grupy tiolowej, którego

wartość pK_a wynosi 8,18 oraz Tyr, dla którego pK_a wynosi 9,11 [76]. Dla kompleksów Zn-Tyr i Zn-Cys proces kompleksowania jest niekorzystny z uwagi na dodatnią energię swobodną wiązania.

W przypadku procesu wiązania jonów srebra do β LG najsilniejsze miejsca wiązania jonów srebra zaobserwowano odpowiednio dla Asp^- i Glu^- , Tyr, Met, Lys. Podobnie jak w przypadku wiązania jonów cynku zaobserwowano, że miejsca wiązania jonów srebra z wymienionymi aminokwasami zwiększają się wraz ze wzrostem stężenia jonów srebra. Ponadto, w oparciu o podejście symulacji dynamiki molekularnej i obliczeń mechaniki kwantowej zaproponowano mechanizm wiązania jonów srebra i tworzenia się nanocząstek srebra. Srebro oddziałujące z β LG przy niższych stężeniach jonów srebra (6, 60 mg/L) prowadzi do tworzenia metalokompleksów. Natomiast stosując wyższe stężenie jonów srebra (600 mg/L) obserwuje się różnicę, a mianowicie powstawanie metalokompleksów wraz z tworzeniem się nanocząstek srebra tworzących układ hybrydowy $Ag\beta$ LG/ $AgNPs\beta$ LG. Wynika to z silnego powinowactwa Glu^- i Asp^- przy wyższym stężeniu srebra (600 mg/L) na mol β LG (20 jonów srebra/cząsteczka β LG). Zainicjowany proces redukcji wynika z przeniesienia elektronów z reszt aminokwasowych β LG na zaadsorbowane kationy srebra, co prowadzi do powstania srebra atomowego (Ag^0). Następnie zredukowane srebro (Ag^0) działa jako miejsca nukleacji, na których w procesie elektrochemicznym kationy srebra (Ag^+) są zredukowane do srebra atomowego, co prowadzi do powstania nanoklastrów srebra (Ag^0). Nanoklastry te ulegają koalescencji tworząc nanocząstki stabilizowane przez cząsteczki białka [77]. Na podstawie wyników izoterm oraz przeprowadzonych badań TEM, obecność nanocząstek srebra o wielkości około 5 nm zaobserwowano w przypadku nanokompleksu $Ag\beta$ LG300, czyli tego o najwyższym stężeniu jonów srebra (600 mg/L).

Dziedziną wchodzącą w skład modelowania molekularnego jest dokowanie molekularne (MD, ang. *Molecular Docking*). Dokowanie molekularne pomaga przewidzieć miejsca i charakter oddziaływania pomiędzy cząsteczkami. Najczęściej wykorzystuje się makrocząsteczkę receptora lub strukturę białka oraz ligand, taki jak jon metalu lub mały związek organiczny. Zasadniczą ideą symulacji jest wykorzystanie co najmniej dwóch niepowiązanych ze sobą struktur i znalezienie najsilniejszego połączenia, jakie może istnieć między nimi. W pracy [P4] po raz pierwszy przedstawiono badania dokowania molekularnego jonów Zn_{aq}^{2+} związanych z poszczególnymi izoformami kazeiny (α_{S1} -, β - i κ -CN). Uzyskane wyniki wskazały, że zdeprotonowana grupa karboksylowa Glu^- , jak również pierścień imidazolowy His były dominującymi aminokwasami α_{S1} - i β CN najsilniej oddziałującymi z jonami Zn_{aq}^{2+} . Intrygująco, w oddziaływaniu κ CN z cynkiem, istotną rolę może odgrywać

siarka pochodząca z cysteiny. Wynik modelowania, a tym samym przewidywane miejsce przyłączenia jonu metalu do struktury białka w dużym stopniu zależy od sekwencji i konformacji przestrzennej struktury białka. Między otrzymanymi wynikami w wyniku dokowania molekularnego, a technikami instrumentalnymi uzyskano dużą zgodność. Protokoły dokowania są zazwyczaj szybkie i wymagają niewielkiej mocy obliczeniowej ze względu na dużą liczbę przybliżeń [78], [79].

Dużą zaletą dokowania molekularnego jest fakt, że są one tanimi technikami. Niemniej jednak, połączenie droższych, ale dokładniejszych technik symulacji modelowania molekularnego może być lepszym uzupełnieniem dokowania. Symulacje MDs prowadzą intensywniejsze poszukiwania konformacyjne niż metody dokowania molekularnego i zapewniają dokładniejsze przedstawienie białek i ich oddziaływań. Należy jednak podkreślić fakt, że połączenie metod instrumentalnych i teoretycznych stanowi komplementarne podejście analityczne. Obie metody potwierdziły i uzupełniły informacje na temat zachodzących mechanizmów w tworzeniu kompleksów typu metal-białko.

3.3. Innowacyjne rozwiązanie w walce z lekoopornością

Na przestrzeni ostatnich dziesięcioleci, jednym z największych zagrożeń dla globalnego zdrowia publicznego uznaje się zjawisko lekooporności na leki. Oporność ta ogranicza leczenie infekcji, podważając tym samym wiele postępów w medycynie np. chirurgii, leczeniu raka i zmniejszaniu immunosupresji, których efektywność zależy od umiejętności skutecznego leczenia infekcji. Mikroorganizmy na przestrzeni lat opracowały mechanizmy pozwalające im chronić się przed szkodliwym działaniem i przekazywaniu tych mechanizmów ochronnych innym mikrokom. Dynamiczny wzrost oporności na leki przeciwdrobnoustrojowe w XX i XXI wieku jest efektem wspomnianych potężnych mechanizmów ewolucyjnych w zestawieniu z działalnością człowieka, która wpływa na świat drobnoustrojów [80]. Nieprawidłowe decyzje dotyczące terapii bywają powiązane z niepewnością diagnostyczną. Pacjenci bardzo często nie mają przeprowadzonego szybkiego i dokładnego testu, który określiłby czy przyczyną choroby jest patogen bakteryjny. Skutkiem tej niepewności włącznie z niechęcią do podejmowania ryzyka wśród lekarzy i pacjentów oraz nieprawidłowym przekonaniem, że dany antybiotyk nie zaszkodzi co roku miliony antybiotyków są przyjmowane chociaż nie są potrzebne [80], [81]. Ponadto niejasność ewolucji bakterii skutkuje tym, że oporność nie jest przewidywalna, stąd też brakuje rozwoju nowych leków, gdyż producenci inwestujący w opracowywanie antybiotyków mogą uznać, że zyski są niewystarczające, jako że odporność na nowe antybiotyki utrudnia pomyślne wprowadzenie produktu na rynek [82]. Niewątpliwie, problem lekooporności występuje w coraz to częściej wzrastającej ilości ran przewlekłych i ciężkich infekcjach ran. Tego typu rany stwarzają korzystne podłoże dla inwazji i proliferacji patogenów co powoduje, że często dochodzi do ich zakażeń. Z uwagi na zachodzące zmiany demograficzne w kierunku społeczeństwa w podeszłym wieku, wśród którego znajdują się pacjenci z wieloma schorzeniami, wzrasta obciążenie zdrowotne i zainteresowanie humanitarne skutecznym leczeniem zakażeń ran [83]. W związku z powyższym, opisany problem lekooporności, wymusza badaczy do poszukiwania środków przeciwdrobnoustrojowych, które mogłyby pomóc w walce z patogennymi drobnoustrojami. Obiecującą odpowiedzią na zjawisko lekooporności jest opracowanie nowych związków opartych na jonach metali w połączeniu z białkami jako potencjalne nowej generacji preparaty przeciwdrobnoustrojowe, na które mikroorganizmy nie będą w stanie wytworzyć mechanizmów lekoopornych.

Powyższa problematyka została uwzględniona i podjęta w pracy *Metal-protein action for the wound healing process using murine model C57BL/6J mouse* [P8], w której jednym z celów było zbadanie skuteczności przeciwdrobnoustrojowej zsyntetyzowanych kompleksów.

Wśród zbadanych szczepów znalazły się te, które występują w ostrych i przewlekłych ranach czy też wywołują infekcje u pacjentów z obniżoną odpornością takie jak: (I) *Proteus mirabilis* PX 220 86112 MLD, (II) *Escherichia coli* MB 11464 1 CHB, (III) *Pseudomonas aeruginosa* DSM 5007717 HAM, (IV) *Staphylococcus aureus* ATCC 33591 THL – wyizolowane z odleżyn; (V) *Candida albicans* ATCC 10231 THL, (VI) *Candida krusei* CBS 2107 CBS – wyizolowane ze stopy cukrzycowej; oraz te, które są uważane za bezpieczne i korzystne dla mikroflory człowieka takie jak: (VII) *Lactobacillus paracasei* DSM 2649 DSM, (VIII) *Lactococcus lactis* ATCC 10231 – wyizolowane z serwatki. Zainteresowanie bakteriami prozdrowotnymi przejawia się w coraz większej liczbie opracowywanych produktów żywności funkcjonalnej trafiających na rynek, a także w rosnących przychodach i zyskach zwłaszcza suplementów bakteryjnych na świecie [84]. W pracy [P8] zastosowano dwie różne metodologie, a mianowicie wyznaczenie minimalnego stężenia hamującego (MIC, ang. *Minimal Inhibitory Concentration*) oraz klasyczne wyznaczenie liczby tworzącej kolonie (CFU, ang. *Colony Forming Unit*). Wyniki wskazały na dobrą aktywność przeciwbakteryjną i przeciwgrzybiczą otrzymanych kompleksów kazeiny i β LG – zaobserwowano zahamowanie wzrostu badanych szczepów po zastosowaniu kompleksów, a wartości MIC mieściły się w zakresie 6,25–200 ug/ml.

W pracy [P8] podjęto się również problemu badawczego jakim jest zastosowanie *in vivo* preparatów kompleksowych Zn β LG i Ag β LG na gojenie się ran stosując model zwierzęcy (myszy). Dodatkowo, zwrócono uwagę na określenie akumulacji cynku i srebra w próbkach tkanki wątroby i krwi. Zamknięcie rany było monitorowane za pomocą mikroskopu stereoskopowego, a badanie lokalizacji metali w tkankach wątroby i krwi przeprowadzono za pomocą spektrometru masowego ICP-MS. Proces gojenia się ran prowadzony był przez dziesięć dni. Przez cały czas trwania eksperymentu były monitorowane waga i zachowanie gryzoni. Zastosowanie preparatów na bazie nanokompozytów metalowo-białkowych w końcowym etapie obserwacji wykazało pojawienie się strupa wskazującego na właściwości wysuszające i ściągające. Cynk jest mikroelementem naturalnie występującym w organach takich jak wątroba, nerki, płuca, śledziona czy mózg. Przy zastosowaniu opatrunku cynkowego Zn β LG (MIC) i Zn β LG (110% MIC) stwierdzono wzrost poziomu tego pierwiastka we krwi względem poziomu w tkance kontrolnej. Natomiast poziom cynku w wątrobie był porównywalny z poziomem w wątrobie myszy kontrolnych. W przypadku srebra odnotowano nieznaczne ilości srebra zarówno w próbkach wątroby jak i krwi. Przyjmuje się, że organizm, absorbując związki srebra, tworzy kompleksy głównie z białkami, a także z RNA i DNA,

wiążąc się z grupami sulfhydrylowymi, aminowymi, karboksylowymi, fosforanowymi i imidazolowymi.

Wstępne eksperymenty, które oceniały bezpieczeństwo nanokompozytów opartych na białkach wykazały satysfakcjonujące rezultaty. Wyniki te wskazują, że owe nanokompozyty mogą mieć praktyczne zastosowanie jako potencjalne, nietoksyczne substancje do terapii trudno leczących się ran w obszarze medycyny. Mogą one pełnić rolę innowacyjnych środków antyseptycznych. Innymi słowy, początkowe badania na temat nanokompozytów bazujących na białkach potwierdziły, że są one bezpieczne. Z tego powodu mogą one być wykorzystane jako nowe, nieszkodliwe dla organizmu środki do leczenia problematycznych ran. Tego typu nanokompozyty mogą stanowić nowoczesne antyseptyki w medycynie.

3.4. Bibliografia

- [1] A. Płodzich, Proteomika i jej zastosowanie w wybranych jednostkach chorobowych, *Journal of Transfusion Medicine*. 6 (2013) 48–59.
- [2] A. Haug, A.T. Høstmark, O.M. Harstad, Bovine milk in human nutrition - a review, *Lipids in Health and Disease*. 6 (2007) 1–16. <https://doi.org/10.1186/1476-511X-6-25>.
- [3] K. Petrotos, E. Tsakali, P. Goulas, A.G. D'Alessandro, Casein and Whey Proteins in Human Health, in: *Milk and Dairy Products as Functional Foods*, John Wiley & Sons, Ltd, 2014: pp. 94–146. <https://doi.org/10.1002/9781118635056.CH4>.
- [4] S. Bradbury, Wound healing: is oral zinc supplementation beneficial?, *Wounds UK*. 2 (2006) 54–61.
- [5] C. Graham, The role of silver in wound healing, *British Journal of Nursing*. 14 (2005) 22–28. <https://doi.org/10.12968/bjon.2005.14.sup5.19954>.
- [6] T. Bruna, F. Maldonado-Bravo, P. Jara, N. Caro, Silver nanoparticles and their antibacterial applications, *International Journal of Molecular Sciences*. 22 (2021) 1–21. <https://doi.org/10.3390/ijms22137202>.
- [7] D. Figeys, Proteomics approaches in drug discovery, *Analytical Chemistry*. 74 (2002) 412 A-419 A. <https://doi.org/10.1021/ac022079r>.
- [8] P. Pomastowski, B. Buszewski, Two-dimensional gel electrophoresis in the light of new developments, *TrAC - Trends in Analytical Chemistry*. 53 (2014) 167–177. <https://doi.org/10.1016/j.trac.2013.09.010>.
- [9] F. Di Domenico, G. Pupo, E. Giraldo, M.C. Badia, P. Monllor, A. Lloret, M. Eugenia Schininà, A. Giorgi, C. Cini, A. Tramutola, D.A. Butterfield, J. Viña, M. Perluigi, Oxidative signature of cerebrospinal fluid from mild cognitive impairment and Alzheimer disease patients, *Free Radical Biology and Medicine*. 91 (2016) 1–9. <https://doi.org/10.1016/j.freeradbiomed.2015.12.004>.
- [10] C.A. Ross, M.A. Poirier, Protein aggregation and neurodegenerative disease, *Nature Medicine*. 10 (2004) S10. <https://doi.org/10.1038/nm1066>.
- [11] D. Fraser-Pitt, D. O'Neil, Cystic fibrosis - a multiorgan protein misfolding disease, *Future Science OA*. 1 (2015). <https://doi.org/10.4155/fso.15.57>.
- [12] A.M. Smith, Interaction of metal ions with proteins as a source of inspiration for biomimetic materials, in: *Functional Metallosupramolecular Materials*, 2015: pp. 1–31. <https://doi.org/10.1039/9781782622673-00001>.
- [13] B. Buszewski, P. Pomastowski, A. Król, A. Rogowska, A. Rodzik, G. Sagandykova, V.

- Railean-Plugaru, Spectroscopic Techniques in Research of Biocolloids, in: I.B. Bogusław Buszewski (Ed.), Handbook of Bioanalytics, Springer Cham, 2022: pp. 805–832. https://doi.org/10.1007/978-3-030-95660-8_39.
- [14] D.J. McMahon, B.S. Oommen, Casein micelle structure, functions, and interactions, in: Advanced Dairy Chemistry: Volume 1A: Proteins: Basic Aspects, 4th Edition, Springer, Boston, MA, 2003: pp. 185–209. https://doi.org/10.1007/978-1-4614-4714-6_6.
- [15] P. Martin, C. Cebo, G. Miranda, Inter-Species Comparison of Milk Proteins: Quantitative Variability and Molecular Diversity, Encyclopedia of Dairy Sciences. (2011) 821–842. <https://doi.org/10.1016/B978-0-12-374407-4.00438-6>.
- [16] V. Abrahão, Nourishing the dysfunctional gut and whey protein, Current Opinion in Clinical Nutrition and Metabolic Care. 15 (2012) 480–484. <https://doi.org/10.1097/MCO.0b013e328356b71e>.
- [17] A.R. Madureira, C.I. Pereira, A.M.P. Gomes, M.E. Pintado, F. Xavier Malcata, Bovine whey proteins - overview on their main biological properties, Food Research International. 40 (2007) 1197–1211. <https://doi.org/10.1016/j.foodres.2007.07.005>.
- [18] G.I. Imafidon, N.Y. Farkye, A.M. Spanier, Isolation, purification, and alteration of some functional groups of major milk proteins: A review, Critical Reviews in Food Science and Nutrition. 37 (1997) 663–689. <https://doi.org/10.1080/10408399709527794>.
- [19] T. Huppertz, P.F. Fox, A.L. Kelly, The caseins: structure, stability, and functionality, in: Proteins in Food Processing, Second Edition, Elsevier Ltd., 2018: pp. 49–92. <https://doi.org/10.1016/B978-0-08-100722-8.00004-8>.
- [20] E.W. Bingham, N. Parris, H.M. Farrell, Phosphorylation of β -Casein and α -Lactalbumin by Casein Kinase from Lactating Bovine Mammary Gland, Journal of Dairy Science. 71 (1988) 324–336. [https://doi.org/10.3168/JDS.S0022-0302\(88\)79561-2](https://doi.org/10.3168/JDS.S0022-0302(88)79561-2).
- [21] C.W. Slattery, R. Evard, A model for the formation and structure of casein micelles from subunits of variable composition, Biochimica et Biophysica Acta. 317 (1973) 529–538. [https://doi.org/10.1016/0005-2795\(73\)90246-8](https://doi.org/10.1016/0005-2795(73)90246-8).
- [22] C. Holt, Structure and Stability of Bovine Casein Micelles, Advances in Protein Chemistry. 43 (2015) 63–151. [https://doi.org/10.1016/S0065-3233\(08\)60554-9](https://doi.org/10.1016/S0065-3233(08)60554-9).
- [23] D.S. Horne, Casein interactions: casting Light on the black boxes, the structure in dairy products, International Dairy Journal. 8 (1998) 171–177. [https://doi.org/10.1016/S0958-6946\(98\)00040-5](https://doi.org/10.1016/S0958-6946(98)00040-5).
- [24] C.S. Tai, Y.Y. Chen, W.L. Chen, β -Lactoglobulin influences human immunity and promotes cell proliferation, BioMed Research International. 2016 (2016) 1–12.

<https://doi.org/10.1155/2016/7123587>.

- [25] A.R. Corrochano, V. Buckin, P.M. Kelly, L. Giblin, Invited review: whey proteins as antioxidants and promoters of cellular antioxidant pathways, *Journal of Dairy Science*. 101 (2018) 4747–4761. <https://doi.org/10.3168/jds.2017-13618>.
- [26] K. Marshall, Therapeutic applications of whey protein, *Alternative Medicine Review*. 9 (2004) 136–156.
- [27] S. Le Maux, S. Bouhallab, L. Giblin, A. Brodkorb, T. Croguennec, Bovine β -lactoglobulin/fatty acid complexes: binding, structural, and biological properties, *Dairy Science and Technology*. 94 (2014) 409–426. <https://doi.org/10.1007/s13594-014-0160-y>.
- [28] K. Sakai, K. Sakurai, M. Sakai, M. Hoshino, Y. Goto, Conformation and stability of thiol-modified bovine beta-lactoglobulin, *Protein Science*. 9 (2000) 1719–1729.
- [29] M.D. Pérez, M. Calvo, Interaction of β -Lactoglobulin with Retinol and Fatty Acids and Its Role as a Possible Biological Function for This Protein: A Review, *Journal of Dairy Science*. 78 (1995) 978–988. [https://doi.org/10.3168/jds.S0022-0302\(95\)76713-3](https://doi.org/10.3168/jds.S0022-0302(95)76713-3).
- [30] K.M.G. Oliveira, V.L. Valente-Mesquita, M.M. Botelho, L. Sawyer, S.T. Ferreira, I. Polikarpov, Crystal structures of bovine β -lactoglobulin in the orthorhombic space group C222 1, *European Journal of Biochemistry*. 268 (2001) 477–484. <https://doi.org/10.1046/j.1432-1033.2001.01918.x>.
- [31] X. Meng, Y. Bai, J. Gao, X. Li, H. Chen, Effects of high hydrostatic pressure on the structure and potential allergenicity of the major allergen bovine β -lactoglobulin, *Food Chemistry*. 219 (2017) 290–296. <https://doi.org/10.1016/j.foodchem.2016.09.153>.
- [32] P. Pomastowski, J. Walczak, M. Gawin, S. Bocian, W. Piekoszewski, B. Buszewski, HPLC separation of casein components on a diol-bonded silica column with MALDI TOF/TOF MS identification, *Analytical Methods*. 6 (2014) 5236–5244. <https://doi.org/10.1039/c4ay00895b>.
- [33] C.N. Pace, G.R. Grimsley, J.M. Scholtz, Protein ionizable groups: pK values and their contribution to protein stability and solubility, *Journal of Biological Chemistry*. 284 (2009) 13285–13289. <https://doi.org/10.1074/jbc.R800080200>.
- [34] L.P. Kozłowski, Proteome-pI 2.0: proteome isoelectric point database update, *Nucleic Acids Research*. 50 (2022) D1535–D1540. <https://doi.org/10.1093/nar/gkab944>.
- [35] P.P. Pomastowski, E. Dziubakiewicz, B. Buszewski, Potencjał zeta - jego rola i znaczenie, *Analityka*. 2 (2012) 19–23.
- [36] B. Buszewski, P. Pomastowski, Wpływ heterogeniczności powierzchni biokoloidów na

- ich rozdzielanie elektroforetyczne, *Wiadomości Chemiczne*. 69 (2015) 9–10.
- [37] M. Corredig, P.K. Nair, Y. Li, H. Eshpari, Z. Zhao, Invited review: understanding the behavior of caseins in milk concentrates, *Journal of Dairy Science*. 102 (2019) 4772–4782. <https://doi.org/10.3168/jds.2018-15943>.
- [38] D.G. Dalgleish, Measurement of electrophoretic mobilities and zeta-potentials of particles from milk using laser Doppler electrophoresis, *Journal of Dairy Research*. 51 (1984) 425–438. <https://doi.org/10.1017/S0022029900023724>.
- [39] P. Edman, Method for determination of the amino acid sequence in peptides., *Acta Chemica Scandinavica*. 4 (1950) 283–293.
- [40] H. Kamińska, H. Podbielska, Identyfikacja białek z wykorzystaniem techniki Peptide Mass Fingerprinting (PMF). Część I - charakterystyka eksperymentu identyfikacji, *Acta Bio-Optica et Informatica Medica*. 17 (2011) 153–160.
- [41] J.R. Yates, C.I. Ruse, A. Nakorchevsky, Proteomics by mass spectrometry: approaches, advances, and applications, *Annual Review of Biomedical Engineering*. 11 (2009) 49–79. <https://doi.org/10.1146/annurev-bioeng-061008-124934>.
- [42] P.K. Rout, M. Verma, Post translational modifications of milk proteins in geographically diverse goat breeds, *Scientific Reports*. 11 (2021) 1–16. <https://doi.org/10.1038/s41598-021-85094-9>.
- [43] L. Zhan, Y. Liu, X. Xie, C. Xiong, Z. Nie, Heat-induced rearrangement of disulfide bond of lactoglobulin characterized by multiply charged MALDI-TOF/TOF mass spectrometry, *Analytical Chemistry*. 90 (2018) 10670–10675. <https://doi.org/10.1021/acs.analchem.8b02563>.
- [44] X. Wu, Y. Lu, H. Xu, D. Lin, Z. He, H. Wu, L. Liu, Z. Wang, Reducing the allergenic capacity of β -lactoglobulin by covalent conjugation with dietary polyphenols, *Food Chemistry*. 256 (2018) 427–434. <https://doi.org/10.1016/j.foodchem.2018.02.158>.
- [45] D. Mercadante, L.D. Melton, G.E. Norris, T.S. Loo, M.A.K. Williams, R.C.J. Dobson, G.B. Jameson, Bovine β -Lactoglobulin is dimeric under imitative physiological conditions: Dissociation equilibrium and rate constants over the pH range of 2.5-7.5, *Biophysical Journal*. 103 (2012) 303–312. <https://doi.org/10.1016/j.bpj.2012.05.041>.
- [46] A. Gołębiowski, P. Pomastowski, A. Rodzik, A. Król-Górniak, T. Kowalkowski, M. Górecki, B. Buszewski, Isolation and self-association studies of beta-lactoglobulin, *International Journal of Molecular Sciences*. 21 (2020) 1–21. <https://doi.org/10.3390/ijms21249711>.
- [47] A.J. Thomson, H.B. Gray, Bio-inorganic chemistry, *Current Opinion in Chemical*

- Biology. 2 (1998) 155–158. [https://doi.org/10.1016/s1367-5931\(98\)80056-2](https://doi.org/10.1016/s1367-5931(98)80056-2).
- [48] A. Rodzik, P. Pomastowski, V. Railean-Plugaru, B. Buszewski, Hybrydowe nanokompozyty typu metal-białko serwatkowe, *Analityka*. (2021) 4–12.
- [49] K. Kluska, J. Adamczyk, A. Krężel, Metal binding properties, stability and reactivity of zinc fingers, *Coordination Chemistry Reviews*. 367 (2018) 18–64. <https://doi.org/10.1016/j.ccr.2018.04.009>.
- [50] Y. Lu, Metalloprotein and metallo-DNA/RNAzyme design: current approaches, success measures, and future challenges, *Inorganic Chemistry*. 45 (2006) 9930–9940. <https://doi.org/10.1021/ic052007t>.
- [51] A. Basu, Metals in medicine: an overview, *Scientific Reviews & Chemical Communications*. 5 (2015) 77–87. www.sadgurupublications.com.
- [52] A. Krężel, W. Maret, The biological inorganic chemistry of zinc ions, *Archives of Biochemistry and Biophysics*. 611 (2016) 3–19. <https://doi.org/10.1016/j.abb.2016.04.010>.
- [53] S. Medici, M. Peana, V.M. Nurchi, M.A. Zoroddu, Medical Uses of Silver: History, Myths, and Scientific Evidence, *Journal of Medicinal Chemistry*. 62 (2019) 5923–5943. <https://doi.org/10.1021/acs.jmedchem.8b01439>.
- [54] L. Xu, Y.Y. Wang, J. Huang, C.Y. Chen, Z.X. Wang, H. Xie, Silver nanoparticles: Synthesis, medical applications and biosafety, *Theranostics*. 10 (2020) 8996–9031. <https://doi.org/10.7150/thno.45413>.
- [55] I. Michalak, K. Chojnacka, A. Witek-Krowiak, State of the art for the biosorption process - a review, *Applied Biochemistry and Biotechnology*. 170 (2013) 1389–1416. <https://doi.org/10.1007/s12010-013-0269-0>.
- [56] G. William Kajjumba, S. Emik, A. Öngen, H. Kurtulus Özcan, S. Aydın, Modelling of adsorption kinetic processes—errors, theory and application, *Advanced Sorption Process Applications*. (2019) 1–19. <https://doi.org/10.5772/intechopen.80495>.
- [57] M. Pooresmaeil, H. Namazi, Application of polysaccharide-based hydrogels for water treatments, Elsevier Inc., 2020. <https://doi.org/10.1016/B978-0-12-816421-1.00014-8>.
- [58] M.B. Desta, Batch sorption experiments: Langmuir and freundlich isotherm studies for the adsorption of textile metal ions onto teff straw (*eragrostis tef*) agricultural waste, *Journal of Thermodynamics*. 1 (2013). <https://doi.org/10.1155/2013/375830>.
- [59] A.M. Aljeboree, A.N. Alshirifi, A.F. Alkaim, Kinetics and equilibrium study for the adsorption of textile dyes on coconut shell activated carbon, *Arabian Journal of Chemistry*. 10 (2017) S3381–S3393. <https://doi.org/10.1016/j.arabjc.2014.01.020>.

- [60] V. Railean-Plugaru, P. Pomastowski, K. Meller, M. Złoch, K. Rafinska, B. Buszewski, Lactococcus lactis as a safe and inexpensive source of bioactive silver composites, *Applied Microbiology and Biotechnology*. 101 (2017) 7141–7153. <https://doi.org/10.1007/s00253-017-8443-x>.
- [61] V. Railean-Plugaru, P. Pomastowski, T. Kowalkowski, M. Sprynskyy, B. Buszewski, Physicochemical study of natural fractionated biocolloid by asymmetric flow field-flow fractionation in tandem with various complementary techniques using biologically synthesized silver nanocomposites, *Analytical and Bioanalytical Chemistry*. 410 (2018) 2837–2847. <https://doi.org/10.1007/s00216-018-0967-0>.
- [62] D.W.S. Wong, W.M. Camirand, A.E. Pavlath, Structures and functionalities of milk proteins, 1996. <https://doi.org/10.1080/10408399609527751>.
- [63] A.B.T. Ghisaidoobe, S.J. Chung, Intrinsic tryptophan fluorescence in the detection and analysis of proteins: a focus on Förster resonance energy transfer techniques, *International Journal of Molecular Sciences*. 15 (2014) 22518–22538. <https://doi.org/10.3390/ijms151222518>.
- [64] L.J. Juszczak, Eisenberg. Azaria S., The color of cation- π interactions: subtleties of amine-tryptophan interaction energetics allow for radical-like visible absorbance and fluorescence, *Journal of the American Chemical Society*. 139 (2017) 8302–8311. <https://doi.org/10.1021/jacs.7b03442>.
- [65] A. Król, V. Railean-Plugaru, P. Pomastowski, M. Złoch, B. Buszewski, Mechanism study of intracellular zinc oxide nanocomposites formation, *Colloids and Surfaces A: Physicochemical and Engineering Aspects*. 553 (2018) 349–358. <https://doi.org/10.1016/j.colsurfa.2018.05.069>.
- [66] A. Król, V. Railean-Plugaru, P. Pomastowski, B. Buszewski, Phytochemical investigation of *Medicago sativa* L. extract and its potential as a safe source for the synthesis of ZnO nanoparticles: the proposed mechanism of formation and antimicrobial activity, *Phytochemistry Letters*. 31 (2019) 170–180. <https://doi.org/10.1016/J.PHYTOL.2019.04.009>.
- [67] F.X. Schmid, Biological macromolecules: UV-visible spectrophotometry, *Encyclopedia of Life Sciences*. (2001) 1–4. <https://doi.org/10.1038/npg.els.0003142>.
- [68] J.E. Kinsella, D.M. Whitehead, Proteins in whey: chemical, physical, and functional properties, *Advances in Food and Nutrition Research*. 33 (1989) 343–438. [https://doi.org/10.1016/S1043-4526\(08\)60130-8](https://doi.org/10.1016/S1043-4526(08)60130-8).
- [69] P. Žuvela, J.J. Liu, M. Yi, P.P. Pomastowski, G. Sagandykova, M. Belka, J. David, T.

- Bączek, K. Szafranski, B. Żołnowska, J. Sławiński, C.T. Supuran, M.W. Wong, B. Buszewski, Target-based drug discovery through inversion of quantitative structure-drug-property relationships and molecular simulation: CA IX-sulphonamide complexes, *Journal of Enzyme Inhibition and Medicinal Chemistry*. 33 (2018) 1430–1443. <https://doi.org/10.1080/14756366.2018.1511551>.
- [70] I. Müllerová, L. Frank, Role of the high-angle BSE in SEM imaging, in: *14th European Microscopy Congress*, Springer, Berlin, Heidelberg, 2008: pp. 585–586. https://doi.org/10.1007/978-3-540-85156-1_293.
- [71] G.E. Lloyd, Atomic number and crystallographic contrast images with the SEM: a review of backscattered electron techniques, *Mineralogical Magazine*. 51 (1987) 3–19. <https://doi.org/10.1180/MINMAG.1987.051.359.02>.
- [72] B.G. Poulson, K. Szczepski, J.I. Lachowicz, L. Jaremko, A.H. Emwas, M. Jaremko, Aggregation of biologically important peptides and proteins: Inhibition or acceleration depending on protein and metal ion concentrations, *RSC Advances*. 10 (2020) 215–227. <https://doi.org/10.1039/c9ra09350h>.
- [73] J. Polte, Fundamental growth principles of colloidal metal nanoparticles - a new perspective, *CrystEngComm*. 17 (2015) 6809–6830. <https://doi.org/10.1039/c5ce01014d>.
- [74] V. Railean-Plugaru, P. Pomastowski, B. Buszewski, Use of *Lactobacillus paracasei* isolated from whey for silver nanocomposite synthesis: antiradical and antimicrobial properties against selected pathogens, *Journal of Dairy Science*. 104 (2021) 2480–2498. <https://doi.org/10.3168/jds.2020-19049>.
- [75] T. Dudev, Modeling metal binding sites in proteins by quantum chemical calculations, *Computational Chemistry*. 2 (2014) 19–21. <https://doi.org/10.4236/cc.2014.22003>.
- [76] R.J. Ouellette, J.D. Rawn, Amino Acids, peptides, and proteins, in: *Organic Chemistry Study Guide*, 2015: pp. 569–586. <https://doi.org/10.1016/b978-0-12-801889-7.00027-3>.
- [77] P. Pomastowski, M. Sprynskyy, P. Žuvela, K. Rafińska, M. Milanowski, J.J. Liu, M. Yi, B. Buszewski, Silver-Lactoferrin Nanocomplexes as a Potent Antimicrobial Agent, *Journal of the American Chemical Society*. 138 (2016) 7899–7909. <https://doi.org/10.1021/jacs.6b02699>.
- [78] L.H.S. Santos, R.S. Ferreira, E.R. Caffarena, Integrating molecular docking and molecular dynamics simulations, in: *Docking Screens for Drug Discovery*, 2019: pp. 13–34. https://doi.org/10.1007/978-1-4939-9752-7_2.
- [79] S. Singh, Q. Bani Baker, D.B. Singh, Molecular docking and molecular dynamics

- simulation, in: *Bioinformatics: Methods and Applications*, Elsevier, 2021: pp. 291–304. <https://doi.org/10.1016/B978-0-323-89775-4.00014-6>.
- [80] E. Jamrozik, M.J. Selgelid, Drug-Resistant Infection: Causes, Consequences, and Responses, in: *Ethics and Drug Resistance: Collective Responsibility for Global Public Health*, Springer, Cham, 2020: pp. 3–18. https://doi.org/10.1007/978-3-030-27874-8_1.
- [81] C.L. Ventola, The antibiotic resistance crisis, *Pharmacy and Therapeutics*. 40 (2015) 277–283. <https://doi.org/10.1016/B978-1-4831-9711-1.50022-3>.
- [82] I.M. Gould, A.M. Bal, New antibiotic agents in the pipeline and how they can help overcome microbial resistance, *Virulence*. 4 (2013) 185–191. <https://doi.org/10.4161/viru.22507>.
- [83] P. Kaiser, J. Wächter, M. Windbergs, Therapy of infected wounds: overcoming clinical challenges by advanced drug delivery systems, *Drug Delivery and Translational Research*. 11 (2021) 1545–1567. <https://doi.org/10.1007/s13346-021-00932-7>.
- [84] F.P. Douillard, W.M. de Vos, Biotechnology of health-promoting bacteria, *Biotechnology Advances*. 37 (2019) 107369. <https://doi.org/10.1016/j.biotechadv.2019.03.008>.
- [85] C. Broyard, F. Gaucheron, Modifications of structures and functions of caseins: a scientific and technological challenge, *Dairy Science and Technology*. 95 (2015) 831–862. <https://doi.org/10.1007/s13594-015-0220-y>.
- [86] D.G. Dalgleish, M. Corredig, The structure of the casein micelle of milk and its changes during processing, *Annual Review of Food Science and Technology*. 3 (2012) 449–467. <https://doi.org/10.1146/ANNUREV-FOOD-022811-101214>.
- [87] S. Sandra, M. Alexander, D.G. Dalgleish, The rennet coagulation mechanism of skim milk as observed by transmission diffusing wave spectroscopy, *Journal of Colloid and Interface Science*. 308 (2007) 364–373. <https://doi.org/10.1016/J.JCIS.2007.01.021>.
- [88] K. Garai, P. Sengupta, B. Sahoo, S. Maiti, Selective destabilization of soluble amyloid beta oligomers by divalent metal ions, *Biochemical and Biophysical Research Communications*. 345 (2006) 210–215. <https://doi.org/10.1016/J.BBRC.2006.04.056>.
- [89] G. Navarra, M. Leone, V. Militello, Thermal aggregation of beta-lactoglobulin in presence of metal ions, *Biophysical Chemistry*. 131 (2007) 52–61. <https://doi.org/10.1016/J.BPC.2007.09.003>.
- [90] J. Choi, D.S. Horne, J.A. Lucey, Effect of Insoluble Calcium Concentration on Rennet Coagulation Properties of Milk, *Journal of Dairy Science*. 90 (2007) 2612–2623. <https://doi.org/10.3168/JDS.2006-814>.

- [91] G.J.O. Martin, R.P.W. Williams, D.E. Dunstan, Effect of manufacture and reconstitution of milk protein concentrate powder on the size and rennet gelation behaviour of casein micelles, *International Dairy Journal*. 20 (2010) 128–131. <https://doi.org/10.1016/J.IDAIRYJ.2009.08.007>.
- [92] S. Sandra, M. Corredig, Rennet induced gelation of reconstituted milk protein concentrates: The role of calcium and soluble proteins during reconstitution, *International Dairy Journal*. 29 (2013) 68–74. <https://doi.org/10.1016/J.IDAIRYJ.2012.10.011>.
- [93] N. Tang, L.H. Skibsted, Calcium binding to amino acids and small glycine peptides in aqueous solution: Toward peptide design for better calcium bioavailability, *Journal of Agricultural and Food Chemistry*. 64 (2016) 4376–4389. <https://doi.org/10.1021/acs.jafc.6b01534>.
- [94] T. Huppertz, Chemistry of the Caseins, in: *Advanced Dairy Chemistry*, Springer, Boston, MA, 2013: pp. 135–160. https://doi.org/10.1007/978-1-4614-4714-6_4.
- [95] E. Miquel, A. Alegría, R. Barberá, R. Farré, Casein phosphopeptides released by simulated gastrointestinal digestion of infant formulas and their potential role in mineral binding, *International Dairy Journal*. 16 (2006) 992–1000. <https://doi.org/10.1016/j.idairyj.2005.10.010>.
- [96] H. Singh, A. Flynn, P.F. Fox, Binding of zinc to bovine and human milk proteins, *The Journal of Dairy Research*. 56 (1989) 235–248. <https://doi.org/10.1017/S0022029900026455>.
- [97] X. Wang, J. Zhou, P.S. Tong, X.Y. Mao, Zinc-binding capacity of yak casein hydrolysate and the zinc-releasing characteristics of casein hydrolysate-zinc complexes, *Journal of Dairy Science*. 94 (2011) 2731–2740. <https://doi.org/10.3168/JDS.2010-3900>.
- [98] T. Kočańczyk, A. Drozd, A. Krężel, Relationship between the architecture of zinc coordination and zinc binding affinity in proteins - insights into zinc regulation, *Metallomics*. 7 (2015) 244–257. <https://doi.org/10.1039/c4mt00094c>.
- [99] A. Krężel, W. Maret, The biological inorganic chemistry of zinc ions, *Archives of Biochemistry and Biophysics*. 611 (2016) 3–19. <https://doi.org/10.1016/j.abb.2016.04.010>.
- [100] L. Ehrl, Z. Jia, H. Wu, M. Lattuada, M. Soos, M. Morbidelli, Role of Counterion Association in Colloidal Stability, *Langmuir*. 25 (2009) 2696–2702. <https://doi.org/10.1021/LA803445Y>.
- [101] F. Roosen-Runge, B.S. Heck, F. Zhang, O. Kohlbacher, F. Schreiber, Interplay of pH

- and binding of multivalent metal ions: charge inversion and reentrant condensation in protein solutions, *Journal of Physical Chemistry B*. 117 (2013) 5777–5787. <https://doi.org/10.1021/jp401874t>.
- [102] H.A. Alhazmi, W. Ahsan, A.M.M. Ibrahim, R.A.Y. Khubrani, Z.A.A. Haddadi, A.Y.F. Safhi, N. Shubayr, M. Al Bratty, A. Najmi, Investigation of bovine serum albumin aggregation upon exposure to silver(i) and copper(ii) metal ions using Zetasizer, *Open Chemistry*. 19 (2021) 987–997. <https://doi.org/10.1515/CHEM-2021-0089/MACHINEREADABLECITATION/RIS>.
- [103] J. Zhang, H. Li, S. Li, X. Hou, Effects of metal ions with different valences on colloidal aggregation in low-concentration silica colloidal systems characterized by continuous online zeta potential analysis, *Colloids and Surfaces A: Physicochemical and Engineering Aspects*. 481 (2015) 1–6. <https://doi.org/10.1016/j.colsurfa.2015.04.024>.
- [104] A. Chakraborty, S. Basak, Interaction with Al and Zn induces structure formation and aggregation in natively unfolded caseins, *Journal of Photochemistry and Photobiology B: Biology*. 93 (2008) 36–43. <https://doi.org/10.1016/j.jphotobiol.2008.06.011>.

4. Publikacje naukowe

4.1. Hybrydowe układy metal-białko w ujęciu serwatkowym

[P1] **A. Rodzik**, P. Pomastowski, V. Railean-Plugaru, B. Buszewski, *Hybrydowe układy metal-białko w ujęciu serwatkowym*, *Analityka: nauka i praktyka*, 2021, 2, 4-12.



AGNIESZKA RODZIK

PAWEŁ POMASTOWSKI

VIORICĂ RAILEAN-PLUGARU

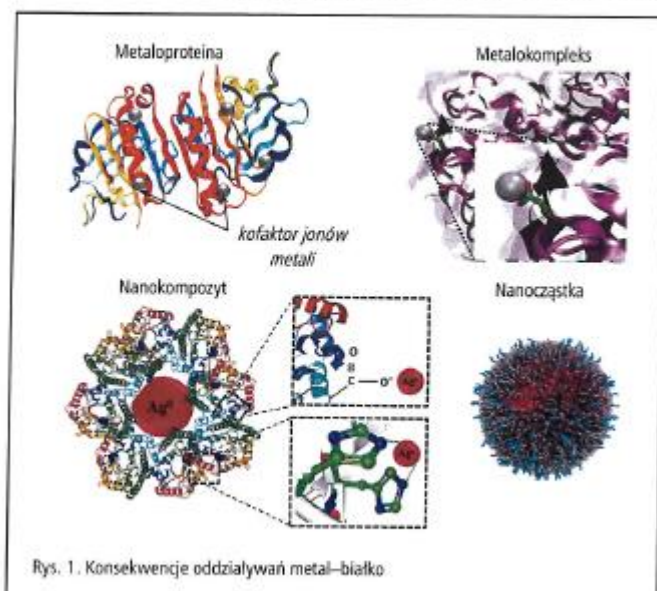
BOGUSŁAW BUSZEWSKI

Obok całej gamy związków nieorganicznych i organicznych ważną i interesującą grupę związków biologicznie aktywnych stanowią białka serwatkowe. Mają one zdolność do oddziaływania z jonami metali. Aby zrozumieć zjawiska oddziaływań metal–białko, ważne jest opracowanie i wdrożenie nowych, innowacyjnych metod analitycznych, połączonych z badaniami zmian aktywności biologicznej oraz analizą wpływu tych oddziaływań.

Hybrydowe nanokompozyty typu metal–białko serwatkowe

Mleko, skład i jego bogactwo obok znanych faktów prozdrowotnych i odżywczych ciągle stanowi inspirację do poszukiwania nowych, interesujących i ważnych wyzwań. Jest ono bowiem źródłem substancji biologicznie aktywnych i zapasowych, mających wpływ na procesy życiowe i prozdrowotne. To kolejny argument do szczegółowego poznania i opisu jego składu, właściwości i możliwości wykorzystania jako surowiec do pozyskania nowych produktów i preparatów. Obok całej gamy związków nieorganicznych (mikro- i makroelementy, sole etc.) i organicznych (substancje budulcowe i odżyw-

cze, tj.: różne typy białka, tłuszcze, witaminy, cukry etc.) ważną i interesującą grupę związków biologicznie aktywnych stanowią białka serwatkowe. Mają one zdolność do oddziaływania z jonami metali. Ma to przełożenie na różne dziedziny związane z postępowaniem cywilizacyjnym i jakością życia człowieka. Oddziaływania te mają dwójaki charakter. Po pierwsze mogą one stanowić szeroki wachlarz możliwości zastosowania w żywności, nutraceutykach czy przemyśle farmaceutycznym, a po drugie mogą być prawdziwym wyzwaniem analitycznym dla badaczy związanym z ich badaniem mechanizmu wiązania prowadzącym do powstania metaloprotein, metalokompleksów, nanocząstek czy nanokompozytów. Aby zrozumieć zjawiska oddziaływań metal–białko, ważne jest opracowanie i wdrożenie nowych, innowacyjnych metod analitycznych, połączonych z badaniami zmian aktywności biologicznej oraz analizą wpływu tych oddziaływań.



Oddziaływanie białek serwatkowych z metalami

Jony metali oddziałują z białkami, wpływając w ten sposób na ich aktywność biologiczną. Ocena tych zmian ma duże znaczenie, ponieważ białka pełnią wiele funkcji w organizmie człowieka i znajdują zastosowanie w wielu gałęziach przemysłu. Dla oceny zmian wywołanych oddziaływaniem z metalami istotne są następujące czynniki:

- tworzenie nowych miejsc wiążących, które determinują oddziaływanie białka z innymi ligandami,
- zmiany w strukturze białka,
- grupy oddziałujące, umożliwiające badanie charakteru, a tym samym siły oddziaływania,
- agregacja białka.

Wynikiem oddziaływań metal–białko mogą być metaloproteiny, metalokompleksy, nanocząstki oraz nanokompozyty, co zostało przedstawione na rysunku 1.

Metaloproteiny powstają głównie poprzez wiązania koordynacyjne pomiędzy jonami metali i grupami funkcyjnymi aminokwasów, na przykład karboksylowymi, wbudowując się w ten sposób w strukturę białka. Te grupy funkcyjne białka tworzą specjalne miejsce wiążące w formie „wnęki” (ang. cave), która jest określona przez strukturę czwartorzędową białka i jego aktywność biologiczną. Ponadto, białka z grupy metaloprotein mogą oddziaływać z jonami metali, tworząc albo metalokompleksy, albo nanocząstki metalu/tlenku metalu. Metalokompleks z kolei jest sztucznym układem zdefiniowanym przez słabe oddziaływania, takie jak oddziaływania elektrostatyczne, wiązanie wodorowe, siły van der Waalsa czy wiązania donorowo-akceptorowe, które sumarycznie są silniejsze od wcześniej wymienionych oddziaływań. Oddziaływania białka i jonów metali z aktywnymi grupami funkcyjnymi aminokwasów mogą być odwracalne i labilne oraz prowadzić do powstawania nanocząstek, czyli struktur o wymiarach w zakresie 1 nm – 100 nm. Powstały układ składający się z utworzonego metalokompleksu i nanocząstek może tworzyć nanokompozyt. Dodatkowo warto wspomnieć, że statystycznie różne rodzaje oddziaływań jonu metalu i różnych grup funkcyjnych białka mogą zachodzić, a nawet z teoretycznego punktu widzenia, zachodzą jednocześnie. Jednak ostateczny wynik tych oddziaływań zależy od wielu czynników i warunków (temperatury, pH itp.). Determinują one konformację białka, jego fałdowanie/rozfałdowanie, a tym samym tworzenie miejsc wiązania dla jonu metalu. Ponadto mają wpływ na orientację grup funkcyjnych białka (czynnik steryczny dla oddziaływania). Wyjaśnia to również silne wiązania koordynacyjne jonów metali i białek w metaloproteinie, ponieważ wiele czynników może prowadzić do powstawania „wgnębień” jako miejsc wiążących dla jonów metali, które są dość trudne do odtworzenia w sztucznym układzie. Umożliwia to syntezę głównie metalokompleksów, podczas gdy metaloproteiny powstają przede wszystkim na drodze naturalnej. Oprócz tworzenia się nanokompozytów dochodzi również do indukowanej metalami agregacji białek (wpływ ładunku), która powoduje utratę aktywności biologicznej i wytrącanie się białek z roztworu. To z kolei negatywnie wpływa na jakość produktu. Chemia agregacji białek indukowanej metalami może być wyjaśniona przez teorię oddziaływań wewnątrzcząsteczkowych Derjagina-Landau-Verwey-Overbeek (DLVO), która traktuje stabilność układu biokoloidalnego w kategoriach równowagi pomiędzy przyciągającymi siłami van der Waalsa i odpychającymi elektrycznymi siłami dwuwarsztwowymi (potencjał zeta). Dodatek jonów metali powoduje wzrost sił przyciągających, co wzmacnia oddziaływania pomiędzy jednostkami białkowymi, powodując powstawanie dużych agregatów.

Metale przejściowe (metale d-elektronowe) są najbardziej powszechnymi kofaktorami nieorganicznymi w układach biologicznych, które implikują różne funkcje białek i ich kompleksów. Metale d-elektronowe mają naturalne powinowactwo do oddziaływania z białkami ze względu

IKA® POL

Przedstawiciel w Polsce
Firmy IKA WERKE GmbH

Działalność firmy obejmuje doradztwo techniczne, dystrybucję i handel sprzętem laboratoryjnym, pomiarowo-analitycznym i produkcyjnym:

Sprzęt laboratoryjny

- mieszadła magnetyczne, mieszadła mechaniczne, homogenizatory, wyrzaskarki, młynki, łaznie wodne, płyty grzewcze, pompy próżniowe i perystaltyczne, wyparki, ekstraktory substancji stałych, reaktory laboratoryjne

Sprzęt pomiarowo-analityczny

- zetowniki, analizatory elektrochemicznej syntezy organicznej, termogravimetry, kalorymetry, analizatory laboratoryjne C, S, N, O, H, CO₂

Sprzęt produkcyjny

- pojemnościowy – homogenizatory, turbulatory, rululatory
- przepływowy – homogenizatory, dispax reaktory, młyny koloidalne
- emulgatory – mieszalniki (o poj. od 10 – 4000 L), dla substancji o różnej lepkości

IKA POL

ul. Przy Bażantarni 4/6, 02-793 Warszawa
tel. +48 22 649 24 05, fax: +48 22 859 14 39
e-mail: info@ikapol.pl, www.ikapol.pl

na brak elektronów, dzięki czemu mogą koordynować się z bogatymi w elektrony cząsteczkami w białkach. Powoduje to, że metaloproteiny są szeroko rozpowszechnione w przyrodzie. Szacuje się, że ponad 50% wszystkich białek to właśnie metaloproteiny. Ponadto, takie jony metali jak miedź (II), żelazo (II), mangan (II) i molibden (II) mają zdolność do najsilniejszej koordynacji ze względu na swoje właściwości, takie jak gęstość i mały promień atomowy. Co ważniejsze, obecność metali przejściowych jest wszechobecna w środowisku, a źródła i drogi narażenia człowieka mogą być bardzo różne. Ponadto, kompleksy metali znajdują zastosowanie jako leki dla pacjentów z niedokrwistością z niedoboru żelaza, chorobami nerek, nowotworami (kompleksy palladu, rutenu i platyny) oraz dotkniętych niedożywieniem.

Wreszcie, zwiększone spożycie mikroelementów metali jako suplementów żywności zwiększa prawdopodobieństwo ich oddziaływania z białkami, ponieważ globalne zapotrzebowanie na żywność bogatą w białko wzrosło wraz z poprawą standardu życia oraz z dominującym udziałem procentowym funkcji białek w organizmie człowieka.

Natura oddziaływań metal-białko

Natura oddziaływań metal-białko pozwala na poznanie rodzaju i siły tych oddziaływań, jak również zaangażowania grup funkcyjnych białka w proces wiązania. Przykładowo sorpcja na powierzchni białka, która jest charakterystyczna dla metalokompleksów, może zachodzić poprzez słabe oddziaływania niekowalencyjne, które są niestabilne i odwracalne. Silniejsze są wiązania koordynacyjne, które umożliwiają wbudowanie metalu w strukturę białka.

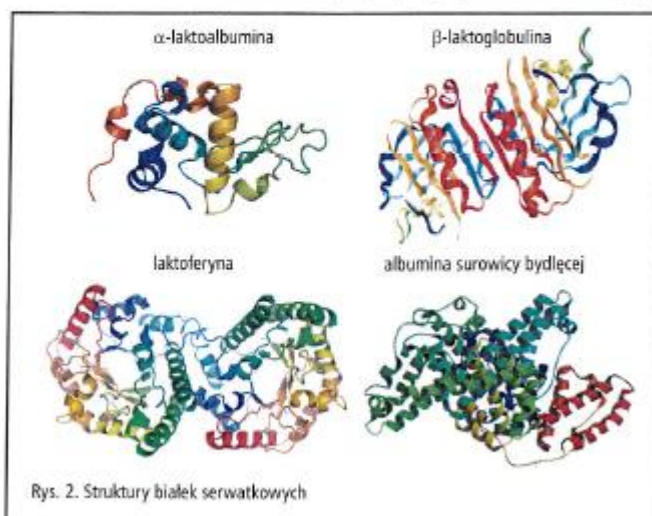
Łańcuchy polipeptydowe białek zwykle koordynują z jonami metali, a łańcuchy boczne z grupami funkcyjnymi mogą stanowić dodatkowe miejsce wiązania dla metali, między innymi grupa imidazolowa histydyny

(His), grupa karboksylowa asparagianu (Asp) i glutaminianu (Glu), pierścień fenolowy tyrozyny (Tyr), azot łańcuchów bocznych lizyny (Lys) i argininy (Arg). Istotne znaczenie dla oddziaływania metal-białko mają wiązania wodorowe, elektrostatyczne, hydrofobowe oraz oddziaływania van der Waalsa, co ma znaczący wpływ na stabilizację struktur białkowych. Czynniki wpływającymi na wiązanie metalu z białkami są właściwości metalu, takie jak stan walencyjny, promień jonowy, zdolność do przyjmowania ładunku oraz stężenie wolnego metalu. Jednakże, badania nad naturą oddziaływań metal-białko oraz charakterystyka wiązania metali z białkami stanowią wyzwanie i są prowadzone przy użyciu instrumentalnych technik analitycznych, jak również kombinacji różnych technik instrumentalnych.

Kolejnym czynnikiem wpływającym na oddziaływanie metal-białko jest pH. Wpływ pH na takie oddziaływania można wytłumaczyć stanem protonowania aminokwasów w białkach. Po pierwsze, Asp, Glu i His reagują na zmiany pH prowadzące do asocjacji/dysocjacji ich kompleksów z jonami metali i ulegają deprotonacji w pH obojętno-zasadowym, co prowadzi do wzrostu przyciągania elektrostatycznego i wzmocnienia kompleksu, natomiast w pH kwaśnym następuje protonacja i osłabienie sił przyciągania. Ponadto, cysteina (Cys) posiada grupę tiolową, która musi być zdeprotonowana, aby mogła uczestniczyć w wiązaniu metalu, jak również Tyr może być zdeprotonowany, aby wytworzyć fenolowy atom donora tlenu, który na przykład może być dobrym ligandem dla żelaza (III). Interesujące jest, że w przypadku wpływu pH na powinowactwo wiązania żelaza do laktoferyny zaangażowany jest jon węglanowy, gdyż jest on niezbędny do wiązania żelaza, a jon ten jest niestabilny w niskim pH, co prowadzi do uwolnienia żelaza z laktoferyny. Inny aspekt wpływu pH związany jest ze zmianami konformacyjnymi w strukturze białka, na przykład β -laktoglobulina w warunkach kwaśnych powodowała dimeryzację, która wiązała się ze zmianami w eksponowanych pasmach β , natomiast w warunkach zasadowych obserwowano denaturację.

Wykazano również, że Glu i Asp powinny być połączone z donorem azotu lub donorem siarki, aby ułatwić wiązanie cynku w peptydach lub białkach, stosując izotermiczne miareczkowanie kalometryczne ITC (ang. *Isothermal Titration Calorimetry*). Białka serwatkowe (rys. 2), takie jak laktoferyna (LTF), α -laktoalbumina (α -LA) i β -laktoglobulina (β -LG), wykazywały silne, zbliżone do siebie powinowactwa wiązania cynku. Warto zaznaczyć, że wiązanie cynku z albuminą surowicy bydłowej (BSA i LTF) jest egzotermiczne, podczas gdy wiązanie z α -LA i β -LG jest lekko endotermiczne. Sugeruje się, że cynk wiąże się z wiązaniami disiarczkowymi utlenionej Cys w LTF oraz z grupą tiolową cysteiny (Cys34) w BSA z istotnym wydzielaniem ciepła, podczas gdy cynk wiąże się z His, Asp lub Glu w α -LA i β -LG.

Dodatkowo, badania wykazały, że oddziaływanie kompleksu lantan (III)-cysteina z β -LG i BSA wywołuje zmiany konformacyjne obu białek. Ponadto, kompleks lantan



Rys. 2. Struktury białek serwatkowych

(III)-cysteina silnie wygasza fluorescencję fluoroforu Trp w β -LG i BSA w trybie wygaszania statycznego. Wiązania wodorowe i siły van der Waalsa stabilizują kompleksy dla obu białek. Podobne badania dotyczące oddziaływań lantan-białko przeprowadzono dla kompleksu lantanu (III) z tryptofanem (Trp) i fenyloalaniną (Phe) w odniesieniu do albuminy surowicy ludzkiej (HSA). Kompleks lantanu z Trp wykazuje również umiarkowaną do dobrej aktywność przeciwbakteryjną wobec różnych szczepów bakterii. Porównywalne wyniki uzyskano dla oddziaływań pomiędzy HSA i β -LG z kompleksami palladu (II). Badania spektroskopowe wykazały zmiany konformacyjne białek w wyniku działania kompleksu palladu (II). Dane dotyczące parametrów termodynamicznych oddziaływań pokazują, że w asocjacjach HSA/ β -LG i kompleksów palladu (II) istotną rolę odgrywają wiązania wodorowe i oddziaływania van der Waalsa. Wyniki badań wykazały silne wygaszenie fluorescencji HSA i β -LG przez kompleks palladu (II) na drodze mechanizmu statycznego.

Techniki analityczne w rozdzielaniu i analizie białek serwatkowych

Metody rozdzielania białek serwatkowych obejmują metody membranowe (ultrafiltracja i mikrofiltracja), elektroforetyczne oraz chromatograficzne (powinowactwa, anionowej i kationowej wymiany, odwróconej fazy) czy przepływowe frakcjonowanie w polu zewnętrznym FFF (ang. *Field Flow Fractionation*).

Metody oparte na technikach ultrafiltracji membranowej są bardzo zróżnicowane i mogą być stosowane do izolacji białek serwatkowych z rzeczywistych matryc. Ponadto skutecznie mogą być stosowane do przygotowania koncentratu białek serwatkowych WPC (ang. *Whey Protein Concentrate*) i izolatu białek serwatkowych WPI (ang. *Whey Protein Isolate*) oraz do rozdzielania przed końcową analizą/detekcją.

Techniki elektroforetyczne obejmują elektroforezę kapilarną CE (ang. *Capillary Electrophoresis*), żelową SDS PAGE, Native PAGE (ang. *Sodium Dodecyl Sulfate Polyacrylamide Gel Electrophoresis*) i mikrochipową MCE (ang. *Microchip Electrophoresis*). Technika mikroprzepływowa „lab-on-a-chip” do rozdzielania białek została opisana jako wysokowydajna i zautomatyzowana alternatywa dla konwencjonalnej SDS PAGE, która pozwala na rozdzielanie i kwantyfikację wielu próbek w ciągu 30 minut. Kolejną zaletą jest mała wymagana objętość próbki i materiału, która jest zwykle mniejsza niż 0,5 mL całkowitej objętości chipa (10 próbek). Dla porównania, SDS PAGE wymaga kilku litrów materiałów (roztwory akrylamidu, bufor i roztwory barwiące/odbarwiający). Głównym ograniczeniem systemu kapilarnego i mikroprzepływowego jest jednak stosunkowo niska odwarzalność rozdzielania elektroforetycznego. Wynika to z adhezji białek do kapilary, denaturacji i wrażliwości systemu na zmiany pH oraz siły jonowej buforów. Wykazano, że dodanie buforów do solubilizacji TPS (ang. *Total Protein Solubilization*) i rozdziela-

nia białek SEP (ang. *Separating Milk Protein Buffer*) do mleka przed separacją miało doskonały wpływ na α -LA i β -LG. Wykazano też, że separacja kazein była lepsza przy użyciu buforu SEP, a wyniki były porównywalne z tymi uzyskanymi metodą SDS PAGE.

Techniki chromatograficzne służące do rozdzielania białek serwatkowych są zróżnicowane. Separacja w tym przypadku oparta jest na oddziaływaniach hydrofobowych, jonowych oraz specyficznych (opartych na powinowactwie molekularnym) i polega na adsorpcji białek na ciele stałym (kolumnie lub membranie), które są eluowane fazą ciekłą. Chromatografia jonowymieniana ma wiele zalet w porównaniu z technologią kolumnowo-pakowaną, takie jak szybki stopień asocjacji pomiędzy białkiem docelowym a grupami funkcyjnymi, krótki czas przetwarzania, łatwość skalowania, brak ciepła i chemicznych obróbek wstępnych lub zmian pH, które mogłyby wpływać na strukturę białka, zmieniając jego właściwości. Ponadto, technika chromatografii kolumnowej jest kosztowna i dlatego nie jest ekonomicznie opłacalna do zastosowania na skalę przemysłową w przemyśle spożywczym. Kolumny membranowe anionowe i kationowymienne wykorzystano do frakcjonowania białek serwatkowych z WPC i serwatki z sera mozzarella, a następnie do rozdzielania za pomocą szybkiej chromatografii cieczowej białek FPLC (ang. *Fast Protein Liquid Chromatography*) i wysokosprawnej chromatografii cieczowej HPLC (ang. *High Performance Liquid Chromatography*), wykrywania za pomocą UV Vis i identyfikacji za pomocą SDS PAGE. Stwierdzono, że jeden system wymiany jonowej może być wykorzystywany do różnych celów w zależności od buforu elucyjnego. Pierwszy etap obejmuje wychwytywanie dodatnio naładowanych białek serwatkowych w kolumnie kationowymiennej, drugi etap to usuwanie niezwiązanych zanieczyszczeń przez płukanie, a ostatni etap obejmuje selektywną desorpcję jednego lub więcej interesujących białek. Jedną z zalet tego badania było wykorzystanie niedrogich, spożywczych buforów w jednej kolumnie do uzyskania białek o wysokiej czystości. Jednak metody chromatograficzne w porównaniu z klasycznymi technikami elektroforetycznymi, na przykład dwuwymiarową elektroforezą żelową, mają wciąż dość niską zdolność rozdzielczą.

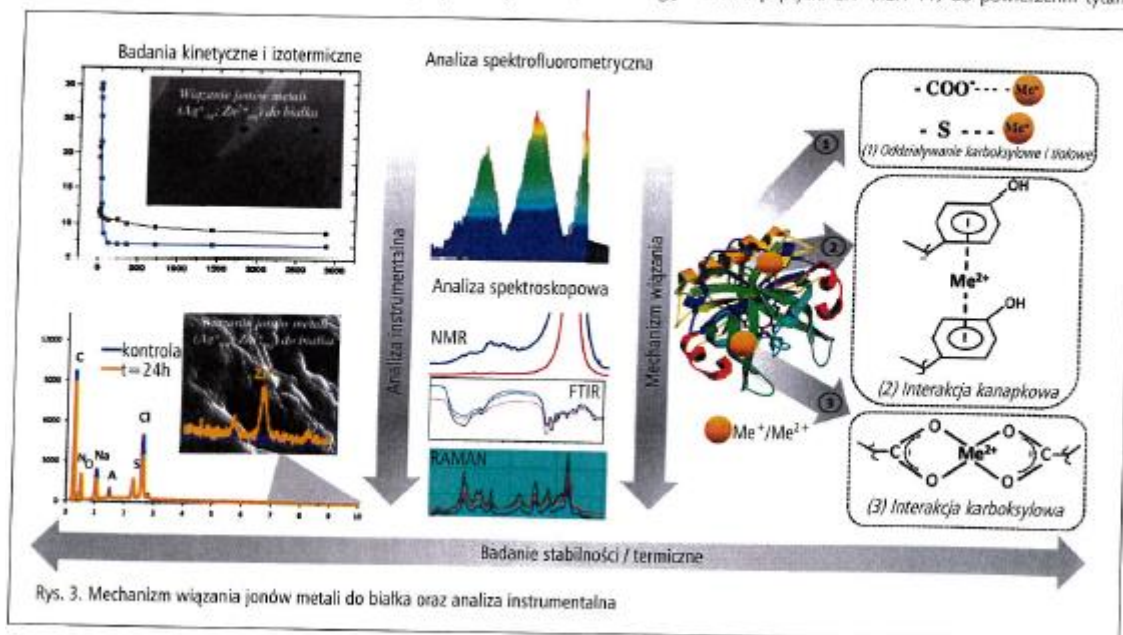
Pewną alternatywą do rozdzielania i charakteryzowania białek serwatkowych jest przepływowe frakcjonowanie w polu zewnętrznym (FFF). Proces przebiega w specjalnie zaprojektowanych kanałach, gdzie generowany jest przepływ laminarny fazy ruchomej (newtonowski, paraboliczny profil) z uwzględnieniem gradientu pola zewnętrznego. Różnica w natężeniu przepływu i sterowanie natężeniem tego pola (grawitacyjne, magnetyczne, elektryczne etc.) pozwala na wstępne i całkowite frakcjonowanie białek, a następnie ich oznaczenie za pomocą on-line detektorów [UV Vis, elektrochemiczne, fluorescencyjne czy układy laserowe jak wielokątowe rozproszenie światła czy spektrometria mas (MS) oraz sprzężenie z plazmą indukcyjną (ICP MS)].

Techniki analityczne do badania oddziaływań białek serwatkowych z jonami metali

Metody spektrometrii mas, jako wysoce czułe techniki o niskich granicach wykrywalności, zostały zastosowane do badania oddziaływań metal–białko poprzez pomiar stężenia jonów metalu i białka. Spektrometria mas ze wzbudzeniem w plazmie indukcyjnie sprzężonej ICP MS (ang. *Inductively Coupled Plasma Mass Spectrometry*) jest zdolna do wykrywania stężeń metali, co zostało odnotowane w naszych pracach w przypadku oznaczenia stężenia jonów srebra (I), jonów cynku (II) w celu zbadania mechanizmu wiązania srebra z LTF i cynku z β -LG. Chromatografia wykluczenia wielkości SEC (ang. *Size Exclusion Chromatography*) w połączeniu z ICP MS została zastosowana do oznaczania takich metali, jak mangan, kobalt, miedź i selen obecnych w różnych frakcjach białek serwatkowych mleka ludzkiego (HBM) w celu wykrycia pierwiastków z odpowiednią czułością i dokładnością, podczas gdy metoda laserowej jonizacji/desorpcji próbki wspomaganą matrycą z analizatorem czasu przelotu MALDI TOF MS (ang. *Matrix-Assisted Laser Desorption Ionization technique coupled to Time-Of-Flight Mass Spectrometry*) i wysokosprawna chromatografia cieczowa z tandemową spektrometrią mas LC MS MS (ang. *Liquid Chromatography coupled with tandem Mass Spectrometry*) zostały użyte do analizy składu frakcji białek i profilu ilościowego. Pomimo zalet i szybkiego rozwoju protokołów MALDI TOF MS do analizy białek złotym standardem do określania masy, sekwencji białek, ich analizy i charakterystyki jest jonizacja przez rozpylenie w polu elektrycznym ESI MS (ang. *Electrospray Ionization*). Ograniczeniami ESI MS dla oddziaływań metal–białko mogą być reakcje redoks, które mogą

zachodzić podczas jonizacji, ciśnienie atmosferyczne, które może przyczynić się do utleniania wrażliwych gatunków, wymagania dotyczące wysokiej czystości próbki oraz niekompatybilność z najczęściej stosowanymi nieorganicznymi buforami i solami.

Oprócz technik spektrometrii mas inne metody stosowane w celu zrozumienia mechanizmu wiązania srebra z LTF czy też cynku z β -LG obejmowały spektroskopię w podczerwieni z transformacją Fouriera FTIR (ang. *Fourier Transformed Infrared Spectroscopy*) oraz spektroskopię Ramana (RS). Zarówno analiza FTIR, jak i spektroskopię Ramana wykazały znaczące różnice w widmach metal–białko w stosunku do natywnego białka w postaci dodatkowych sygnałów. Techniki te są komplementarne do badania oddziaływań jonów metali z aktywnymi grupami funkcyjnymi białek. Jednakże FTIR w porównaniu z RS jest mniej specyficzna i czuła ze względu na obecność wody w układzie, co ogranicza udział grupy hydroksylowej w oddziaływaniu. Alternatywnie, RS jest ograniczona przez procesy fluorescencji reszt aromatycznych LTF i wymaga zastosowania procedur wspomaganych powierzchniowo, na przykład poprzez napylenie nanocząstek złota lub srebra. Dodatkowo, aby precyzyjnie wskazać miejsce wiązania kationu srebra z LTF, można zastosować analizę dynamiki molekularnej MD (ang. *Molecular Dynamics*). Ponadto, określając miejsca wiązania kationów srebra z LTF, wskazano redukcję jonów srebra do srebra elementarnego za pomocą teorii funkcjonalów gęstości DFT (ang. *Density Functional Theory*). Z drugiej strony, rentgenowska spektroskopia fotoelektronów XPS (ang. *X-ray Photoelectron Spectroscopy*) została wykorzystana do potwierdzenia przyłączenia peptydu LTF (hLF1-11) do powierzchni tytanu

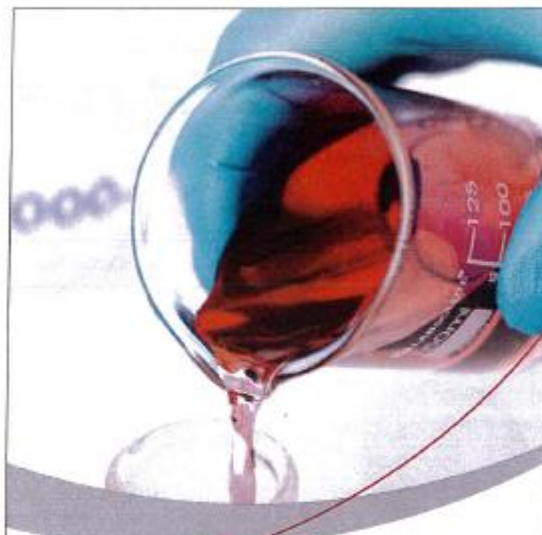


Rys. 3. Mechanizm wiązania jonów metali do białka oraz analiza instrumentalna

poprzez określenie składu chemicznego powierzchni układu. Inną ważną techniką jest spektroskopia fluorescencyjna, która pozwoliła na określenie powinowactwa wiązania białek serwatkowych i jonów metali poprzez pomiar wygaszonej fluorescencji białka po dodaniu metalu. Metoda ta jest jednak odpowiednia głównie dla umiarkowanych i silnych powinowactw i zawiera szereg szczegółów, które należy uwzględnić podczas pomiarów. Powinowactwa wiązania różnych jonów metali i białek serwatkowych były najczęściej określane za pomocą spektroskopii fluorescencyjnej. Drugą metodą, która została wykorzystana do określenia powinowactwa wiązania oddziaływań jonów metali i białek serwatkowych była izotermiczna kalorymetria miareczkowa ITC (ang. *Isothermal Titration Calorimetry*). ITC opiera się na pomiarach zmian ciepła podczas oddziaływania. Zaletą tej metody w stosunku do innych technik jest możliwość pomiaru parametrów termodynamicznych oddziaływania wraz z powinowactwem wiązania, jednak w przypadku kompleksów o bardzo wysokim lub niskim powinowactwie jest to trudne.

Techniki mikroskopowe mogą służyć jako pośrednie metody badania skutków oddziaływań i opisu mechanizmu wiązania jonów metali z białkiem prowadzącego do powstania nanocząstek poprzez ich obrazowanie. Analizy skaningowej mikroskopii elektronowej SEM (ang. *Scanning Electron Microscope*) przeprowadzane są w celu monitorowania zmian w morfologii struktury białka przed procesem wiązania dla natywnych białek (LTF i β -LG) oraz po procesie wiązania z jonami metali (srebra, cynku). Badania wskazały, iż jony cynku są równomiernie immobilizowane na/w wielowymiarowej strukturze mikroporowatej β -LG. Z kolei analizy z zastosowaniem transmisyjnej mikroskopii elektronowej TEM (ang. *Transmission Electron Microscope*) posłużyły dodatkowo do fizykochemicznej charakterystyki nanocząstek powstałych w wyniku oddziaływania LTF z jonami srebra. Analiza TEM pozwoliła określić morfologię i wielkość nanocząstek, natomiast SEM pozwoliła stwierdzić, że otrzymane cząstki mają kształt sferyczny w zakresie 90 nm – 110 nm. Dodatkowo, badania oparte na dynamicznym rozpraszaniu światła wykazały, że średnica hydrodynamiczna otrzymanych nanocząstek LTF wynosi 150 nm \pm 20 nm. Różnice te można wytłumaczyć faktem, że analiza dynamicznego rozpraszania światła DLS (ang. *Dynamic Light Scattering*) uwzględnia hydrodynamiczny rozmiar rozpuszczonego białka, natomiast metody mikroskopii elektronowej są wykorzystywane do badania topologii, porowatości i rozmiaru rdzenia metaloorganicznego. Morfologię nanocząstek LTF scharakteryzowano także, używając zarówno SEM, jak i mikroskopii sił atomowych AFM (ang. *Atomic Force Microscopy*), która wykazała, że nanocząstki miały kształt sferyczny i średnicę 50 nm – 60 nm (rys. 3).

Technika jonizacji desorpcji laserowej wspomaganej matrycą (MALDI) sprzężona ze spektrometrią mas w czasie przelotu (TOF MS) stała się jedną z powszechnie stosowanych metod charakteryzacji białek obok



WSZYSTKO NA POTRZEBY TWOJEGO LABORATORIUM W JEDNYM MIEJSCU

Nawet w tych trudnych czasach, jesteśmy zobowiązani do zapewnienia Tobie wszystkiego, czego potrzebujesz do swojego laboratorium.

- Materiały eksploatacyjne laboratoryjne
- Sprzęt laboratoryjny
- Meble laboratoryjne
- Odczynniki chemiczne
- Produkty life science

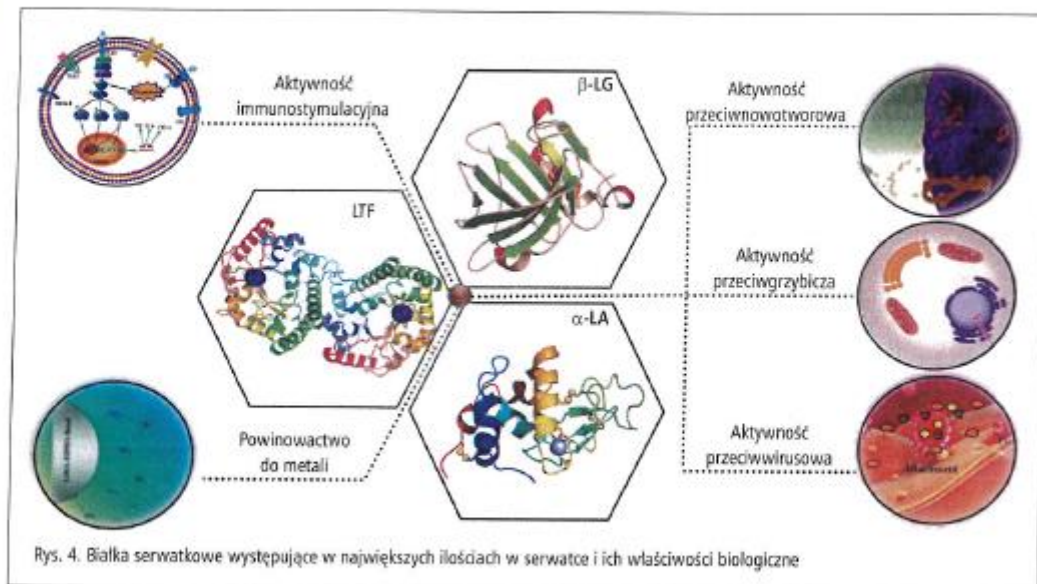
Co czyni firmę Th. Geyer twoim idealnym Partnerem w Polsce?

- Wybór spośród ponad 200 producentów
- Najlepsze marki, takie jak LABSOLUTE® & CHEMSOLUTE®
- Szybka i niezawodna logistyka
- Usługi serwisowe zakresie urządzeń laboratoryjnych
- Kompetentnie, dedykowane osoby kontaktowe

Nasi eksperci laboratoryjni z przyjemnością doradzą Państwu pod numerem telefonu +48 22 427 64 64 lub pocztą elektroniczną pod adresem sales@thgeyer.pl

W naszym sklepie internetowym znajdziesz wszystko, co jest niezbędne do codziennej pracy w laboratorium. Zarejestruj się! Odwiedź nas na www.thgeyer.pl

 **TH.GEYER**
SUPPLYING YOUR IDEAS



Rys. 4. Białka serwatkowe występujące w największych ilościach w serwatce i ich właściwości biologiczne

innych podejść opartych na spektrometrii mas. Do zalet MALDI TOF MS należy zaliczyć prostotę użycia, czułość, duży zakres mas i względną odporność na interferencje z matrycą. Ponadto, technika ta może być wykorzystywana nie tylko do charakterystyki białek, ale również do badania ich interakcji, ponieważ aktywność biologiczna i rozpoznawanie biomolekuł są definiowane przez oddziaływania niekowalencyjne. Interakcje różnych ligandów z białkami są interesujące, ponieważ pełnią one wiele funkcji zarówno w przyrodzie, jak i w organizmie człowieka. Przykładowo, analiza MALDI TOF MS β-LG została wykorzystana do badania jej wpływu na odporność człowieka i promocję proliferacji komórek, a analiza kompleksów anhidrazy węglowej IX z potencjalnymi syntetycznymi inhibitorami pozwoliła na identyfikację jedynie silnie wiążących się z białkami inhibitorów dzięki naturze jonizacji MALDI. W niektórych przypadkach w badaniach nad genetyką chorób rola kompleksów metal-białko i specjacja metali są przedmiotem dużego zainteresowania, szczególnie w przypadku choroby Alzheimera i jej implikacji. Chociaż MALDI MS nie jest w stanie określić ilości metali w próbkach biologicznych, jak również w systemach modelowych, do takich badań może być wykorzystana do ilościowego oznaczania białek i identyfikacji miejsc modyfikacji potranslacyjnych PTM (ang. *Posttranslational Modifications*). Pomimo wyzwań związanych z kwantyfikacją MALDI MS związanych z odtwarzalnością wyników, podejścia takie jak wykorzystanie znaczników izobarycznych do względnej i absolutnej kwantyzacji iTRAQ (ang. *isobaric Tags for Relative and Absolute Quantization*) są szeroko stosowane do różnicowania wyrażonych białek w proteomice porównawczej ze względu na dużą skalę, wysoką przepustowość i wysoką czułość procedur różnych podejść

opartych na spektrometrii mas. W technologii tej stosuje się 4-krotny zestaw aminowo reaktywnych znaczników izobarycznych do derywatacji peptydów na N-końcu i na łańcuchach bocznych lizyny, znakując w ten sposób wszystkie peptydy w mieszaninie trawionej.

Ponadto, PTM są kluczowe dla aktywności biologicznej białek, a ich identyfikacja jest ważnym wyzwaniem analitycznym. Technika MALDI TOF MS może być zastosowana do tego celu poprzez trawienie białek do peptydów, a następnie identyfikację miejsc PTM. Chociaż MALDI TOF MS jest szeroko stosowana również do analizy strawionych białek, analiza peptydów niskocząsteczkowych może być skomplikowana ze względu na interferencję z matrycą, a co za tym idzie tłumienie sygnału (< 700 Da). Podejścia bezmatrycowe obejmują wiele metod analizy z wykorzystaniem materiałów zastępujących matrycę. Obiecującą techniką jest jonizacja/desorpcja laserowa wspomagana nanostrukturami NALDI (ang. *Nano-Assisted Laser Desorption Ionization*). Nanomateriały wspomagają jonizację, co prowadzi do wzmocnienia sygnału dzięki powierzchniowemu rezonansowi plazmonowemu. Przykładowo, badania donoszą, że płytka NALDI zapewnia wyniki o lepszej czułości w porównaniu z płytką na porowatym krzemieniu (DIOS), proszkiem węglowym i porowatą krzemionką dla modelowych peptydów w zakresie 519-2853 Da. Co ciekawe, podejście NALDI może być obiecujące dla badań interakcji metal-peptyd, co jest również ważną częścią badań interakcji metal-białko, ponieważ może wskazać, czy niektóre peptydy mogą być specyficznie związane z interesującym nas metalem.

Tak więc, techniki MALDI i NALDI mogą być komplementarne względem siebie w zakresie obrazowania i charakterystyki oddziaływań metal-białko, gdy są połą-

Tabela. Badanie oddziaływań metal-białko i ich potencjalne zastosowanie

lp.	Oddziaływanie metal-białko	Aktywność biologiczna	Aplikacja
1	Ag-LTF	Przeciwbakteryjna wobec: <i>Pseudomonas aeruginosa</i> , <i>Staphylococcus aureus</i> , <i>Escherichia coli</i> , <i>Enterococcus faecalis</i>	Leczenie trudno gojących się ran, odleżyn
2	Zn-LTF	Przeciwbakteryjna wobec <i>Escherichia coli</i>	Leczenie zakażenia pałeczkami okrężnicy u prosiąt
3	Zn-β-LG	Przeciwnowotworowa wobec linii komórkowych raka piersi MCF-7 Przeciwutleniająca wobec rodnika DPPH (2,2-difenylo-1-pikrylohydrazyl)	Leczenie raka
4	Zn-LTF Zn-β-LG Zn-α-LA Zn-BSA	Prekursor jonów cynku	Zwiększenie biodostępności cynku w żywności

czone z innymi technikami instrumentalnymi w następujących przypadkach:

- analiza i charakterystyka nienaruszonych i strawionych białek, analiza adduktów metal-białko za pomocą MALDI,
- analiza peptydów strawionych z białek wyjściowych w zakresie niskich mas cząsteczkowych, adduktów peptydowych z metalami i miejscami PTM zlokalizowanymi na peptydach o niskiej masie cząsteczkowej

za pomocą NALDI w zakresie średnich i wysokich mas za pomocą MALDI,

- analiza ilościowa białek za pomocą MALDI/NALDI.

Znaczenie oddziaływania białek serwatkowych z metalami

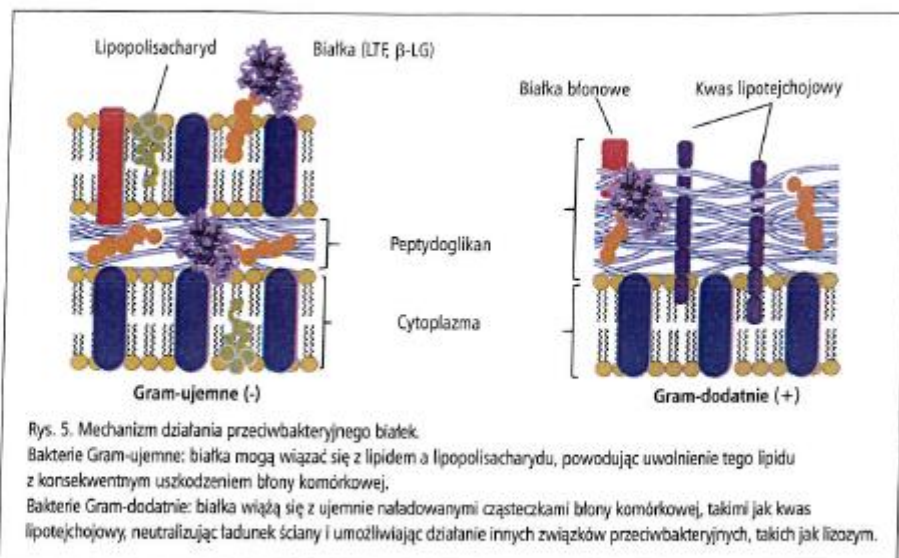
Białko serwatkowe zawiera głównie β-LG, α-LA oraz LTF, które charakteryzują się wysoką wartością biologiczną przewyższającą inne typowe białka pokarmowe (rys. 4).



www.testchem.pl

Od ponad 30 lat Testchem jest liderem innowacji technologicznych wspierających rozwój laboratoriów w całym kraju. Dzięki bogatej ofercie i kompleksowej obsłudze, pomożemy wprowadzić Twój biznes w przyszłość.





Rys. 5. Mechanizm działania przeciwbakteryjnego białek.

Bakterie Gram-ujemne: białka mogą wiązać się z lipidem a lipopolisacharydu, powodując uwolnienie tego lipidu z konsekwentnym uszkodzeniem błony komórkowej.

Bakterie Gram-dodatnie: białka wiążą się z ujemnie naładowanymi cząsteczkami błony komórkowej, takimi jak kwas lipoteichojuowy, neutralizując ładunek ściany i umożliwiając działanie innych związków przeciwbakteryjnych, takich jak lizozym.

Białka serwatkowe wykazują aktywność antyoksydacyjną poprzez tworzenie glutationu (GSH). Może to być związane z aktywnością przeciwnowotworową. GSH może powstawać dzięki wysokiej zawartości siarki w białkach serwatkowych zapewnionej przez obecność cysteiny, która tworzy γ -glutamylcysteinę, a etap ten jest ograniczający w syntezie GSH. Ponadto, LTF może pełnić funkcję przeciwutleniacza poprzez wiązanie żelaza w formie, która uniemożliwia mu pełnienie funkcji katalizatora Habera-Weissa. Natomiast kompleksy białek serwatkowych z metalami wykazują aktywność przeciwnowotworową, służąc jako nośniki dla kompleksów metali takich jak kompleksy lantanu (III) z β -LG oraz kompleksy kobaltu i niklu z HSA i β -LG.

Niemniej jednak wpływ metali na aktywność przeciwnowotworową białek serwatkowych można wykażać na przykładzie LTF. Nienasycona żelazem apo-LTF hamuje wzrost komórek raka szyjki macicy (HeLa) po 48 h leczenia, podczas gdy diferric-bLf nie była skuteczna. Dodatkowo wskazano, że zarówno nienasycona żelazem apo-LTF, jak i nasycona żelazem LTF (> 90 % wysycenia Fe^{3+}) wykazują właściwości przeciwnowotworowe, jednak forma apo-LTF wykazywała większy efekt w indukowaniu cytotoxiczności w obu liniach komórkowych (MDA-MB-231 i MCF-7) w porównaniu z Fe-LTF, która była bardziej skuteczna w indukowaniu apoptozy w liniach komórkowych MCF-7. Badania przeprowadzone na myszach wykazały, że chemioterapia zlikwidowała chłoniaki EL-4 u myszy, które otrzymywały LTF nasyconą żelazem przez 6 tygodni przed chemioterapią, ale nie u myszy otrzymujących formy mniej nasycone żelazem. Stwierdzono, że LTF może być potencjalnym naturalnym środkiem wspomagającym chemioterapię, ale nasycona żelazem może być bardziej skuteczna.

LTF β -LG same w sobie posiadają aktywność przeciwbakteryjną, co przedstawiono na rysunku 5, oraz funkcje immunomodulacyjne.

Natomiast stwierdzono, że nanokompozyt w wyniku interakcji jonów srebra z LTF i spontaniczną redukcją jonów srebra do nanocząstek wykazuje silną aktywność przeciwbakteryjną wobec *Pseudomonas aeruginosa*, *Staphylococcus aureus*, *Escherichia coli* i *Enterococcus faecalis*. Wzrost lekoopornego szczepu *P. aeruginosa* został zahamowany o ponad 97 %, co było porównywalne z tradycyjnym antybiotykiem cefotaksymem (tab.). Ponadto wykazano, że LTF może być stosowana w celu zmniejszenia ryzyka aspiracyjnego zapalenia płuc u osób starszych, u których pielęgnacja jamy ustnej jest utrudniona. Dodatkowo, działanie przeciw pasożytnicze LTF jest różne w zależności od gatunku. LTF zakłóca przyswajanie żelaza przez niektóre pasożyty, jednak może ona działać jako specyficzny donator żelaza dla niektórych pasożytów, które wykorzystują LTF do swojego wzrostu. Dokładniej mówiąc, holo-LTF oddziałuje z receptorami błony komórkowej, a komórka zaczyna wydzielać kompleks reduktazy żelaza, która zawiera NADPH, wymagając reduktazy, a ta oddaje elektrony, zmieniając w ten sposób potencjał błony i prowadząc do jej rozpadu.

Agnieszka Rodzik, Paweł Pomastowski, Viorica Railean-Plugaru, Bogusław Buszewski

Katedra Chemii Środowiska i Bioanalitki, Wydział Chemii, Uniwersytet Mikołaja Kopernika, Toruń, Interdyscyplinarne Centrum Nowoczesnych Technologii, Uniwersytet Mikołaja Kopernika, Toruń

Podziękowania:

Praca została wsparta finansowo przez Narodowe Centrum Nauki w ramach projektu Opus 14 nr 2017/27/B/ST4/02628 (2018–2021)

4.2. A study of zinc ions immobilization by β -lactoglobulin

[P2] B. Buszewski, **A. Rodzik**, V. Railean-Plugaru, M. Sprynskyy, P. Pomastowski, *A study of zinc ions immobilization by β -lactoglobulin*, Colloids and Surfaces A, 2020, 591, 1-13, doi: 10.1016/j.colsurfa.2020.124443.



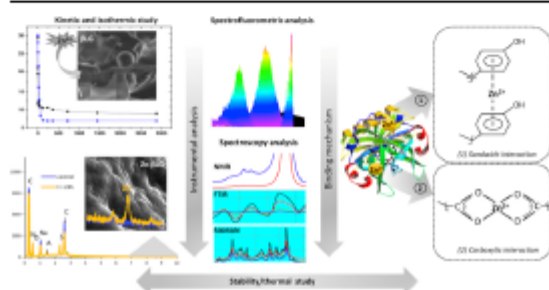
A study of zinc ions immobilization by β -lactoglobulin

Bogusław Buszewski^{a,b,*}, Agnieszka Rodzik^{a,b}, Viorica Railean-Plugaru^{a,b}, Myroslav Sprynskyy^a, Paweł Pomastowski^b

^a Department of Environmental Chemistry and Bioanalysis, Faculty of Chemistry, Nicolaus Copernicus University in Toruń, Gagarina 7, 87-100, Toruń, Poland

^b Centre for Modern Interdisciplinary Technologies, Nicolaus Copernicus University in Toruń, Wileńska 4, 87-100, Toruń, Poland

GRAPHICAL ABSTRACT



ARTICLE INFO

Keywords:

β -Lactoglobulin
Zinc ions
Zinc- β -lactoglobulin complex
Sorption
Synthetic physiological fluids

ABSTRACT

The aim of the study was to immobilize zinc ions by β -lactoglobulin (β LG) micelles. The investigation focused on physicochemical properties of β -lactoglobulin and zinc- β -lactoglobulin complexes as well as the stability of the obtained complex in synthetic physiological fluids. Kinetic and isothermal studies of zinc ion immobilization by β LG were conducted based on batch sorption approach, while the mechanism of binding zinc ions to β LG was determined and described by application of several kinetic and isotherm models, such as zero order, first and pseudo-first order, intraparticle Weber-Morris diffusion, Langmuir and Freundlich models. The nature of binding/immobilization of zinc ions to β LG was determined with instrumental complementary analysis by using the spectrometric, spectroscopic, microscopic, thermal and X-ray diffraction methods. The results revealed that zinc ion binding to β LG is a heterogeneous process which consists of three main stages: the stage one was associated with rapid sorption of zinc ions on the surface of β LG micelles, while stages two and three resulted from intramolecular diffusion of zinc ions. Moreover, based on instrumental and stability study it was proven that acidic (Glu, Asp) and aromatic (Tyr, Trp, Phe) amino acid groups participate in formation of Zn- β LG complex as a metallocomplex with nutraceutical potential.

1. Introduction

Whey has been considered for a long time exclusively as cheese

production waste. Nowadays it has become a focus of scientific interest due to its ingredients: in addition to providing nutrients, it can also prevent or alleviate diseases and their effects [1]. One of the dominant

* Corresponding author at: Department of Environmental Chemistry and Bioanalysis, Faculty of Chemistry, Nicolaus Copernicus University in Toruń, Gagarina 7, 87-100, Toruń, Poland.

E-mail address: bbusz@umk.pl (B. Buszewski).

<https://doi.org/10.1016/j.colsurfa.2020.124443>

Received 6 November 2019; Received in revised form 8 January 2020; Accepted 8 January 2020

Available online 09 January 2020

0927-7757 / © 2020 Elsevier B.V. All rights reserved.

wey proteins is β -lactoglobulin (β LG), which accounts for more than 50 % of the total whey protein content [2]. β -Lactoglobulin is a small globular protein belonging to the lipocalin family, consisting of 162 amino acid residues [3]. There are several genetic variants (A, B, C, D, E, F, G, H and W) differing in one or two exchanges of amino acids, of which the complete primary structures A, B and W have been established. Godovac-Zimmermann et al. isolated two new variants I and J, differing in two amino acids at positions 108 and 126 [4].

β -Lactoglobulin is a source of essential and branched-chain amino acids such as leucine, isoleucine and valine [5]. Moreover, the β LG contains two disulfide bonds (Cys-66 to Cys-160, Cys-106 to Cys-119) and one free thiol group (Cys-121), which prevent oxidation by capturing reactive oxygen species (ROS) [6]. β -Lactoglobulin exhibits antibacterial properties affecting the human immune system by stabilizing cell proliferation [2]. It thus contributes to protection against diseases such as sepsis and septic shock with subsequent multi-organ failure, which are currently increasingly frequent causes of death [7].

Despite its many advantages, this protein is considered to be the main milk allergen, which is responsible for allergic effects of milk, especially among young children. However, many studies carried out on conformational β -lactoglobulin changes contribute to changes in the emerging allergenicity [8].

A key structural element of β -lactoglobulin is the β -barrel, which is a hydrophobic ligand-binding pocket and ligand transport pocket. The mechanism of ligand binding inside the β -barrel depends on the environmental conditions [9]. Due to the nature of β -barrels, β -lactoglobulin has a natural ability to bind to retinol, triglycerides, long-chain fatty acids or vitamins [10], and even drugs such as platinum-based oxaliplatin used against colorectal cancers [11]. Binding of different molecules or metal cations (such as zinc ions) to β -lactoglobulin changes their biological activity [2].

Zinc ions (Zn^{2+}) play a major role in the control of redox biology [12]. Zinc can act as a catalytic, structural and regulatory cofactor in enzymes [13]. In the 1980s a remarkable discovery was the so-called *zinc fingers* in which zinc performs structural functions in domains, interacting with other biomolecules [13]. In a way, proteins are the major ligands for divalent zinc ions, and zinc-dependent proteins have many essential functions in cells, such as transcription regulation, DNA repair, and apoptosis [14,15]. Besides that, this element is one of the minerals most important for human health because of its antioxidant properties – metabolic disorders caused by oxidative stress contribute to damage to cells and tissues, leading to chronic diseases such as obesity, diabetes or cancer [16]. Supplementation of zinc has a positive effect on glycemic control [17], osteoporosis [18], and wound healing process [15]; it also has the ability to regulate immunological homeostasis [19]. However, the nature of binding molecules and metal ions to the multidimensional structure of biocolloids (proteins) is complicated, sometimes unexpected and astonishing [20]. Researchers are thus currently seeking new approaches to studying the mechanism of binding molecules [21] or metal ions such as zinc cations to proteins [22] in order to eliminate the toxicity of free zinc ions.

Therefore, this work was focused on the immobilization of zinc ions by β LG in order to comprehend the binding mechanism and its nature. With this goal in view, kinetics and isothermal experiments using batch sorption approach were carried out. In order to investigate the obtained Zn- β LG complex, the instrumental analysis such as spectrometric, spectroscopic, microscopic, thermal and X-ray diffraction measurements were conducted. Also the stability of obtained Zn- β LG complexes in synthetic physiological fluids was investigated.

2. Experimental

2.1. Characteristics of β -lactoglobulin

2.1.1. Matrix-assisted laser desorption/ionization – time of flight mass spectrometry (MALDI-TOF/TOF-MS) analysis

This study was conducted using MALDI-TOF/TOF mass spectrometer (Bruker Daltonik, Bremen, Germany) equipped with a modified Nd:YAG laser operating at the wavelength of 355 nm and frequency of 2 kHz. Reagents used for MALDI-TOF MS analysis were purchased from Sigma-Aldrich (Steinheim, Germany) in the highest commercially available purity. α -cyano-4-hydroxycinnamic acid was used as a matrix, while Protein Calibration Standards II and Peptide Calibration Standard II (all from Bruker Daltonics, Bremen) was selected for calibration. Samples were applied to ground steel targets purchased from Bruker Daltonik (Bremen, Germany) by dry dropped methods.

Sample preparation of intact and digested protein for spectrometric analysis involved several steps. Initially, the studied proteins were tested for their purity with the use of gel electrophoretic method, according to the procedure described by Pomastowski et al., 2014 [23]. Then, the step of in-gel protein digestion with trypsin was performed, conforming to Bruker Proteomic protocols for mass spectrometry. Finally, the prepared samples (intact and digested protein) were subjected to spectrometric analysis.

MS spectra of intact β -lactoglobulin were recorded in a linear positive mode within a m/z range of 5000–100 000 while peptide mass fingerprint (PMF) spectra of the protein digested with trypsin were recorded in reflectron positive mode within a m/z range of 40–3050. For both cases, measurements were conducted at an accelerating voltage equal to 25 kV. The mass tolerance for all spectra was set to 0.3 Da and calibrated internally on immonium ions. The LIFT post source decay (PSD) technique in the range of m/z was used for determination of fragment spectra. The resulted peptides after tryptic digestion of β -lactoglobulin were identified by application of BioTools software (Bruker Daltonik).

2.1.2. Isoelectric point determination

The isoelectric point of β -lactoglobulin (Sigma-Aldrich, Poland) was determined using diffraction light scattering technique (Zetasizer, Malvern Instruments, Malvern, United Kingdom). The protein was suspended in 0.09 % NaCl (Sigma-Aldrich, Poland) at different pH (2–11), then sonicated (10 s) and analyzed.

2.2. Kinetic study of zinc ions binding to β -lactoglobulin

β -Lactoglobulin (Sigma-Aldrich, Poland) was dispersed in 0.09 % NaCl at pH = pI (4.6) of β LG and sonicated for 5 min. β -lactoglobulin with final concentration (FC) 5000 mg/L was mixed with $Zn(NO_3)_2$ (FC = 30 mg/L) (Sigma-Aldrich, Poland) at the ratio 1:1. The samples were then incubated for different periods of time (2, 5, 10, 20, 30, 60, 120, 240, 360, 720, 1440 and 2880 min) and centrifuged (4 °C, 12 000 rpm, 10 min). After that, an aliquot of supernatant was mineralized in *aqua regia* and diluted to 1 % HNO_3 (Sigma-Aldrich, Poland), and the concentration of zinc ions was determined with the use of Inductively Coupled Plasma-Mass Spectrometry ICP-MS (7900 ICP-MS, Agilent Technologies, Warsaw, Poland).

2.2.1. Sorption kinetics modelling

For this step, zero, first and pseudo-first order kinetics models and intraparticle diffusion models were used for interpretation of experimental results in order to explain the mechanism of zinc ion sorption by β -lactoglobulin.

- The zero order kinetics model was expressed by the following formula:

$$C = C_0 - k_0 t \quad (1)$$

Where: C – the concentration of zinc ions in aqueous solution for a certain period of time [mg/L], C_0 – the initial concentration of zinc ions in aqueous solution [mg/L], k_0 – the adsorption rate constant [(mg/L)/min], t – the adsorption duration [min].

- The amount of zinc sorption by β -lactoglobulin from an aqueous solution for a first order reaction was calculated as follows:

$$C = C_0 e^{-k_1 t} \quad (2)$$

Where: k_1 – the rate constant of first order sorption kinetics [1/min].

- The pseudo-first order kinetics model was expressed by the following formula:

$$q_t = q_e (1 - e^{-k_2 t}) \quad (3)$$

Where: q_e – the amount of zinc sorbed at equilibrium [mg/g].

- The Weber-Morris intraparticle diffusion model was expressed by the following formula:

$$q_t = A + K_{sp} t^{0.5} \quad (4)$$

Where: A – a constant indicating the thickness of the boundary layer diffusion or external surface adsorption [mg/g], K_{sp} – the diffusion rate constant [mg/g min^{0.5}]

- The amount of zinc sorption by β -lactoglobulin from an aqueous solution was calculated as follows:

$$q_t = (C_0 - C) \frac{V}{m} \quad (5)$$

Where: q_t – the amount of zinc ions sorbed for a certain period of time [mg/g], V – the volume of solution from which sorption occurs [L], m – the sorbent mass [g].

2.2.2. Determination of thermodynamic parameters

On the basis of kinetic data at equilibrium time, distribution coefficient (K_d) of zinc ion sorption by β -lactoglobulin was calculated. The following equation was used:

$$K_d = \frac{q_e}{C_e} \quad (6)$$

Where: q_e – the amount of zinc sorbed by β -lactoglobulin at equilibrium time [mg/g], C_e – the equilibrium concentrations of zinc in solution [mg/L].

The distribution coefficient was used as an index of adsorbent affinity to metal ions sorption, because high K_d value corresponds to higher sorption capacity of sorbent, and for calculation of the change in the Gibbs' free energy (ΔG^0).

The value of Gibbs' free energy change (ΔG^0) for adsorption of zinc by β -lactoglobulin was calculated according to the formula:

$$\Delta G^0 = -RT \ln K_d \quad (7)$$

Where: ΔG^0 – the energy of adsorption [kJ/mol], R – the gas constant (8.314 J/mol·K), T – the adsorption absolute temperature (295 K), K_d – the distribution coefficient.

The correlation of experimental data to the models was determined using the Pearson correlation coefficient (R) and standard error (S).

2.3. Isothermal study of zinc ions binding to β -lactoglobulin

Firstly, β -lactoglobulin was suspended in 0.09 % NaCl at pH = pI (4.6) and sonicated for 5 min. Then, β -lactoglobulin (FC = 5000 mg/L) was mixed at the ratio 1:1 with Zn(NO₃)₂ in the following final concentrations of zinc ions: 0.5, 2.5, 7.5, 15, 30, 37.5, 50, 100, 150, 250 mg/L, incubated (21 °C, 900 rpm) for 60 min and centrifuged (4 °C, 12 000 rpm, 10 min). Afterwards, zinc ions were determined according to the procedure described in paragraph 2.2.

2.3.1. Sorption isotherm modelling

In order to study the mechanism of zinc ion sorption by β -lactoglobulin, the experimental results were examined with the use of Freundlich isotherm, Langmuir isotherm and isotherm as function C_e/C_0 , where C_e is equilibrium concentration of the zinc ions in the solution (mg/mL) [24].

- The Freundlich isotherm was expressed by the following formula:

$$q = K_F C_e^n \quad (8)$$

Where: K_F – constant division (L/g), n – an empirical constant, characterized by the heterogeneity of the adsorption process. This model is generally used to describe the sorption process on the surface of heterogeneous hydrocolloids.

- The Langmuir isotherm was expressed by the following formula:

$$q = \frac{q_m K_L C_e}{1 + K_L C_e} \quad (9)$$

Where: q_m – maximum amount of zinc adsorbed in monolayer (mg/g), K_L – constant Langmuir division (L/mg). This model assumes that on the surface of adsorbent forms a monolayer of molecules which interact with adsorption sites, and do not interact with each other, and that there is no possibility to create a multilayer as well as that the adsorption energy is constant [25].

The degree of model matching to experimental isothermal data was determined using the Pearson correlation coefficient (R) and standard error (S).

2.4. Instrumental analysis

For the purpose of all measurements related to the instrumental analysis step, the zinc- β -lactoglobulin complex (Zn- β LG) was obtained according to the optimal parameters resulting from the kinetics study: the time of incubation (10 min, 6 h, 24 h), zinc ions and β -lactoglobulin concentrations at final concentration 30 mg/L and 5000 mg/L respectively. Once the Zn- β LG complex had been obtained, it was centrifuged (12 000 rpm, 10 min) and the supernatant was separated from the pellets (precipitate). The resulting pellets have been washed two times with distilled water and subjected to studies with further instrumental techniques.

2.4.1. Ultraviolet-visible spectroscopy and spectrofluorometric analysis

1.5 mg of Zn- β LG complex was dissolved in 2 mL of 0.09 % NaCl solution, pH 4.6 and analyzed with a UV-vis spectrometer (NanoDrop ND2000, Thermo Scientific) and Jasco FP-8300 spectrofluorometer (JASCO, Europe). UV-vis spectra were registered at $\lambda = 190 - 850$ nm while three-dimensional (3D) excitations and emission spectra were recorded with 1 nm wavelength interval in the range $\lambda = 200 - 350$ nm and 206–650 nm, respectively.

2.4.2. Fourier transform infrared spectroscopic (FT-IR) and Raman spectroscopy analysis

In order to verify the binding of zinc to β -lactoglobulin, the FT-IR and Raman analyses were carried out.

FT-IR spectra were measured using a Spectrum 2000 from Perkin-Elmer, Waltham, MA. The sample was prepared by application KBr disc approach. The FT-IR spectra of the samples were recorded in the 4000–400 cm⁻¹ range.

Raman spectra were captured using a Raman Spectrometer (Senterra, Bruker Optik). The sample was prepared by applying it to a microscope slide. The spectra were registered in the region 4000–400 cm⁻¹ at the wavelength equal to $\lambda = 532$ nm as excitation light, with the power of approximately 20 mW and the counting time spectrum at 30 s with 10 s accumulation. The spectroscopic data were processed with OPUS software.

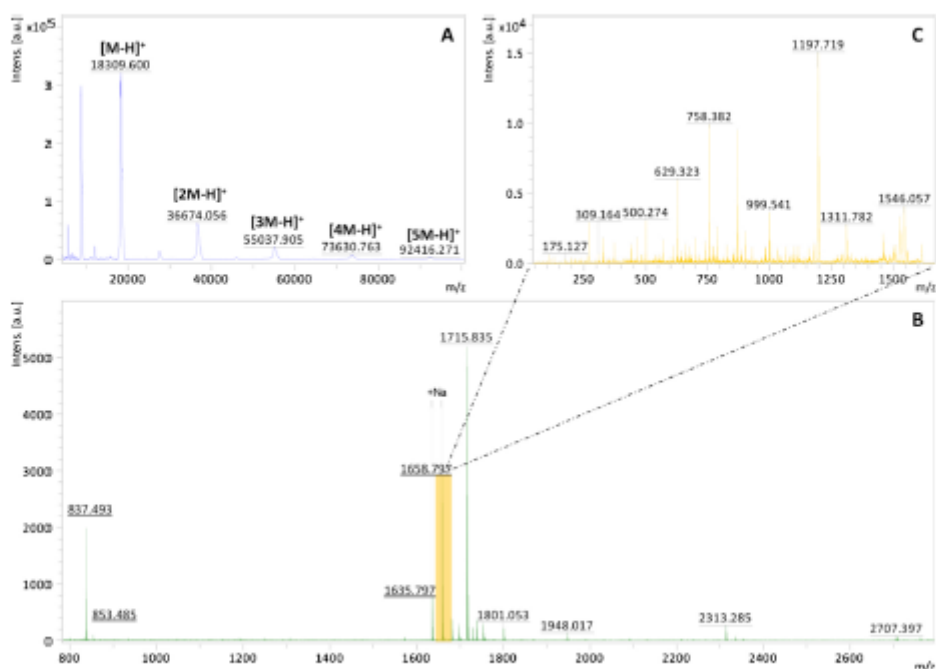


Fig. 1. Mass spectra of β -lactoglobulin components in the intact state – A. The tryptic digestion spectrum recorded for β -lactoglobulin – B. MS/MS spectrum analysis of a selected peptide m/z 1658.803 (adduct with Na^+ ion from signal 1635.797 – C.

2.4.3. Nuclear magnetic resonance (NMR) spectroscopy

Both the control sample (β LG) as well as Zn- β LG complex were suspended in dimethyl sulfoxide- d_6 and sonicated for 5 min. Then the samples were transferred to the NMR tube with the glass Pasteur pipette and analyzed using Bruker Avance III 700 MHz. The recorded data were processed using MestReNova program.

2.4.4. Thermogravimetric analysis

Thermal analyses of β LG and Zn- β LG complex were carried out using TA Instruments type SDT 2960 (Artisan Technology). All data were processed by TGA-DTA thermal analysis software. Native β LG powder and Zn- β LG complex obtained after 24 h of incubation were subjected to heating over a range of 0–600°C with the air flow rate of 100 mL/min and heating rate of 10 °C/min.

2.4.5. Electron microscopy approach (SEM, TEM) and energy dispersive X-ray (XRD) analysis

Morphology, topography and quantitative analysis of elements were carried out with the use of scanning electron microscopy analysis (SEM) and transmission electron microscope (TEM) (model G2 F20X-Twin 200 kV, FEI) in combination with EDX detector (Energy Dispersive X-ray, RTEM SN9577, 134 eV, Edax), respectively. In order to monitor the changes in the morphology of the protein structure, the analyses were performed for both native protein (used as a control) and Zn- β LG complex.

For SEM analysis, the powder was applied on the grid while for TEM, the samples were prepared by dispersing several milligrams of the sample in ethanol solution (99.8 % anhydrous) and applying a drop on a carbon coated grid (Lacey type Cu 400 mesh, Plano) after the solvent was evaporated at room temperature [26].

In order to provide information on the structure, form and nature of the obtained Zn- β LG complex, the X-ray diffractometer (X'Pert Pro Analytical Phillips) equipped with Ni filter and CuK α radiation source

($\lambda = 1.54056 \text{ \AA}$) was used. The sample was prepared by depositing an aliquot on a microscope slide. The registered XRD pattern was processed using XRD Malvern Panalytical software.

2.5. Applications of the Zn- β -lactoglobulin complex

2.5.1. Stability study of the Zn- β -lactoglobulin complex in synthetic physiological fluids

2.5.1.1. Procedure for the preparation of Zn- β -lactoglobulin complex. The Zn- β LG complex was prepared according to the procedure described in Section 2.3. For this investigation, only three final concentrations of zinc ions (30, 50, 100 mg/L) had been chosen for mixing with β -lactoglobulin (PC = 5000 mg/L) at ration 1:1. Once prepared, the samples were incubated for 60 min at 21 °C, 900 rpm and then centrifuged (4 °C, 12 000 rpm, 10 min). The supernatant was removed and the precipitate analyzed. The obtained Zn- β LG precipitate was weighed and then tested for stability in synthetic physiological fluids such as gastric fluid and intestinal fluid.

2.5.1.2. Procedure for the preparation of physiological fluids. In order to study the stability of the complex, synthetic gastric fluid with and without pepsin enzyme and synthetic intestinal fluid with and without pancreatin enzyme was prepared according to the procedure described by Pryschecha et al., 2019 [27].

The obtained Zn- β LG complex (0.1 mg) was added to 500 μ L of physiological fluid. The solution was then transferred to reverse-spin tubes (Amicon 3 K, Merck, Warsaw, Poland). The respective tubes were incubated ($T = 37 \text{ }^\circ\text{C}$, $t = 24 \text{ h}$, 900 rpm) and centrifuged (RT, $t = 10 \text{ min}$, 14000 rpm). Then the obtained filtrate and precipitate, separately, were subjected to the mineralization step, and the concentration of zinc ions was determined using Inductively Coupled Plasma-Mass Spectrometry ICP-MS (7900 ICP-MS, Agilent Technologies, Warsaw, Poland).

Table 1
MS and MS/MS identification of β -lactoglobulin peptides.

Mass [Da]		Intensity	Sequence range	Sequence
Measured	Theoretical			
837.493	837.476	1936.753	158-164	ALPMHR
853.485	853.471	94.534	158-164	ALPMHR 4: Oxidation (M)
1635.793	1635.775	755.294	141-154	TPEVDEALEKFDK
1715.835	1715.806	5226.022	165-178	LSFNFTQLEEQCHI 12: Carbamidomethyl (C)
1801.053	1801.022	200.712	92-107	TKIPAVFKIDALNENK
1948.017	1947.991	95.769	141-157	TPEVDEALEKFDKALK
2313.285	2313.259	179.586	57-76	VYVEELKPTPEGDLELLQK
2707.397	2707.376	47.536	31-56	VAGTWYSLAMAASDISLLDAQAPLR

3. Results and discussion

3.1. Characteristics of β -lactoglobulin

MALDI-TOF MS analysis was carried out to characterize and confirmed the primary structure, molecular masses of intact β -lactoglobulin sorbent, as a part of preliminary sorbent physicochemical analysis.

The mass of β -lactoglobulin was found to be $18\,309 \pm 0.132$ Da. Slight variations of β -lactoglobulin masses may be caused by the presence of posttranslational modifications [28] and the analytical method used for their analysis [29]. In our study, it was observed that β -lactoglobulin may occur in the form of dimers $[2M-H]^+$ or even trimers $[3M-H]^+$, tetramers $[4M-H]^+$ or pentamers $[5M-H]^+$ (Fig. 1A).

Moreover, the β -lactoglobulin was subjected to additional in-depth study by using fingerprint analysis in positive mode, after tryptic digestion. The resulting peptides were identified by the application of BioTools software using non-standard search parameters: cysteine modified by carbamidomethylation and oxidation. The mass spectrum of β -lactoglobulin tryptic peptides is presented in Fig. 1B,C. Table 1 shows the masses of detected peptides, their intensity and sequences.

In order to predict the isoelectric point of β LG, the electrokinetic potential was measured. Zeta potential was determined as a function of different pH (2–12) at the initial time, after 1 h and after 5 h (Fig. 2). Over time, changes in the value of the zeta potential were observed. The initial zeta potential values at pH values 2 and 3 ranged from 19 to 21 mV. Then, at pH values 4 and 5 a decrease in potential values from +18.5 to -12.3 mV was observed. Zeta potential values above pH 5 present unstable tendency of the system and indicate protein degradation. When measuring the zeta potential after 1 h, the zeta potential values were found to be for pH 2 and 3, between 11 and 28 mV

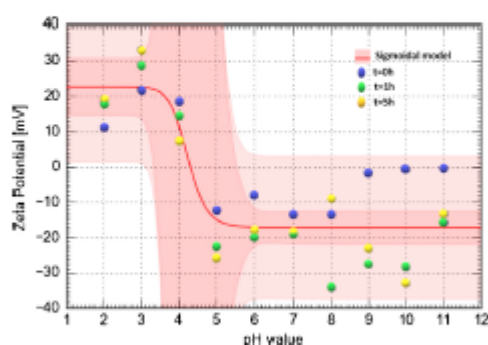


Fig. 2. Zeta potential of β -lactoglobulin in a function of pH. The red line represents the sigmoidal fit trend line. Darker red indicates a confidence band, while lighter indicates a prediction band. (For interpretation of the references to colour in this figure legend, the reader is referred to the web version of this article).

and after 5 h, between 18 and 33 mV, respectively. The isoelectric point of β LG was noted to be equal to 4.6, which is in concordance with the literature [30]. For further analysis, protein solutions were prepared at $\text{pH} = \text{pI}$ (4.6). According to the literature, β -lactoglobulin is a dimer at neutral pH. On the other hand, below pH 3 and above pH 7.5 it occurs as a monomer, but near its isoelectric point it can form tetramers or even higher oligomers [31]. According to the literature, the surface charge of a protein plays a role in ensuring protein stability, which can be controlled by (de)protonation of functional groups of the surface or counterion condensation on the protein surface. The study shows that different metals cations, pH [32–35] different electrolyte solutions [36] not only compensate the protein charge, but also provide attractive interaction between proteins represented by the cross-links of multivalent cations in protein crystals and by varied surface patterns of charges and hydrophobicity.

3.2. Kinetic and isothermic study of the zinc binding process

Kinetic and isothermal studies allow understanding the mechanism of formation of Zn- β LG complex and the factors influencing the rate of zinc ions binding to β -lactoglobulin. Therefore, the experimental kinetic data obtained were subjected to zero order, first, pseudo-first order and Weber-Morris intraparticle diffusion kinetics models.

The kinetics of zinc cation sorption to β -lactoglobulin for experimental data are presented in Fig. 3A. The plot shows the changes of zinc ion concentration in solution per unit time. According to Fig. 3A, it was noticed that the sorption kinetics process occurs as a non-homogeneous process and consists of three distinct stages: rapid initial sorption (stage I), gradual sorption (stages II and III) followed by chemical equilibrium. In order to calculate the reaction rate constants for the obtained steps, a zero-order kinetics model was applied as it describes in a simple way the individual steps of sorption characterized by a linear course. The unit of reaction rate constants obtained by using this model is the actual physical parameter that characterizes the rate of the process of zinc ion binding to β LG. The reaction rate constant for steps one, two and three were 4.23, 0.49 and 1.53 (mg/L)/min respectively. For step I the velocity of zinc ion sorption was definitely the highest. It results probably from protein surface saturation by zinc ions and interfaces the binding process during the first step of sorption. The constant velocity values are summarized in Table 2.

In order to better highlight the accuracy of the obtained experimental data, the first order and pseudo-first order kinetics model was used. Due to poor fitting of the first order model to the obtained experimental data, the pseudo-first order model was used. The standard error and Pearson correlation coefficient are given in Table 2. At stage I, the sorption process was achieved in the first 2 min. The molar ratio of zinc ions to β -LG at the maximum sorption capacity was 4 : 1. The sorption efficiency of β -lactoglobulin was 28.86 ± 1.19 % and the sorption capacity was 3.39 ± 0.14 mg/g. Stage II was completed after 5 min of incubation, and its efficiency of Zn^{2+} sorption increased to 33.86 ± 1.32 % while its sorption capacity was found to be 3.97 ± 0.16 mg/g. In case of stage III, the sorption process was

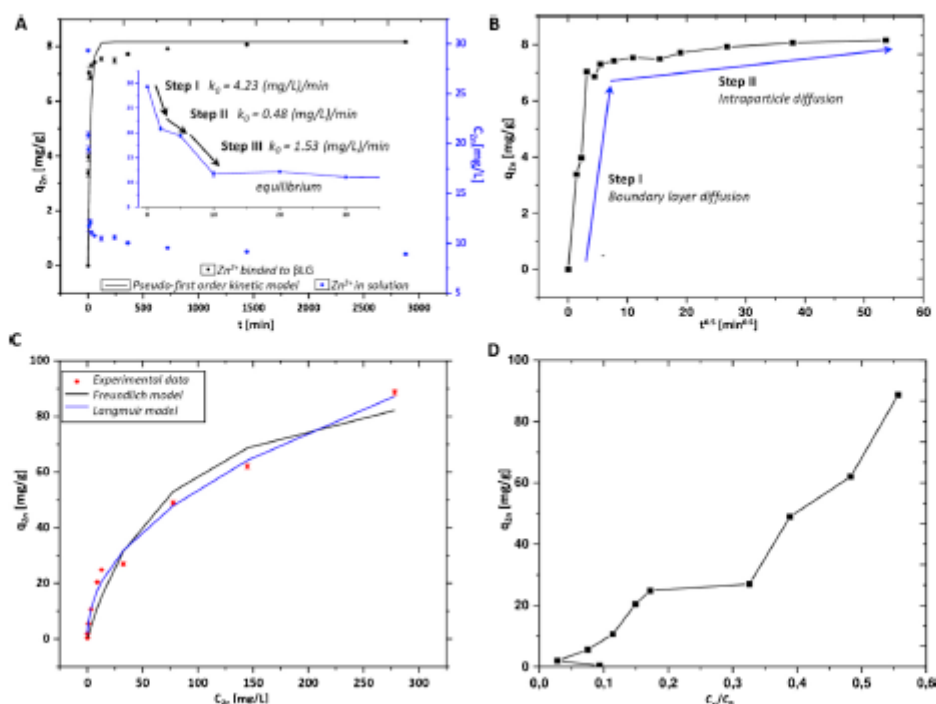


Fig. 3. Kinetics and isotherm of the process of zinc sorption onto β -lactoglobulin. The kinetic steps of the zinc ion sorption by β -lactoglobulin and values of the rate constants determined using: A – the concentration of zinc ions in aqueous solution at a certain period of time and the amount of zinc ions sorbed on β -lactoglobulin in time function for experimental data and pseudo-first order kinetic model. B – the Weber-Morris intraparticle diffusion model, C – isotherm of Zn^{2+} sorption onto β -lactoglobulin and fitting of the Freundlich and Langmuir isotherm models, D – sorption isotherm of Zn^{2+} as a function of C_e/C_0 .

Table 2
Kinetic model parameters for the zinc ions sorption by β -lactoglobulin.

Kinetics model	Parameter
Zero order kinetic model	
First step	$k_0 = 4.23$ [(mg/L)/min]
Second step	$k_0 = 0.48$ [(mg/L)/min]
Third step	$k_0 = 1.53$ [(mg/L)/min]
First order kinetic model	$k_1 = 0.05$ [1/min] $S = 11.1745$ $R^2 = 1.66$
Pseudo-first order kinetic model	$k_1 = 0.17$ [1/min] $S = 0.57$ $R^2 = 0.96$
Intraparticle diffusion model	$A = 7.31$ [mg/g] $K_p = 0.017$ [mg/g min ^{0.5}] $S = 0.10$ $R^2 = 0.88$

completed after 10 min, its efficiency was 60.02 ± 1.96 % and the quantity of Zn^{2+} adsorbed per 1 g of protein was 7.04 ± 0.23 mg/g. After 10 min of the sorption process, the chemical equilibrium was achieved. The maximum sorption efficiency and sorption capacity were 69.55 ± 0.37 % and 8.16 ± 0.04 mg/g, respectively.

Kinetic research of Pomastowski et al. [22] on the immobilization of zinc on casein also indicates a heterogeneous process – however, with two main stages and a stage of chemical equilibrium formed after 50 min. The differences in equilibrium time probably result from the structure of the protein. Casein is a large protein in the form of micelles formed from subunits consisting of four fractions of α_{s1} , α_{s2} , β , and κ -casein [37] in comparison with low-molecular (about 18 kDa) β -lactoglobulin. Moreover, the studies conducted by Pryschecha et al. in 2019

on casein binding to silver ions also confirm the heterogeneous character of the binding process with the first stage involving fast sorption combined with interface processes and the second stage involving gradual sorption followed by chemical equilibrium [27].

Kinetic data were also modeled for Weber-Morris intraparticle diffusion as a functional dependence of the zinc ions adsorption on $t^{0.5}$ (Fig. 3B). The initial step (Step I) can be attributed to the diffusion effects of the boundary layer or to the external process of surface sorption, while the second step may result from intraparticle diffusion of zinc ions. The values of the limit layer diffusion or surface adsorption constant (A) and the diffusion rate constant (K_p) are shown in Table 2. Additionally, the distribution coefficient (K_d) and Gibbs' free energy (ΔG), which amount to 913.43 and -16.72 kJ/mol respectively, were calculated (Table 3). The negative value of Gibbs' free energy indicates the spontaneous exoergic process of zinc binding to β -lactoglobulin.

The adsorption isothermal results are presented as a plot of the change of sorption capacity to zinc concentration in the solution (Fig. 3C). Additionally, the obtained experimental data were compared with the results obtained for Freundlich and Langmuir models. The parameters obtained from experimental data that characterize isothermal models are presented in Table 4. The rate constants for the Freundlich and Langmuir models are 6.18 L/g and 0.013 L/mg,

Table 3
Values of the distribution coefficient and the Gibbs' free energy change of the metal ions sorption.

q_e [mg/g]	C_e [mg/L]	K_d	T [K]	ΔG_0 [kJ/mol]
8.16	8.93	913.43	295	-16.72

Table 4
Parameters of Freundlich and Langmuir approximation mathematical models of adsorption isotherms to the experimental data.

Isotherm model	Parameter
Freundlich	$K_F = 6.18$ [L/g]
	$n = 0.47$
	$S = 22.95$
	$R^2 = 0.99$
Langmuir	$K_L = 0.013$ [L/mg]
	$q_m = 104.40$ [mg/g]
	$S = 25.63$
	$R^2 = 0.95$

respectively. It emerges from the calculated constants that the Freundlich model provides a better fit to the obtained experimental data. Therefore it can be assumed that the process has a surface character.

Isotherm as a function of C_e/C_0 indicates a more complex character of the process (Fig. 3D). The application of this dependence enables the identification of the two dominant steps in the sorption of zinc ions. In the first step, a monolayer of zinc ions is formed on the surface of β -lactoglobulin. Further, after the initial application of the zinc ion concentration of 37.5 mg/L, a second layer is formed with an intermediate step to the zinc ion concentration of 50 mg/L by binding the zinc ions to the already adsorbed monolayer. In addition, it can be observed that for zinc ion concentrations of 0.5 mg/L and 30 mg/L, the experimental data overlap with Freundlich and Langmuir models. The Freundlich and Langmuir models do not take into account the formation of multilayer layers. With this arrangement, the interaction between the first layer of zinc ions and β -lactoglobulin is strongest and decreases with each subsequent layer.

3.3. Spectroscopic analysis

UV-Vis spectroscopy and fluorescence measurements were used to understand the physicochemical properties of the obtained Zn- β LG complex. The maximum absorption for β LG was observed at 270–280 nm (Fig. S1), which is typical of proteins and is due to the absorption of aromatic amino acids included in the structure of β -lactoglobulin, which constitute 6.17 % of 162 amino acids – tryptophan (1.23 %), tyrosine (2.47 %) and phenylalanine (2.47 %) [38,39]. After addition of zinc ions to β -lactoglobulin, decrease in absorbance intensity with increasing time has been observed. This phenomenon may result from shielding aromatic chromophores of Tyr, Trp and Phe by zinc ions [21].

Moreover, the obtained UV-vis results were compared with fluorescence spectroscopy study. Fig. 4 shows the 3D profiles of the native protein (Fig. 4A) and zinc metal complex after 10 min (Fig. 4B), after 6 h (Fig. 4C), after 24 h (Fig. 4D) of incubation.

In the case of native protein, two main fluorescence bands were noticed at excitation (λ_{ex}) and emission wavelengths (λ_{em}) of 238, 326 nm (I); 278, 328 nm (II), respectively, while in the case of the metal complex a new fluorescence band appears. For the obtained Zn- β LG complex, the excitation and emission wavelengths were found to be as follows: 226, 328 nm (I), 278, 332 nm (II) and 270, 540 nm (I) after 10 min; 226, 328 nm (I), 278, 334 nm (II) and 268, 534 nm (III) after 6 h and 226, 328 nm (I), 276, 330 nm (II), 268, 534 nm (III) after 24 h of incubation, respectively. In case of the β -lactoglobulin treated with zinc ions, first, a slight shift of λ_{ex} / λ_{em} of the I and II fluorescence bands was observed. Then a drastic increase of fluorescence bands I and II was seen after 10 min, 6 h and 24 h of incubations compared to the native protein. However, the intensity of the fluorescent bands decreased with increasing incubation time.

This phenomenon can be connected with the amount of zinc ions involved in the process of binding to β LG protein, leading to the

possible conformation change around the aromatic amino acids contained in the protein structure. Atri et al. proved the effects of zinc binding on the aromatic amino acids structure and thermal stability of camel α -lactalbumin, which accounts for 3.25 % of the 123 amino acids in α -lactalbumin [40]. Moreover, changes in λ_{ex} / λ_{em} of Zn- β LG complex in comparison to the fluorescence of native protein can also result from the mechanism of resonance energy transfer or Förster resonance energy, caused by interaction of d-electron of zinc ions with π -electron of aromatic rings or Trp, Tyr and Phe [41]. The fluorescence changes observed after the immobilization process could be also caused by interaction of zinc ions with β LG via “sandwich” type binding, characteristic of zinc cation- π interaction of Trp [42].

In order to monitor the changes on the β LG structure after treatment with zinc ions during different periods of time (10 min, 6 h, 24 h), the Fourier transform spectroscopy method was used. Fig. 5A represents the spectra of native β -lactoglobulin (control), as well as the β -lactoglobulin after zinc binding reaction during 10 min, 6 h and 24 h.

The bands appearing in the 3270–3310 cm^{-1} range results from N–H stretching vibrations of the amide A band, whose frequency depends on the strength of hydrogen bond. In turn, the bands in the 3030–3100 cm^{-1} range are part of Fermi's resonance double and correspond to amide B [43].

The signals localized in the 2800–3000 cm^{-1} range derived from aliphatic primary amines due to the asymmetric and symmetric $-(\text{NH}_2)^+$ stretch and to CH aliphatic stretching [43].

The random coil region wavenumbers, i.e. (1640–1650 cm^{-1}) is associated with secondary protein structures such as β -sheets, random coils and α -helix in particular random coils [44]. The band at 1600–1700 cm^{-1} indicates the presence of amide I vibrations caused by stretching vibrations C=O with the participation of stretching vibrations C–N outside the phase, deformation CCN and the N–H in plane bend [43], [45].

The bands in the range of 1500–1600 cm^{-1} represent the area of amide II as a result of plane bending N–H and the C–N stretching vibrations with smaller contributions from CO plane bending and stretching C–C and C–N [43,45]. The bands at 1394 cm^{-1} and 1449 cm^{-1} are assigned to amino acid side chains in peptides and proteins caused by the asymmetric and symmetric CH_2 bending vibrations [46].

In the range of 1220–1330 cm^{-1} there is an area of amide III, resulting also from bending N–H and stretching C–N [45,47], while the signals in the 600–700 cm^{-1} range are derived from aliphatic monocarboxylic acids attached to the α -carbon atom [48].

All the signals recorded in MIR range (500–4000 cm^{-1}) were noticed to be present almost in all tested samples. The only exception were bands at 2168 cm^{-1} , 932 cm^{-1} , 883 cm^{-1} appeared only in control sample. This phenomenon is a consequence of zinc ions binding probably by the aromatic residues of amino acids present in β -lactoglobulin structure. Moreover, have been observed a trend of signal intensity during the incubation time - with increasing of the incubation time the intensity of signals increases.

The Raman spectroscopy (Fig. 5B) was used as a complementary technique to understand the process of binding zinc to β -lactoglobulin. Raman's spectroscopy simultaneously supplemented the information obtained in FT-IR analysis. Similarly to FT-IR spectra, Raman spectra were registered for native β -lactoglobulin (control) as well as for the β -lactoglobulin after zinc binding reaction during 10 min, 6 h and 24 h. Raman spectra recorded in the range of 400–4000 cm^{-1} also indicate changes in intensity depending on the incubation time of zinc ions with β -lactoglobulin in comparison to native protein as well as changes in signal shifts. Symmetrical vibrations, such as e.g. C–C and S–S bonds, are more clearly visible in Raman scattering, while asymmetrical vibrations, such as e.g. C=O, N–H and O–H, show strong absorption in infrared [49].

The signals at 2844 cm^{-1} , 2930 cm^{-1} , 3060 cm^{-1} noticed in both β -lactoglobulin (control) as well as in the β -lactoglobulin samples after

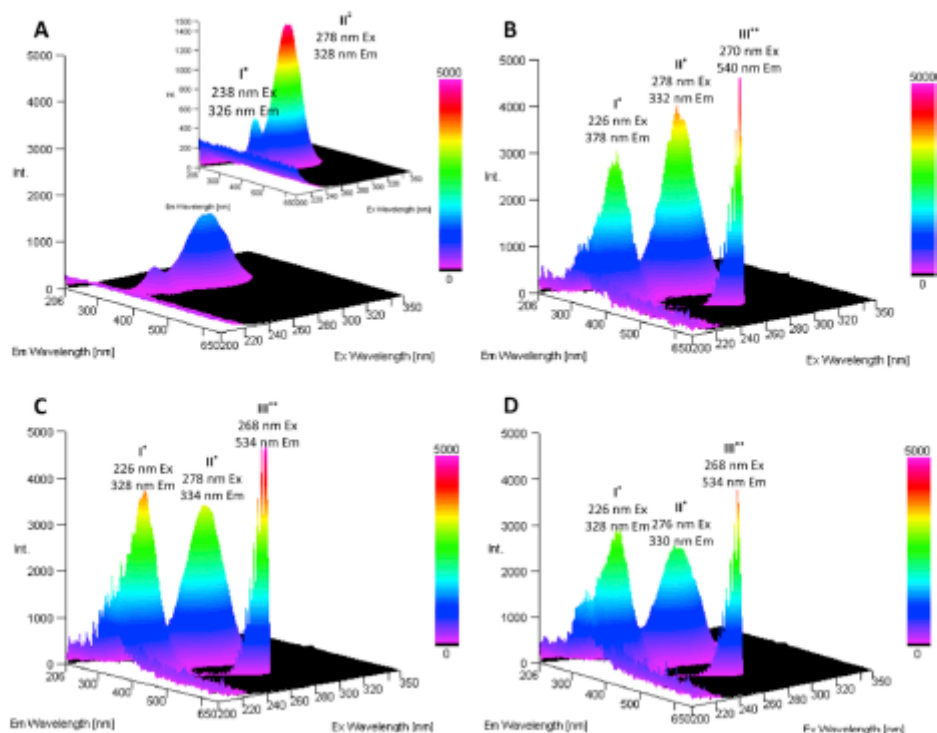


Fig. 4. Fluorescence of native β -lactoglobulin – A and Zn- β -lactoglobulin complex in 10 min – B, 6 h – C, 24 h – D, *occurred changes; **new signals.

zinc binding reaction during 10 min, 6 h and 24 h, derived from —C—H or —C—H stretch and the 3200 cm^{-1} band from O—H stretch [50]. The Raman spectra illustrate as well two regions of amides: (i) amide I ($1640\text{--}1680\text{ cm}^{-1}$) representing C—O stretching and a small amount of out-of-phase C—N stretching, (ii) amide III ($1200\text{--}1340\text{ cm}^{-1}$) comprising C—N stretching and N—H bending [51]. The location of the amide I band in the Raman spectrum depends on hydrogen binding and conformation of a polypeptide or protein molecule [52]. Amide I is usually assigned to unordered or disordered secondary protein structures such as α -helix, β -sheet, β -turn and random coil [51,52]. The band around $1400\text{--}1420\text{ cm}^{-1}$ changes the intensity and wavelength in the spectra at different times, which may be due to the involvement of COO^- groups in the Zn-BLG interaction [53,54]. This probably results from the interaction of zinc ions with carboxyl groups of Glu and Asp [52]. In turn, the change in the shape of the 1447 cm^{-1} band is presumably due to a different orientation of CH_3 and CH_2 groups because of the Zn interaction with the protein [49]. The band detected at 1274 cm^{-1} correspond to the structure of the β -sheet [52]. In addition, the $1020\text{--}1060\text{ cm}^{-1}$ band may also come from β -sheet vibrations [52].

The bands 757 cm^{-1} , 829 cm^{-1} , 1005 cm^{-1} are derived from amino acids such as Trp, Tyr, Phe respectively [49] while the $600\text{--}750\text{ cm}^{-1}$ region, resulting from the C—S stretching vibrations corresponding to the Met and Cys [52].

For both control samples as well as for β -lactoglobulin incubated with zinc ions during the 10 min, 6 h and 24 h, almost for all the signals registered in MIR range, the same trend of intensity changes has been noticed. Exceptions are the bands recorded at 557 cm^{-1} , 449 cm^{-1} , 435 cm^{-1} intensity that are present only in control sample. Moreover, the intensity of the respective bands, that most likely coming from helix breathing, torsions, and skeletal deformations [55], decreased in the

sample of β -lactoglobulin incubated with zinc ions. The same phenomenon has been noticed at 1095 cm^{-1} intensity, resulting from C—N stretching vibrations [62]. Moreover, the respective signal has been noticed to be splits in β -lactoglobulin samples incubated with zinc ions into three separate bands at 1098 cm^{-1} , 1035 cm^{-1} and 1023 cm^{-1} intensity caused by the vibrations of the aromatic residues.

Decreasing or disappearance of the signals in β -lactoglobulin samples incubated with zinc ions is a results of zinc ions interaction to the characteristic functional groups involved in the binding process. This results are in concordance with the FTIR analysis.

In order to find information about the local magnetic fields around atomic nuclei, and at the same time about conformational changes, NMR technique needed to be used. Therefore, the ^1H NMR method was used to provide information on different parts of the protein [56].

The ^1H NMR spectrum was obtained for resonance signals in the scale of chemical shift $0\text{--}12\text{ ppm}$. The position of resonance signals within the range of $6.6\text{--}8.8$ (Fig. 6A) ppm represents the aromatic and amide regions; therefore more HN nuclei are included in this range. The changes of chemical shift in the range of $0\text{--}5\text{ ppm}$ (Fig. 6B,C) indicates an aliphatic region with more HC nuclei. This result may suggest also the contribution of aromatic amino acids in binding zinc ions to β LG. Additionally, based on the obtained NMR spectra it can be concluded that the range characteristic for amide is less shielded and has a higher resonance frequency, while the resonance signals located in the range of aliphatic compounds are more shielded and their resonance frequency is lower. Analyzing the control spectrum of β -lactoglobulin and β LG complex, one can see that the resonance signals for the metallo-complex are sharper and more narrow while the signals for the control are wider.

Moreover, for metal complexes in both the aromatic as well as aliphatic ranges, the lowering or even the loss of intensity of certain

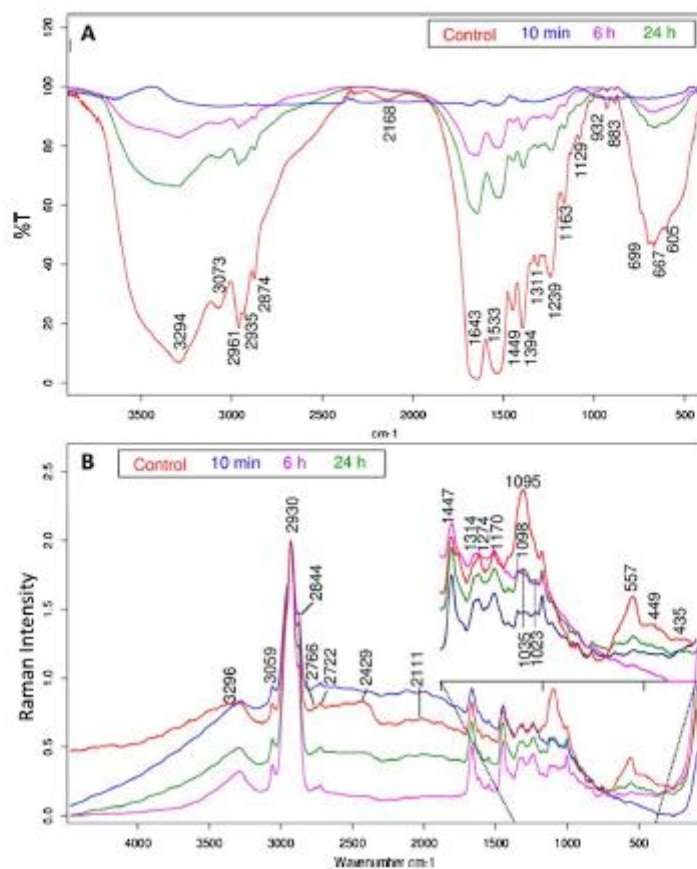


Fig. 5. Infrared spectra – A and Raman spectra – B for the β -lactoglobulin (control) and the β -lactoglobulin after zinc binding reaction during 10 min, 6 h and 24 h.

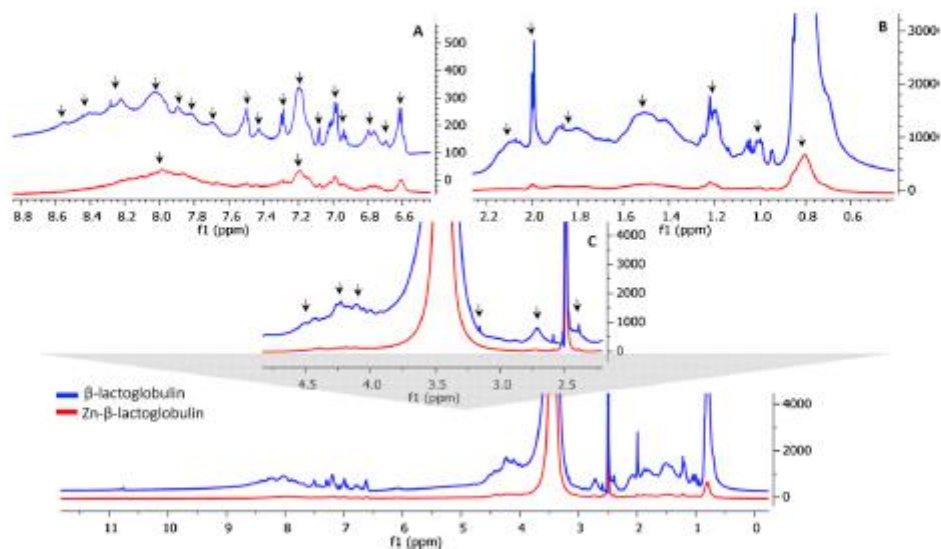


Fig. 6. NMR analysis of native β -lactoglobulin and Zn- β -lactoglobulin complexes. A – aromatic and amide regions; B, C – aliphatic region.

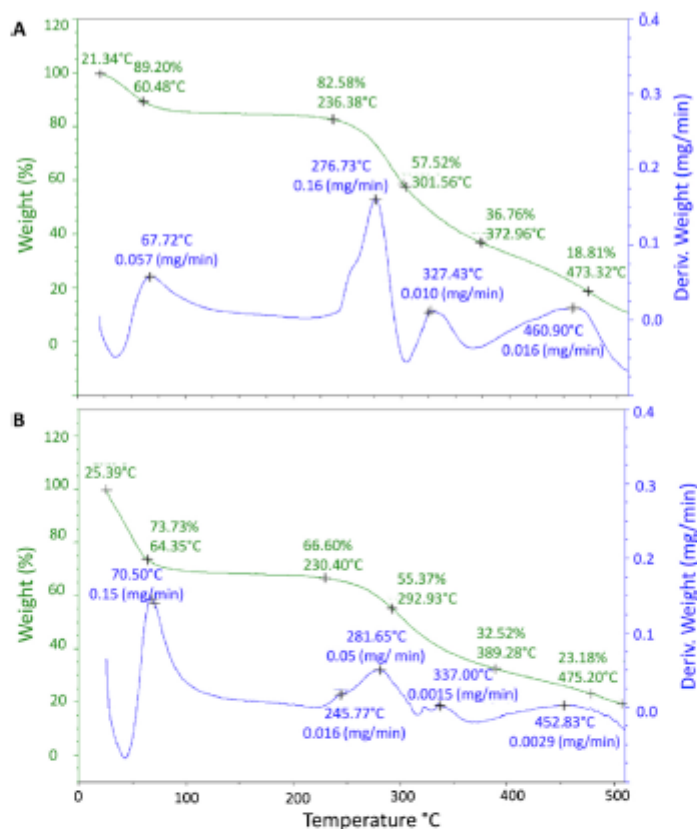


Fig. 7. Thermogravimetry and derivative thermogravimetric analysis of native β -lactoglobulin – A and Zn- β -lactoglobulin complexes after 24 h – B.

signals can be noticed. No significant chemical shifts were observed throughout the spectrum.

Decrease of the signal intensity on NMR spectra, analogous to FTIR and Raman results, in the case of Zn- β LG complex was observed. Binding of metal ions to aromatic residues of protein can be identified through a reduction intensities in bands of obtained complexes, as a interaction results of zinc ions d-electron with π -electrons of Trp, Phe [57].

3.4. Thermogravimetric analysis

In order to determine the thermostability of the obtained complex, thermal analysis was applied and, as it is known, proteins are thermally denatured during heating. Thermogravimetric results, ranged from 0 °C to 500 °C, of native β LG and Zn- β LG complex are shown in Fig. 7A,B. The obtained TG and DTG curves indicate that the breakdown of both native protein and Zn- β LG complex takes place in three main steps and each mass loss corresponds to a different kind of degradation. The first step is related to dehydration at 60.48 °C (loss in weight of 10.8 % for native protein) and at 64.35 °C (loss in weight of 35.65 % for zinc complex). The rate of weight loss of the Zn- β LG complex (0.15 mg/min) is higher than that of native β LG (0.057 mg/min). The data obtained in the first step show that native β -lactoglobulin is more thermally stable up to 236.38 °C.

The second step may be related to the thermal decomposition of the structure of protein and its components, i.e. amino acids.

During this step, in case of β LG, the weight loss occurred in the

temperature range from 236.38–372.96 °C with the evaluated mass loss up to 46 %, at degradation rate 0.16 mg/min (276.73 °C) and 0.010 mg/min (327.43 °C). As for the Zn- β -lactoglobulin complex, the weight loss process took place mainly in the range of 230.40–389.28 °C. Its mass loss was approximately 34.08 %. The mass loss rate in this range was 0.016 mg/min for 245.77 °C, 0.05 mg/min for 281.65 °C and 0.001491 mg/min for 337.00 °C. Another loss of mass was registered at the temperature of 473.32 °C (β LG) and 475.20 °C (Zn- β LG complex), exhibiting a single weight loss stage of 18.8 % and 19.25 %, respectively.

3.5. Microscopic (SEM/TEM/EDX) analysis and X-ray diffraction

The results of SEM and TEM studies presented in Fig. 8A-E indicate that zinc ions are immobilized uniformly on/into a multidimensional structure of microporous β LG protein. Moreover, according to the uniform dispersion of zinc element, represented as a bright light reflected on TEM/SEM images, the Zn- β LG complex occurs in the form of a homogeneous metallocomplex.

The obtained EDX spectra of Zn- β LG complex (Fig. 8F, G) indicated the presence of elemental zinc. In addition to zinc, a number of elements such as carbon, oxygen, copper, nitrogen and sulfur were also detected. The presence of these elements indicates the presence of organic matter on the surface of the Zn- β LG complex. The presence of Cu is related to the grid used for TEM analysis. The obtained Zn- β LG complex has an amorphous structure characteristic for protein samples visualized by application of TEM approach, in contrast to cryo-scanning

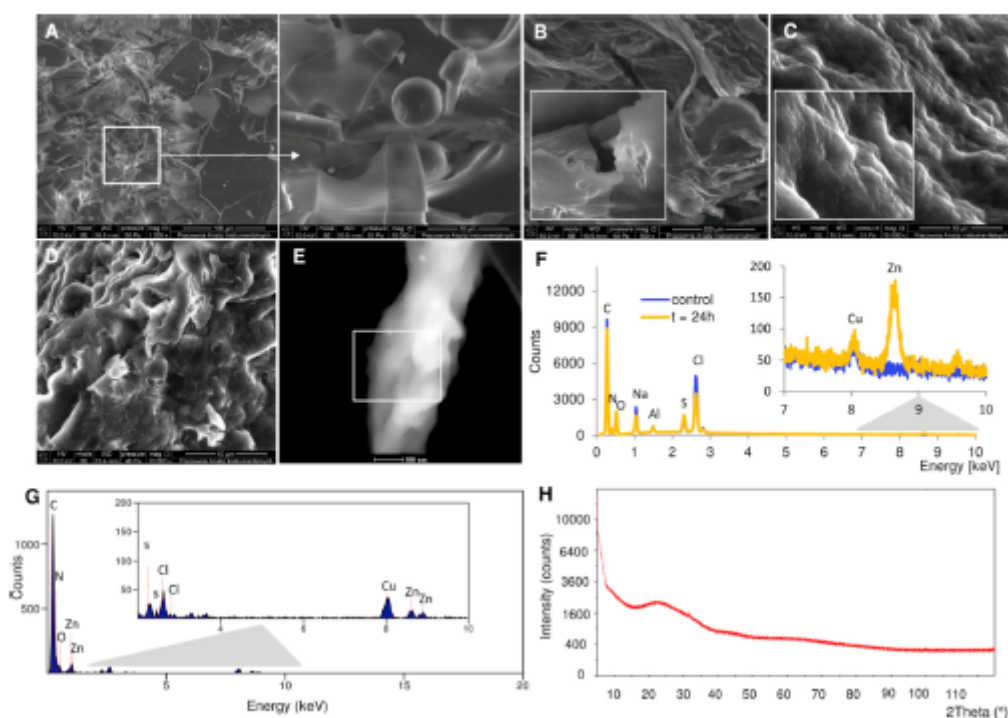


Fig. 8. SEM image of native β -lactoglobulin – A and Zn- β -lactoglobulin complex in 10 min – B, 6 h – C, 24 h – D. TEM image of Zn- β -lactoglobulin complex in time 24 h – E. SEM-EDX spectrum of native β -lactoglobulin and Zn- β -lactoglobulin complex in time 24 h – F. TEM-EDX spectrum of Zn- β -lactoglobulin complex in 24 h – G. X-ray diffraction of Zn- β -lactoglobulin complex in 24 h – H.

transmission electron microscopy (cryo-STEM), where single protein molecules with metal atoms can be visible [58].

Additionally, in order to highlight the provided information on structure, form and nature of the obtained complex, X-ray analysis with energy diffraction (XRD) was performed. XRD results presented in Fig. 8H proved the amorphous nature of Zn- β -LG complex and confirmed the absence of any crystal structure such as wurtzite form of zinc oxide nanoparticles. Those result are in contrast to our previous work where has been proven the metal nanoparticle formation as a results of metal ions interaction with protein [59].

3.6. Stability study of the Zn- β -lactoglobulin complex in synthetic physiological fluids

The stability of Zn- β -LG complex in synthetic models of (artificial) gastric (SGF) and intestinal fluids (SIF) was investigated. For this purpose the synthetic models in two variants – without (SGF, SIF) and with enzymes: SGF with Pepsin (SGFPs) and SIF with Pancreatin (SIFPN) (Section 2.5.1) – were applied. For this step, three concentrations (30, 50, 100 mg/L) of zinc ions were chosen for the synthesis of Zn- β -LG complexes (Zn- β -LG30; Zn- β -LG50 and Zn- β -LG100). As described in section 2.5.1, both filtrate and precipitate were subjected to ICP/MS analysis.

Fig. 9 represents the zinc ion concentration (C_{Zn}) of both Zn- β -LG precipitate (A) and Zn- β -LG filtrate (B) after evaluation in SGF/SIF and SGFPs/SIFPN models. In the case of Zn- β -LG precipitate (Fig. 9A), the C_{Zn} in SGF and SIF models was found to be 43.40 ± 0.95 ppb, 44.77 ± 0.57 ppb for Zn- β -LG30, 54.85 ± 0.47 ppb, 53.22 ± 0.93 ppb for Zn- β -LG50, and 110.76 ± 0.54 ppb, 110.77 ± 0.37 ppb for Zn- β -LG100, while in the case of SGFPs and SIFPN models, lower values of

C_{Zn} were recorded: 37.68 ± 1.20 and 34.06 ± 0.82 ppb (Zn- β -LG30), 40.01 ± 0.38 and 31.58 ± 0.58 ppb (Zn- β -LG50), 84.61 ± 0.89 and 78.46 ± 0.86 (Zn- β -LG100), respectively.

As for Zn- β -LG filtrate (Fig. 9B) without enzymes, the C_{Zn} in SGF and SIF models were undetectable (below LOQ) while in the case of Zn- β -LG filtrate with enzymes the C_{Zn} values in SGFPs and SIFPN models were noted as follows: 4.22 ± 0.10 ppb and 5.70 ± 0.54 ppb (Zn- β -LG30), 11.76 ± 0.60 ppb and 15.49 ± 1.17 ppb (Zn- β -LG50) and 23.75 ± 2.10 ppb and 28.68 ± 0.87 ppb (Zn- β -LG100), respectively. Lack of detectable zinc ions in the filtrate suggests high stability of Zn- β -LG complex in acidic (SGF) and alkaline environment (SIF). Calculated Gibbs' free energy (ΔG) of Zn- β -LG complex formation equal to -16.72 kJ/mol. It indicates spontaneous binding process of zinc ions to β -LG. This range of negative values of ΔG confirms that the system is thermodynamically stable.

SGF and SIF with enzymes simulate the digestion process taking place in the stomach and intestines. Zn- β -LG protein complex in selected systems is digested to low-molecular peptides. The enzyme pepsin cuts the peptide between amino acids containing a phenyl group in the side chain, such as tyrosine or phenylalanine, and amino acids containing two carboxylic groups, glutamic acid or aspartic acid [60]. In the case of trypsin present in pancreatin, the peptide bond is split between lysine and arginine [61]. Because of the fact that 3 kDa cut-off was used for ultrafiltration, the obtained peptides together with the zinc-bound peptides moved to the filtrate. In case of Zn- β -LG30 complex, 11.20 % (SGF) and 16.73 % (SIF) of zinc ions moved from the Zn- β -LG precipitate to the filtrate. For Zn- β -LG100 complex, the percentage values of zinc ions detected in the filtrate were found to be 28.06 % (SGFPs) and 36.55 % (SIFPN) in respective selected artificial models. The obtained results indicate that with the increase of C_{Zn} used for the Zn- β -LG

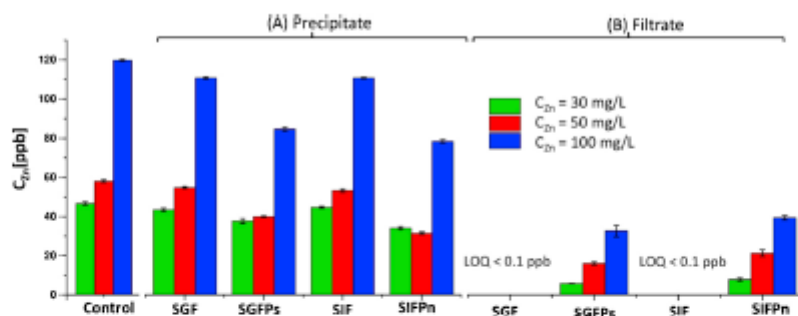


Fig. 9. Concentrations of zinc ions after evaluation of Zn- β -lactoglobulin complex in synthetic physiological fluid models.

Table 5

Percentage of zinc transferred into the filtrate.

	30 mg/L	50 mg/L	100 mg/L
SGFPs [%]	11.20	29.40	28.06
SIFPn [%]	16.73	49.03	36.55

synthesis, the amount of zinc ions transferred to the filtrate also increases. The percentage of total zinc concentration that penetrated the enzyme-filled Zn- β LG filtrate at zinc ion concentrations of 30, 50 and 100 mg/L is shown in Table 5.

According to the previous study conducted by our group [27] investigating the immobilization of silver ions by casein and stability of the silver-casein nanocomplex (Ag-CN) with and without enzyme, it was observed for both of the studied artificial (with enzyme and enzyme-free) systems that silver ions were recorded below LOQ. This is due to the fact that the Ag-CN system is a system of silver nanoparticles and metal complexes Ag-CN, which are a minority. In contrast to the present study, the enzymes used did not digest nanoparticles. Furthermore, digestion of Zn- β LG complex to zinc-peptides should be the starting point for further nutraceutical research.

4. Conclusion

The obtained results indicate that zinc ions are effectively immobilized by native β LG protein. Kinetic studies of zinc binding to β LG indicate that it is a heterogeneous process consisting of four steps: an initial step (I), a very fast step (2 min) associated with rapid sorption, two steps associated with gradual sorption (II, III), ending with reaching a chemical equilibrium. Additionally, isothermal studies indicate two dominant steps in the sorption of zinc ions. In the first step, a monolayer of zinc ions is formed on the surface of β LG, followed by a second intermediate layer with an already adsorbed monolayer. Spectroscopic study demonstrated that zinc ions are bonded to aromatic rings of tyrosine, tryptophan and phenylalanine, carboxylic groups of aspartic acid and glutamate. On the other hand, the use of thermal and electron microscopy proved that the zinc ion immobilization by β LG involves formation of a thermally stable, homogenous and amorphous Zn- β LG complex. Investigating the stability of the synthesized complex in synthetic physiological fluids confirmed its stability in acidic and alkaline conditions; it also offers an opportunity to expand the application research on zinc supplementation.

Conflict of interest

There are no conflicts of interest regarding this paper.

CRediT authorship contribution statement

Bogusław Buzewski: Conceptualization, Project administration. **Agnieszka Rodzik:** Methodology, Investigation, Writing - original draft. **Viorica Railean-Plugaru:** Methodology. **Myroslav Sprynskyy:** Formal analysis. **Paweł Pomastowski:** Conceptualization, Methodology, Project administration, Funding acquisition.

Acknowledgements

This work was financially supported by the National Science Centre within the framework of Opus 14 project No. 2017/27/B/ST4/02628 (2018-2021). We would like to thank Professor Tomasz Kowalkowski for technical assistance in the ICP-MS analysis.

Appendix A. Supplementary data

Supplementary material related to this article can be found, in the online version, at doi:<https://doi.org/10.1016/j.colsurfa.2020.124443>.

References

- [1] V. Abrahão, Nourishing the dysfunctional gut and whey protein, *Curr. Opin. Clin. Nutr. Metab. Care* 15 (2012) 480–484, <https://doi.org/10.1097/MCO.0b013e328356b71e>.
- [2] C.S. Tai, Y.Y. Chen, W.L. Chen, β -Lactoglobulin Influences Human Immunity and Promotes Cell Proliferation, *Biomed Res. Int.* 2016 (2016) 1–12, <https://doi.org/10.1155/2016/7123587>.
- [3] A.R. Corrochano, V. Buckin, P.M. Kelly, I. GIMin, invited review: whey proteins as antioxidants and promoters of cellular antioxidant pathways, *J. Dairy Sci.* 101 (2018) 4747–4761, <https://doi.org/10.3168/jds.2017-13618>.
- [4] J. Godovac-Zimmermann, I. Krause, M. Baranyi, S. Fischer-Frühholz, J. Juszcak, G. Erhardt, J. Buchberger, H. Klostermeyer, Isolation and rapid sequence characterization of two novel bovine β -Lactoglobulins I and J, *J. Protein Chem.* 15 (1996) 743–750, <https://doi.org/10.1007/BF01887148>.
- [5] K. Marshall, Therapeutic applications of whey protein, *Altern. Med. Rev.* 9 (2004) 136–156.
- [6] K. Sakai, K. Sakurai, M. Sakai, M. Hoshino, Y. Goto, Conformation and stability of thiol-modified bovine beta-lactoglobulin, *Protein Sci.* 9 (2000) 1719–1729.
- [7] R.S. Hotchkiss, L.L. Moldawer, S.M. Opal, K. Reinhart, L.R. Turnbull, J.-L. Vincent, Sepsis and septic shock, *Nat. Rev. Dis. Prim.* 2 (2016) 1–47, <https://doi.org/10.1016/j.physbeh.2017.03.040>.
- [8] X. Meng, Y. Bai, J. Gao, X. Li, H. Chen, Effects of high hydrostatic pressure on the structure and potential allergenicity of the major allergen bovine β -lactoglobulin, *Food Chem.* 219 (2017) 290–296, <https://doi.org/10.1016/j.foodchem.2016.09.153>.
- [9] S. Świątek, P. Komorek, G. Turner, B. Jachimska, β -Lactoglobulin as a potential carrier for bioactive molecules, *Bioelectrochemistry* 126 (2019) 137–145, <https://doi.org/10.1016/j.biochem.2018.12.006>.
- [10] M.C. Yang, H.H. Guan, M.Y. Liu, Y.H. Lin, J.M. Yang, W.L. Chen, C.J. Chen, S.J.T. Mao, Crystal structure of a secondary vitamin D3 binding site of milk β -lactoglobulin, *Protein Struct. Funct. Genet.* 71 (2008) 1197–1210, <https://doi.org/10.1002/prot.21811>.
- [11] B. Ghalandari, A. Ditsvilar, M. Esami-Moghadam, A.A. Saboury, T. Haertle, M. Amanlou, K. Purvar, Probing of the Interaction Between β -Lactoglobulin and the Anticancer Drug Oxaliplatin, *Appl. Biochem. Biotechnol.* 175 (2014) 974–987, <https://doi.org/10.1007/s12010-014-1341-0>.
- [12] W. Maret, The redox biology of redox-inert zinc ions, *Free Radic. Biol. Med.* 134

- (2019) 311–326, <https://doi.org/10.1016/j.frescradbiomed.2019.01.006>.
- [13] W. Maret, Zinc biochemistry: from a single zinc enzyme to a key element of life, *Adv. Nutr.* 4 (2013) 82–91, <https://doi.org/10.3945/an.112.003038.82>.
- [14] J.G. Cho, S. Park, C.H. Lim, H.S. Kim, S.Y. Song, T.-Y. Roh, J.-H. Sung, W. Suh, S.-J. Ham, K.-H. Lim, S.G. Park, ZNF224, Krüppel like zinc finger protein, induces cell growth and apoptosis-resistance by down-regulation of p21 and p53 via miR-663a, *Oncotarget* 7 (2016) 31177–31190, <https://doi.org/10.18632/oncotarget.8870>.
- [15] P.H. Lin, M. Sormersheim, H. Li, P.H.U. Lee, S.M. Steinberg, J. Ma, Zinc in wound healing modulation, *Nutrients* 10 (2018) 1–20, <https://doi.org/10.3390/nu10010016>.
- [16] Ddo N. Marreiros, K.J.C. Cruz, J.B.S. Morais, J.B. Beserra, J.S. Severo, A.R. Soares de Oliveira, Zinc and oxidative stress: current mechanisms, *Antioxidants* 6 (2017) 1–9, <https://doi.org/10.3390/antiox6020024>.
- [17] M. Ruz, F. Carrasco, P. Rojas, J. Codocero, J. Inostroza, K. Basfi-Fer, A. Valencia, K. Vásquez, J. Galgani, A. Pérez, G. López, M. Arredondo, F. Perez-Bravo, Zinc as a potential adjuvant in therapy for type 2 diabetes, *Food Nutr. Bull.* 34 (2013) 215–221, <https://doi.org/10.1177/156482651303400210>.
- [18] A. Carovic, I. Miletic, S. Sobajic, D. Blagojevic, M. Radusinovic, A. El-Sohemy, Effects of zinc on the mineralization of bone nodules from human osteoblast-like cells, *Biol. Trace Elem. Res.* 116 (2007) 61–71, <https://doi.org/10.1007/sf02685919>.
- [19] N.Z. Gammoh, L. Rink, Zinc in infection and inflammation, *Nutrients* 9 (2017) 1–25, <https://doi.org/10.3390/nu9060624>.
- [20] P. Pomastowski, M. Sprzynsky, P. Żurawka, K. Rafińska, M. Milanowski, J.J. Liu, M. Yi, B. Buzowski, Silver-Lactoferrin Nanocomplexes as a Potent Antimicrobial Agent, *J. Am. Chem. Soc.* 138 (2016) 7899–7909, <https://doi.org/10.1021/jacs.6b02699>.
- [21] P. Żurawka, J.J. Liu, M. Yi, P.P. Pomastowski, G. Sagandykova, M. Belka, J. David, T. Bączak, K. Szafranski, B. Żołowska, J. Stawinski, C.T. Supuran, M.W. Wong, B. Buzowski, Target-based drug discovery through inversion of quantitative structure–drug property relationships and molecular simulation: Ca IX-sulphonamide complexes, *J. Enzyme Inhib. Med. Chem.* 33 (2018) 1430–1443, <https://doi.org/10.1080/14756366.2018.1511551>.
- [22] P. Pomastowski, M. Sprzynsky, B. Buzowski, The study of zinc ions binding to casein, *Colloids Surf. B Biointerfaces* 120 (2014) 21–27, <https://doi.org/10.1016/j.colsurfb.2014.03.009>.
- [23] P. Pomastowski, J. Walczak, M. Gawin, S. Bocian, W. Piekoszowski, B. Buzowski, HPLC separation of casein components on a diol-bonded silica column with MALDI TOF/TOF MS identification, *Anal. Methods* 6 (2014) 5236–5244, <https://doi.org/10.1039/c4ay00895h>.
- [24] M. Sprzynsky, T. Kowalkowski, H. Tutu, E.M. Cukrowska, B. Buzowski, Ionic liquid modified diatomite as a new effective adsorbent for uranium ions removal from aqueous solution, *Colloids Surf. A Physicochem. Eng. Asp.* 465 (2015) 159–167, <https://doi.org/10.1016/j.colsurfa.2014.10.042>.
- [25] R.E. Reed, M.R. Matsumoto, Modeling cadmium adsorption by activated carbon using the Langmuir and Freundlich isotherm expressions, *Sep. Sci. Technol.* 28 (1993) 2179–2195, <https://doi.org/10.1080/01496399308816742>.
- [26] I. Gölseren, Y. Fang, M. Corredig, Whey protein nanoparticles prepared with desolvation with ethanol: Characterization, thermal stability and interfacial behavior, *Food Hydrocol.* 29 (2012) 258–264, <https://doi.org/10.1016/j.foodhyd.2012.03.015>.
- [27] O. Pryshchepa, G.N. Sagandykova, P. Pomastowski, V. Raftoon-Plugaru, A. Król, A. Rogowska, A. Rodzik, M. Sprzynsky, B. Buzowski, A new approach for spontaneous silver ions immobilization onto Casein, *Int. J. Mol. Sci.* 20 (2019) 1–18, <https://doi.org/10.3390/ijms20163864>.
- [28] L. Zhan, Y. Liu, X. Xie, C. Xiong, Z. Nie, Heat-Induced Rearrangement of Disulfide Bond of Lactoglobulin Characterized by Multiply Charged MALDI-TOF/TOF Mass Spectrometry, *Anal. Chem.* 90 (2018) 10670–10675, <https://doi.org/10.1021/acs.analchem.8b02563>.
- [29] X. Wu, Y. Lu, H. Xu, D. Lin, Z. He, H. Wu, L. Liu, K. Gao, Z. Wang, X. Lin, J. Huang, G. Wang, C. Zhu, Reducing the Allergenic Capacity of β -Lactoglobulin by Covalent Conjugation With Dietary Polyphenols, *Food Chem.* 256 (2018) 427–434, <https://doi.org/10.1016/j.foodchem.2018.02.158>.
- [30] L. Pérez-Panles, C. Drummond, J. Faruado, D. Bastos-González, Adsorption of milk proteins (β -Casein and β -Lactoglobulin) and BSA onto hydrophobic surfaces, *Materials (Basel)* 10 (2017) 1–25, <https://doi.org/10.3390/ma10080893>.
- [31] D. Mercadante, L.D. Melton, G.E. Norris, T.S. Loo, M.A.K. Williams, R.C.J. Dobson, G.B. Jameson, Bovine β -Lactoglobulin is dimeric under imitative physiological conditions: Dissociation equilibrium and rate constants over the pH range of 2.5–7.5, *Biophys. J.* 103 (2012) 303–312, <https://doi.org/10.1016/j.bpj.2012.05.041>.
- [32] F. Roosen-Runge, B.S. Hock, F. Zhang, Q. Kohlbacher, F. Schreiber, Interplay of pH and binding of multivalent metal ions: Charge inversion and renaturation condensation in protein solutions, *J. Phys. Chem. B* 117 (2013) 5777–5787, <https://doi.org/10.1021/jp401874i>.
- [33] F. Roosen-Runge, F. Zhang, F. Schreiber, R. Roth, Ion-activated attractive patches as a mechanism for controlled protein interactions, *Sci. Rep.* 4 (2014) 1–5, <https://doi.org/10.1038/srep07016>.
- [34] B. Braunschweig, F. Schulze-Zachau, E. Nagel, K. Engelhardt, S. Stoyanov, G. Gochev, K. Khristov, E. Mileva, D. Exerowa, R. Miller, W. Peukert, Specific effects of Ca²⁺ ions and molecular structure of β -lactoglobulin interfacial layers that drive macroscopic foam stability, *Soft Matter* 12 (2016) 5995–6004, <https://doi.org/10.1039/c6sm00636a>.
- [35] M.E. Richter, G.G. Gochev, B. Braunschweig, Specific Ion Effects of Trivalent Cations on the Structure and Charging State of β -Lactoglobulin Adsorption Layers, *Langmuir* 35 (2019) 11299–11307, <https://doi.org/10.1021/acs.langmuir.9b01803>.
- [36] F.R. Beterlein, T. Clark, B. Braunschweig, K. Engelhardt, L. Glas, W. Peukert, Carboxylate Ion Pairing with Alkali-Metal Ions for β -Lactoglobulin and Its Role on Aggregation and Interfacial Adsorption, *J. Phys. Chem. B* 119 (2015) 5505–5517, <https://doi.org/10.1021/acs.jpch.5b01944>.
- [37] D.G. Dalgleish, M. Corredig, The structure of the casein micelle of milk and its changes during processing, *Annu. Rev. Food Sci. Technol.* 3 (2012) 449–467, <https://doi.org/10.1146/annurev-food-022811-101214>.
- [38] F.X. Schmid, Biological Macromolecules: UV-Visible Spectrophotometry, *Encycl. Life Sci.* (2001) 1–4, <https://doi.org/10.1038/npg.els.0003142>.
- [39] J.E. Kinsella, D.M. Whitehead, Proteins in whey: chemical, physical, and functional properties, *Adv. Food Nutr. Res.* 33 (1989) 343–438, [https://doi.org/10.1016/S1043-4526\(08\)60130-8](https://doi.org/10.1016/S1043-4526(08)60130-8).
- [40] M.S. Alri, A.A. Saboury, A.A. Moosavi-Movahedi, K. Kavousi, S. Arfaeizadeh, Effects of zinc binding on the structure and thermal stability of camel alpha-lactalbumin, *J. Therm. Anal. Calorim.* 120 (2015) 481–488, <https://doi.org/10.1007/s10973-014-4274-5>.
- [41] A.B.T. Ghisaldoo, S.J. Chung, Intrinsic tryptophan fluorescence in the detection and analysis of proteins: A focus on Förster resonance energy transfer techniques, *Int. J. Mol. Sci.* 15 (2014) 22518–22538, <https://doi.org/10.3390/ijms15122518>.
- [42] L.J. Juszczyk, A.S. Eisenberg, The Color of Cation- π Interactions: Subtleties of Amino-Tryptophan Interaction Energetics Allow for Radical-like Visible Absorbance and Fluorescence, *J. Am. Chem. Soc.* 139 (2017) 8302–8311, <https://doi.org/10.1021/jacs.7b03442>.
- [43] A. Barth, Infrared spectroscopy of proteins, *Biochim. Biophys. Acta Bioenerg.* 1767 (2007) 1073–1101, <https://doi.org/10.1016/j.bbabio.2007.06.004>.
- [44] X. Luo, T. Vastljovic, L. Ramchandran, Effect of adjusted pH prior to ultrafiltration of skim milk on membrane performance and physical functionality of milk protein concentrate, *J. Dairy Sci.* 99 (2016) 1083–1094, <https://doi.org/10.3168/jds.2015-9842>.
- [45] T. Kramić, N.S. Obrađović, M.B. Rakin, Application of whey protein and whey protein hydrolysate as protein based carrier for probiotic starter culture, *Food Chem.* 293 (2019) 74–82, <https://doi.org/10.1016/j.foodchem.2019.04.062>.
- [46] M. Gastelli Guidi, C. Mirri, E. Fratini, V. Licursi, R. Negri, A. Marcolli, R. Amendola, In vivo skin leptin modulation after 14 MeV neutron irradiation: A molecular and FT-IR spectroscopic study, *Anal. Bioanal. Chem.* 404 (2012) 1317–1326, <https://doi.org/10.1007/s00216-012-6018-3>.
- [47] E.L. Farguhar, The Infrared Spectra of Primary Aromatic Amides, Iowa State University of Science and Technology, 1962.
- [48] S. Pandharajan, M. Umadevi, R.K. Rajaram, V. Ramakrishnan, Infrared and Raman spectroscopic studies of L-valine L-valinium perchlorate monohydrate, *Spectrochim. Acta - Part A Mol. Biomol. Spectrosc.* 62 (2006) 630–636, <https://doi.org/10.1016/j.saa.2005.02.008>.
- [49] S. Ikeda, E.C.Y. Li-Chan, Raman spectroscopy of heat-induced fine-stranded and particulate β -lactoglobulin gels, *Food Hydrocol.* 18 (2004) 489–498, <https://doi.org/10.1016/j.foodhyd.2003.07.003>.
- [50] E.C.Y. Li-Chan, Vibrational spectroscopy applied to the study of milk proteins, *Dairy Sci. Technol.* 87 (2007) 443–458, <https://doi.org/10.1051/lait:2007023>.
- [51] D. Karouski, R.P. Van Duyn, I.K. Lednev, Exploring the structure and formation mechanism of amyloid fibrils by Raman spectroscopy: a review, *Analyst* 140 (2015) 4967–4980, <https://doi.org/10.1039/c5an00342c>.
- [52] E. Li-Chan, S. Nakai, M. Hirotsuka, Raman spectroscopy as a probe of protein structure in food systems, *Protein Struct. Relationships Foods* (1994) 163–197, https://doi.org/10.1007/978-1-4615-2670-4_8.
- [53] A.D. Roddick-Lanzetta, P.A. Connor, A.J. McQuillan, An in situ infrared spectroscopic study of the adsorption of lysine to TiO₂ from an aqueous solution, *Langmuir* 14 (1998) 6479–6484, <https://doi.org/10.1021/la980425n>.
- [54] M. Nara, H. Torii, M. Tasumi, Correlation between the vibrational frequencies of the carboxylate group and the types of its coordination to a metal ion: An ab initio molecular orbital study, *J. Phys. Chem.* 100 (1996) 19812–19817, <https://doi.org/10.1021/jp9615924>.
- [55] F. Zhu, N.W. Isaacs, L. Hecht, L.D. Barron, Raman optical activity: a tool for protein structure analysis, *Structure* 13 (2005) 1409–1419, <https://doi.org/10.1016/j.str.2005.07.009>.
- [56] J. Belloque, G.M. Smith, Thermal Denaturation of β -Lactoglobulin. A 1H NMR Study, *J. Agric. Food Chem.* 46 (1998) 1805–1813, <https://doi.org/10.1021/jf9709313>.
- [57] W. Becker, K.C. Bhattiprolu, N. Gubensik, K. Zangger, Investigating protein-ligand interactions by solution nuclear magnetic resonance spectroscopy, *ChemPhysChem* 19 (2018) 895–906, <https://doi.org/10.1002/cphc.201701253>.
- [58] N. Elad, G. Bellapadrona, I. Houben, I. Sagl, M. Elbaum, Detection of isolated protein-bound metal ions by single-particle cryo-STEM, *Proc. Natl. Acad. Sci. U. S. A.* 114 (2017) 11139–11144, <https://doi.org/10.1073/pnas.1708609114>.
- [59] A. Król, P. Pomastowski, K. Rafińska, V. Raftoon-Plugaru, B. Buzowski, Zinc oxide nanoparticles: synthesis, antiseptic activity and toxicity mechanism, *Adv. Colloid Interface Sci.* 249 (2017) 37–52, <https://doi.org/10.1016/j.cis.2017.07.033>.
- [60] J. Tang, R.N.S. Wong, Evolution in the structure and function of aspartic proteases, *J. Cell. Biochem.* 33 (1987) 53–63, <https://doi.org/10.1002/jcb.240330106>.
- [61] Eastwood Leung Hon-Chiu, Integrative Proteomics, Croatia, (2012).
- [62] S. Parker, Applications of Infrared, Raman, and resonance raman spectroscopy in biochemistry, *Book Review* 9 (6) (1983).

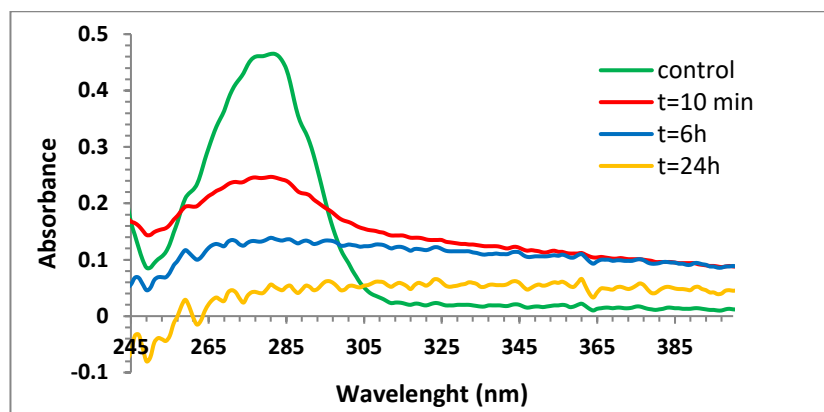


Fig. S1. UV-Vis spectra of native β -lactoglobulin – **A** and Zn- β -lactoglobulin complex in time 10 min – **B**, 6 h – **C**, 24 h – **D**.

4.3. The study of zinc ions binding to α_{S1} -, β -, κ -casein

[P3] **A. Rodzik**, P. Pomastowski, V. Railean-Plugaru, M. Sprynskyy, B. Buszewski, *The study of zinc ions binding to α_{S1} -, β -, κ -casein*, International Journal of Molecular Sciences, 2020, 21(21), 1-18, doi: 10.3390/ijms21218096.



Article

The Study of Zinc Ions Binding to α_{S1} -, β - and κ -Casein

Agnieszka Rodzik ^{1,2}, Paweł Pomastowski ^{2,*}, Viorica Railean-Plugaru ^{1,2},
Myroslav Sprynskyy ¹ and Bogusław Buszewski ^{1,2}

¹ Department of Environmental Chemistry and Bioanalysis, Faculty of Chemistry, Nicolaus Copernicus University, Gagarina 7, 87-100 Toruń, Poland; agnieszka.rodzik1@gmail.com (A.R.); rviorela@yahoo.com (V.R.-P.); mspryn@chem.umk.pl (M.S.); bbusz@chem.umk.pl (B.B.)

² Centre for Modern Interdisciplinary Technologies, Nicolaus Copernicus University, Wileńska 4, 87-100 Toruń, Poland

* Correspondence: p.pomastowski@umk.pl; Tel.: +48-56-6114308; Fax: +48-56-6656038

Received: 7 September 2020; Accepted: 28 October 2020; Published: 30 October 2020



Abstract: The presented studies focused on the specificity binding of particular casein fractions: α_{S1} -, β - and κ -casein (α_{S1} CN, β CN, κ CN), with zinc ions. The binding mechanism was determined by kinetic modeling using results of batch sorption. For this goal, models of zero-order kinetics, pseudo-first-order, pseudo-second-order and Weber–Morris intraparticle diffusion were used. The formation of Zn- α_{S1} CN, Zn- β CN and Zn- κ CN complexes was additionally monitored using spectroscopic methods such as Fourier transform infrared spectroscopy (FT-IR) and Raman spectroscopy, characterizing active functional groups involved in the binding process. Additionally, a mass spectrometry technique—matrix-assisted laser desorption/ionization time-of-flight mass spectrometry (MALDI-TOF MS)—was used to characterize respective protein fractions and obtained complexes. Spectroscopic and spectrometric studies were carried out both before and after binding the protein with zinc ions. The obtained results showed the difference in Zn- α_{S1} CN, Zn- β CN and Zn- κ CN complexes created at separate kinetic stages. On the basis of instrumental studies, a significant influence of acidic (glutamic acid (Glu), aspartic acid (Asp)) and aromatic (tryptophan (Trp), phenylalanine (Phe), tyrosine (Tyr)) amino acids on the formation of metal complexes was proven. In turn, spectrometric studies allowed determining the molecular masses of casein isoforms before and after binding to zinc ions.

Keywords: α -casein; β -casein; κ -casein; zinc ions; sorption; kinetic; FT-IR; Raman; MALDI-TOF MS

1. Introduction

Casein is recognized as the main cow's milk protein, accounting for about 80% of the total milk protein content [1]. It is not a homogeneous protein but consists of several fractions. The main fractions are α (α_{S1} , α_{S2})-, β - and κ -casein (α CN, β CN and κ CN). They form colloidal aggregates called micelles in combination with calcium phosphate [2]. The primary role of caseins in milk is to ensure the effective transport of calcium and phosphate from the mammary gland directly to the newborn baby [3]. The main components of casein (α CN, β CN and κ CN) form a strong micellar complex stabilized by van der Waals forces, hydrophobic effects, hydrogen bonding and electrostatic and steric stabilization [2]. In addition, micelles are stabilized by physicochemical properties such as the ability of phosphorylated serine residues to bind to calcium ions and the amphiphilic nature of κ CN, which is a fraction that is glycosylated and responsible for stabilizing micelles on the surface [4]. The size of micelles varies depending on the amount of specific fractions—mainly κ CN—cow feed and season (in summer, the micelles are smaller, and in winter, the opposite is true) [5]. The amount of calcium ions is also

important in forming stable micelles [5]. In addition, during casein hydrolysis, caseinophosphopeptides are formed, which bind calcium through their phosphoserine residues, affecting casein stability [6]. It turns out that caseins have a natural ability to bind to other metal ions such as silver [7], iron [8] and zinc [9,10]. Despite this knowledge, there are still many uncertainties in the mechanism of binding metal ions to casein fractions, especially their quantitative contribution and the role of the active functional group in this process.

Fraction α_{S1} CN accounts for 40% overall casein in bovine milk. It is a single-chain polypeptide with a sequence containing 199 amino acid residues containing sixteen serine (Ser) residues, eight of which are phosphorylated and seven of which occur between 43 and 80 residues [11]. Furthermore, this highly acidic segment also contains twelve carboxyl residues and is responsible for the negative charge of the molecule [4,11]. As a result of negative charges at neutral pH, phosphoric residues and secondary carboxylic acid residues have a strong affinity for metals [9]. The second significant fraction in the total amount of caseins in milk is β CN. β CN is a single-chain polypeptide with five residual phosphoserines with the first four forming the phosphorylation center [4,11]. It represents about 35% of bovine milk casein content and consists of 209 amino acids residues. β CN is strongly amphipathic and the N-terminal part of the β CN molecule (1–43 residues) contains a negative protein charge, has low hydrophobicity and consists of only two prolines (Pro) residues, representing about 17%. The β CN central section, i.e., residues 44–135, has a low charge and moderate hydrophobicity, while the C-terminal part of the molecule (136–209 residues) contains many non-polar residues and is therefore highly hydrophobic [4]. κ CN is the third main but smallest casein protein (169 residues) with a low calcium sensitivity. It is the only form of casein that can be glycosylated in addition to phosphorylation [4]. Phosphorylation compared to α CN and β CN can also take place in the rest of the threonine (Thr). Thr takes part in binding with zinc ions [9]. Due to the considerable distances between residues of SerP and ThrP κ -casein, there is no phosphorylation center [4].

The structure of casein micelles most probably consists of a form of α CN and β CN located in the inside of the micelles and κ CN forming the outside layer stabilizing the micelles sterically [12]. The stabilization of micelles is possible thanks to the hydrophilic part of κ CN protruding into an aqueous surrounding—glycomacropeptide. The actual internal structure of casein micelles is not fully understood and explained [13]. For this reason, several models were developed to characterize casein micelle [14]. The main models proposed are (i) the submicellar (subunit) model [15], (ii) the coat-core model [16] and (iii) the internal structure model [17].

The colloidal nature of milk poses a great challenge to isolate proteins. Casein micelles and fat globules function as separate phases, preventing milk filtration and complicating the usual separation methods [18]. Since purified individual milk proteins have better functionality than their native protein mixtures, there is great interest in developing easier methods of preparing pure casein and its isoforms on a large scale [2]. To eliminate protein–protein interactions, different concentrations of urea [19], dimethylformamides [20], β mercaptoethanol [21] or dithiothreitol [19] are used, among other things, to change the structure of proteins by splitting hydrogen bonds and reducing disulphide bonds. Differences in α CN, β CN and κ CN solubility in urea solution allow for separating different components [2]. In addition, the combination of proteins with d-electron metal ions allows for obtaining nanocomposites such as metallocomplexes (with zinc ions [9], uranium(VI) [22]) and nanoparticles (with silver ions) [23] with a wider spectrum of biological activity. The mechanisms by which a protein binds metal ions, which often improve protein function, are not well known [24].

Zinc ions are essential for many living systems, playing a significant role in physiological reactions and diseases [25]. Zinc is a structural and catalytic component of many proteins. It modulates the functions of glutamate and neurotransmitter receptors, regulates transcription factors and inhibits tyrosine phosphatase proteins [26]. This element is also essential for the functioning of many enzymes. Its deficiency contributes to congenital defects and acquired immunological responses [27]. Understanding the mechanism of zinc ion binding to casein and structural changes in protein induced by these ions can prevent immune deficiencies or disease changes [10]. The use of knowledge about the

mechanism of binding zinc to casein can be a tool in their medical application [28]. Pomastowski and co-authors studied the interaction of zinc ions with casein [9], however, the distribution of the zinc ion binding in various casein fractions was not known.

Hence, the main goal of this study was to explain the binding process of zinc ions to individual casein fractions. Therefore, models of zero-order kinetics, pseudo-first-order, pseudo-second-order and Weber–Morris intraparticle diffusion were applied. This objective has been achieved by previous characterization of individual casein fractions (α_{S1} CN, β CN, κ CN) isolated from cow's milk, and the study of their dispersion stability, isoelectric point and molecular masses. In addition, spectroscopic (FT-IR, Raman) and spectrometric (MALDI-TOF MS) studies were carried out to determine the contribution of the active functional group in the binding process of zinc ions to casein fractions.

2. Results and Discussion

2.1. Characteristics of α_{S1} CN, β CN, κ CN

In order to determine the isoelectric point and to examine protein stability, the zeta potential value was measured for the initial time ($t = 1$ min), after one hour ($t = 1$ h) and after five hours ($t = 5$ h). The zeta potential results of α_{S1} CN, β CN and κ CN as a function of pH (2–11) are presented in Figure 1. Isoelectric points (pI) for α_{S1} CN, β CN and κ CN were found to be 4.80 ± 0.72 , 4.55 ± 2.15 and 4.40 ± 0.28 , respectively. The surface charges of all investigated proteins are in the range of -35 – $+32$ mV. In addition, it was observed that with increasing time, the zeta potential values changed and protein stability was noticed after $t = 1$ h and $t = 5$ h. At low pH values, the surface charge of proteins was positive and the zeta potentials became more negative with increasing pH. The results show that the more stable proteins are β CN and κ CN and the least stable is α_{S1} CN. The potential values of α_{S1} CN, β CN and κ CN at pH = 2 and pH = 3 were found between +15 and +32 mV, except $t = 1$ min for α_{S1} CN, for which the zeta potential was noticed between +3 and +14 mV. Above pH = 3, a decrease in the zeta potential to -20 – -30 mV at pH = 5 for each protein was observed. In the case of $t = 1$ min for α_{S1} CN, the decrease in the zeta potential occurred from pH = 4 to pH = 6.

The zeta potential provides an indicative measure of dispersion stability. The chemical properties of the surface of the particles affect the zeta potential of each dispersion. The surface chemistry can be modified by changing the pH, surfactant concentration and salt concentration. Therefore, it is important to determine the effect of pH on the zeta dispersion potential [29].

The protein charge is mainly controlled by two processes: (de)protonation of functional surface groups and counter-ions condensation on the protein surface [30]. Farrel et al., 2004 [31], indicated that pI for α_{S1} CN, β CN and κ CN were 4.92–5.05, 5.41 and 5.77, respectively, while according to Egito et al., 2002 [32], the pI values for α_{S1} CN, β CN and κ CN were 4.4–6.3, 4.4–5.9 and 3.5–5.5, respectively. The pI depend on the origin of the sample, the method of determination and the used electrolyte [23].

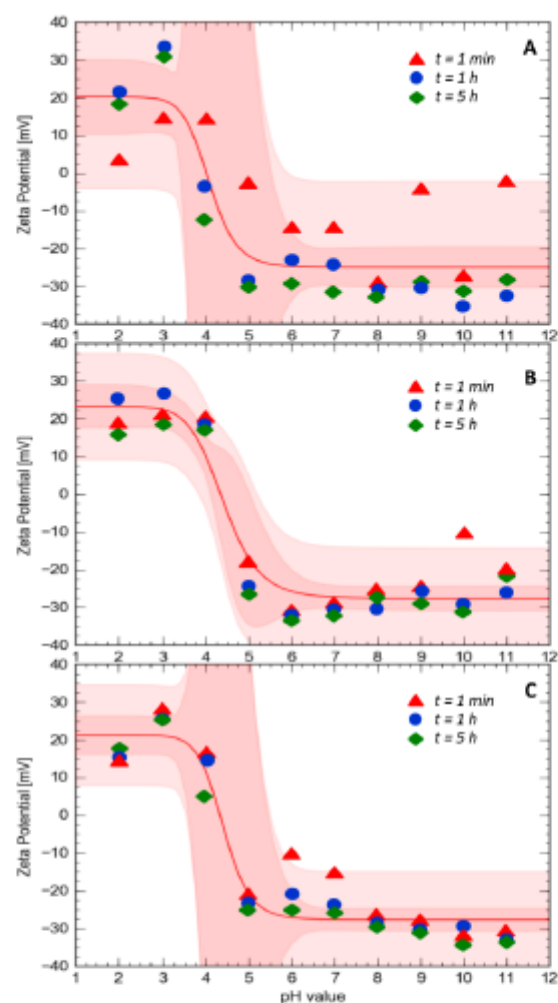


Figure 1. Zeta potential of α_{S1} CN (A), β CN (B) and κ CN (C) as a function of pH. The red line represents the sigmoidal fit trend line. Darker red indicates a confidence band, while lighter indicates a prediction band.

2.2. Kinetic Study of the Zinc Binding Process

Kinetic studies contribute to the understanding of the mechanism of binding casein isoforms (α_{S1} CN, β CN and κ CN) with zinc ions. The obtained experimental kinetic data were examined with reference to zero-, pseudo-first- and pseudo-second-order kinetic models and the Weber–Morris intraparticle diffusion model. Matching the experimental kinetic data to the models allowed for explaining the rate of the binding of zinc ions to proteins, but also for determining the degree of adsorption of zinc ions on the protein adsorbent.

Figure 2A shows the kinetics of the binding process of zinc ions to casein fractions in the form of a plot of concentration of zinc ions in solution per unit of time. For α_{S1} CN, three steps were identified, while for β CN and κ CN, two steps were identified. Step I in α_{S1} CN, β CN and κ CN is associated with rapid initial sorption. Meanwhile, Step II for β CN and κ CN is related to slower sorption and gradual achievement of the sorption equilibrium. A different situation is observed in the case of α_{S1} CN. Namely, Step II is also associated with gradual sorption, after which Step III appears with an even

slower sorption compared to Step II without achieving a state of equilibrium. However, Step II in the case of β CN and κ CN is significantly faster compared to α_{S1} CN. The obtained results indicate that the process of zinc ion sorption for all three proteins: α_{S1} CN, β CN and κ CN, is not linear and several separate steps can be identified.

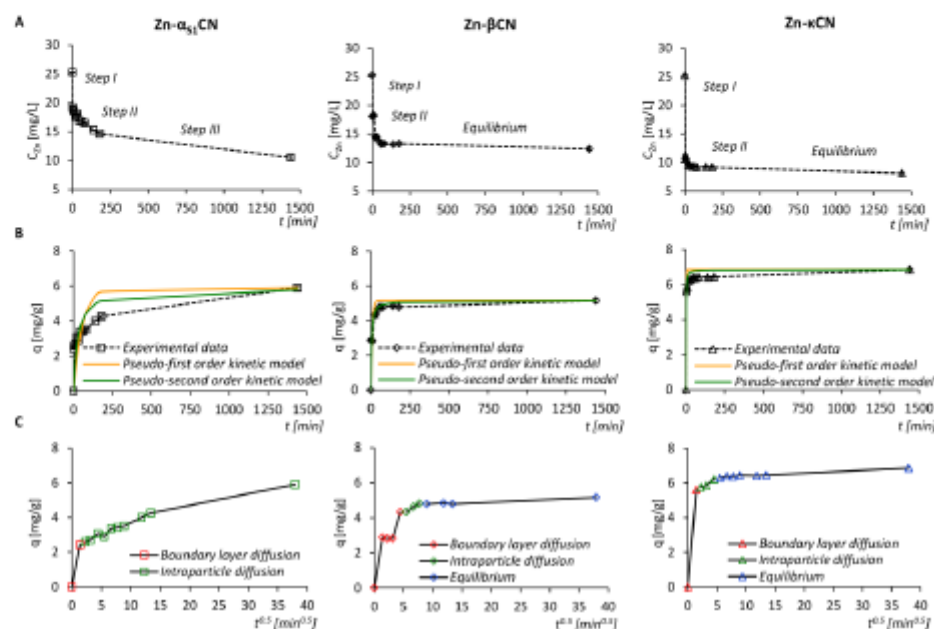


Figure 2. The kinetic steps of the Zn^{2+} sorption onto α_{S1} CN, β CN and κ CN using the zero-order kinetic model (A), experimental data and fitted pseudo-first- and pseudo-second-order kinetics models of the Zn^{2+} sorption by isoforms of casein (B) and the Weber–Morris intraparticle diffusion model (C).

In order to calculate the rate constants of the sorption kinetics of zinc ions for linear segments of the obtained steps, a zero-order kinetics model was used, which describes in detail the successive steps of sorption. The values of the rate constants for Step I in the case of α_{S1} CN, β CN and κ CN were noticed to be equal to 3.02, 0.54 and 7.0 (mg/L)/min, whereas they were 0.026, 0.030 and 0.085 (mg/L)/min for Step II, respectively. For Step III in the case of α_{S1} CN, the rate constant was found to be 0.0033 (mg/L)/min. The results are summarized in Table 1, and in Figure 3, the sorption effectiveness per time unit is shown.

A pseudo-first- and pseudo-second-order kinetic model was applied to the experimental data as well (Figure 2B). The calculated values of the determination coefficient (R^2) and standard deviation (S) indicated a more accurate description of the kinetics of the sorption of zinc ions to casein proteins by means of a pseudo-second-order kinetics model. The obtained values of the determination coefficient for α_{S1} CN and β CN, in comparison to κ CN, in the case of both pseudo-second-order kinetics models, indicate low values of the determination coefficient to the obtained experimental results. The not accurate fitting of α_{S1} CN and β CN to the classical kinetics model determines the contradictory nature of metal ions sorption in comparison to the glycosylated form of κ CN. The calculated kinetic constants are summarized in Table 1. The fast sorption step (Step I) for the two proteins: α_{S1} CN and κ CN, occurs during the first 2 min of the process, in which $23.88 \pm 0.21\%$ of zinc ions were bound to α_{S1} CN and the sorption capacity of the protein was 2.41 ± 0.02 mg/g, while for κ CN, these values increased slightly and amounted to $55.41 \pm 0.13\%$ and 5.60 ± 0.00 mg/g, respectively. For Step I, in the case of β CN, the effectiveness of binding to protein was $42.88 \pm 0.20\%$ and the amount of zinc ions absorbed on the protein was 4.33 ± 0.02 mg/g. The sorption process in Step II in the case of α_{S1} CN, β CN and

κ CN ends after 180, 60 and 20 minutes, respectively. The sorption effectiveness of zinc ions by casein isoforms for this step was $42.08 \pm 1.31\%$, $47.62 \pm 0.72\%$ and $61.48 \pm 0.32\%$; the sorption capacity was found to be 4.25 ± 0.14 , 4.81 ± 0.08 and 6.21 ± 0.05 mg/g. In the last step, Step III, the sorption process for α CN is completed after an incubation period of 1440 min, with a sorption effectiveness of $58.31 \pm 1.31\%$ and a sorption capacity of 5.89 ± 0.12 mg/g. The maximum sorption effectiveness and sorption capacity of α_{S1} CN, β CN and κ CN were $58.31 \pm 1.31\%$ and 5.89 ± 0.12 mg/g (α_{S1} CN), $51.05 \pm 0.97\%$ and 5.16 ± 0.11 mg/g (β CN) and $67.81 \pm 0.30\%$ and 6.85 ± 0.05 mg/g (κ CN).

Table 1. Kinetic model parameters for the zinc ions sorption by α_{S1} CN, β CN and κ CN and values of the distribution coefficient and the Gibbs' free energy change of the metal ions sorption.

		Zn- α_{S1} CN	Zn- β CN	Zn- κ CN
Zero-order kinetic model	k_0 [(mg/L)/min]	3.02	0.54	7.00
		0.026	0.030	0.085
		0.0033		
Pseudo-first-order kinetic model	k_1 [1/min]	0.018	0.13	0.76
	S	1.32	0.70	0.58
	R ²	0.075	0.78	0.90
Pseudo-second-order kinetic model	k_2 [(g/mg)/min]	0.0065	0.050	0.21
	S	1.02	0.80	0.40
	R ²	0.45	0.71	0.96
Intraparticle diffusion model	A [mg/g]	2.58	3.56	5.30
	K_{ip} [(mg/g)/min ^{-0.5}]	0.094	0.16	0.19
	S	0.25	0.083	0.066
	R ²	0.94	0.92	0.96
Distribution coefficient, the Gibbs' free energy change of the metal ions sorption	q_e [mg/g]	5.89	5.16	6.85
	C_e [mg/L]	10.53	12.37	8.13
	K_d	559.49	417.25	842.62
	T [K]	295	295	295
	ΔG^0 [kJ/mol]	-15.52	-14.80	-16.52

K_{ip} —the intraparticle diffusion rate constant; q_e —the amount of zinc sorbed by casein isoforms at equilibrium time; C_e —the equilibrium concentrations of zinc in solution; K_d —the distribution coefficient of zinc ions sorption by α_{S1} CN, β CN and κ CN.

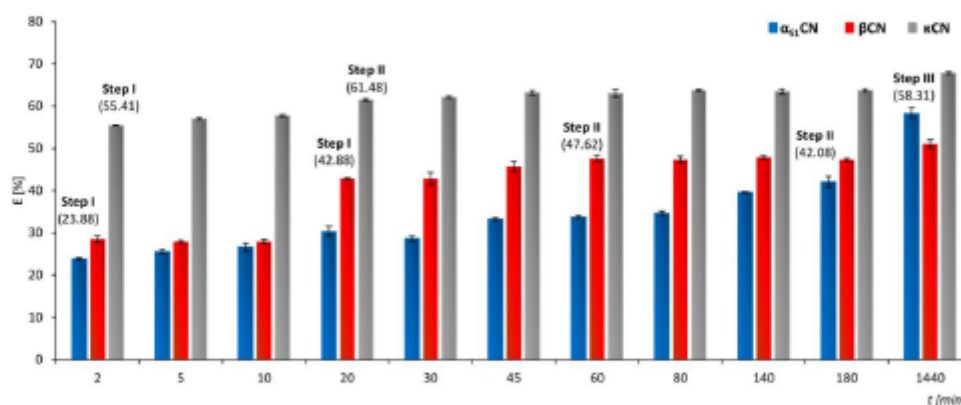


Figure 3. Sorption effectiveness of Zn²⁺ by α_{S1} CN, β CN and κ CN.

In order to determine the mechanism involved in the process of binding zinc ions to casein isoforms, experimental data were also subjected to the Weber–Morris intraparticle diffusion model (Figure 2C). The Weber–Morris model revealed two steps of sorption. Step I was attributed to adsorption on the

external surface of proteins or diffusion of zinc ions through the boundary layer as well as a sharp drop in zinc ion concentration. In turn, Step II corresponds to intraparticle diffusion that limits the speed of the process, thus indicating the absorption of zinc ions into the protein structure. In the final step, a sorption equilibrium was noticed. The Weber–Morris model revealed that zinc ions are mainly adsorbed on the external surface of casein isoforms. Then, gradual sorption of zinc ions causes their further diffusion inside the proteins structure.

In addition, the values of the change of Gibbs' free energy (ΔG^0) and the distribution coefficient (K_d) of sorption of zinc ions to α_{S1} CN, β CN and κ CN were calculated, which were found to be -15.52 kJ/mol and 559.49 , -14.80 kJ/mol and 417.25 and -16.52 kJ/mol and 842.62 , respectively. Negative values of Gibbs' free energy for α_{S1} CN, β CN and κ CN confirm that the process of zinc ion binding to these proteins is spontaneous. The obtained values are presented in Table 1.

The obtained results indicate that at the initial stage of rapid sorption, 1 mole of α_{S1} CN, β CN and κ CN sorbed 0.86 (α_{S1} CN), 1.59 (β CN) and 1.63 (κ CN) mole of zinc ions. It turns out that according to the Weber–Morris model, most zinc ions are surface-bound to κ CN and the least to α_{S1} CN. The situation changes rapidly in a second, slower stage, namely, per one mole of α_{S1} CN, β CN and κ CN, 2.12, 1.76 and 1.81 mole of zinc ions is sorbed, respectively. This shows that zinc ions are further diffused and absorbed to the greatest extent into the internal structure of α_{S1} CN. These results are consistent with the assumptions of the models characterizing casein micelles, where κ CN constitutes the outer shell of the micelles, and α_{S1} CN is localized in the interior of the casein micelle [14]. Assuming that the synthesis of the binding of zinc ions with individual casein fractions is completed with a state of equilibrium (except for α_{S1} CN) after external adsorption steps and penetration of zinc ions into the internal structure of proteins, κ CN binding zinc ions on the external surface is the most spontaneous reaction ($\Delta G^0 = -16.52$ kJ/mol).

2.3. Spectroscopic Analysis

Spectral characteristics of unmodified (control) α_{S1} CN, β CN and κ CN as well as the zinc ion-modified ones were determined to establish active chemical groups involved in the zinc ion binding process. The resulting FT-IR spectrum is shown in Figure 4. The obtained FT-IR spectra prove that zinc binding influences the spectrum of individual caseins in infrared. It was observed that after binding zinc to casein, the intensity of selected bands was significantly reduced and the appearance of the spectra changed.

As a result of NH stretching vibrations, the amide band A was observed in the range of 3429 – 3100 cm^{-1} . Its frequency depends on the strength of the hydrogen bond. The amide A band is usually part of Fermi's resonance double [33]. For unmodified proteins, a shift appeared from 3301 (α_{S1} CN) to 3289 cm^{-1} (β CN and κ CN). On the other hand, comparing the unmodified proteins (Figure 4A) with Zn-protein complexes (modified, Figure 4B), the shift occurred from the bands of about 3289 to 3429 cm^{-1} , respectively.

The spectral range between 3000 and 2840 cm^{-1} is dominated by the absorption of hydrophobic hydrocarbons residue [34]. After binding proteins with zinc ions, bands in the respective region are visible only for the Zn- κ CN complex.

The FT-IR spectrum is dominated by the protein amide I (~ 1650 cm^{-1}) and amide II (~ 1550 cm^{-1}) bands, mainly due to the C=O stretching and the NH bending of the peptide bond. The amide I band is extremely sensitive to secondary protein structures (α -helix, β -sheets, random coils) and to the presence of intermolecular β -sheets in protein aggregates [34]. According to Herskovits and co-authors' [35] studies, the percentage of α -helix in α_{S1} CN is estimated at 5–15%, and comparable values of α -helix occur in β CN—7–25%, and κ CN—10–20% [4,35]. The percentage of β -sheet in α_{S1} CN is between 18 and 20% [36] and 34 and 46% for β -sheet-like [37]. Both α_{S1} CN and β CN have around 20–30% turns. The turns are clearly distinguishable from what are commonly called undefined, random or structureless [36]. For β CN, the presence of 15–33% β -sheet has been reported and in the case of κ CN, 20–30% of β -structure has been reported [36]. Comparison of the unmodified (control) proteins

and zinc-protein complexes for amide I resulted in a shift from the bands of 1650 (control, Figure 4A) to 1633, 1632 and 1635 cm^{-1} (α_{S1} CN, β CN and κ CN, respectively, Figure 4B). In addition, amide I vibrations, absorbing nearly 1650 cm^{-1} , also originate from the stretching vibrations of C=O with a small proportion of CN out-of-phase stretching vibrations, CN deformation and bending in the NH plane. Amide I vibrations are slightly dependent on the nature of the side chain [33]. In amide II, there is an out-of-phase NH in the bend flat, CN stretching vibrations and CN stretching vibrations with less CO in the plane bend and CC and NC stretching vibrations [34]. For amides II, shifts between control proteins and Zn-protein complexes were observed from 1540 (α_{S1} CN), 1539 (β CN) and 1544 (κ CN) (Figure 4A) to 1548 (Zn- α_{S1} CN), 1549 (Zn- β CN) and 1546 (Zn- κ CN) cm^{-1} (Figure 4B). Signals at $\sim 1400 \text{ cm}^{-1}$ from amino acid side chains in peptides and proteins are related to CH_3 asymmetrical and symmetrical bending vibrations [38]. The band in this range corresponds to proline (Pro), the amino acid most commonly found both in β CN and κ CN, representing 16.7% and 11.8%, respectively, which can make a significant contribution to the binding with zinc ions [33]. However, the bands at ~ 1540 and $\sim 1400 \text{ cm}^{-1}$ may also be assigned to the deprotonated carboxylic groups COO^- asparagine (Asp) and glutamine (Glu) residues [39]. The most Glu is contributed by α_{S1} CN representing 12.6% of total amino acid residues, being the most common amino acid, followed by β CN at 9.1%, and κ CN at 7.1%. Therefore, the binding of zinc ions to α_{S1} CN, β CN and κ CN can be carried out by coordinating with the oxygen of the side chain Asp and Glu [40,41].

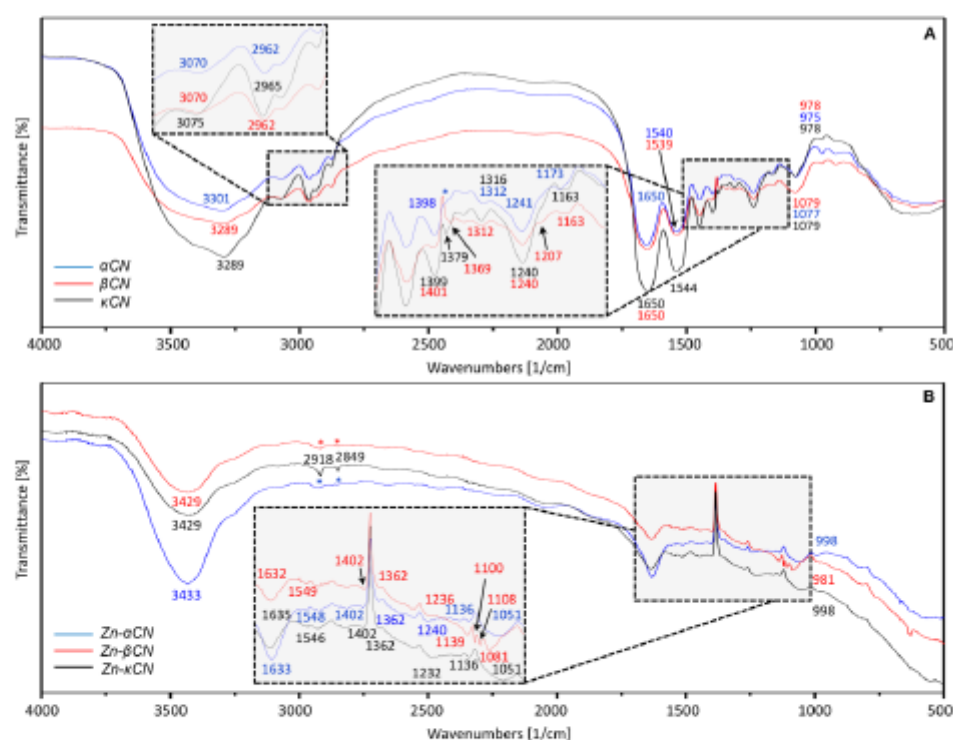


Figure 4. Infrared spectra of the α_{S1} CN, β CN and κ CN casein isoforms control (A) and casein isoforms after binding of zinc ions (B). Asterisks (*) indicate signal disappearance.

The spectral area 1500–1200 cm^{-1} also includes the area of amide III bands, resulting from bending NH and stretching CN [34]. For the band at about 1401 cm^{-1} corresponding to unmodified β CN, a slight change was observed as opposed to unmodified α_{S1} CN and κ CN (1398 and 1399 cm^{-1} , respectively). However, the bands 1398, 1399 and 1401 cm^{-1} , corresponding to unmodified α_{S1} CN,

κ CN and β CN, respectively, after binding to zinc ions are shifted to 1402 cm^{-1} for all proteins. Moreover, for unmodified β CN and κ CN, a new band at 1369 cm^{-1} (not seen in α_{S1} CN) appeared with a slight shift of κ CN to 1379 cm^{-1} . After binding of proteins to zinc ions, a shift in the 1369 to 1362 cm^{-1} band for β CN was observed and a new 1362 cm^{-1} band for α_{S1} CN and κ CN was noticed. The bands occurring at ~ 1240 and $\sim 1079\text{ cm}^{-1}$ are caused by the asymmetrical and symmetrical stretching of ionized PO_3^{2-} , respectively [38]. The control protein bands 1241 (α_{S1} CN) and 1240 cm^{-1} (β CN, κ CN) were slightly shifted in complexes to 1240 cm^{-1} for α_{S1} CN, 1236 cm^{-1} for β CN and 1232 cm^{-1} for κ CN. In turn, the bands 1079 (β CN, κ CN) and 1077 cm^{-1} (α_{S1} CN) were shifted to 1051 (α_{S1} CN, κ CN) and 1081 cm^{-1} (β CN) after binding to zinc ions. For β CN (unmodified, Figure 4A), a new 1207 cm^{-1} signal was registered, while for α_{S1} CN (unmodified) at 1173 cm^{-1} , a shift to 1163 cm^{-1} for β CN and κ CN (unmodified) was observed. However, comparing these signals (1173 , 1163 cm^{-1}) with the signals obtained after binding with zinc ions (1136 cm^{-1} for α_{S1} CN and κ CN, 1139 cm^{-1} for β CN), a shift occurs. For the Zn- β CN complex (Figure 4B), two new 1108 and 1100 cm^{-1} bands were observed. In the case of control proteins (Figure 4A), the bands 975 , 978 and 978 cm^{-1} (α_{S1} CN, β CN and κ CN, respectively) corresponding to the $-\text{PO}_3^{2-}$ moiety of the serine phosphate residue were observed. For complexes (Figure 4B), there was a shift in the bands to a value of about 998 (Zn- α_{S1} CN, Zn- κ CN) and 981 cm^{-1} (Zn- β CN) to assign the phosphate ions HPO_4^{2-} . The presence of the 978 cm^{-1} band means that CCP (colloidal calcium phosphate) molecules are released from the phosphate residues, causing an increase in the negative charge of casein particles. The appearance of the first band ($\sim 978\text{ cm}^{-1}$) suggests that the CCP particle dissociates into Ca^{2+} and HPO_4^{2-} when the serine phosphate residue is released [42]. In α_{S1} CN, there are two phosphorylation centers containing serine (Ser), which is 8.0% and crucial for stabilizing calcium phosphate nanoclusters in casein micelles [4]. These changes may indicate the binding of zinc ions to casein fractions with phosphate ions.

All shifts and appearances of new signals, especially in the range of 1650 – 978 cm^{-1} , occurring in the obtained complexes are correlated with metal-protein binding.

Moreover, the use of Raman spectroscopy allowed the observation of vibrational spectra. The Raman spectra provided complementary information to that obtained by IR spectroscopy that showed that apart from carboxylic and phosphate groups, aromatic amino acids also play an important role in metal-protein interaction. The Raman spectra were registered in the 400 – 4000 cm^{-1} frequency range and are shown in Figure 5.

The Raman protein spectra are dominated by bands associated with the main peptide chain, aromatic side chains and sulphur-containing side chains, and therefore are group vibrations that are either multiple related or electron-rich such as C=O, C=N, C=C, S-S, S-C and S-H. Therefore, changes may result in β CN being similar to complexes rather than to other control proteins [43]. Polar functional groups are characterized by stronger signals in the infrared spectrum, while non-polar functional groups are associated with more intense Raman bands [44].

Figure 5A represents the Raman spectra of unmodified protein fractions. Comparing the spectra for unmodified protein fractions (α_{S1} CN, β CN, κ CN), similarities were observed in the case of α_{S1} CN and κ CN, while β CN indicated large differences in the shape of the registered bands. Raman bands in the range 2428 – 3381 cm^{-1} were assigned to bond CH (CH_2 , CH_3), C-H or =C-H stretch [44]. For the bands 3380 (α_{S1} CN) and 3381 cm^{-1} (κ CN), a shift was observed for β CN to 3293 cm^{-1} (Figure 5A), while after binding to zinc ions (Figure 5B), a shift was observed to 3260 , 3255 and 3258 cm^{-1} for α_{S1} CN, β CN and κ CN, respectively. For unmodified β CN, the 3058 cm^{-1} band was observed, which is not found in unmodified α_{S1} CN and κ CN. However, after binding to zinc ions, this band (3058 cm^{-1}) is present in all complexes. Shifts were also observed between bands for unmodified proteins— 2971 (κ CN), 2966 (α_{S1} CN) and 2930 cm^{-1} (β CN). After binding of proteins to zinc ions, the absorbance of those bands was similar to unmodified β CN (2929 cm^{-1} for Zn- β CN and Zn- κ CN, 2932 cm^{-1} for Zn- α_{S1} CN). Similarly, it was observed in the case of bands 2818 and 2718 cm^{-1} (α_{S1} CN), 2820 and 2718 cm^{-1} (κ CN) and 2876 and 2725 cm^{-1} (β CN) that, after binding, they corresponded to the value of unmodified β CN bands (2875 , 2723 cm^{-1} for complexes).

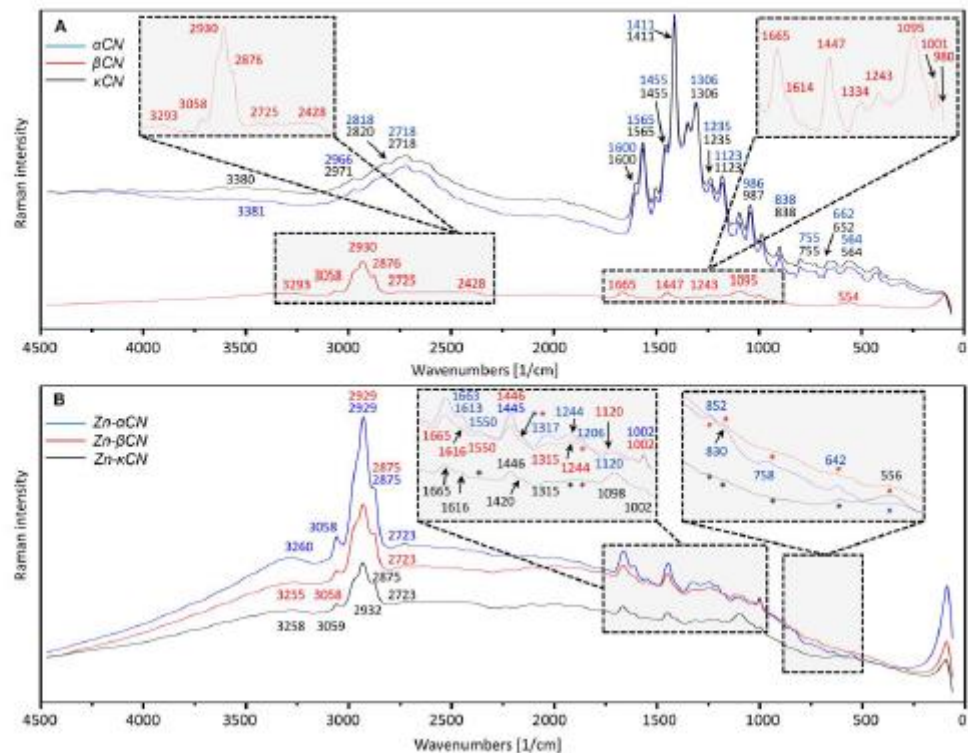


Figure 5. Raman spectra of the α_{S1} CN, β CN and κ CN casein isoforms control (A) and casein isoforms after binding of zinc ions (B). Asterisks (*) indicate band disappearance.

The spectra registered at amide and amino acids region $500\text{--}1655\text{ cm}^{-1}$ illustrate the changes between the modified samples and unmodified. The signals noticed at $1663/1665\text{ cm}^{-1}$ correspond to the C=O stretching mode associated with the CONH protein group (amide I) [45,46], but the bands registered at 1600 and at $1613/1616\text{ cm}^{-1}$ are generated by Tyr-OH [45]. In turn, the 1455 cm^{-1} band is assigned to the NH deformation and CN stretching [46] in amide II. The common bands ($1663/1665$, $1613/1616$, 1550 , $1445/1446$, $1315/1317$, 1244 , 1120 and 1002 cm^{-1}) have been also noticed for the modified α_{S1} CN and β CN protein samples. The bands 1665 , 1616 , 1446 , 1315 and 1002 cm^{-1} were also observed for modified κ CN, while bands 1550 and 1244 cm^{-1} for modified κ CN disappeared. The 1120 cm^{-1} band corresponding to modified α_{S1} CN and β CN for modified κ CN has been shifted to 1098 cm^{-1} . Disappearance of the band also occurred for unmodified α_{S1} CN and κ CN at 1665 cm^{-1} and β CN at 1600 , 1565 and 1123 cm^{-1} . However, the 1411 cm^{-1} band for unmodified α_{S1} CN and κ CN for unmodified β CN disappeared, and after binding with zinc ions, this band with a shift to 1420 cm^{-1} occurred only for κ CN. The mentioned bands, 1002 cm^{-1} for Zn- α_{S1} CN, Zn- β CN and Zn- κ CN for unmodified proteins, are shifted to 986 (α_{S1} CN), 987 (κ CN) and 1001 cm^{-1} (β CN). The 1002 cm^{-1} band (Figure 5B) corresponds to phenylalanine (Phe) [47]. This amino acid constitutes about 4.0% of the total of residues in α_{S1} CN, 4.3% in β CN and 2.4% in κ CN and may be responsible for protein binding with zinc ions. The new signals were observed at 1206 and 852 cm^{-1} only for the modified α_{S1} CN.

The Raman's spectra illustrate the amide region III ($1200\text{--}1340\text{ cm}^{-1}$), including C-N tension and N-H bending [48]. The signal observed at $1306/1315\text{ cm}^{-1}$ is assigned to the alanine (Ala) bands. The band registered at $1235/1244\text{ cm}^{-1}$ corresponds to the CH_2 carbohydrate twisting mode. The most important current vibration modes have been assigned to CO stretching and deformation of CC and COH ($1120\text{--}1064\text{ cm}^{-1}$), as well as deformation of COC ($950\text{--}870\text{ cm}^{-1}$) [46]. What is more, the bands

at 852, 830 and 642 cm^{-1} can correspond to the tyrosine (Tyr) vibration [45] and the bands 758 and 556 cm^{-1} to the tryptophan (Trp) [45]. The regions 630–670 cm^{-1} and 700–745 cm^{-1} found in α_{S1} CN and κ CN control and Zn- α_{S1} CN complex originate from C-S stretch cysteine and methionine [44]. The occurrence of residues of Cys11 and Cys88 results in the formation of a complex disulphide bond pattern among κ -CN molecules, with all possible combinations being observed (Cys11-Cys11, Cys11-Cys88 and Cys88-Cys88). There is also a certain amount of monomeric κ CN associated with an intramolecular disulphide bond, but it is no more than 10% κ CN [49]. In turn, the 564 and 755 cm^{-1} bands are assigned to the tryptophan (Trp) residues [45], which occupy about 1% [4]. Signal shifts in complexes may indicate their participation in the bond with zinc ions.

Similarly, kinetic and spectroscopic studies on the binding of zinc ions to casein carried out by Pomastowski et al. indicate the dominant presence of carboxyl groups Asp and Glu and phosphate groups involved in the binding [9]. In turn, studies on the binding of zinc ions to α CN carried out by Srinivas and Prakash [10] indicate the initial binding to serine phosphates. The binding process is fast, while the affinity of the binding is weak and does not cause any structural changes. However, further reaction with zinc ions leads to binding with aromatic amino acids, including Trp [10]. Zinc binding causes the rearrangement of the secondary protein structure and increases orderliness. It was also observed in the quenching of intrinsic α CN fluorescence by zinc interacting with histidine (His), glutamic acid (Glu), aspartic acid (Asp) and cysteine (Cys) [10]. The presence of Asp and Glu carboxylic groups has also been found in the case of silver to lactoferrin (LTF) binding [23]. The potential binding sites were determined by means of molecular dynamics simulations, which were consistent with and complemented the instrumental studies carried out. For caseins, which are non-crystalline proteins, their total primary and partially secondary structures are known, but homologous proteins with a known crystallographic structure are unavailable. In Kumosiński et al., 1991 [50], an attempt was made to construct a three-dimensional κ CN structure using molecular modeling, and the structures obtained were preliminary models. Additionally, despite the fact that the computational approach allows for studying the processes and properties of proteins, there are limitations to the possibility of obtaining accurate parameters that would allow for studying posttranslational modifications (PTMs), which are crucial in caseins' structure [51]. The proposed casein models require additional validation using other approaches and deserve further investigation, which will be our goal in future studies.

2.4. Spectrometric Analysis

Studies on control proteins (unmodified) before binding with zinc ions were performed for three casein fractions obtained during chromatographic separation in our previous studies [52]. To determine the masses of casein isoforms both before and after binding of zinc ions, the analysis of intact proteins was carried out using MALDI-TOF MS (Figure 6).

The masses of intact casein isoforms were found to be $23,985.874 \pm 0.326$ and $19,032.393 \pm 0.326$ m/z for β CN and κ CN, respectively. In the case of α_{S1} CN, two overlapping signals were observed. These signals correspond to values $23,530.363 \pm 0.326$ and $23,604.819 \pm 0.326$ m/z. According to the literature data, the registered signals are coming from different genetic forms of α_{S1} CN [53,54].

The respective signals appeared in the sample after zinc ions binding (Zn- α_{S1} CN complex) at 23,507.614 and 23,597.329 m/z. This difference is connected to the degradation of some parts of the protein structure during the zinc ions binding process. Compared to the unmodified protein (control), in the case of the Zn- α_{S1} CN complex, a new signal has been observed (8661.218 and 9257.008 m/z). This observation is the result of protein decay to the more hydrophobic fragments, e.g., 8661.218 and 9257.008 m/z (Figure 6). A different situation was observed in the case of the β CN protein. The characteristic signal registered at $23,985.874 \pm 0.326/23$ and 982.382 ± 0.326 m/z was noticed in both the unmodified and modified β CN protein. Moreover, in the case of the Zn- β CN complex, a new signal with the m/z ratio of 8025.292 m/z has been noticed. This signal indicates that hydrophilic zinc ions bind to the hydrophobic protein through indirect interaction with oxygen from water. β CN is more hydrophobic than other casein isoforms. This is due to a negative net charge in the N-terminal

with five phosphoserine and hydrophobic C-terminal residues [55]. In the case of the κ CN protein, which is the smallest of the caseins, the signal is suppressed (in comparison with the control signal 19,032.393 m/z) after binding to the zinc ions. Perhaps it is an effect of glycosylation occurring only in κ CN. The κ CN is a glycoprotein sensitive to the proteinase (chymosin) site, which causes cleavage of the glycoprotein into two parts: the N-terminal para- κ -casein domain and the C-terminal domain of κ -casein with macroglyceride, which is highly heterogeneous in terms of oligosaccharide content [56].

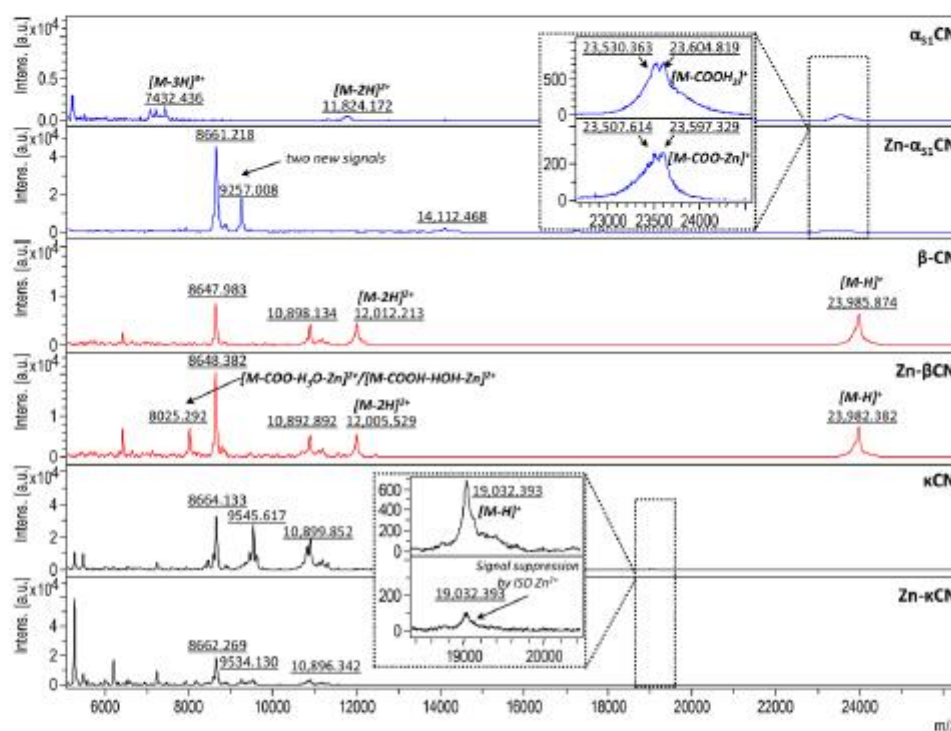


Figure 6. Mass spectra of intact standard solutions of α_{S1} CN, β CN, κ CN and their complexes with zinc ions ($Zn-\alpha_{S1}$ CN, $Zn-\beta$ CN, $Zn-\kappa$ CN).

3. Materials and Methods

3.1. Characteristics of α_{S1} CN, β CN and κ CN

3.1.1. Isolation of α_{S1} CN, β CN and κ CN, Chromatographic Separation and Matrix-Assisted Laser Desorption Ionization–Time of Flight Mass Spectrometry (MALDI-TOF/TOF-MS) Analysis

The casein fractions (α_{S1} CN, β CN, κ CN) used in present study have been previously separated and identified by our research group according to Pomastowski et al. [52] using high-performance liquid chromatography (HPLC) and MALDI-TOF MS techniques, respectively. In the current research, the isolated fractions were used to continue the study by the investigation of the mechanism of binding zinc ions with the obtained casein fractions.

3.1.2. Isoelectric Point Determination

The isoelectric point of casein isolated from milk was determined by the diffraction light scattering technique (Zetasizer, Malvern Instruments, Malvern, UK). The protein was suspended in 0.09% sodium chloride solution (Sigma-Aldrich, Warszawa, Poland) in the range of pH 2–11, sonicated for 10 s and

analyzed using the DTS1070 cuvette (Malvern Panalitical). All the measurements were performed in three repetitions.

3.2. Kinetic Study of Zinc Ions Binding to α_{S1} CN, β CN and κ CN

For the kinetic studies, the samples were prepared by mixing α_{S1} CN, β CN, κ CN and zinc nitrate (V) (Sigma-Aldrich, Warszawa, Poland) solutions at a ration of 1:1 (v/v) with the final concentration of 5000 and 25 mg/L. The protein samples were suspended in 0.09% sodium chloride at pH = pI. Then, the samples were incubated at 4 °C and analyzed after a certain period of time: 2, 5, 10, 20, 30, 45, 60, 80, 140, 180 and 1440 min, and centrifuged (12,000 rpm, 10 min). Part of the supernatant was mineralized in aqua regia and diluted to 1% nitric acid (V) (Sigma Aldrich, Poland). The concentration of zinc ions was determined by inductively coupled plasma-mass spectrometry ICP-MS (7900 ICP-MS, Agilent Technologies).

To explain the mechanism of zinc ion sorption by casein isoforms, zero kinetics, pseudo-first and pseudo-second-order kinetics models, and intraparticle diffusion models were used to analyze the results.

The kinetic models were expressed with the following formulas:

- The zero-order kinetics model:

$$C = C_0 - k_0t \quad (1)$$

where: C —the concentration of zinc ions in aqueous solution for a certain period of time [mg/L], C_0 —the initial concentration of zinc ions in aqueous solution [mg/L], k_0 —the adsorption rate constant [(mg/L)/min], and t —the adsorption duration [min].

- The pseudo-first-order kinetics model:

$$q_t = q_e(1 - e^{-k_1t}) \quad (2)$$

where: q_t —the amount of zinc ions sorbed for a certain period of time [mg/g], q_e —the amount of zinc sorbed at equilibrium [mg/g], and k_1 —the rate constant of the pseudo-first-order sorption kinetics [1/min].

- The pseudo-second-order kinetics model:

$$q_t = \frac{q_e^2 k_2 t}{1 + q_e k_2 t} \quad (3)$$

where: k_2 —the rate constant of the pseudo-second-order sorption kinetics [(g/mg)/min].

- The Weber-Morris intraparticle diffusion model:

$$q_t = A + K_{ip}t^{0.5} \quad (4)$$

where: A —a constant indicating the thickness of the boundary layer diffusion or external surface adsorption [mg/g], and K_{ip} —the intraparticle diffusion rate constant [(mg/g)/min^{0.5}]

The amount of zinc sorption by casein isoforms from an aqueous solution (for experimental data) was determined as follows:

$$q_t = (C_0 - C) \frac{V}{m} \quad (5)$$

where: V —the volume of solution from which sorption occurs [L], and m —the sorbent mass [g].

Additionally, the distribution coefficient (K_d) of zinc ions sorption by α_{S1} CN, β CN and κ CN and Gibbs' free energy for zinc adsorption were calculated.

The following equations were used:

$$K_d = \frac{q_e}{C_e} \quad (6)$$

where: q_e —the amount of zinc sorbed by casein isoforms at equilibrium time [mg/g], and C_e —the equilibrium concentrations of zinc in solution [mg/L].

$$\Delta G^0 = -RT \ln K_d \quad (7)$$

where: ΔG^0 —the energy of adsorption [kJ/mol], R —the gas constant (8.314 J/mol·K), T —the adsorption absolute temperature (295 K), and K_d —the distribution coefficient

3.3. Spectroscopic and Spectrometric Analysis

For the FT-IR, Raman and MALDI-TOF MS studies, the complexes were prepared by mixing α_{S1} CN, β CN, κ CN and zinc nitrate (V) (Sigma-Aldrich, Warszawa, Poland) solutions at a ratio of 1:1 (v/v) with the final concentrations of 5000 and 25 mg/L. The protein samples were suspended in 0.09% sodium chloride at pH = pI. Then, the samples were incubated at 4 °C for 24 h (because, after this time, we are sure that the metal–protein binding will take place). After the incubation time, the samples were centrifuged (12,000 rpm, 10 min). The supernatant was removed and the resulting sediment was lyophilized and submitted to further spectroscopic and spectrometric analyses. In turn, isolated CN (control) was prepared by dissolving in distilled water.

3.3.1. Fourier Transform Infrared Spectroscopic (FT-IR) and Raman Spectroscopy (Raman) Analysis of α_{S1} CN, β CN and κ CN

Spectroscopic methods (FT-IR, Raman) have been used as techniques for analyzing the changes of the active functional group and the secondary structure of the protein system.

Spectra in FT-IR analysis were recorded by using a Spectrum 2000 from Perkin-Elmer, Waltham, MA, and were recorded in the MIR range from 400 to 4000 cm^{-1} , and 15 scans were averaged at a resolution of 4. The samples were prepared in three repetitions by grinding them with potassium bromide powder (KBr) and pressed into a disc.

The Raman signals were recorded with the Raman Spectrometer (Senterra, Bruker Optik) in a spectral range of 400–4000 cm^{-1} with an integration time of 3×30 s using a 532 nm laser excitation, at 20×5 mW power, in combination with 10 fM accumulation. The samples were prepared in three repetitions by direct application of the sample on a microscope slide.

All spectra were processed using ORIGIN software.

3.3.2. Matrix-Assisted Laser Desorption Ionization–Time of Flight Mass Spectrometry (MALDI-TOF/TOF-MS) Analysis before and after Zinc Binding to Isoforms of Casein

MALDI mass spectra were acquired using a Bruker UltrafleXtreme II mass spectrometer provided with 2 kHz speed in TOF mode and 1 kHz speed in TOF/TOF mode equipment with a modified Nd:YAG laser operating at the wavelength of 355 nm. For MALDI-TOF MS analysis of the intact proteins before and after binding of zinc to isoforms of casein, samples were prepared according to the dried droplet method using sinapinic acid (SA) as matrix, and next, the samples were applied to ground steel. In turn, Protein Calibration Standards II was selected for calibration. Spectra were obtained in linear positive ion mode over an m/z range of 5000–100,000.

4. Conclusions

This study describes for the first time the mechanism of binding zinc ions to individual casein fractions, causing the formation of complexes, and thus indicating the precise contribution of individual

fractions to the binding. The performed kinetic studies of the binding of zinc ions with α_{S1} CN, β CN and κ CN indicate a heterogeneous kinetic process carried out in three steps for Zn- α_{S1} CN, Zn- β CN and Zn- κ CN. The initial stage is associated with rapid initial sorption, the second stage with moderate sorption and the third stage with gradual achievement of the sorption equilibrium. Experimental data subjected to the Weber–Morris model indicated two stages of sorption ending in a sorption equilibrium step. The first step was related to adsorption occurring on the external surface of proteins, while the second step was related to intraparticle diffusion of zinc ions.

Spectroscopic studies (FT-IR) have proven that the main role in the binding of zinc ions to α_{S1} CN, β CN and κ CN complexes is played phosphate groups and carboxylic groups of Glu and Asp. Raman's spectroscopy supplemented the information from the gap in the information obtained from FT-IR analysis and indicates that the presence of aromatic amino acids such as Tyr, Trp and Phe was involved in the binding with zinc ions.

The use of mass spectrometry allows the accurate determination of masses and thus the identification of α_{S1} CN, β CN and κ CN. The mass spectra obtained after binding the protein with zinc ions indicate that in the case of α_{S1} CN, the carboxylic groups Asp and Glu play a key role. β CN binds to zinc ions through indirect interactions with oxygen ions, whereas in κ CN, the binding of zinc ions takes place probably through weak electrostatic interactions with deprotonated functional groups. However, the proposed binding mechanism requires additional validation using complementary approaches, especially molecular modeling methods.

Author Contributions: Conceptualization, P.P.; methodology, A.R. and V.R.-P.; software, A.R. and V.R.-P.; investigation, A.R.; writing—original draft preparation, A.R.; writing—review and editing, V.R.-P., P.P., M.S. and B.B.; visualization, A.R. and V.R.-P.; supervision, B.B.; project administration, P.P.; funding acquisition, P.P. All authors have read and agreed to the published version of the manuscript.

Funding: This work was financially supported by the National Science Centre in frame of Opus 14 project No. 2017/27/B/ST4/02628 (2018–2021).

Acknowledgments: Paweł Pomastowski and Bogusław Buszewski are members of Toruń Center of Excellence “Towards Personalized Medicine” operating under Excellence Initiative—Research University.

Conflicts of Interest: The authors declare no conflict of interest.

Abbreviations

α_{S1} CN	α_{S1} -casein
β CN	β -casein
κ CN	κ -casein
Ala	Alanine
Asp	Aspartic acid
Glu	Glutamic acid
Phe	Phenylalanine
Pro	Proline
Thr	Threonine
Trp	Tryptophan
Tyr	Tyrosine
Ser	Serine
CCP	Colloidal calcium phosphate
FT-IR	Fourier transform infrared spectroscopy
HPLC	High-performance liquid chromatography
MALDI-TOF MS	Matrix-assisted laser desorption/ionization time-of-flight mass spectrometry

References

- Bhat, M.Y.; Dar, T.A.; Singh, L.R. Casein Proteins: Structural and Functional Aspects. In *Milk Proteins—From Structure to Biological Properties and Health Aspects*; IntechOpen: London, UK, 2016; pp. 3–18.
- Imafidon, G.I.; Farkye, N.Y.; Spanier, A.M. Isolation, purification, and alteration of some functional groups of major milk proteins: A review. *Crit. Rev. Food Sci. Nutr.* **1997**, *37*, 663–689. [CrossRef]
- Müller-Buschbaum, P.; Gebhardt, R.; Roth, S.V.; Metwalli, Z.E.; Doster, W. Effect of calcium concentration on the structure of casein micelles in thin films. *Biophys. J.* **2007**, *93*, 960–968. [CrossRef]
- Huppertz, T.; Fox, P.F.; Kelly, A.L. *The Caseins: Structure, Stability, and Functionality*, 2nd ed.; Elsevier Ltd.: Amsterdam, The Netherlands, 2018; ISBN 9780081007297.
- Glantz, M.; Devold, T.G.; Vegarud, G.E.; Lindmark Månsson, H.; Stålhammar, H.; Paulsson, M. Importance of casein micelle size and milk composition for milk gelation. *J. Dairy Sci.* **2010**, *93*, 1444–1451. [CrossRef]
- Péres, J.M.; Bouhallab, S.; Petit, C.; Bureau, E.; Maubois, J.L.; Arhan, P.; Bouglé, D. Improvement of zinc intestinal absorption and reduction of zinc/iron interaction using metal bound to the caseinophosphopeptide 1-25 of β -casein. *Reprod. Nutr. Dev.* **1998**, *38*, 465–472. [CrossRef]
- Pryshchepa, O.; Sagandykova, G.N.; Pomastowski, P.; Railean-Plugaru, V.; Król, A.; Rogowska, A.; Rodzik, A.; Sprynskyy, M.; Buszewski, B. A New Approach for Spontaneous Silver Ions Immobilization onto Casein. *Int. J. Mol. Sci.* **2019**, *20*, 3864. [CrossRef]
- Demott, B.J.; Dincer, B. Binding Added Iron to Various Milk Proteins. *J. Dairy Sci.* **1976**, *59*, 1557–1559. [CrossRef]
- Pomastowski, P.; Sprynskyy, M.; Buszewski, B. The study of zinc ions binding to casein. *Colloids Surf. B Biointerfaces* **2014**, *120*, 21–27. [CrossRef]
- Srinivas, S.; Prakash, V. Interaction of Zn (II) with bovine milk α -casein: Structure-function study. *J. Food Biochem.* **2011**, *35*, 1311–1326. [CrossRef]
- Farrell, H.M. Models for Casein Micelle Formation. *J. Dairy Sci.* **1973**, *56*, 1195–1206. [CrossRef]
- Broyard, C.; Gaucheron, F. Modifications of structures and functions of caseins: A scientific and technological challenge. *Dairy Sci. Technol.* **2015**, *95*, 831–862. [CrossRef]
- Głąb, T.K.; Boratyński, J. Potential of Casein as a Carrier for Biologically Active Agents. *Top. Curr. Chem.* **2017**, *375*, 71. [CrossRef] [PubMed]
- Hristov, P.; Mitkov, I.; Sirakova, D.; Mehandgiiski, I.; Radoslavov, G. Measurement of Casein Micelle Size in Raw Dairy Cattle Milk by Dynamic Light Scattering. In *Milk Proteins—From Structure to Biological Properties and Health Aspects*; Intech: London, UK, 2016.
- Morr, C.V. Effect of Oxalate and Urea upon Ultracentrifugation Properties of Raw and Heated Skimmilk Casein Micelles. *J. Dairy Sci.* **1967**, *50*, 1744–1751. [CrossRef]
- Wauugh, D.F.; Noble, R.W. Casein Micelles. Formation and Structure. *J. Am. Chem. Soc.* **1965**, *87*, 2246–2257. [CrossRef]
- Rose, D. Relation Between Micellar and Serum Casein in Bovine Milk. *J. Dairy Sci.* **1968**, *51*, 1897–1902. [CrossRef]
- Wilkins, T.D.; Velander, W. Isolation of recombinant proteins from milk. *J. Cell. Biochem.* **1992**, *49*, 333–338. [CrossRef]
- Donnelly, W.J. Chromatography of milk proteins on hydroxyapatite. *J. Dairy Res.* **1977**, *44*, 621–625. [CrossRef]
- Yang, X.; Jiang, L.; Jia, Y.; Hu, Y.; Xu, Q.; Xu, X.; Huang, H. Counteraction of trehalose on N, N-dimethylformamide-induced *Candida rugosa* lipase denaturation: Spectroscopic insight and molecular dynamic simulation. *PLoS ONE* **2016**, *11*, e0152275. [CrossRef] [PubMed]
- Rouhier, N.; Gelhaye, E.; Jacquot, J.P. Glutaredoxin-dependent peroxiredoxin from poplar: Protein-protein interaction and catalytic mechanism. *J. Biol. Chem.* **2002**, *277*, 13609–13614. [CrossRef] [PubMed]
- Zänker, H.; Heine, K.; Weiss, S.; Brendler, V.; Husar, R.; Bernhard, G.; Glöe, K.; Henle, T.; Barkleit, A. Strong Uranium(VI) Binding onto Bovine Milk Proteins, Selected Proteins Sequences, and Model Peptides. *Inorg. Chem.* **2019**, *58*, 4173–4189. [CrossRef]
- Pomastowski, P.; Sprynskyy, M.; Žuvela, P.; Rafińska, K.; Milanowski, M.; Liu, J.J.; Yi, M.; Buszewski, B. Silver-Lactoferrin Nanocomplexes as a Potent Antimicrobial Agent. *J. Am. Chem. Soc.* **2016**, *138*, 7899–7909. [CrossRef]

24. Dokmanić, I.; Šikić, M.; Tomić, S. Metals in proteins: Correlation between the metal-ion type, coordination number and the amino-acid residues involved in the coordination. *Acta Crystallogr. Sect. D Biol. Crystallogr.* **2008**, *64*, 257–263. [CrossRef] [PubMed]
25. Miki, T.; Awa, M.; Nishikawa, Y.; Kiyonaka, S.; Wakabayashi, M.; Ishihama, Y.; Hamachi, I. A conditional proteomics approach to identify proteins involved in zinc homeostasis. *Nat. Methods* **2016**, *13*, 931–937. [CrossRef] [PubMed]
26. Watt, N.T.; Taylor, D.R.; Kerrigan, T.L.; Griffiths, H.H.; Rushworth, J.V.; Whitehouse, I.J.; Hooper, N.M. Prion protein facilitates uptake of zinc into neuronal cells. *Nat. Commun.* **2012**, *3*, 1112–1134. [CrossRef]
27. Kitamura, H.; Morikawa, H.; Kamon, H.; Iguchi, M.; Hojyo, S.; Fukada, T.; Yamashita, S.; Kaisho, T.; Akira, S.; Murakami, M.; et al. Toll-like receptor-mediated regulation of zinc homeostasis influences dendritic cell function. *Nat. Immunol.* **2006**, *7*, 971–977. [CrossRef]
28. Harzer, G.; Kauer, H. Binding of zinc to casein. *Am. J. Clin. Nutr.* **1982**, *35*, 981–987. [CrossRef]
29. Pomastowski, P.P.; Dziubakiewicz, E.; Buszewski, B. Potencjał zeta—jego rola i znaczenie. *Analityka* **2012**, *2*, 19–23.
30. Roosen-Runge, E.; Heck, B.S.; Zhang, E.; Kohlbacher, O.; Schreiber, F. Interplay of pH and binding of multivalent metal ions: Charge inversion and reentrant condensation in protein solutions. *J. Phys. Chem. B* **2013**, *117*, 5777–5787. [CrossRef]
31. Farrell, H.M.; Jimenez-Flores, R.; Bleck, G.T.; Brown, E.M.; Butler, J.E.; Creamer, L.K.; Hicks, C.L.; Hollar, C.M.; Ng-Kwai-Hang, K.F.; Swaisgood, H.E. Nomenclature of the proteins of cow's milk—Sixth revision. *J. Dairy Sci.* **2004**, *87*, 1641–1674. [CrossRef]
32. Egitto, A.S.; Miclo, L.; López, C.; Adam, A.; Girardet, J.M.; Gaillard, J.L. Separation and characterization of mares' milk α s1-, β -, κ -caseins, γ -casein-like, and proteose peptone component 5-like peptides. *J. Dairy Sci.* **2002**, *85*, 697–706. [CrossRef]
33. Barth, A. Infrared spectroscopy of proteins. *Biochim. Biophys. Acta Bioenerg.* **2007**, *1767*, 1073–1101. [CrossRef]
34. Ami, D.; Lavatelli, F.; Rognoni, P.; Palladini, G.; Raimondi, S.; Giorgetti, S.; Monti, L.; Doglia, S.M.; Natalello, A.; Merlini, G. In situ characterization of protein aggregates in human tissues affected by light chain amyloidosis: A FTIR microspectroscopy study. *Sci. Rep.* **2016**, *6*, 1–12. [CrossRef] [PubMed]
35. Herskovits, T.T. On the Conformation of Caseins. Optical Rotatory Properties. *Biochemistry* **1966**, *5*, 1018–1026. [CrossRef] [PubMed]
36. Michael Byler, D.; Farrell, H.M.; Susi, H. Raman Spectroscopic Study of Casein Structure. *J. Dairy Sci.* **1988**, *71*, 2622–2629. [CrossRef]
37. Malin, E.L.; Brown, E.M.; Wickham, E.D.; Farrell, H.M. Contributions of terminal peptides to the associative behavior of α s1-casein. *J. Dairy Sci.* **2005**, *88*, 2318–2328. [CrossRef]
38. Cestelli Guidi, M.; Mirri, C.; Fratini, E.; Licursi, V.; Negri, R.; Marcelli, A.; Amendola, R. In vivo skin leptin modulation after 14 MeV neutron irradiation: A molecular and FT-IR spectroscopic study. *Anal. Bioanal. Chem.* **2012**, *404*, 1317–1326. [CrossRef]
39. Parikh, S.J.; Kubicki, J.D.; Jonsson, C.M.; Jonsson, C.L.; Hazen, R.M.; Sverjensky, D.A.; Sparks, D.L. Evaluating Glutamate and Aspartate Binding Mechanisms to Rutile (α -TiO₂) via ATR-FTIR Spectroscopy and Quantum Chemical Calculations. *Langmuir* **2011**, *27*, 1778–1787. [CrossRef]
40. Ryde, U. Carboxylate binding modes in zinc proteins: A theoretical study. *Biophys. J.* **1999**, *77*, 2777–2787. [CrossRef]
41. Krężel, A.; Maret, W. The biological inorganic chemistry of zinc ions. *Arch. Biochem. Biophys.* **2016**, *611*, 3–19. [CrossRef]
42. Gebhardt, R.; Takeda, N.; Kulozik, U.; Doster, W. Structure and stabilizing interactions of casein micelles probed by high-pressure light scattering and FTIR. *J. Phys. Chem. B* **2011**, *115*, 2349–2359. [CrossRef]
43. Thomas, G.J. Raman spectroscopy of protein and nucleic acid assemblies. *Annu. Rev. Biophys. Biomol. Struct.* **1999**, *28*, 1–27. [CrossRef]
44. Li-Chan, E.C.Y. Vibrational spectroscopy applied to the study of milk proteins. *Dairy Sci. Technol.* **2007**, *87*, 443–458. [CrossRef]
45. Li-Chan, E.; Nakai, S.; Hirotsuka, M. Raman spectroscopy as a probe of protein structure in food systems. In *Protein Structure-Function Relationships in Foods*; Springer: Boston, MA, USA, 1994; pp. 163–197.
46. Almeida, M.R.; Oliveira, K.D.S.; Stephani, R.; De Oliveira, L.F.C. Fourier-transform Raman analysis of milk powder: A potential method for rapid quality screening. *J. Raman Spectrosc.* **2011**, *42*, 1548–1552. [CrossRef]

47. Jarvis, R.M.; Blanch, E.W.; Golovanov, A.P.; Screen, J.; Goodacre, R. Quantification of casein phosphorylation with conformational interpretation using Raman spectroscopy. *Analyst* **2007**, *132*, 1053–1060. [CrossRef] [PubMed]
48. Kurouski, D.; Van Duyne, R.P.; Lednev, I.K. Exploring the structure and formation mechanism of amyloid fibrils by Raman spectroscopy: A review. *Analyst* **2015**, *140*, 4967–4980. [CrossRef]
49. Farrell, H.M.; Kumosinski, T.F.; Cooke, P.H.; King, G.; Hoagland, P.D.; Wickham, E.D.; Dower, H.J.; Groves, M.L. Particle sizes of purified κ -casein: Metal effect and correspondence with predicted three-dimensional molecular models. *J. Protein Chem.* **1996**, *15*, 435–445. [CrossRef] [PubMed]
50. Kumosinski, T.F.; Brown, E.M.; Farrell, H.M. Three-Dimensional Molecular Modeling of Bovine Caseins: κ -Casein. *J. Dairy Sci.* **1991**, *74*, 2879–2887. [CrossRef]
51. Audagnotto, M.; Dal Peraro, M. Protein post-translational modifications: In silico prediction tools and molecular modeling. *Comput. Struct. Biotechnol. J.* **2017**, *15*, 307–319. [CrossRef]
52. Pomastowski, P.; Walczak, J.; Gawin, M.; Bocian, S.; Piekoszewski, W.; Buszewski, B. HPLC separation of casein components on a diol-bonded silica column with MALDI TOF/TOF MS identification. *Anal. Methods* **2014**, *6*, 5236–5244. [CrossRef]
53. Vincent, D.; Elkins, A.; Condina, M.R.; Ezernieks, V.; Rochfort, S. Quantitation and identification of intact major milk proteins for high-throughput LC-ESI-Q-TOF MS analyses. *PLoS ONE* **2016**, *11*, e0163471. [CrossRef]
54. Mamone, G.; Caira, S.; Garro, G.; Mauriello, R.; Nicolai, M.A.; Picariello, G.; Calabrese, M.G.; Ferranti, P.; Chianese, L.; Addeo, F. Challenging the heterogeneity of casein by an IEF/MALDI-TOF “virtual 2D-like” approach. *Food Res. Int.* **2013**, *54*, 1263–1272. [CrossRef]
55. Wong, D.W.S.; Camirand, W.M.; Pavlath, A.E. *Structures and Functionalities of Milk Proteins*; Taylor & Francis: Abingdon, UK, 1996; Volume 36, ISBN 1040839960952.
56. Pisano, A.; Packer, N.H.; Redmond, J.W.; Williams, K.L.; Gooley, A.A. Characterization of O-linked glycosylation motifs in the glycopeptide domain of bovine κ -casein. *Glycobiology* **1994**, *4*, 837–844. [CrossRef]

Publisher’s Note: MDPI stays neutral with regard to jurisdictional claims in published maps and institutional affiliations.



© 2020 by the authors. Licensee MDPI, Basel, Switzerland. This article is an open access article distributed under the terms and conditions of the Creative Commons Attribution (CC BY) license (<http://creativecommons.org/licenses/by/4.0/>).

4.4. Study on zinc ions binding to the individual casein fractions α_{S1} , β - and κ -casein

[P4] A. Rodzik, A. Król-Górniak, V. Railean, M. Sugajski, A. Gołębiowski, D. S. Horne, B. Michalke, M. Sprynskyy, P. Pomastowski, B. Buszewski, *Study on zinc ions binding to the individual casein fractions α_{S1} , β - and κ -casein*, Journal of Molecular Structure, 2023, 1272, doi: 10.1016/j.molstruc.2022.134251.



Study on zinc ions binding to the individual casein fractions: α_{S1} -, β - and κ -casein



Agnieszka Rodzik^{a,b}, Anna Król-Górniak^{a,b}, Viorica Railean^{a,c}, Mateusz Sugajski^{a,b}, Adrian Gołębowski^{a,b}, David S. Horne^d, Bernhard Michalke^e, Myrosław Spryński^b, Paweł Pomastowski^{a,*}, Bogusław Buszewski^{a,b}

^aCentre for Modern Interdisciplinary Technologies, Nicolaus Copernicus University in Toruń, Włocławska 4, Toruń 87-100, Poland

^bDepartment of Environmental Chemistry and Bioanalysis, Faculty of Chemistry, Nicolaus Copernicus University in Toruń, Gagarina 7, Toruń 87-100, Poland

^cDepartment of Public Health Protection and Animal Welfare, Faculty of Biological and Veterinary Sciences, Nicolaus Copernicus University in Toruń, Gagarina 7, Toruń 87-100, Poland

^dWisconsin Center for Dairy Research, University of Wisconsin–Madison, Madison, WI, United States

^eResearch Unit Analytical BioGeoChemistry, Helmholtz Center Munich-German Research Center for Environmental Health, Neuherberg 85764, Germany

ARTICLE INFO

Article history:

Received 7 September 2022

Revised 24 September 2022

Accepted 30 September 2022

Available online 1 October 2022

Keywords:

Zinc

Caseins

Spectroscopic study

Molecular docking

MALDI-TOF/MS

ABSTRACT

The presented work is focused on the isotherm study on the Zn^{2+} ions binding to the individual casein fractions: α_{S1} -, β - and κ -casein ($\alpha_{S1}CN$, βCN and κCN). The experimental isotherms were evaluated using Freundlich and Langmuir models. Subsequently, the stability of the obtained complexes in the respective Zn^{2+} ion concentrations (120, 350, 600 mg/L) was determined by carrying out zeta potential measurements. Capillary electrophoresis combined with inductively coupled plasma mass spectrometry (CE-ICP-MS) confirmed the occurring binding process. Additionally, physicochemical characteristics of the obtained metal-protein complexes was performed including scanning electron microscopy (SEM) in two modes (SE and Z-contrast) and the binding sites of caseins to Zn^{2+} ions were indicated using attenuated total reflectance infrared spectroscopy (FTIR-ATR) and Raman analysis as well as mass spectrometry technique (MALDI-TOF MS). Isothermal studies indicated a heterogeneously complex zinc ion adsorption process, and a stability study showed that the zeta potential is strongly related to the hydrophobicity, size and structure of the casein isoforms studied. Electron microscopy confirmed the modification of casein surfaces due to the addition of Zn^{2+} ions. Spectroscopic techniques indicated the interaction of zinc ions with polar amino acids of casein, such as glutamic acid (Glu) and aspartic acid (Asp), but also His, Cys. The influence of phosphate groups was also observed. Finally, the study culminated in a molecular docking study of the Zn^{2+} ion binding process, which confirmed the presence of the listed amino acids responsible for the binding process.

© 2022 The Author(s). Published by Elsevier B.V.

This is an open access article under the CC BY license (<http://creativecommons.org/licenses/by/4.0/>)

1. Introduction

Nowadays, one of the main research paths is the in-depth knowledge and use of the properties of compounds present in our environment. One of the top-reach issue attracting attention are metal-proteins interactions, mainly due to fact the metal-protein binding results, e.g. metallocomplexes might be successfully implemented in fields such as food processing, pharmacology or medicine [1]. Moreover, the use of food proteins is of particular interest. The use of specific food proteins is also of ecological importance. An example could be milk – using this raw material as

a source of biologically active proteins in an alternative way fits perfectly into the idea of sustainable development. The main protein of milk (about 75–80% w/v) are caseins (CNs). They form the largest protein component in most milks of industrial significance. The casein complex is divided into three fractions: α_{S1} and α_{S2} (alpha), β (beta) and κ (kappa) [2]. Casein is the basic building material for the formation of hemoglobin and blood plasma proteins, and also stimulates the proliferation of lymphocytes and activates macrophages [3]. A special feature for this type of proteins is the presence of a bond to a phosphate group, moreover, all polypeptide chains contain at least one of these groups in their structure – the unique sequence of amino acids leads to phosphorylation [4]. In this sequence, serine occurs first, then any amino acid, and then glutamic acid or serine again. The phosphorylated portions of the

* Corresponding author.

E-mail address: p.pomastowski@umk.pl (P. Pomastowski).

polypeptide form specific clusters with the phosphoserine on the outer side. This has a particularly important effect on the possibility of forming a bond with the metals. One of the main characteristics is the presence of casein in the form of large colloidal particles or micelles. Their size ranges from 50 to 300 nm and may contain from 20 to 150,000 casein particles [5,6]. A typical micelle consists of 92% α_{S1} -, α_{S2} -, β -, κ -caseins in the ratio 3: 1: 3: 1, 8% of inorganic compounds such as: calcium (2.87%), phosphates (2.89%), citrates (0.4%), and small amounts of sodium, magnesium and potassium [6]. The dispersion stability of casein micelles depend is related with their structure. Among many proposed micelles models, three main can be divided: (1) the sub-micelle model of Slatery and Evard [7]; (2) the Holt nanocluster model [8] and (3) the dual-binding model proposed by Horne [9]. Nevertheless, the precise stability of α_{S1} -, β -, κ -CN micelles is still under debates and requires further research in this area. Functionalization of casein micelles by metal ions or other chemical might find the application not only in food industry as nutraceutical ingredients but also in medicine as a novel antimicrobial and anticancer agents [1,10–14]. The production of casein-metal based pharmaceuticals complexes is often the subject of the patents [15–17].

Zinc participates in many biological processes and has exceptional coordination chemistry – in the acidic aqueous solution it forms the stable aqua complexes able to exchange water molecules when binding to other ligands [18]. Due its high affinity for functional groups, such as carboxyl or amino [19], binding zinc to proteins create a new application. Zinc, as one of one of the most essential microelements, has been shown to be crucial for the proper function of a large number of macromolecules and enzymes, where it has both catalytic (active center of enzymes) and structural roles [20–22]. Importantly, the human body is not able to store zinc, so that a daily intake of this element is required for normal health and maintenance [23]. Fortification of food products with zinc has thus been commonly used to prevent deficiencies. Here dairy products are of the special interest – they do not contain a high level of zinc, but the addition of it to milk, yogurts or cheese might provide replenishment of zinc levels in groups at risk of its deficiency. However, the addition of elements to dairy products might effect on the protein stability. The colloidal properties of the casein micelles play a major role in the structural properties of dairy products [24,25]. Interestingly, except the crucial role of zinc ions (Zn^{2+}) for human health, the free Zn^{2+} might play a critical role in neuronal damage and neurodegenerative disorders [26]. Then, the specific binding of Zn^{2+} to proteins seems to be necessary to eliminate the toxic effect. The results of metal–protein interactions may include metalloproteins, metallocomplexes, nanocomposites and nanoparticles [1]. The previous works of our group have shown the successful binding of zinc to milk and whey proteins resulting in both metallocomplexes such as: zinc-casein (ZnCN) [27,28] and zinc- β lactoglobulin (Zn β LG), which is a whey protein [29], as well as nanocomposites: zinc oxide-ovalbumin (ZnO-OVA), which is protein isolated from egg white [30]. However, the exact mechanism of zinc binding to the proteins is still unclear. The papers from the last few years gave some insight in this complex process by implementation of various instrumental and computational techniques (spectroscopy, spectrometry, molecular modelling or density functional theory calculations).

Therefore, the presented scientific problem prompted our research group to complement our previous studies with isothermal studies of Zn^{2+} ions binding to individual casein isoforms: α_{S1} -, β - and κ CN. As a complementary method, the CE-ICP-MS was performed to confirm the zinc binding to the caseins. Moreover, microscopic (Scanning Electron Microscopy; SEM), spectroscopic (Fourier Transform Infrared Spectroscopic with Attenuated Total Reflectance (FTIR-ATR), Raman) and spectrometric (MALDI-

TOF-MS) analyses were used to monitor the binding of Zn^{2+} ions (120, 350 and 600 mg/L) to individual casein fraction. Additionally, zeta potential measurements were performed to determine the stability of the casein fractions. In the final step, the experimental results were confronted with the theory by using the molecular docking, allowing for deeper understanding of the potential Zn^{2+} -CN binding sites.

2. Experimental

2.1. Isothermal study

For isothermal studies, samples were conducted based on batch sorption approach by mixing solutions of α_{S1} CN, β CN, κ CN, and zinc nitrate (V) (Sigma-Aldrich, Warsaw, Poland) at a ratio of 1:1 (v/v). Proteins were suspended in 0.09% sodium chloride solution at pH = pI (concentration 5000 mg/L) according to our previous work (pI α_{S1} CN = 4.80 ± 0.72 , pI β CN = 4.55 ± 2.15 , pI κ CN = 4.40 ± 0.28 [27]). Then, the proteins were sonicated for 10 min. The Zn^{2+} ion concentrations used in present study was as follow: 1, 6, 12, 40, 60, 120, 180, 300, 350 and 600 mg/L. The samples were incubated for 1440 min ($T = 21^\circ C$), centrifuged ($4^\circ C$, 12,000 rpm, 10 min) and mineralized in aqua regia and diluted to 1% nitric acid (V) (Sigma Aldrich, Poland) and the concentration of Zn^{2+} ions involved in the metal-protein binding process was determined using Inductively Coupled Plasma-Mass Spectrometry ICP-MS (Shimadzu ICPMS 2030, Kyoto, Japan).

The experimental results of Zn^{2+} ion sorption process by α_{S1} CN, β CN, κ CN were analyzed using Freundlich isotherm, Langmuir isotherm. The Freundlich and Langmuir isotherms were chosen due to the fact that they are the best known and popular isotherms and additionally they describe in a simple way the process of adsorption on the surface of biocolloids.

- The Freundlich isotherm was explained by the following formula:

$$q = K_F C_e^n \quad (1)$$

Where: K_F – constant division (L/g), C_e – the equilibrium concentrations of zinc in solution [mg/L], n – an empirical constant, characterizing the heterogeneity of the adsorption process. The above model is widely used to describe the sorption process on the surface of heterogeneous proteins.

The Langmuir isotherm was explained by the following formula:

$$q = \frac{q_m K_L C_e}{1 + K_L C_e} \quad (2)$$

Where: q_m – maximum amount of zinc adsorbed in monolayer (mg/g), K_L – constant Langmuir division (L/mg). This is a model that assumes that a monolayer of molecules forms on the adsorbent surface, interacting with the adsorption sites rather than interacting with each other, and that there is no possibility of forming a multilayer, and that the adsorption energy is constant.

2.2. Capillary electrophoresis coupled with inductively coupled plasma mass spectrometry analysis (CE-ICP-MS)

The CE-ICP-MS analysis was performed for the Zn β CN complexes (precipitates) at all Zn^{2+} isotherm concentrations (1, 6, 12, 40, 60, 120, 180, 300, 350 and 600 mg/L) to observe the effect of applied binding procedure as a screening method. For this purpose, a Prince CE 760 system (Prince Technologies B.V.) coupled to a NexION 300 D ICP mass spectrometer (Perkin Elmer) by a house-made interface [31,32] were used. Moreover, the uncoated fused-silica capillaries (length 1 m; i.d. 75 μ m) and the background electrolyte (BGE; Na-borate buffer at pH 7.8) were applied. Zinc was

Table 1
Optimal running parameters of CE-ICP-MS.

Parameter	Value
CE voltage	20 kV
Sample injection	hydrodynamically for 20 s
CE capillary	uncoated fused-silica capillaries i.d. 75 μm, 1 m length
Running buffer solution	Na-Borat buffer, pH 7.8
RF power	1250W
Outer plasma gas	16 L Ar/min
Carrier gas	0.98 L Ar/min
Monitored isotopes	⁶⁶ Zn, ⁴⁸ [SO]

monitored at the ⁶⁶Zn isotope, whereas the βCN protein at ⁴⁸[SO], as far as sulfur is considered as the natural tag in proteins and dynamic reaction cell technology with oxygen as a reaction gas for mass shift to the non-interfered *m/z* = 48. All of ZnβCN complexes were dissolved in the BGE at the protein sulfur concentration of 1000 ppm for the further analysis. The CE-ICP-MS measurements were carried out in triplicates. The applied CE-ICP-MS parameters are summarized in the Table 1.

2.3. Zeta potential (ZP) measurement

The stability of casein fractions after binding to Zn²⁺ ions was determined using dynamic light scattering technique (Zetasizer, Malvern Instruments, Malvern, UK). Metallocomplexes were suspended in 0.09% sodium chloride solution (Sigma-Aldrich, Poland) at several Zn²⁺ ion concentrations (1, 6, 12, 40, 60, 120, 180, 300, 350 and 600 mg/L). Directly before the ZP measurements, all samples were sonicated (10 s) by using the ultrasonic cleaner (USC THD model with 45 kHz ultrasonic frequency and degassing function, WWR International, Poland). The measurements have been performed in three replicates.

2.4. Microscopic study

Changes in native α₅₁CN, βCN, κCN and Znα₅₁CN, ZnβCN, ZnκCN metallocomplexes surface morphology were investigated by Scanning Electron Microscopy (SEM, LEO model 1430 VP), using two modes: secondary electrons (SE) and Z-contrast backscattered electron (Z contrast BSE). All images were acquired from the same region, allowing for a better comparison of the image acquisition modes. Images were taken at the same high voltage and magnification, and contrast and brightness were kept constant for each mode. The sample were dropped on the microscopic glass, dried and then analyzed while for elemental analysis the samples powder was used.

2.5. Spectroscopic study of the Zn²⁺ ions binding process

FTIR-ATR and Raman spectroscopy were used to evaluate the changes in caseins (CN) structure before and after Zn²⁺ ions binding.

FTIR-ATR spectra were collected in the MIR range by 15 scans at 4 cm⁻¹ resolution using a Bruker FTIR-ATR (Billerica, Massachusetts, USA). Approximately 1 mg of native α₅₁CN, βCN, κCN powder and Znα₅₁CN, ZnβCN, ZnκCN metallocomplexes for spectral analysis were applied to a platinum-ATR with a durable monolithic diamond measurement interface.

Raman spectra in the MIR range were measured at a wavelength of λ = 532 nm as excitation light, with a power of about 20 mW and a counting time spectrum of 2 × 30 s with an accumulation of 10 fM using a Raman spectrometer (Senterra, Bruker Optik). Sample preparation consisted of applying the samples to

ZnSe lenses, Focal length 50.8mm, 12 mm, 2.4 mm (IUVO-LASER, Poland), drying at room temperature for 24 h and analysis.

2.6. Polyacrylamide gel electrophoresis study

The standard solutions of α₅₁-, β- and κCN each casein fraction before and after the Zn²⁺ binding was investigated by using a one-dimensional sodium dodecyl sulfate-polyacrylamide gel electrophoresis (1D SDS-PAGE) (Bolt™ Mini Gel Tank, Novex Life Technologies, Carlsbad, CA, USA). As a marker, the SeeBlue™ Plus2 Pre-stained Protein Standard was used (Novex Life Technologies, Europe, Bleiswijk, Netherlands). The preparation of samples was based on the standard procedure recommended by the manufacturer

2.7. Mass spectrometric study

MALDI mass spectra were obtained using a Bruker UltrafleX-treme II mass spectrometer at 2 kHz in TOF mode and 1 kHz in TOF/TOF mode by a modified 355 nm Nd:YAG laser. The spectra were recorded in the positive ion linear mode in the range *m/z* 5000 – 100000. Analysis has been performed according to the manufacturer guidelines. For intact analyses, sinapic acid (SA) as a matrix was used, and Protein Calibration Standard II was applied for calibration. Samples (both control and complex at concentrations of Zn²⁺ ions 120, 350, and 600 mg/L) were dissolved in water and applied to a MALDI steel target by the dried droplet method after mixing with the matrix.

Protein Calibration Standard II and matrix (SA) were purchased from Bruker Daltonics, and all other reagents were purchased from Sigma Aldrich (Steinheim, Germany) with the highest possible commercially offered purity.

2.8. Molecular docking

When performing molecular docking, we may encounter many different approaches depending on the structures available and the results we want to achieve. In our previous work [33] one example approach is presented. The free and trial software were used to simulate the attachment of the metal-ion to the protein. The 3D structures of the proteins in the .pdb extension were downloaded from <https://alphafold.ebi.ac.uk/>. The environment in which the analysis was conducted and visualized was Metal Ion-Binding Site Prediction and Docking Server (MIB) <http://bioinfo.cmu.edu.tw/MIB/>. MIB is an extremely fast server that allows to predict where the bonding between the metal ion and the protein chain occurs. Notable that the MIB is based on the fragment transformation method, which allows for high accuracy and sensitivity; in the case of matching the Zn²⁺ ion, these parameters assume 94.8% and 71.7%, respectively. These values are constantly improving as new structures appear in MIBs. Additionally, the Chem3D Pro 12 trial version, <https://cs-chem3d-std.software.informer.com/4.0> and Molegro Molecular Viewer 7, <http://molexus.io/molegro-7> were used to optimize the 3D structures of the proteins. The PyMol program was employed to visualize the obtained results (<https://pymol.org/2/>).

In the first step all 3D structures of α₅₁CN, βCN, κCN were downloaded from AlphaFold Protein Structure Database. *Bos taurus* was chosen as the source organism for all structures. All files were downloaded in .pdb format. The acquired structures were single-chain and did not include post-translational modifications. In method we use only native primary structures can be used as a basis. Using a Molegro Molecular Viewer 7 we delete all water particles from the files. Next using the same software, we made a simple energy optimization. We could upload the prepared struc-

Table 2
Isothermal model parameters for Zn²⁺ ions sorption by α_{S1} -, β - and κ CN.

Casein fraction	Freundlich model				Langmuir model			
	K_F	n	S	R^2	K_L	q_m	S	R^2
α_{S1} CN	1.55	0.70	26.82	0.96	0.0015	285.56	28.14	0.95
β CN	0.66	0.92	30.71	0.98	0.00074	685.20	31.08	0.99
κ CN	1.07	0.81	29.10	0.99	0.0015	338.07	30.02	0.99

tures to the server performing automated calculations without user intervention.

The MIB interface is user-friendly and intuitive. The website also provides a simple instruction that allows less experienced users to carry out the analysis. To perform the analysis, we upload the files with the prepared proteins (one at a time). Next, we select the metal ion we want to attach, we choose Zn²⁺ but there are 12 different options. Calculations to predict the potential site of ion attachment to the structure are based on the Fragment Transformation Method and do not require user intervention. The method used is described in detail in the paper Lin et al. [34]. After just a few minutes, the results in the form of a short report were sent to an e-mail address [35,36].

The sites of the anticipated metal ion attachments to the protein proposed by the program were collected in the .pdb format and further visualized in the PyMol program.

3. Results and discussion

3.1. Isothermal study

Isothermal adsorption studies were carried out to better understand the process of zinc ion binding to individual casein fractions. The obtained experimental data are presented as a plot of sorption capacity change versus zinc concentration in solution (Fig. 1).

The experimental results obtained in the used concentration range indicate that with increasing zinc ion concentration, the adsorption capacity of different protein fractions increases. The adsorption phenomenon was additionally described by two adsorption isotherms: Langmuir and Freundlich. The Langmuir model predicts adsorption in a monolayer when the probability of all adsorption sites is equal, with no interactions between adsorbed molecules while the Freundlich model, represents adsorption of molecules in multiple layers with heterogeneous adsorption energies and interactions between adsorbed molecules [37].

The equilibrium constants for the Freundlich and Langmuir models were 1.55 l/g and 0.0015 l/mg for α_{S1} CN, 0.66 l/g and 0.000745 l/mg for β CN, 1.07 l/g and 0.0015 l/mg for κ CN, respectively. The obtained parameters and additionally calculated standard error (S) as well as correlation coefficient (R²) are summarized in Table 2. These two models have a high degree of fit to the experimental data. Successfully, applied Freundlich adsorption isotherm for all three fractions, indicating multilayer adsorption of zinc ions. Based on the theory of Freundlich isotherm model [38,39], the heterogeneous surface of CN protein might have various kinds of adsorption sites, and the affinities of these adsorption sites on the Zn²⁺ ions are different.

Much more information was obtained by running the isotherm as a function of C_e/C_0 . Consideration of this kind of dependence made it possible to identify two dominant steps in the sorption of Zn²⁺ ions on all three fractions of casein. First, the formation of a monolayer of Zn²⁺ ions is observed on the surface of each casein. In turn, after the initial step, a second layer is formed involving the binding of Zn²⁺ ions to the already adsorbed monolayer. In the case of β CN, the obtained curves both for Freundlich and Langmuir isotherms and as a function of C_e/C_0 are slightly steeper, which

may indicate that this protein shows much stronger hydrophobic properties than α_{S1} CN or κ CN. Based on the obtained isothermal results, three highest concentrations with zinc ion concentrations of 120, 350 and 600 mg/L were selected for comparison, to observe differences in the binding process and structure of casein fractions. Isothermal studies indicate that the number of zinc moles for particular concentrations at 120, 350, and 600 mg/L for α_{S1} CN are 10 moles, 22 moles, 36 moles, for β CN 9 moles, 29 moles, 44 moles, for κ CN 7 moles, 21 moles, 32 moles, respectively. Hence, it can be concluded that the amount of binding zinc to the protein increases with increasing zinc ion concentration.

3.2. Capillary electrophoresis coupled with inductively coupled plasma mass spectrometry analysis (CE-ICP-MS)

Metal-protein interactions were investigated by the comparison of the zinc composition of the β CN and the Zn β CN complexes (obtained by the using different Zn²⁺ concentration: 1, 120, 350 and 600 mg/L). The assigning of zinc peaks to protein in CE-ICP-MS was made by comparison of their migration times. Fig. 2 presents the ⁶⁶Zn specific electropherogram of native protein and its zinc complexes.

In all samples the detectable ⁶⁶Zn levels in the β CN protein were recorded (Fig. 2B-D), with the exception of sample prepared by 1 mg/L of zinc level (Fig. 2A). From analysis of Zn β CN complex at the lowest Zn²⁺ concentration (1 mg/L) it can be noticed the unbound zinc monitored 100 s, while the β CN migrates at 200 s (Fig. 2A). The higher concentration of Zn²⁺ used for the binding process resulted in the detection of protein containing zinc. Zinc binding was found to be concentration-dependent – with the increase of Zn²⁺ concentration, the intensity of ⁶⁶Zn peaks was also increased. The peaks assigned to the 350 and 600 mg/L of zinc level was wider than the 120 mg/L. Additionally, the peaks of the highest zinc concentration was shifted, compared to 120 mg/L Zn²⁺ concentration. The slight time migration shift can be explained by the higher salinity of the sample with highest concentration of zinc, and in the consequence, the higher conductivity of the sample. Similar effect was observed by many authors including Michalke et al. [32] who have noticed that migration times of iron species in biological samples were higher than used standards solutions.

What is interesting, the analysis of native β CN protein suspended in the BGE at pH=7.8 resulted in the two separate peaks indicating the probable dimer of β CN [40].

3.3. Zeta potential measurements

The stability of the obtained metallocomplexes was measured by using zeta potential (ZP) at all isotherm points (1, 6, 12, 40, 60, 120, 180, 300, 350 and 600 mg/L). The zeta potential is a parameter commonly used to characterize the stability of colloidal systems in solution. Based on the electrokinetic theory and Smoluchowski equation, biocolloids have a surface charge that attracts a thin layer of ions of the opposite charge to the protein surface. The electric potential at the boundary of the double layer is called the zeta potential [41–43].

The ZP of α_{S1} CN was registered in the range of -31.8 ± 2.8 (1 mg/L Zn²⁺ ions) to 17.3 ± 1.7 (600 mg/L Zn²⁺ ions) mV (Fig. 3).

The zeta potential of the β CN varied the most during the binding process (Fig. 3) – it was the most stable during the complexation in the range of 40 to 180 mg/L of Zn²⁺ ions (-25.9 ± 1.86 to -27.9 ± 3.0 mV). On the other hand, it was unstable at the lowest (1 mg/L Zn²⁺ ions) and highest (600 mg/L Zn²⁺ ions) concentration of zinc with the ZP at -5.1 ± 0.6 mV and -5.9 ± 3.8 mV, respectively (Fig. 3). According to the ZP value, the less stability has been presented by the κ CN form with the ZP registered in the range from

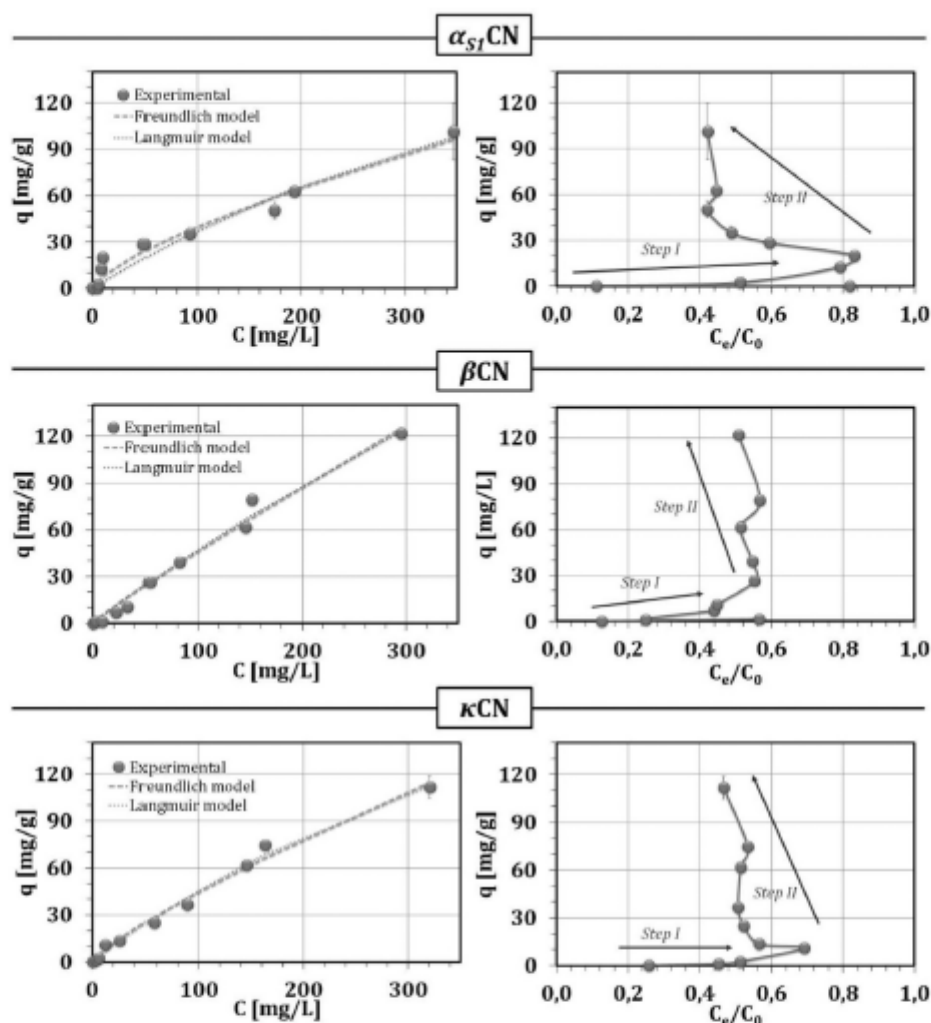


Fig. 1. The binding isotherms of Zn^{2+} ions by $\alpha_{S1}CN$, βCN , and κCN and the fit to Freundlich and Langmuir isotherm models, as well as the sorption isotherm of Zn^{2+} ions considering the C_e/C_0 relationship.

-12.5 ± 1.1 mV at the lowest to -1.3 ± 0.2 mV at the highest concentration of Zn^{2+} ions (Fig. 3). This phenomenon might be correlated with the hydrophobicity properties of the all three form of casein; $\alpha_{S1}CN$ form is shown to have the hydrophilic properties whereas βCN and κCN have hydrophobic properties, the higher hydrophobicity is shown by βCN [24,44]. Therefore, the affinity to the solvent occurred in different manner. Moreover, from the experimental results it can be concluded that in the case of $\alpha_{S1}CN$ and κCN , addition of zinc did not affect the stability of this protein. At the $Zn\alpha_{S1}CN$ and $Zn\kappa CN$ complexes preparation step (See the *Materials and Methods* section), no considerable changes in sample turbidity after the Zn^{2+} addition were observed. Differently, binding the zinc onto βCN at 350 and 600 mg/L concentration considerably decreased its stability, and it was also visible as a change in the turbidity of $Zn\beta CN$ sample.

The colloidal behaviour of various caseins forms during the metal binding process is crucial for the further modulation of their

stability during the dairy technological processes [45] described in detail in the **Supplement section**.

3.4. Microscopic study

The Fig. 4 presents the scanning electron microscopy (SEM) images of α_{S1} -, β -, κCN before and after the Zn^{2+} ions binding process in two modes, secondary electron (SE) and Z-contrast backscattered electron (BSE). The SE mode permits description of the surface topography and size of tested materials. On the other hand, the BSE SEM images can be applied to confirm their chemical composition as well as the distribution of different elements in the samples [46]. Due to fact that BSE images show high sensitivity to differences in atomic number (Z number) it is possible to visualize the elements with the higher atomic number as the brighter spots in the SEM image [47].

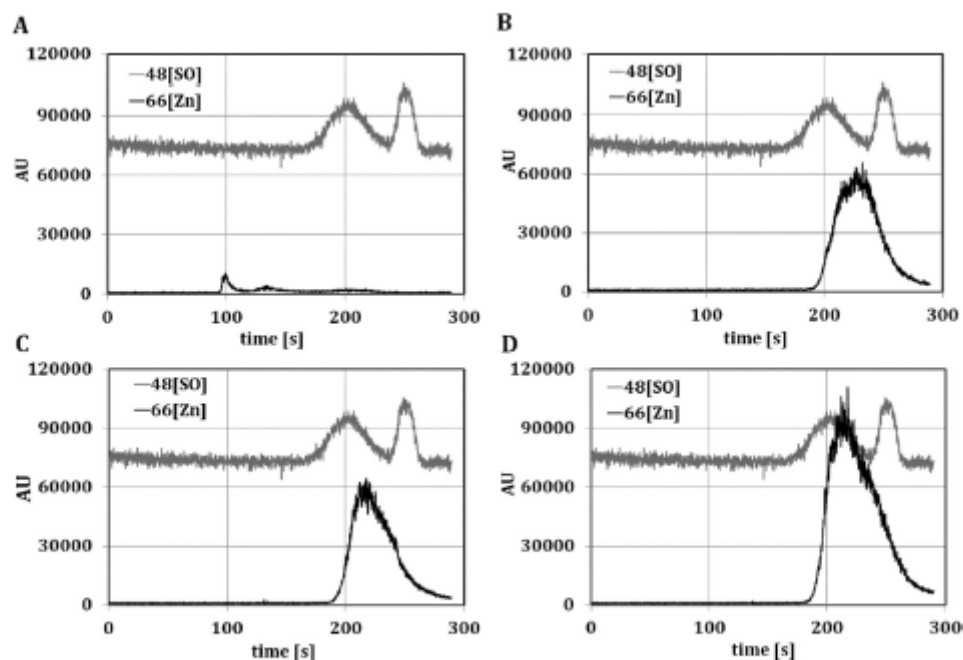


Fig. 2. CE-ICP-MS electropherograms of $Zn\beta CN$ complexes at 1 (A), 120 (B), 350 (C) and 600 mg/L of Zn^{2+} (D); all compared to the native βCN protein (grey line). Conditions of CE-ICP-MS – injection: 250 mbar, voltage: 25 kV, time: 300s, BGE: borate buffer at pH=7.8.

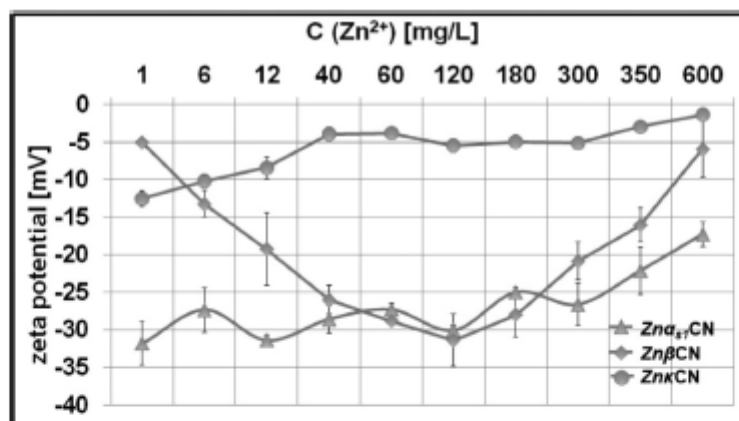


Fig. 3. The zeta potential of $\alpha_{S1}CN$, βCN and κCN after the Zn^{2+} ions binding in all tested concentrations (1, 6, 12, 40, 60, 120, 180, 300, 350 and 600 mg/L).

In the case of our study, Z-contrast BSE detection provides improved imaging of deposited zinc ions on the surface of casein fractions. Then, the brighter spots shown in the Fig. 4 indicates the zinc deposition on the casein's surfaces. Referring to the received SEM images, the compositional variations of the samples were observed. In the control samples (native proteins) zinc was not detected, both, in the SE and BSE mode.

However, the native proteins were characterized by different surface morphology. Compared to the Zn-CN complex, SEM image of the native protein show a quite smooth and non-porous surface of α_{S1} -, β -, κCN . Instead, the protein surface after the Zn^{2+} ions binding is modified and with the increasing concentration of Zn^{2+}

ions, the greater changes of α_{S1} -, β -, κCN surface topography are noticed. The observed surface modification is generated mainly by the adsorption of Zn^{2+} ions on the tested protein. Explanation of this phenomenon might be based on the fact that at the lower zinc concentration, the casein molecules collapse in on themselves, while on the highest concentration the metal-induced aggregation occurred. It is in a good accordance with the zeta potential values of complexes obtained for the 350 and 600 mg/L Zn^{2+} concentration.

The work of Kumar et al. [71] who have investigated the interaction between caseins and polysaccharides support this hypothesis. They have observed on the SEM images that addition of small

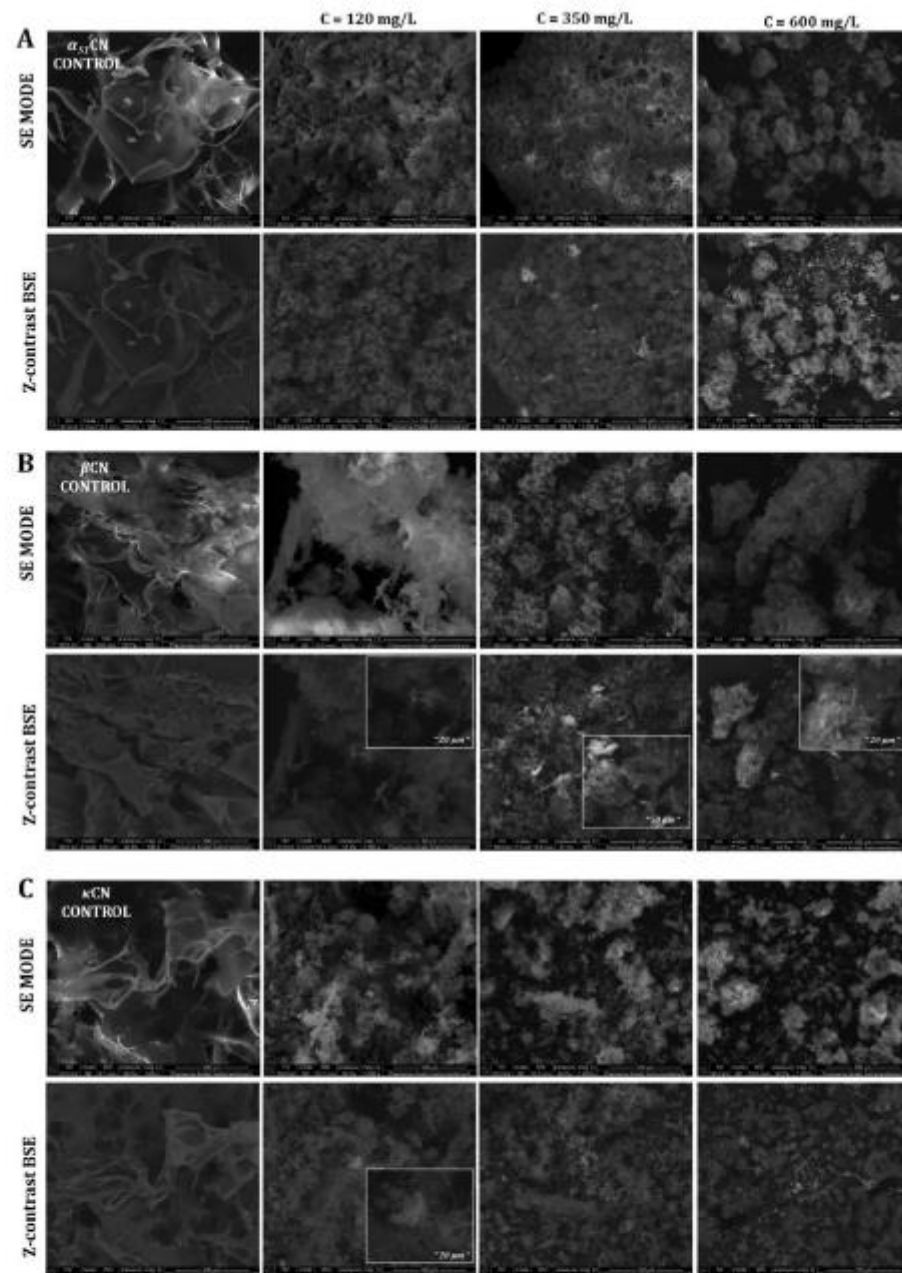


Fig. 4. SEM image of native α_{S1} CN (A), β CN (B), κ CN (C) and after the Zn^{2+} binding at 120, 350 and 600 mg/L concentration of Zn^{2+} ions in two modes: SE and Z-contrast BSE.

amount of λ -carrageenan resulted in the casein molecules collapse, whereas the increasing of carrageenan concentration caused the formation of aggregates [71]. Similar results was also obtained in our previous study [36] during the zinc aqua complexes interaction with ovalbumin from the egg white. The ovalbumin topography modification was generated by two mechanisms including ad-

sorption of Zn^{2+} on the protein surface. Moreover, according to the obtained SEM micrographs, in the case of β - and κ CN the changes in the shape of protein molecules (more globular) was observed at lowest concentration (120 and 300 mg/L) compared to the α_{S1} CN (600 mg/L).

Addition of the highest (600 mg/L) concentration of the metal have caused the self-association of all tested caseins forms. The explanation of this phenomenon can be based on the primary structure of casein amino acids sequence, and in consequence, on their hydrophobicity. The most hydrophobic casein is the β CN, which has a highly hydrophobic C-terminal domain consist of many of the non-polar amino acids residues (such as isoleucine, valine or proline) [48]. In the case of the κ CN, the hydrophobicity is distributed irregularly throughout the protein and it is strongly associated with the amino acid sequence of the κ CN.

As an example, 1 – 20 amino acids show mainly hydrophilic behavior (e.g., arginine, glutamic and aspartic acid), while the aa. from 21 to 110 contains some strongly hydrophobic residues (e.g., tyrosine, alanine or leucine). Furthermore, the post-translational phosphorylation and glycosylation occurring in the κ CN might reduce its hydrophobicity [48,49]. On the other hand, the α_{S1} CN form is considered to exhibit the highest hydrophilic properties. In comparison to other forms of caseins, α_{S1} CN consist of 39 negatively charged aa. residues (β - and κ CN contains 28 negatively charged residues) [48]. Taking into consideration the observed zinc binding to caseins, the attention should be paid to the major amino acids responsible for such metal-protein interactions. Based on the literature reports, zinc cations are mainly bound to proteins through the negatively charged (aspartic (Asp) and glutamic acids (Glu) or polar (cysteine (Cys), histidine (His) and asparagine (Asp)) amino acids residues, but also to the phosphoserine. The works of Pomastowski et al. [28] and Rodzik et al. [27] confirmed that Zn^{2+} -caseins binding process is occurring through their Asp⁻ and Glu⁻ carboxyl groups. In our work, the zinc cations might bind to the phosphate groups of serine, the histidine imidazole ring (mainly nitrogen) or to the deprotonated carboxyl groups of glutamic and aspartic acids. Moreover, the divalent ions such as zinc may take part in the cross-linking of two or more neighboring charged amino acids groups [50,51]. The SEM data revealed that the addition of the same zinc ions concentration resulted in the slightly different shape of ZnCN complexes. Therefore, it can be concluded that more Zn^{2+} ions are required to neutralize the α_{S1} CN charge, in comparison to β - and κ CN (Fig. 4B, C), to achieve the folded, globular structure by the most hydrophilic α_{S1} casein (Fig. 4A). Taking into account the differences between the zinc deposition on the all casein isoforms, the BSE Z-contrast mode should be considered more detailed. The addition of the 600 mg/L Zn^{2+} to the α_{S1} CN resulted in the appearance of much brighter zinc ions in the BSE image, compared to the 120 and 300 mg/L Zn^{2+} concentration (Fig. 4A). The result is a higher number of moles of zinc ions per protein. Similar observation was made for the others proteins (β - and κ CN) (Fig. 4B and C), but here the zinc deposition was not so high. The differences between the tested caseins might be related to the various nature of zinc binding process. Considering the C_e/C_0 isotherm obtained for the β - and κ CN (Fig. 1B and C) it can be concluded that the sorption of zinc ions is occurred mostly on the protein surface, in the multilayer manner. In turn, the Zn^{2+} binding to α_{S1} CN seems to be more complex – more ions have been adsorbed on the already existed monolayer (Fig. 1A).

3.5. Spectroscopic study of the Zn^{2+} ions binding process

In order to describe the functional α_{S1} -, β - and κ CN groups involved in the Zn^{2+} ions binding process, the spectroscopic study including FTIR-ATR and Raman analysis were performed. On the Fig. 5, the FTIR-ATR spectra registered for the proteins before and after the Zn^{2+} ions complexation is presented in three different concentrations of Zn^{2+} ions chosen on the basis of isothermal studies.

In the case of α_{S1} CN metallocomplexes with Zn^{2+} ion concentrations of 120, 350 and 600 mg/L ($Zn\alpha_{S1}CN120/350/600$), it is ob-

served that with increasing Zn^{2+} ion concentration the signal intensity decreases over the entire spectral range while for β CN and κ CN complexes ($Zn\beta CN120/350/600$, $Zn\kappa CN120/350/600$) the signal intensity increases. The reason for the observed changes may be the kinetics of binding Zn^{2+} ions with particular casein fractions. According to our previous studies [27], for a Zn^{2+} ion concentration of 50 mg/L for α_{S1} CN three steps were observed: fast initial sorption, gradual sorption and increasingly slow sorption without reaching equilibrium, in the case of β CN and κ CN equilibrium was reached. When the concentration of Zn^{2+} ions is higher, that is, the bound Zn^{2+} ions are increasingly more. This is due to the structure of the protein itself and its ability to bind to Zn^{2+} ions.

For all three spectra obtained there was a large reduction in intensity in the signal range 1447–940 cm^{-1} (9–16) especially for signals 1307 cm^{-1} (11), 1172 cm^{-1} (13), 974 cm^{-1} (15) and 940 cm^{-1} (16). Comparing the native (control) proteins of each casein fraction among themselves, a decrease in signal intensity 974 cm^{-1} (15) was observed for β CN and κ CN compared to α_{S1} CN. Thus, it can be concluded that Zn^{2+} ions change the structure of the different casein fractions. The highest intensity among native proteins is observed for α_{S1} CN, followed by β CN and κ CN. It may be a result of the fact that α CN occupies the biggest part of casein micelle about 40%, β CN 35% and κ CN 15%, respectively.

The observed signal 3275 cm^{-1} (1) in the case of native CNs (α_{S1} -, β -, κ CN) and their metallocomplexes ($Zn\alpha_{S1}CN120/350/600$, $Zn\beta CN120/350/600$, $Zn\kappa CN120/350/600$) is assigned for the NH stretching vibrations occurring in amide A, whose frequency depends exclusively on the strength of the hydrogen bond. Near the obtained signal is the less intense signal at 3068 cm^{-1} (2) found among all native proteins – amide B, which is also due to NH stretching vibrations. This signal (2) disappeared among $Zn\alpha_{S1}CN120/350/600$ and $Zn\kappa CN120/350/600$ metallocomplexes, and in the case of $Zn\beta$ CN for a concentration of 600 mg/L [52]. The signals at 2959 cm^{-1} (3) and 2931 cm^{-1} (4) are from asymmetric stretching vibrations, and the signal 2875 cm^{-1} (5) is from small stretching bands. For the metallocomplexes $Zn\alpha_{S1}CN350/600$ and $Zn\kappa CN350/600$, there was a disappearance of the band 2931 cm^{-1} (4) [53].

Absorbing at a wavelength of 1636 cm^{-1} (6), amide I vibrations derived from C=O stretching vibrations together with minor contributions from out-of-phase CN stretching vibrations, CCN deformation, and NH in-plane bending were recorded for both native proteins and metallocomplexes, with a significant decrease in the intensity of the obtained signals among metallocomplexes indicative of interference in the protein structure by the presence of Zn^{2+} ions [52]. An out-of-phase combination of NH in-plane vibrations and CN stretching vibrations with smaller contributions from CO in-plane vibrations and CC and NC stretching vibrations is characterized in amide II corresponding to signals 1532 cm^{-1} (7) and 1516 cm^{-1} (8) [52]. For all metallocomplexes ($Zn\alpha_{S1}CN120/350/600$, $Zn\beta CN120/350/600$, $Zn\kappa CN120/350/600$) a disappearance of the signal (7) was noticed. The 1516 cm^{-1} signal (8) similarly to the signal from amide I (6) for metallocomplexes was characterized by a decrease in intensity. A major role for both amide I and amide II are played by the secondary structure of the proteins studied. According to literature data, the α -helix content of α_{S1} CN is estimated to be 5–20%, and the value for β -sheet is 17–46%. In β CN there is 7–25% of α -helix structure, 15–33% of β -sheet and 29–35% of turn. Meanwhile, κ CN suggests a proportion of 10–20% α -helix, 20–30% β -sheet, and 15–25% β -turns [6]. Additionally, spectral bands at 1307 cm^{-1} (11) and 1237 cm^{-1} (12) are derived from amide III as a result of the in-phase combination of the NH bending and the CN stretching vibration with small contributions from the CO in plane bending and the CC stretching vibration. For metallocomplexes $Zn\alpha_{S1}CN600$, $Zn\beta CN120$, $Zn\kappa CN120/350/600$, a

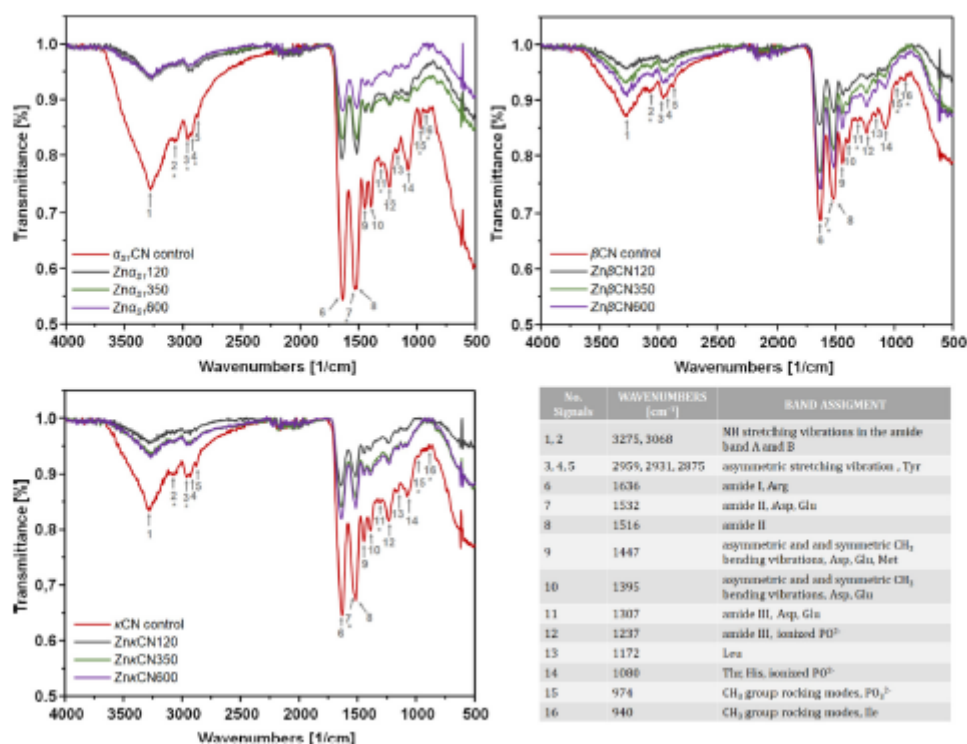


Fig. 5. FTIR-ATR spectra of CN before and after Zn²⁺ ions binding reaction at 120, 350 and 600 mg/L concentration of Zn²⁺ ions.

signal observed at 1307 cm⁻¹ (11) disappeared. The predominant presence of amides I, II, III and the observed changes are due to structural changes of proteins.

The side chains of amino acids provide valuable information, which by interacting with metals, especially in this case zinc ions, affect the structural changes of the protein that are observed in the obtained spectra [52]. Signals at 1447 cm⁻¹ (9) and 1395 cm⁻¹ (10) are associated with asymmetric and symmetric CH₂ bending vibrations and originate from amino acid side chains in peptides and proteins. The band at 1080 cm⁻¹ (14) can be attributed to the presence of threonine (Thr), which is formed by stretching the C-O vibration and rocking of NH₂ structure [54]. In turn, signals appearing at 2959, 2931 and 2875 cm⁻¹ correspond to aliphatic symmetric and asymmetric CH₂ stretching vibrations of tyrosine (Tyr) [55,56]. The 1080 cm⁻¹ signal can also be attributed to His, whose imidazole group has two nitrogen atoms that are coordinated to metal ions [57,58]. The band at 1636 cm⁻¹ (6) may come from stretching the symmetric CCC bond and the guanidyl group of arginine (Arg) [59]. In turn, the signals at 1532 cm⁻¹ (7), 1447 cm⁻¹ (9), 1395 cm⁻¹ (10), and 1307 cm⁻¹ (11) are derived from carboxyl groups of aspartic (Asp) and glutamic (Glu) acids, which confirms the zinc-casein interactions through coordination with the side chain oxygen of acidic amino acids [60]. It is in a good correlation with our previous studies in which similar FTIR-ATR vibrations were observed [14,27,30]. Signal at 1447 cm⁻¹ (9) can be attributed to the CH₂ deformation bands of methionine (Met) but also bands at 974 cm⁻¹ (15) and 940 cm⁻¹ (16) were assigned to CH₃ group rocking modes [61]. The band in region at 940 cm⁻¹ (16) may indicate the presence of isoleucine (Ile) and band at 1172 cm⁻¹ (13) in-

dicates the presence of leucine (Leu). For ZnβCN120/350/600 metallocomplexes, a disappearance of the signal at 974 cm⁻¹ (15) was observed and the signal at 940 cm⁻¹ (16) disappeared for zinc ion concentrations of 120 and 350 mg/L. On the other hand, for ZnκCN120/350/600 metallocomplexes, the signal at 974 cm⁻¹ (15) disappeared.

The observed signals at 1237 cm⁻¹ (12) and 1080 cm⁻¹ (14) may be due to asymmetric and symmetric stretching of ionized PO₄²⁻, respectively [62]. The signal for native proteins and Znα₂CN120/350/600 at 974 cm⁻¹ (15) may correspond to the -PO₃²⁻ moiety of the serine phosphate residue. The presence of the 974 cm⁻¹ (15) band indicates that CCP molecules have been released from the phosphate residues, leading to an increase in the negative charge of casein. The CCP molecule dissociates into Ca²⁺ and HPO₄²⁻ upon release of the serine-phosphate residue [63].

The second spectroscopic technique chosen to determine potential Zn²⁺ ion binding sites to casein fractions is the above-mentioned Raman spectroscopy, which complements the results obtained so far. These results are presented in Fig. 6. From the obtained spectral spectra, it can be concluded that in the whole spectral range 4000–500 cm⁻¹, the native (control) α₂CN, which is located in the inside of the casein micelle, and its metallocomplexes show the highest intensities of the obtained bands. Successively, lower signal intensities are observed for the control proteins βCN and κCN and their complexes. The observed signal at 3309 cm⁻¹ (1) can be attributed to the NH₂ band and the signal at 3059 cm⁻¹ (2) to the aromatic CH band. In the range at 2800–3000 cm⁻¹ (2929 cm⁻¹ (3) and 2875 cm⁻¹ (4)) there are C-H stretching

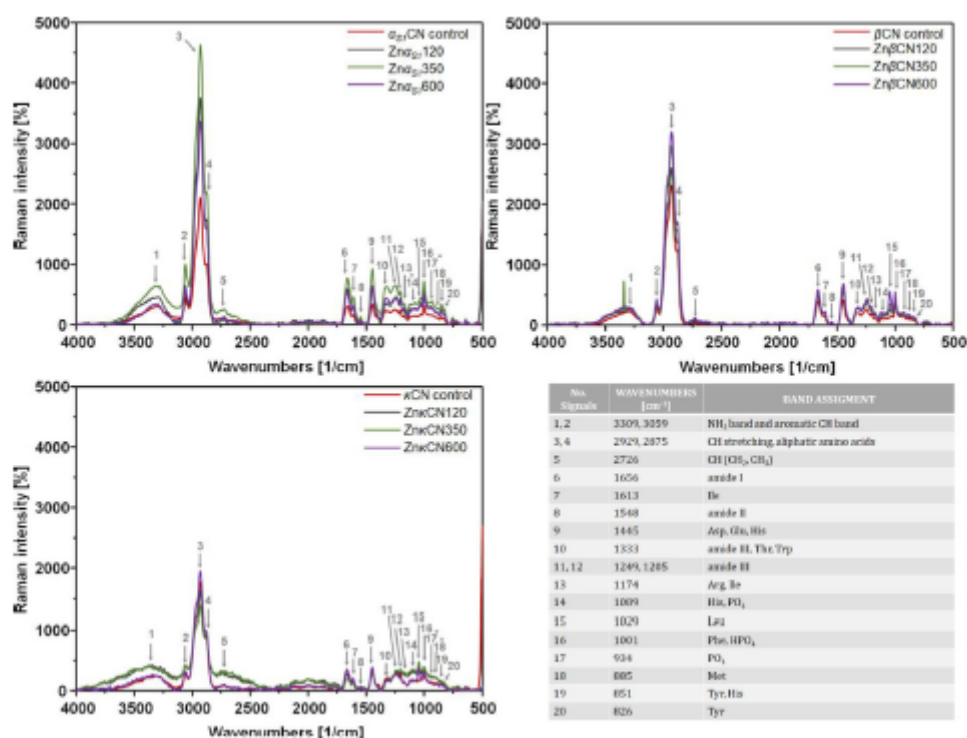


Fig. 6. Raman spectra of CN before and after Zn²⁺ ions binding reaction at 120, 350 and 600 mg/L concentration of Zn²⁺ ions.

and deformation bands of aliphatic amino acids, and the band at 2726 cm⁻¹ (5) corresponds to CH bonds (CH₂, CH₃) [64].

A typical Raman spectrum of proteins consists of signals from three main types of vibrations. These vibrations originate from amide bands and from aromatic and non-aromatic side chains of amino acid residues, which are located in the 1656–826 cm⁻¹ region that is very rich in structural information and changes due to the addition of Zn²⁺ ions [65]. The C–O stretching vibration in plane peptide and, in part, the N–H bending vibration in plane peptide are due to the presence of the amide I band observed for signal 1656 cm⁻¹ (6), which is characterized by high intensity for each of the casein fractions and their complexes [64]. The vibration of amide II corresponds to signal at 1548 cm⁻¹ (8), which is an out-of-phase nonphase combination of C–N stretching and N–H bending motions [65]. Whereas the observed amide III band is mainly due to C–N stretching vibrations and N–H bending vibrations in the peptide bond plane and is located in the 1200–1333 cm⁻¹ region (1333 cm⁻¹ (10), 1249 cm⁻¹ (11) and 1205 cm⁻¹ (12) [65,66]. Because casein proteins are described as natively unfolded with random coil structures, band at 1333 (10) may be associated with the helical conformation of poly(L-proline) II (PPII). This may be due to recent Raman optical activity (ROA) measurements that determine the secondary structure of caseins [67,68].

The vibration of the ionized carboxyl group (COO⁻) of aspartic (Asp) and glutamic (Glu) acids shows a very intense band at 1445 cm⁻¹ (9) [64]. According to the literature data [5,6], α₂₁-, β- and κCN possess 25, 19 and 13 glutamic acid residues, respectively, making this amino acid one of the dominant amino acids in their structure. The observed spectral changes are also in a good agreement with the infrared spectroscopy data. The signal at 1333

cm⁻¹ is attributed to the C–H deformation vibration of threonine (Thr) [66,69] and cystine, but may also correspond to tryptophan (Trp) vibrations. Signal 1174 cm⁻¹ (13) can be attributed to C–N₂–H₂ asymmetric bending of arginine (Arg), but also to isoleucine (Ile) [66,70]. Ile may also correspond to band 1613 cm⁻¹ (7) [66]. Signal 1029 cm⁻¹ (15) with much lower intensity among native α₂₁CN and its metallocomplexes is characterized by bands associated to several C–C and C–N stretching vibrations of leucine (Leu) [71,72]. In contrast, signal 1001 cm⁻¹ (16) was assigned to the aromatic amino acid residue phenylalanine (Phe) [64]. These amino acids may indicate the sites where connections to zinc ions occur. Also, signal 1001 cm⁻¹ (16) may correspond to HPO₄ and signal 851 cm⁻¹ (19) to H₂PO₄. [73]. All casein proteins are phosphorylated and these changes are indicative of the binding of zinc ions to particular casein fractions with phosphate ions. The vibrational modes of tyrosine (Tyr) residues were assigned signals 851 cm⁻¹ (19) and 826 cm⁻¹ (20), which often plays an important role as a coordination ligand for metals [74]. These dual signals arise from the Fermi resonance of the ring breathing vibration and the overtone of the ring bending vibration from the plane of the para-substituted benzene ring [64,74]. From signals at 1443 cm⁻¹ (9), 1089 cm⁻¹ (14) and 851 cm⁻¹ (19), the imidazole group of histidine (His) may be originated [66,75]. Typical phosphate-related oscillations were assigned to signals at 1089 cm⁻¹ (14) and 934 cm⁻¹ (17), which correspond to PO₄. Signal (17) disappeared for native α₂₁CN and the Znα₂₁CN120 metallocomplex and for native κCN and all ZnκCN120/350/600 metallocomplexes. Similarly, there was a disappearance of band at 885 cm⁻¹ (18) for κCN and its complexes, which is attributed to methionine (Met) which is a sulfur-containing amino acid [66].

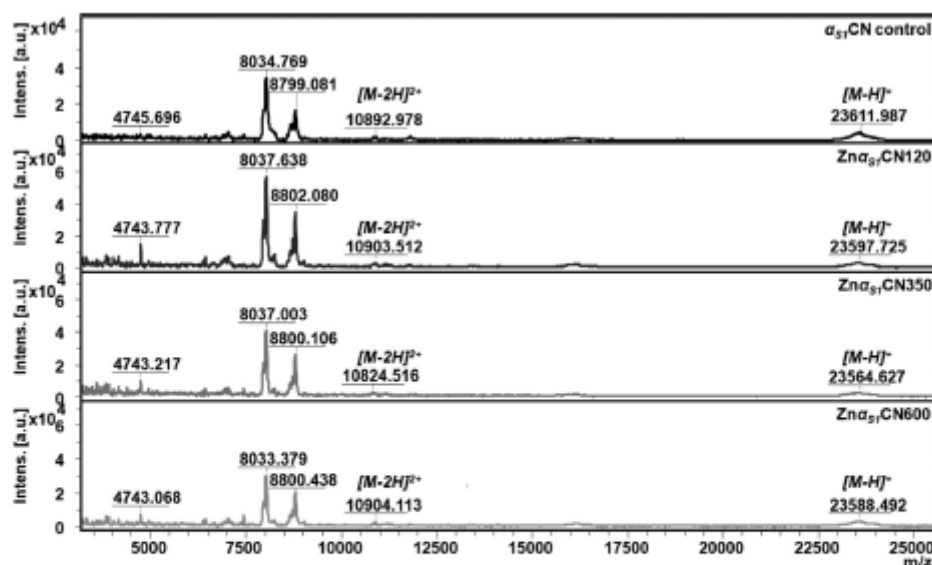


Fig. 7. MALDI-TOF MS intact spectra of native α_{S1} CN and complexes with Zn^{2+} ions ($Zn\alpha_{S1}CN120/350/600$).

3.6. Polyacrylamide gel electrophoresis study

A commonly used method to study proteins is gel electrophoresis, in which the different protein fractions are separated/differentiated based on differences in protein size, charge and conformation. Performed gel electrophoresis, which was subjected to native (control) caseins α_{S1} CN, β CN, κ CN, and the obtained metallocomplexes $Zn\alpha_{S1}$ CN, $Zn\beta$ CN, $Zn\kappa$ CN at three different concentrations of zinc ions 120, 350, and 600 mg/L allowed to determine the purity of the obtained samples, as well as a preliminary determination of their mass. The electrophoresis results were evaluated visually and it was a qualitative assessment (Fig. S1). The obtained bands for α_{S1} CN, β CN, κ CN, and their metallocomplexes indicated contamination in the case of κ CN and its complexes which may be due to the lower purity of the standard used (>70%, Sigma Aldrich). The obtained bands indicate that the mass of α_{S1} CN and $Zn\alpha_{S1}CN120/350/600$ is about 24 kDa, for β CN and $Zn\beta CN120/350/600$ about 23 kDa, and for κ CN and $Zn\kappa CN120/350/600$ about 19 kDa. In addition, polypeptide fragments were observed for each of the casein fractions and their complexes. Additionally, the same bands were obtained for metallocomplexes as for native proteins indicating that Zn^{2+} ions do not contribute to the degradation of native proteins.

3.7. Mass spectrometric study

MALDI-TOF MS was used as a complementary technique to determine intact casein control masses and compare them with complexes to monitor changes due to the addition of different concentrations of Zn^{2+} ions (120, 350, 600 mg/L). Figs. 7–9 shows the spectra obtained for native CNs and their metallocomplexes using the SA matrix.

Based on the results, the intact mass of α_{S1} CN was 23611.987 m/z (Fig. 7). For the complexes, the mass changed ($Zn\alpha_{S1}CN120$ –23597.725 m/z, $Zn\alpha_{S1}CN350$ –23564.627 m/z, $Zn\alpha_{S1}CN600$ –23588.492 m/z). The observed reduction in the mass of the studied complexes is due to the modification of native α_{S1} CN with zinc addition.

Slightly different situation is observed for native β CN and $Zn\beta CN120/350/600$ complexes (Fig. 8), since in addition to monomers, dimers and even trimer are noticed for the studied samples. The obtained intact mass of β CN was 23985.050 m/z, and for $Zn\beta CN120/350/600$ complexes similarly as for α_{S1} CN complexes there was a decrease in mass ($Zn\beta CN120$ –23961.152 m/z, $Zn\beta CN350$ –23962.425 m/z, $Zn\beta CN/600$ –23957.880 m/z). Also, as the zinc ion concentration increases, a marked decrease in signal intensity is observed.

For the smallest native casein protein (κ CN), the intact mass was 19017.846 m/z (Fig. 9). In contrast, suppression for this signal is observed for $Zn\kappa CN120/350/600$ complexes. Based on the comparative analysis of MALDI-TOF MS spectra of control κ CN and complexes with zinc ions additionally, two new intense signals ~7974 m/z and ~8045 m/z are observed for $Zn\kappa CN120/350/600$ complexes. In addition, the appearance of new six signals in the range 5000–7000 m/z (Fig. 9 – A) was also observed for the complexes. The observed signal suppression and the appearance of new signals indicate that zinc interferes with the binding process. These signals occur as a result of the addition of a zinc ion to the native κ CN. Karmakar and Das [76] in their study, performed trypsin digestion of proteins in solution in the presence and absence of zinc ions. It appears that the formation of new peptides is observed when zinc is present [76]. Regarding our results, it can be concluded that zinc ions cause the decay of some fragments in the source, generating new dehydration and decarboxylation which results in the presence of new signals, thus influencing the mass change. In addition, the different result obtained compared with α_{S1} CN and β CN may be due to the fact that κ CN is the only casein protein that undergoes glycosylation.

The combination of gel electrophoresis and MALDI-TOF MS mass spectrometry method provided accurate knowledge of the mass of α_{S1} CN, β CN κ CN.

3.8. Molecular docking

Molecular docking is a useful bioinformatics tool that can predict the sites and/or nature of interaction between molecules. Typ-

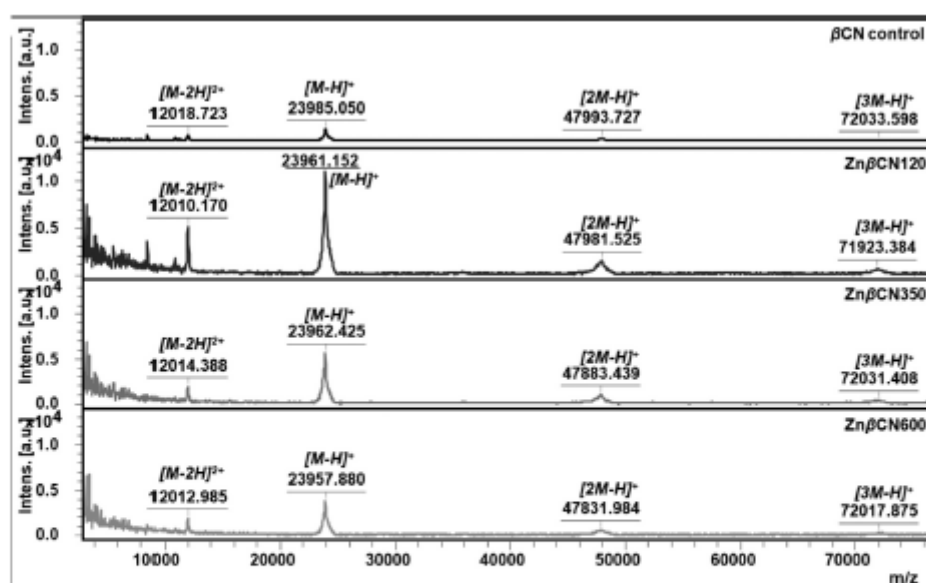


Fig. 8. MALDI-TOF MS intact spectra of native β CN and complexes with Zn^{2+} ions (Zn β CN120/350/600).

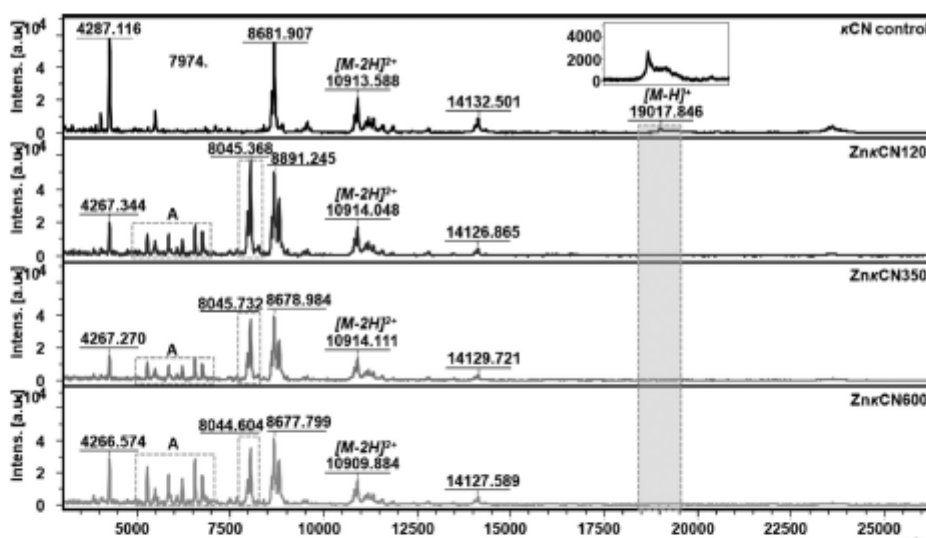


Fig. 9. MALDI-TOF MS intact spectra of native α CN and complexes with Zn^{2+} ions (Zn α CN120/350/600).

ically, a receptor macromolecule, or protein structure and a ligand, such as a small protein, metal ion, or small organic compound are used. The basic idea of the simulation is to use at least two unrelated structures and find the strongest connection that can exist between them [77–79].

Based on the obtained data regarding the interaction between α_{51} CN and the Zn^{2+} ion, it can be concluded that the zinc ion binds preferentially to certain amino acid residues. This group includes: Glu (21 cases, 58%), His (12 cases, 33%), Gln (2 cases, 6%), Ile (1 case, 3%). α_{51} CN shows high binding affinity for Zn^{2+} with docking scores of 1.791, 1.416, 1.327 and 1.234, respectively. Interestingly, for the first two scores the Zn^{2+} binding position is iden-

tical (133E, 136H), the other two scores differ only in the first binding position (132E, 136H). The predicted docking positions for Zn^{2+} with α_{51} CN are shown in Fig. 10 lists the binding positions, interacting amino acids, and binding results for the α_{51} CN interaction with Zn^{2+} .

The operation of the MIB server is based on the collection of protein structures of casein complexes with Zn^{2+} ions in PDB format. Homologous proteins were filtered out. From these metal ion-bound proteins, templates of metal-binding residues were extracted. Each template represented a local structure of metal-binding residues, i.e., residues at least partially located at a distance of 3.5 Å from the metal ion. A metal-binding site had to con-

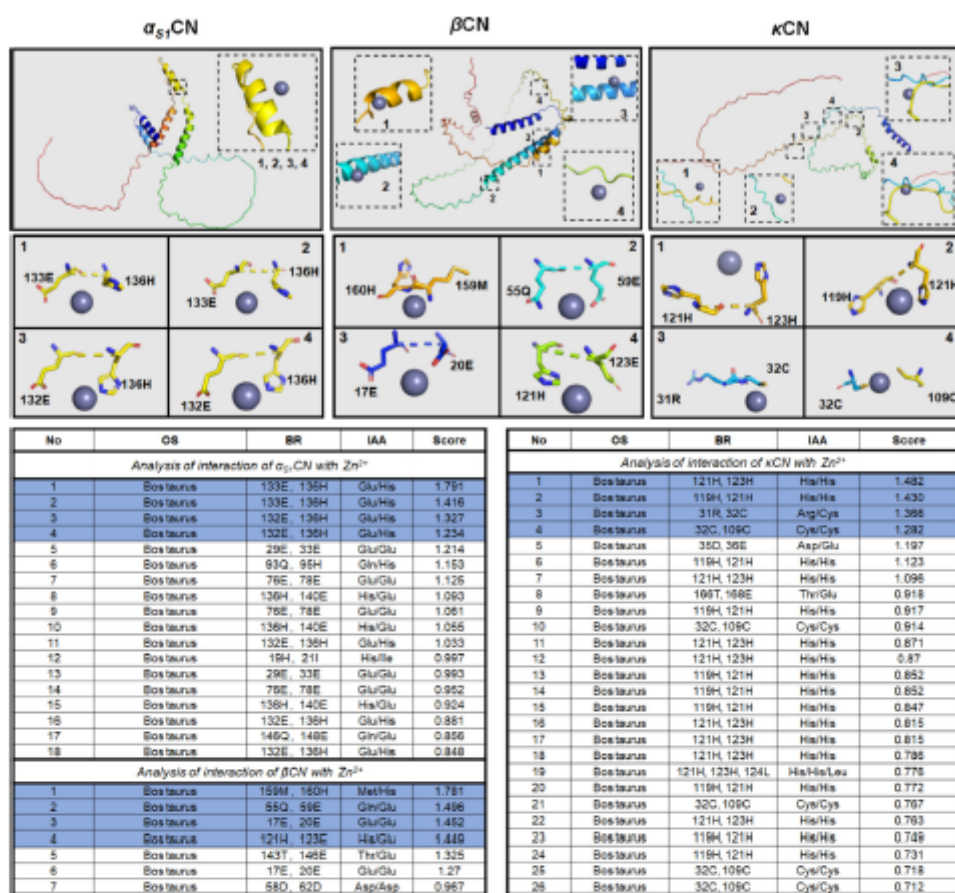


Fig. 10. Molecular docking between $\alpha_{s1}CN$ and Zn^{2+} (1 – score 1.791, 2 – score 1.416, 3 – score 1.327, 4 – 1.234), βCN and Zn^{2+} (1 – score 1.781, 2 – score 1.496, 3 – score 1.452, 4 – 1.449) and κCN and Zn^{2+} (1 – score 1.482, 2 – score 1.430, 3 – score 1.366, 4 – 1.282). (BR) Binding Residues, (IAA) interacting amino acid, (OS) Organism Source. The blue background color in the tables (numbers 1, 2, 3, 4) corresponds to the protein structure in the figure.

tain a metal ion and at least two residues to qualify as a template of metal ion-binding residues. A detailed calculation method with explanation was presented by Liu et al. [34] and Lu et al. [79].

Interpreting the results obtained from the analysis of the interaction between βCN and the Zn^{2+} ion, we can conclude that the zinc ion binds preferentially to certain amino acid residues. This group includes: Glu (7 cases, 50%), His (2 cases, 14%), Asp (2 cases, 14%), Gln (1 case, 7%), Met (1 case, 7%), Thr (1 case, 7%). βCN shows high binding affinity for Zn^{2+} with docking scores of 1.781, 1.496, 1.452 and 1.449. The highest score the Zn^{2+} binding position is for (159M, 160H). The predicted docking positions for Zn^{2+} with βCN are shown in Fig. 10 lists the binding positions, interacting amino acids, and binding results for the βCN interaction with Zn^{2+} . The results obtained from the analysis of the interaction between κCN and the Zn^{2+} ion, conclude that the zinc ion binds preferentially to certain amino acid residues. This group includes: His (36 cases, 68%), Cys (11 cases, 21%), Glu (2 cases, 4%), Arg (1 case, 2%), Asp (1 case, 2%), Thr (1 case, 2%), Leu (1 case, 2%). κCN shows high binding affinity for Zn^{2+} with docking scores of 1.482, 1.430, 1.366 and 1.282. The highest score the Zn^{2+} binding position is (121H, 123H), the second score (119H, 121H). Additionally, only in κCN is zinc ion binding to Cys observed – κCN has two cysteine

residues. The presence of Cys in κCN contributes to the formation of disulfide bridges to form a polymeric structure. Despite accounting for only 13% of all casein, κCN molecules must adhere to each other in micelles to form disulfide-linked aggregates [80].

A computer model generated for κCN by Kumosifski et al. [80] describes that κCN can be viewed as a „horse and rider“. The amino-terminal portion of 110-120 residues represents the „horse“ and the carboxy-terminal portion represents the „rider“. Two distinct legs can be seen in the „horse“ part of the model. These legs are represented by β -sheet regions consisting of residues 20-25; 29-34; 39-45; and 49-55, which are connected by γ - or β -turns. Cys-11 is located between the two segments with the predicted α -helical conformation and is on the left side of the „rider“, and Cys-88 is located in the predicted β -turn on the opposite side. Both of these residues are located close to the surface of the molecule and are more than 33 Å apart. This may explain the ability of the κCN molecule to form inter-chain polymers with disulfide bonds [88]. The predicted docking positions for Zn^{2+} with κCN are shown in Fig. 10 lists the binding positions, interacting amino acids, and binding results for the κCN interaction with Zn^{2+} .

Studies on the prediction of Zn^{2+} ion binding sites using MIB server showed that metal ions have different binding sites for dif-

ferent casein conformations included in the experiment. Studies have shown that the interacting amino acids differ not only depending on the structure and source of the caseins. The result of the study is the determination of the affinity of the Zn^{2+} ion for different casein varieties. Thanks to this *in silico* analysis, information on metal affinity to protein can be extracted before real-time studies using advanced tools, thus avoiding unnecessary costs and making appropriate modifications to the experimental procedure at an early stage. Therefore, this computational analysis will serve as an aid in evaluating the attachment of Zn^{2+} ions to casein.

It is also important to compare the *in-silico* results with publicly available literature data on experimentally determined amino acid residues interacting with Zn^{2+} ions. According to the literature data, Zn^{2+} ions show high affinity towards the following amino acid residues: His, Cys, Glu and Asp. By comparing these data with the tables obtained using MIB we can conclude that the results obtained are complementary to the commonly known knowledge concerning the studied issue. Obviously, the modelling result and thus the predicted site of attachment of the metal ion to the protein structure depends on the sequence and spatial conformation of the protein structure.

The obtained molecular docking results correlate with the obtained instrumental techniques. Nevertheless, using molecular docking we are able to determine potential Zn^{2+} ion binding sites in the IV-order tertiary structure of individual casein proteins, which definitely gives more information in comparison with the spectroscopic method. chain.

4. Conclusion

The present work shows, for the first time, the isothermal study of zinc binding to the particular casein fractions: α_{S1} -, β - and κ CN. As the result of the binding, the specific ZnCN metal complexes were formed. Isothermal studies indicated that zinc adsorption on the casein surface occurs in a heterogeneous and complex way. According to the calculated amount of zinc moles, it was found that as the concentration of zinc ions increased, more zinc ions were involved in the binding process with the different casein protein fractions. Based on the obtained experimental data, it was concluded that the different manner of individual zinc-caseins binding process strongly depends on their size, amino acid's sequence/structure and hydrophobicity. As a complementary method, the CE-ICP-MS was performed and finally confirmed the zinc binding to the β CN. The stability study revealed the zeta potential is strongly associated with the hydrophobicity, size and structure of tested casein fractions. Moreover, the ZP of tested complexes depends on the concentration of the bound Zn^{2+} ions. The α_{S1} CN (average ZP value about -27 mV) located inside the casein micelle appeared to be the most stable over the whole range of zinc concentrations. In the case of the most hydrophobic casein fraction (β CN), the addition of the lowest (1 mg/L Zn^{2+} ions) and highest (600 mg/L Zn^{2+} ions) concentration resulted on the lowest stability of sample. On the other hand, the κ CN was unstable in the all tested Zn^{2+} concentration with the average ZP around -5.9 mV. The colloidal behaviour of caseins as well as the possibility of their easy surface modulation by zinc ions creates new opportunities in the food industry. Scanning electron microscopy indicated the difference between the protein surface before and after the Zn^{2+} binding. The observed surface modifications were generated mainly by the adsorption of Zn^{2+} ions on the tested protein. However, the influence of the Zn^{2+} ions concentration as well as the hydrophobicity of casein on the protein surface changes was also observed. The most hydrophilic α_{S1} CN required the highest concentration of zinc ions to change its structure to more globular. Spectroscopic analysis, including FTIR-ATR and Raman, was employed to evaluate the changes in α_{S1} -, β - and κ CN after the zinc binding. The generated

results have indicated the polar amino acids residues, mainly glutamic and aspartic acid's carboxylic groups, as those mainly contributing in the described phenomenon. The MALDI-TOF MS analysis allowed determination of the molecular profiles obtained native proteins and their metal complexes, and served as an additional method for the binding process.

Finally, the molecular docking study of Zn^{2+} ions bound to individual casein isoforms is reported. Taking into account the obtained experimental and computational data, it can be concluded that the deprotonated carboxyl group of glutamic acid as well as imidazole ring of histidine were the dominant amino acids of α_{S1} - and β CN interacting with Zn^{2+} ions the most. Intriguingly, in the interaction between κ CN and zinc, the sulfur from the cysteine might play a pivotal role. Hence, the great agreement between the molecular docking and spectroscopic results were obtained.

Declaration of Competing Interest

The authors declare that they have no known competing financial interests or personal relationships that could have appeared to influence the work reported in this paper.

CRedit authorship contribution statement

Agnieszka Rodzik: Conceptualization, Methodology, Investigation, Writing – original draft, Visualization, Data curation. **Anna Król-Górniak:** Methodology, Investigation, Writing – original draft. **Viorica Railean:** Methodology, Investigation, Writing – review & editing, Visualization. **Mateusz Sugajski:** Investigation, Data curation, Writing – original draft, Software, Resources. **Adrian Gołębowski:** Methodology, Investigation. **David S. Horne:** Writing – review & editing. **Bernhard Michalke:** Writing – review & editing, Data curation. **Myrosław Sprynsky:** Writing – review & editing. **Paweł Pomastowski:** Conceptualization, Funding acquisition, Project administration. **Bogusław Buszewski:** Conceptualization, Supervision, Resources.

Data Availability

No data was used for the research described in the article.

Acknowledgment

The publication was created thanks to the support of the Ministry of Education and Science, Poland program Innovation Incubator 4.0 at Nicolaus Copernicus University in Torun, Poland, co-financed by the European Union under the European Regional Development Fund (contract No MNIŚW/2020/331/DIR). Anna Król-Górniak obtained funds as part of the financing for a doctoral scholarship from the National Science Centre: Etiuda 7 No. 2019/32/T/ST4/00098 (2019–2020).

Supplementary materials

Supplementary material associated with this article can be found, in the online version, at doi:10.1016/j.molstruc.2022.134251.

References

- [1] A. Rodzik, P. Pomastowski, G.N. Sagandykova, B. Buszewski, Interactions of whey proteins with metal ions, *Int. J. Mol. Sci.* 21 (2020) 1–26, doi:10.3390/ijms21062156.
- [2] C.G. De Kruif, C. Holt, Casein micelle structure, functions, and interactions, in: *Advanced Dairy Chemistry: Volume 1A: Proteins: Basic Aspects*, 4th ed., Springer, Boston, MA, 2003, pp. 185–209, doi:10.1007/978-1-4614-4714-6_6.
- [3] K. Petrotos, E. Tsakali, P. Goulas, A.G. D'Alessandro, Casein and whey proteins in human health, in: *Milk and Dairy Products as Functional Foods*, John Wiley & Sons, Ltd, 2014, pp. 94–146, doi:10.1002/9781118635056.ch4.

- [4] E.W. Bingham, N. Parris, H.M. Farrell, Phosphorylation of β -casein and α -lactalbumin by casein kinase from lactating bovine mammary gland, *J. Dairy Sci.* 71 (1988) 324–336, doi:10.3168/jds.S0022-0302(88)79561-2.
- [5] D.S. Home, Casein micelle structure: models and muddles, *Curr. Opin. Colloid Interface Sci.* 11 (2006) 148–153, doi:10.1016/j.cocis.2005.11.004.
- [6] T. Huppertz, P.F. Fox, A.L. Kelly, The caseins: structure, stability, and functionality, in: *Proteins in Food Processing*, 2nd ed., Elsevier Ltd., 2018, pp. 49–92, doi:10.1016/B978-0-08-100722-8.00004-8.
- [7] C.W. Slattery, R. Evard, A model for the formation and structure of casein micelles from subunits of variable composition, *Biochim. Biophys. Acta* 317 (1973) 529–538, doi:10.1016/0005-2795(73)90246-8.
- [8] C. Holt, Structure and stability of bovine casein micelles, *Adv. Protein Chem.* 43 (2015) 63–151, doi:10.1016/S0065-3233(08)60554-9.
- [9] D.S. Horne, Casein interactions: casting light on the black boxes, the structure in dairy products, *Int. Dairy J.* 8 (1998) 171–177, doi:10.1016/S0958-6946(98)00040-5.
- [10] M. Hayes, R.P. Ross, G.F. Fitzgerald, C. Hill, C. Stanton, Casein-derived antimicrobial peptides generated by *Lactobacillus acidophilus* DPC6026, *Appl. Environ. Microbiol.* 72 (2006) 2260, doi:10.1128/AEM.72.3.2260-2264.2006.
- [11] J. Ma, W. An, Q. Xu, Q. Fan, Y. Wang, Antibacterial casein-based ZnO nanocomposite coatings with improved water resistance crafted via double in situ route, *Prog. Org. Coat.* 134 (2019) 40–47, doi:10.1016/j.porgcoat.2019.05.007.
- [12] J. Huang, W. Qian, L. Wang, H. Wu, H. Zhou, A.Y. Wang, H. Chen, L. Yang, H. Mao, Functionalized milk-protein-coated magnetic nanoparticles for MRI-monitored targeted therapy of pancreatic cancer, *Int. J. Nanomed.* 11 (2016) 3087–3099, doi:10.2147/IJN.S92722.
- [13] X. Li, M. Jian, Y. Sun, Q. Zhu, Z. Wang, The peptide functionalized inorganic nanoparticles for cancer-related bioanalytical and biomedical applications, *Molecules* 26 (2021) 1–30, doi:10.3390/MOLECULES26113228.
- [14] P. Prysichpepa, A. Sagandykova, G.N. Pomastowski, V. Railean-Plugaru, A. Król, A. Rogowska, A. Rodzik, B. Sprynskyy, M. Buszewski, A new approach for spontaneous silver ions immobilization onto casein, *Int. J. Mol. Sci.* 20 (2019) 1–18, doi:10.4018/978-1-7998-8591-7.ch021.
- [15] EP3034512A1, A process for producing iron (III) casein N-acetyl-aspartylated complexes and use thereof in pharmaceutical compositions, 2016. patents.google.com/patent/EP3034512A1/en.
- [16] JP4191261B2, Iron casein complex and its production method, 2008. patents.google.com/patent/JP4191261B2/en?q=A23J3E2F325.
- [17] CN102836419A, Iron protein succinylate oral solution and preparation method thereof, 2014. patents.google.com/patent/CN102836419A/en.
- [18] A. Krężel, W. Maret, The biological inorganic chemistry of zinc ions, *Arch. Biochem. Biophys.* 611 (2016) 3–19, doi:10.1016/j.abb.2016.04.010.
- [19] L. Rulíšek, Z. Havlas, Using DFT methods for the prediction of the structure and energetics of metal-binding sites in metalloproteins, *Int. J. Quantum Chem.* 91 (2003) 504–510, doi:10.1002/qua.10442.
- [20] H. Tapiero, K. Tew, Trace elements in human physiology and pathology: zinc and metallothioneins, *Biomed. Pharmacother.* 57 (2003) 399–411, doi:10.1016/S0753-3322(03)00081-7.
- [21] T. Kambe, T. Tsuji, A. Hashimoto, N. Isumura, The physiological, biochemical, and molecular roles of zinc transporters in zinc homeostasis and metabolism, *Physiol. Rev.* 95 (2015) 749–784, doi:10.1152/physrev.00035.2014.
- [22] W. Maret, Metals on the move: zinc ions in cellular regulation and in the coordination dynamics of zinc proteins, *Biomaterials* 24 (2011) 411–418, doi:10.1007/S10534-010-9406-1.
- [23] R.B. Saper, R. Rash, Zinc: an essential micronutrient, *Am. Fam. Physician* 79 (2009) 768–772.
- [24] M. Corredig, P.K. Nair, Y. Li, H. Eshpari, Z. Zhao, Invited review: Understanding the behavior of caseins in milk concentrates, *J. Dairy Sci.* 102 (2019) 4772–4782, doi:10.3168/JDS.2018.15943.
- [25] M. Glantz, T.G. Devold, G.E. Vegarud, H. Lindmark Månsson, H. Stålhammar, M. Paulsson, Importance of casein micelle size and milk composition for milk gelation, *J. Dairy Sci.* 93 (2010) 1444–1451, doi:10.3168/jds.2009.2856.
- [26] B. Michalke, S. Halbach, V. Nischwitz, Metal speciation related to neurotoxicity in humans, *J. Environ. Monit.* 11 (2009) 939–954, doi:10.1039/b817877h.
- [27] A. Rodzik, P. Pomastowski, V. Railean-Plugaru, M. Sprynskyy, B. Buszewski, The study of zinc ions binding to α S1-, β - and κ -casein, *Int. J. Mol. Sci.* 21 (2020) 1–18, doi:10.3390/ijms21218096.
- [28] P. Pomastowski, M. Sprynskyy, B. Buszewski, The study of zinc ions binding to casein, *Colloids Surf. B* 120 (2014) 21–27, doi:10.1016/j.colsurfb.2014.03.009.
- [29] B. Buszewski, A. Rodzik, V. Railean-Plugaru, M. Sprynskyy, P. Pomastowski, A study of zinc ions immobilization by β -lactoglobulin, *Colloids Surf. A* 591 (2020) 124443, doi:10.1016/j.colsurfa.2020.124443.
- [30] B. Buszewski, P. Zavela, A. Król-Górniak, V. Railean-Plugaru, A. Rogowska, M.W. Wong, M. Yi, A. Rodzik, M. Sprynskyy, P. Pomastowski, Interactions of zinc aqua complexes with ovalbumin at the forefront of the Zn²⁺/ZnO/OVO hybrid complex formation mechanism, *Appl. Surf. Sci.* 542 (2021) 148641, doi:10.1016/j.apsusc.2020.148641.
- [31] B. Michalke, D. Willkommen, V. Venkataramani, Setup of capillary electrophoresis-inductively coupled plasma mass spectrometry (CE-ICP-MS) for quantification of iron redox species (Fe(II), Fe(III)), *J. Vis. Exp. : JoVE* 159 (2020) 1–8, doi:10.3791/61055.
- [32] B. Michalke, D. Willkommen, V. Venkataramani, Iron redox speciation analysis using capillary electrophoresis coupled to inductively coupled plasma mass spectrometry (CE-ICP-MS), *Front Chem.* 7 (2019) 136, doi:10.3389/FCHEM.2019.00136/BIBTEX.
- [33] O. Prysichpepa, K. Rafińska, A. Golebiowski, M. Sugajski, G. Sagandykova, P. Madajski, B. Buszewski, P. Pomastowski, Synthesis and physicochemical characterization of bovine lactoferrin supersaturated complex with iron (III) ions, *Sci. Rep.* 12 (2022) 1–12, doi:10.1038/s41598-022-15814-2.
- [34] Y.F. Lin, C.W. Cheng, C.S. Shih, J.K. Hwang, C.S. Yu, C.H. Lu, MIB: metal ion-binding site prediction and docking server, *J. Chem. Inf. Model.* 56 (2016) 2287–2291, doi:10.1021/acs.jcim.6b00407.
- [35] E. Di Muzio, D. Toti, E. Pollicelli, DockingApp: a user friendly interface for facilitated docking simulations with AutoDock Vina, *J. Comput. Aided Mol. Des.* 31 (2017) 213–218, doi:10.1007/s10822-016-0006-1.
- [36] O. Trott, A.J. Olson, AutoDock vina: improving the speed and accuracy of docking with a new scoring function, efficient optimization, and multithreading, *J. Comput. Chem.* 31 (2012) 455–461, doi:10.1002/jcc.
- [37] E.Da Silva, Y. Kembouche, U. Tegner, A. Baum, K.A. Jensen, Interaction of biologically relevant proteins with ZnO nanomaterials: a confounding factor for in vitro toxicity endpoints, *Toxicol. in Vitro* 56 (2019) 41–51, doi:10.1016/j.tiv.2018.12.016.
- [38] M. Sprynskyy, T. Kowalkowski, H. Tutu, E.M. Cukrowska, B. Buszewski, Ionic liquid modified diatomite as a new effective adsorbent for uranium ions removal from aqueous solution, *Colloids Surf. A* 465 (2015) 159–167, doi:10.1016/j.colsurfa.2014.10.042.
- [39] M. Jaroniec, Adsorption on heterogeneous surfaces: the exponential equation for the overall adsorption isotherm, *Surf. Sci.* 50 (1975) 553–564, doi:10.1016/0039-6028(75)90044-8.
- [40] Y.D. Lányi, A.L. Schwan, D.G. Dalgleish, A study of β -casein tertiary structure by intramolecular p.d.f., *J. Dairy Sci.* 87 (2004) 3638–3647, doi:10.3168/JDS.S0022-0302(04)73502-X.
- [41] Z. Adamczyk, M. Zaucha, M. Zembala, Zeta potential of mica covered by colloid particles: a streaming potential study, *Langmuir* 26 (2010) 9368–9377, doi:10.1021/LA1003534.
- [42] S. Ferraris, M. Gazzola, V. Peretti, B. Stella, S. Spriano, Zeta potential measurements on solid surfaces for an in vitro biomaterials testing: surface charge, reactivity upon contact with fluids and protein adsorption, *Front. Bioeng. Biotechnol.* 6 (2018) 1–7, doi:10.3389/FBIOE.2018.00060.
- [43] J.D. Clogston, A.K. Patri, Zeta potential measurement, in: *Characterization of Nanoparticles Intended for Drug Delivery*, 2010, pp. 63–70, doi:10.1007/978-1-60327-198-1_6.
- [44] D.G. Dalgleish, Measurement of electrophoretic mobilities and zeta-potentials of particles from milk using laser Doppler electrophoresis, *J. Dairy Res.* 51 (1984) 425–438, doi:10.1017/S0022029900023724.
- [45] C. Broyard, F. Gaucheron, Modifications of structures and functions of caseins: a scientific and technological challenge, *Dairy Sci. Technol.* 95 (2015) 831–862, doi:10.1007/s13594-015-0220-y.
- [46] I. Müllerová, L. Frank, Role of the high-angle BSE in SEM imaging, in: *EMC 2008 14th European Microscopy Congress 1-5 September 2008, Aachen, Germany*, Springer, Berlin, Heidelberg, 2008, pp. 585–586, doi:10.1007/978-3-540-85156-1_293.
- [47] G.E. Lloyd, Atomic number and crystallographic contrast images with the SEM: a review of backscattered electron techniques, *Mineral. Mag.* 51 (1987) 3–19, doi:10.1180/MINMAG.1987.051.359.02.
- [48] T. Huppertz, Chemistry of the caseins, in: *Advanced Dairy Chemistry: Volume 1A: Proteins: Basic Aspects*, 4th ed., Springer, Boston, MA, 2013, pp. 135–160, doi:10.1007/978-1-4614-4714-6_4.
- [49] J.W. Holland, H.C. Deeth, P.F. Alewood, Proteomic analysis of kappa-casein micro-heterogeneity, *Proteomics* 4 (2004) 743–752, doi:10.1002/PMIC.200300613.
- [50] C. Loske, A. Gerdemann, W. Schepl, M. Wycislo, R. Schinzel, D. Palm, P. Riederer, G. Münch, Transition metal-mediated glycoxylation accelerates cross-linking of β -amyloid peptide, *Eur. J. Biochem.* 267 (2000) 4171–4178, doi:10.1046/j.1432-1327.2000.01452.x.
- [51] V.N. Uversky, J. Li, A.L. Fink, Metal-triggered structural transformations, aggregation, and fibrillation of human α -synuclein: a possible molecular link between Parkinson's disease and heavy metal exposure, *J. Biol. Chem.* 276 (2001) 44284–44296, doi:10.1074/jbc.M105343200.
- [52] A. Barth, Infrared spectroscopy of proteins, *Biochim. Biophys. Acta* 1767 (2007) 1073–1101, doi:10.1016/j.bbabin.2007.06.004.
- [53] C. Invernizzi, T. Rovetta, M. Licchelli, M. Malagodi, Mid and near-infrared reflection spectral database of natural organic materials in the cultural heritage field, *Int. J. Anal. Chem.* 2018 (2018) 1–16, doi:10.1155/2018/7823248.
- [54] B.L. Silva, P.T.C. Freire, E.E.A. Melo, I. Guedes, M.A. Araújo Silva, J. Mendes Filho, A.J.D. Moreno, Polarized Raman spectra and infrared analysis of vibrational modes in L-threonine crystals, *Braz. J. Phys.* 28 (1998) 19–24, doi:10.1590/S0103-97331998000100003.
- [55] M. Themmachi, R. Mathammal, C. Sekar, Molecular structure and vibrational assignments of L-tyrosine: a detailed experimental and density functional theoretical study, *Comput. Chem.* 64 (2013) 19282–19289.
- [56] S. Kumar, A. Kumar, Vibrational study of tyrosine molecule, *Adv. Sci. Lett.* 21 (2015) 2671–2673.
- [57] S. Kumar, A.K. Rai, S.B. Rai, D.K. Rai, Infrared and Raman spectra of histidine: an ab initio DFT calculations of Histidine molecule and its different protonated forms, *Indian J. Phys.* 84 (2010) 563–573, doi:10.1007/s12648-010-0039-6.
- [58] S. Celik, G. Yilmaz, A.E. Ozel, S. Aktyuz, Structural and spectral analysis of anticancer active cyclo(Ala-His) dipeptide, *J. Biomol. Struct. Dyn.* 40 (2022) 660–672, doi:10.1080/07391102.2020.1817150.

- [59] S. Kumar, S.B. Rai, Spectroscopic studies of L-arginine molecule, *Indian J. Pure Appl. Phys.* 48 (2010) 251–255.
- [60] A. Barth, The infrared absorption of amino acid side chains, *Prog. Biophys. Mol. Biol.* 74 (2000) 141–173, doi:10.1016/S0079-6107(00)00021-3.
- [61] M. Wolpert, P. Hellwig, Infrared spectra and molar absorption coefficients of the 20 alpha amino acids in aqueous solutions in the spectral range from 1800 to 500 cm⁻¹, *Spectrochim. Acta Part A Mol. Biomol. Spectrosc.* 64 (2006) 987–1001, doi:10.1016/j.saa.2005.08.025.
- [62] M. Cestelli Guidi, C. Mirri, E. Fratini, V. Licursi, R. Negri, A. Marcelli, R. Amendola, *In vivo* skin leptin modulation after 14 MeV neutron irradiation: a molecular and FT-IR spectroscopic study, *Anal. Bioanal. Chem.* 404 (2012) 1317–1326, doi:10.1007/s00216-012-6018-3.
- [63] R. Gebhardt, N. Takeda, U. Kulczik, W. Doster, Structure and stabilizing interactions of casein micelles probed by high-pressure light scattering and FTIR, *J. Phys. Chem. B* 115 (2011) 2349–2359, doi:10.1021/jp107622d.
- [64] E. Li-Chan, S. Nakai, M. Hirotsuka, Raman spectroscopy as a probe of protein structure in food systems, in: R.Y. Yada, R.L. Jackman, J.L. Smith (Eds.), *Protein Structure-Function Relationships in Foods*, Springer, Boston, MA, 1994, pp. 163–197, doi:10.1007/978-1-4615-2670-4_8.
- [65] D. Karouski, R.P. Van Dayne, I.K. Lednev, Exploring the structure and formation mechanism of amyloid fibrils by Raman spectroscopy: a review, *Analyst* 140 (2015) 4967–4980, doi:10.1039/c5an00342c.
- [66] G. Zhu, X. Zhu, Q. Fan, X. Wan, Raman spectra of amino acids and their aqueous solutions, *Spectrochim. Acta Part A Mol. Biomol. Spectrosc.* 78 (2011) 1187–1195, doi:10.1016/j.saa.2010.12.079.
- [67] D.S. Home, Casein structure, self-assembly and gelation, *Curr. Opin. Colloid Interface Sci.* 7 (2002) 456–461, doi:10.1016/S1359-0294(02)00082-1.
- [68] C.D. Syme, E.W. Blanch, C. Holt, R. Jakes, M. Goedert, L. Hecht, L.D. Barron, A Raman optical activity study of rheomorphism in caseins, synucleins and tau: new insight into the structure and behaviour of natively unfolded proteins, *Eur. J. Biochem.* 269 (2002) 148–156, doi:10.1046/j.0014-2956.2001.02633.x.
- [69] A.R. Gargaro, L.D. Barron, L. Hecht, Vibrational Raman optical activity of simple amino acids, *J. Raman Spectrosc.* 24 (1993) 91–96, doi:10.1002/jrs.1250240206.
- [70] J. Herrklotz, in: *Analysis of the vibrational spectra of L-lysine and L-arginine*, Universität Wien, 2012, pp. 1–140, doi:10.25365/thesis.24164.
- [71] S. Kumar, Spectroscopic studies of valine and leucine molecules a comparative study, *Vib. Spectrosc.* 39 (2011) 4996–4999.
- [72] P.F. Façanha Filho, P.T.C. Freire, K.C.V. Lima, J. Mendes Filho, E.E.A. Melo, P.S. Pizani, High temperature Raman spectra of L-leucine crystals, *Braz. J. Phys.* 38 (2008) 131–137, doi:10.1590/S0103-9733200800100024.
- [73] R.M. Jarvis, E.W. Blanch, A.P. Golowanov, J. Screen, R. Goodacre, Quantification of casein phosphorylation with conformational interpretation using Raman spectroscopy, *Analyst* 132 (2007) 1053–1060, doi:10.1039/b702944f.
- [74] S. Celik, S. Akyuz, A.E. Özel, Vibrational spectroscopic and structural investigations of bioactive molecule Glycyl-Tyrosine (Gly-Tyr), *Vib. Spectrosc.* 92 (2017) 287–297, doi:10.1016/j.vibspec.2017.08.007.
- [75] E. Deplazes, W. Van Bronswijk, F. Zhu, L.D. Barron, S. Ma, L.A. Nafie, K.J. Jalkanen, A combined theoretical and experimental study of the structure and vibrational absorption, vibrational circular dichroism, Raman and Raman optical activity spectra of the L-histidine zwitterion, *Theor. Chem. Acc.* 119 (2008) 155–176, doi:10.1007/s00214-007-0276-8.
- [76] S. Karmakar, K.P. Das, Identification of histidine residues involved in Zn²⁺ binding to α A- and α B-crystallin by chemical modification and MALDI TOF mass spectrometry, *Protein J.* 31 (2012) 623–640, doi:10.1007/s10930-012-9439-0.
- [77] L. Dreßler, F. Michel, I. Thondorf, J. Mansfeld, R. Golbik, R. Ulbrich-Hofmann, Metal ions and phosphatidylinositol 4,5-bisphosphate as interacting effectors of α -type plant phospholipase D, *Phytochemistry* 138 (2017) 57–64, doi:10.1016/j.phytochem.2017.02.024.
- [78] P. Bazeera Ferdhous, R. Aanandhalakshmi, P. Ramya, B. Vanavil, Scrutiny of metal ion binding sites in different alginate lyases through *in silico* analysis, *Appl. Biochem. Biotechnol.* 194 (2022) 124–147, doi:10.1007/s12010-021-03746-y.
- [79] C.H. Lu, Y.F. Lin, J.J. Lin, C.S. Yu, Prediction of metal ion-binding sites in proteins using the fragment transformation method, *PLoS One* 7 (2012) 1–12, doi:10.1371/JOURNAL.PONE.0039252.
- [80] T.F. Kucosinski, E.M. Brown, H.M. Farrell, Three-dimensional molecular modeling of bovine caseins: κ -casein, *J. Dairy Sci.* 74 (1991) 2879–2887, doi:10.3168/JDS.S0022-0302(91)78469-5.

1 Study on zinc ions binding to the individual casein fractions: α_{S1} -, β - and κ -casein

2 Agnieszka Rodzik^{1,2}, Anna Król-Górniak^{1,2}, Viorica Railean^{2,3}, Mateusz Sugajski^{1,2}, Adrian
3 Gołębiowski^{1,2}, David S. Horne⁴, Bernhard Michalke⁵, Myroslav Sprynskyy¹, Paweł Pomastowski^{2*},
4 Bogusław Buszewski^{1,2}

5 ¹Centre for Modern Interdisciplinary Technologies, Nicolaus Copernicus University in Toruń,
6 Wileńska 4, 87-100, Toruń, Poland

7 ²Department of Environmental Chemistry and Bioanalysis, Faculty of Chemistry, Nicolaus Copernicus
8 University in Toruń, Gagarina 7, 87-100 Toruń, Poland

9 ³Department of Public Health Protection and Animal Welfare, Faculty of Biological and Veterinary
10 Sciences, Nicolaus Copernicus University in Toruń, Gagarina 7, 87-100 Toruń, Poland

11 ⁴Wisconsin Center for Dairy Research, University of Wisconsin—Madison, Madison, WI,
12 United States

13 ⁵Research Unit Analytical BioGeoChemistry, Helmholtz Center Munich—German Research
14 Center for Environmental Health, 85764 Neuherberg, Germany

15 *Corresponding author: Paweł Pomastowski (p.pomastowski@umk.pl)
16

17 The colloidal behaviour of various caseins forms during the metal binding process is crucial for
18 the further modulation of their stability during the dairy technological processes [1]. The reducing of
19 the repulsive forces responsible for the micelles stability, it is possible to induce aggregation of protein.
20 In the consequence, the texture and structure of dairy products are created [2], [3]. The destabilization
21 of caseins is the common process used in e.g. making a cheese – the milk is coagulated by using
22 chymosin in the presence of calcium and at acidic conditions [4]. Furthermore, the aggregation of
23 caseins seems to be metal-dependent. Metal ions can act as both, promoters or inhibitors, of the protein
24 aggregation process [5], [6]. In the case of caseins, the most discussed is the influence of calcium on
25 this process [7], [8], [9]. Choi, Horne and Lucey [7] have demonstrated that removing of insoluble Ca^{2+}
26 from casein micelles strongly influence on rennet gelation properties. The lack of calcium ions have
27 significantly reduced the repulsion forces between phosphoserine residues of caseins, and consequently,
28 the weaker gels were formed. Dalgleish [2], have shown tht Ca^{2+} caused the aggregation of casein
29 micelles by decreasing their zeta potential. The removal of Ca^{2+} have increased the repulsion forces as
30 the phosphoserines are negatively charged and the calcium has been neutraliising this. In the
31 consequence, the gels were found to be weaker. Calcium ions preferably bind to oxygen-containing
32 ligands such as e.g., carboxyl group, but also oxygens of asparagine (Asn), glutamine (Gln), or serine
33 (Ser) [10]. Another important issue, crucial for casein-metal binding is the phosphrylation occurring in
34 their amino acid sequence and the ability of phosphorylated serine residues to bind calcium ions. The
35 amount of Ca^{2+} is important in forming stable micelles [11], [12]. Also zinc might play an important
36 role in casein stabilization through binding to the phosphoserines. Based on the literature, zinc are able

37 to be bound to casein phosphopeptides (CCP) containing the phosphoserine residues [13], [14], [15].
38 Singh, Flynn and Fox [14] have observed that α_{S1} -casein aggregation was observed with the increasing
39 Zn^{2+} concentration. Therefore, the aggregation of the all tested in this study casein fractions might be
40 also zinc-dependent, as it follows from the experimental data we received in the present study. In
41 contrast to calcium, Zn^{2+} ions are able to bind additionally to sulfur and nitrogen [16]. On the other hand,
42 both zinc and calcium, might exist in the aqua complexes forms, which might influence the stability of
43 biocolloids. This process can be described by the bridging effect – divalent aqua complexes screen the
44 charges that make up the electrostatic forces, bind to negatively charged amino acids groups by
45 displacing water molecules from the Stern-Helmholtz layer and, in the consequence, the system charge
46 is increased [17], [18], [19], [20], [21]. As an example, in aqueous solutions, zinc forms stable aqua
47 complexes $[Zn(H_2O)_6]^{2+}$. Polarization of water molecules by the central zinc ion causes proton
48 dissociation and results in formation of an aqua-hydroxo complex $[Zn(OH)(H_2O)_5]^+$, which can be
49 further transformed to $[Zn(OH)_4]^{2-}$ [17], [16]. Finally, the formation of differently-charged species and
50 binding to the protein might modulate the surface charge of metal-protein complexes. It is in a good
51 correlation with results of Alhazmi et al [20] who have examined the zeta potential of bovine serum
52 albumin after the divalent metal ion (Cu^{2+}) exposure. They have observed that protein dispersion
53 stability depends on the coordination capacity of the metal ions. What is more, metal-protein binding
54 involves the formation of intermolecular bridges between the Me^{2+} and protein molecules. Another
55 example can be work of Chakraborty and Basak [22] work, who have investigated the influence of the
56 Zn^{2+} ions on the structure and stability of bovine caseins. At the highest concentration of the added
57 metal, the aggregation and precipitation of protein occurred. Based on our results, due to the various
58 availability of carboxyl groups on the individual caseins surface, the binding of zinc also occur in
59 different manner. It is strongly connected with the generating of stable $Zn\alpha_{S1}CN$ complexes. It has a
60 great reflection in the experimental FTIR-ATR analysis results, which was the crucial step in the proper
61 understanding of the described phenomenon.

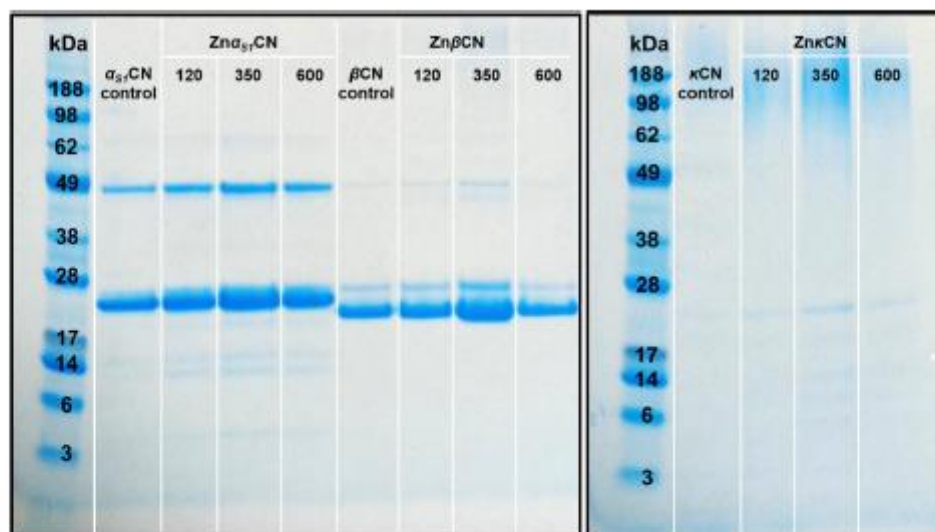
62

63 References

- 64 [1] C. Broyard, F. Gaucheron, Modifications of structures and functions of caseins: a scientific and
65 technological challenge, *Dairy Science and Technology*. 95 (2015) 831–862.
66 <https://doi.org/10.1007/s13594-015-0220-y>.
- 67 [2] D.G. Dalgleish, Measurement of electrophoretic mobilities and zeta-potentials of particles from
68 milk using laser Doppler electrophoresis, *Journal of Dairy Research*. 51 (1984) 425–438.
69 <https://doi.org/10.1017/S0022029900023724>.
- 70 [3] D.G. Dalgleish, M. Corredig, The structure of the casein micelle of milk and its changes during
71 processing, *Annual Review of Food Science and Technology*. 3 (2012) 449–467.
72 <https://doi.org/10.1146/ANNUREV-FOOD-022811-101214>.
- 73 [4] S. Sandra, M. Alexander, D.G. Dalgleish, The rennet coagulation mechanism of skim milk as

- 74 observed by transmission diffusing wave spectroscopy, *Journal of Colloid and Interface Science*.
 75 308 (2007) 364–373. <https://doi.org/10.1016/J.JCIS.2007.01.021>.
- 76 [5] K. Garai, P. Sengupta, B. Sahoo, S. Maiti, Selective destabilization of soluble amyloid beta
 77 oligomers by divalent metal ions, *Biochemical and Biophysical Research Communications*. 345
 78 (2006) 210–215. <https://doi.org/10.1016/J.BBRC.2006.04.056>.
- 79 [6] G. Navarra, M. Leone, V. Militello, Thermal aggregation of beta-lactoglobulin in presence of
 80 metal ions, *Biophysical Chemistry*. 131 (2007) 52–61.
 81 <https://doi.org/10.1016/J.BPC.2007.09.003>.
- 82 [7] J. Choi, D.S. Horne, J.A. Lucey, Effect of Insoluble Calcium Concentration on Rennet
 83 Coagulation Properties of Milk, *Journal of Dairy Science*. 90 (2007) 2612–2623.
 84 <https://doi.org/10.3168/JDS.2006-814>.
- 85 [8] G.J.O. Martin, R.P.W. Williams, D.E. Dunstan, Effect of manufacture and reconstitution of milk
 86 protein concentrate powder on the size and rennet gelation behaviour of casein micelles,
 87 *International Dairy Journal*. 20 (2010) 128–131.
 88 <https://doi.org/10.1016/J.IDAIRYJ.2009.08.007>.
- 89 [9] S. Sandra, M. Corredig, Rennet induced gelation of reconstituted milk protein concentrates: The
 90 role of calcium and soluble proteins during reconstitution, *International Dairy Journal*. 29 (2013)
 91 68–74. <https://doi.org/10.1016/J.IDAIRYJ.2012.10.011>.
- 92 [10] N. Tang, L.H. Skibsted, Calcium binding to amino acids and small glycine peptides in aqueous
 93 solution: Toward peptide design for better calcium bioavailability, *Journal of Agricultural and
 94 Food Chemistry*. 64 (2016) 4376–4389. <https://doi.org/10.1021/acs.jafc.6b01534>.
- 95 [11] T. Huppertz, P.F. Fox, A.L. Kelly, The caseins: structure, stability, and functionality, in: *Proteins
 96 in Food Processing: Second Edition*, Second Edi, Elsevier Ltd., 2018: pp. 49–92.
 97 <https://doi.org/10.1016/B978-0-08-100722-8.00004-8>.
- 98 [12] T. Huppertz, Chemistry of the Caseins, in: *Advanced Dairy Chemistry: Volume 1A: Proteins:
 99 Basic Aspects*, 4th Edition, Springer, Boston, MA, 2013: pp. 135–160.
 100 https://doi.org/10.1007/978-1-4614-4714-6_4.
- 101 [13] E. Miquel, A. Alegria, R. Barberá, R. Farré, Casein phosphopeptides released by simulated
 102 gastrointestinal digestion of infant formulas and their potential role in mineral binding,
 103 *International Dairy Journal*. 16 (2006) 992–1000. <https://doi.org/10.1016/j.idairyj.2005.10.010>.
- 104 [14] H. Singh, A. Flynn, P.F. Fox, Binding of zinc to bovine and human milk proteins, *The Journal
 105 of Dairy Research*. 56 (1989) 235–248. <https://doi.org/10.1017/S0022029900026455>.
- 106 [15] X. Wang, J. Zhou, P.S. Tong, X.Y. Mao, Zinc-binding capacity of yak casein hydrolysate and
 107 the zinc-releasing characteristics of casein hydrolysate-zinc complexes, *Journal of Dairy
 108 Science*. 94 (2011) 2731–2740. <https://doi.org/10.3168/JDS.2010-3900>.
- 109 [16] T. Kochańczyk, A. Drozd, A. Krężel, Relationship between the architecture of zinc coordination
 110 and zinc binding affinity in proteins - insights into zinc regulation, *Metallomics*. 7 (2015) 244–

- 111 257. <https://doi.org/10.1039/c4mt00094c>.
- 112 [17] A. Krężel, W. Maret, The biological inorganic chemistry of zinc ions, *Archives of Biochemistry*
113 *and Biophysics*. 611 (2016) 3–19. <https://doi.org/10.1016/j.abb.2016.04.010>.
- 114 [18] L. Ehrl, Z. Jia, H. Wu, M. Lattuada, M. Soos, M. Morbidelli, Role of Counterion Association in
115 Colloidal Stability, *Langmuir*. 25 (2009) 2696–2702. <https://doi.org/10.1021/LA803445Y>.
- 116 [19] F. Roosen-Runge, B.S. Heck, F. Zhang, O. Kohlbacher, F. Schreiber, Interplay of pH and binding
117 of multivalent metal ions: charge inversion and reentrant condensation in protein solutions,
118 *Journal of Physical Chemistry B*. 117 (2013) 5777–5787. <https://doi.org/10.1021/jp401874t>.
- 119 [20] H.A. Alhazmi, W. Ahsan, A.M.M. Ibrahim, R.A.Y. Khubrani, Z.A.A. Haddadi, A.Y.F. Safhi, N.
120 Shubayr, M. Al Bratty, A. Najmi, Investigation of bovine serum albumin aggregation upon
121 exposure to silver(i) and copper(ii) metal ions using Zetasizer, *Open Chemistry*. 19 (2021) 987–
122 997. <https://doi.org/10.1515/CHEM-2021-0089/MACHINEREADABLECITATION/RIS>.
- 123 [21] J. Zhang, H. Li, S. Li, X. Hou, Effects of metal ions with different valences on colloidal
124 aggregation in low-concentration silica colloidal systems characterized by continuous online zeta
125 potential analysis, *Colloids and Surfaces A: Physicochemical and Engineering Aspects*. 481
126 (2015) 1–6. <https://doi.org/10.1016/j.colsurfa.2015.04.024>.
- 127 [22] A. Chakraborty, S. Basak, Interaction with Al and Zn induces structure formation and
128 aggregation in natively unfolded caseins, *Journal of Photochemistry and Photobiology B:*
129 *Biology*. 93 (2008) 36–43. <https://doi.org/10.1016/j.jphotobiol.2008.06.011>.
- 130



131
132 **Fig. S1.** Electrophoretic separation of casein fractions and their complexes with zinc ions.
133

4.5. Immobilized enzyme microreactors for efficient analysis of tryptic peptides in β -casein and β -lactoglobulin

[P5] A. Rodzik, V. Railean, P. Pomastowski, B. Buszewski, M. Szumski, *Immobilized enzyme microreactors for efficient analysis of tryptic peptides in β -casein and β -lactoglobulin*, Scientific Reports, Submission ID 5d953fac-cd31-4150-9da3-e4e688f203eb.

1 **Immobilized Enzyme Microreactors for Efficient Analysis of Tryptic Peptides in**
2 **β -Casein and β -Lactoglobulin**

3
4 Agnieszka Rodzik^{1,2*}, Viorica Railean^{1,3}, Paweł Pomastowski¹, Bogusław Buszewski^{1,2}, Michał
5 Szumski^{1*}

6
7 ¹ Centre for Modern Interdisciplinary Technologies, Nicolaus Copernicus University in Toruń,
8 Wileńska 4, 87-100, Toruń, Poland

9 ² Department of Environmental Chemistry and Bioanalysis, Faculty of Chemistry, Nicolaus
10 Copernicus University in Toruń, Gagarina 7, 87-100 Toruń, Poland

11 ³ Department of Infectious, Invasive Diseases and Veterinary Administration, Institute of Veterinary
12 Medicine, Nicolaus Copernicus University in Toruń, Gagarina 7, 87-100 Toruń, Poland

13 *Corresponding author: Agnieszka Rodzik (agnieszka.rodzik94@gmail.com), Michał Szumski
14 (michu@umk.pl)

15
16 **Abstract**

17
18 In this study, our primary objective was to develop an effective analytical method for studying trypsin-
19 digested peptides of two proteins commonly found in cow's milk: β -casein (β CN) and β -lactoglobulin
20 (β LG). To achieve this, we employed two distinct approaches: traditional in-gel protein digestion and
21 protein digestion using immobilized enzyme microreactors (μ -IMER). Both methods utilized ZipTip
22 pipette tips filled with C18 reverse phase media for sample concentration. The μ -IMER was fabricated
23 through a multi-step process that included preconditioning the capillary, modifying its surface,
24 synthesizing a monolithic support, and further surface modification. Its performance was evaluated
25 under HPLC chromatography conditions using a small-molecule trypsin substrate (BAEE).
26 Hydrolysates from both digestion methods were analyzed using MALDI-TOF MS. Our findings indicate
27 that the μ -IMER method demonstrated superior sequence coverage for oxidized molecules in β CN
28 ($33\pm 1.5\%$) and β LG ($65\pm 3\%$) compared to classical in-gel digestion ($20\pm 2\%$ for β CN; $49\pm 2\%$ for β LG).
29 The use of ZipTip pipette tips further improved sequence coverage in both classical in-gel digestion
30 ($26\pm 1\%$ for β CN; $60\pm 4\%$ for β LG) and μ -IMER ($41\pm 3\%$ for β CN; $80\pm 5\%$ for β LG). Additionally,
31 phosphorylations were identified. For β CN, no phosphorylation was detected using classical digestion,
32 but the use of ZipTip pipette tips showed a value of $27\pm 4\%$. With μ -IMER and μ -IMER-ZipTip, the
33 values increased to $30\pm 2\%$ and $33\pm 1\%$, respectively. For β LG, the use of ZipTip enabled the detection
34 of a higher percentage of modified peptides in both classical ($79\pm 2\%$) and μ -IMER ($79\pm 4\%$) digestions.
35 By providing a comprehensive comparison of traditional in-gel digestion and μ -IMER methods, this
36 study offers valuable insights into the advantages and limitations of each approach, particularly in the
37 context of complex biological samples. The findings set a new benchmark in protein digestion and
38 analysis, highlighting the potential of μ -IMER systems for enhanced sequence coverage and post-
39 translational modification detection.

40
41 **Introduction**

42
43 Proteins, which are abundant macromolecules in cells, are composed of linear chains of amino
44 acids connected by peptide bonds. A valuable source of biologically active proteins is cow's milk,
45 providing essential bioactive components to the body, including high-quality proteins, lactose as a
46 carbohydrate source, mineral salts (such as calcium and phosphorus compounds), and vitamins¹. Milk
47 consists of two main groups of proteins: casein (α_{S1} , α_{S2} , β , κ -CN) and whey proteins (β -lactoglobulin,
48 α -lactalbumin, lactoferrin, bovine serum albumin). Among these proteins, beta-casein (β CN) and beta-

49 lactoglobulin (β LG) are of particular interest due to their significant differences in various aspects,
50 including primary structure, secondary structure, tertiary structure, solubility, function, allergenicity,
51 occurrence, and polymorphism. These differences distinguish β -casein and β -lactoglobulin as distinct
52 milk proteins with unique characteristics. In terms of primary structure, β -casein consists of 209 amino
53 acids, while β -lactoglobulin is composed of 162 amino acids, indicating a difference in their amino acid
54 sequences. When it comes to secondary structure, β LG contains α -helical and β -sheet structures,
55 whereas β CN is an intrinsically disordered protein and lacks regular secondary structures². The
56 differences extend to their tertiary structures as well. β -lactoglobulin has a well-defined tertiary structure
57 with a hydrophobic ligand-binding pocket. In contrast, β -casein does not have a defined tertiary
58 structure. The solubility of these proteins also differs. β -casein is highly soluble in water, while β -
59 lactoglobulin is less soluble and can form aggregates when heated. Functionally, β CN plays a vital role
60 in the stability of casein micelles and calcium binding, whereas β LG is a lipid and vitamin-binding
61 protein. In terms of allergenicity, β -lactoglobulin is a major cow's milk allergen, while β -casein is less
62 allergenic. Furthermore, β -casein is specific to milk, whereas β -lactoglobulin also occurs in other body
63 fluids³. Finally, both β -casein and β -lactoglobulin exhibit polymorphism, but the different forms of these
64 proteins have different properties. For instance, different forms of β -casein (A1, A2, B) vary in their
65 calcium-binding ability⁴, while different forms of β -lactoglobulin (A, B) differ in their thermal stability
66 and allergenicity. In conclusion, β -casein and β -lactoglobulin, despite both being milk proteins, exhibit
67 a wide range of differences in their structure, modifications, and properties.

68 Enzymatic hydrolysis of proteins leads to the release of fragments that can contribute to the
69 overall health of various systems, including the immune, cardiovascular, nervous, and digestive
70 systems⁵. Protein hydrolysates, primarily composed of dipeptides and tripeptides, are known to be
71 absorbed more rapidly compared to free amino acids or intact proteins, thereby enhancing the absorption
72 capacity of dietary supplements⁶. Furthermore, protein hydrolysates have found applications in animal
73 nutrition⁷. **Proteins frequently experience alterations in their native sequences through a process known**
74 **as post-translational modifications (PTMs), which can profoundly impact their functional activity.** One
75 such PTM is phosphorylation. Post-translational modifications also vary between the two proteins. β -
76 casein is phosphorylated at multiple serine residues, which is crucial for its calcium-binding ability⁸. On
77 the other hand, β -lactoglobulin is not typically phosphorylated. Additionally, β -casein can be also
78 glycosylated, which impacts its functional properties, while β -lactoglobulin is not typically
79 glycosylated. However, the phosphorylation of β -lactoglobulin under artificial conditions has been
80 observed in various studies⁹. In the study by Sato et al. different molar ratios of $\text{POCl}_3/\text{protein}$ were
81 employed to phosphorylate β -lactoglobulin, with the presence of either triethylamine or hexylamine as
82 the base. The use of aqueous conditions facilitated the phosphorylation process. Hence, the development
83 of efficient and precise methods for studying protein digestion is of paramount importance.

84 **A promising approach in the field of proteomic research is the use of microreactors with**
85 **immobilized enzymes (μ -IMERs)¹⁰.** These flow systems encapsulate or preserve the catalytic activity of
86 enzymes, facilitating sequential or continuous digestion processes. The appeal of μ -IMERs over **in-gel**
87 **digestion** lies in their numerous advantages, such as reduced digestion times, enhanced sample
88 throughput due to improved mass transfer, increased enzyme concentration, and prevention of self-
89 digestion. Additionally, the absence of enzyme molecules in the final sample and the extended reuse of
90 μ -IMERs add to their appeal. Proteomics research predominantly employs μ -IMERs in conjunction with
91 MS or MS/MS detection due to their capacity to provide valuable insights into peptide identification
92 and potential modifications, such as oxidation or post-translational modifications (PTMs)¹¹. Matrix-
93 assisted laser desorption/ionization (MALDI) coupled with a time-of-flight (TOF) mass spectrometer is
94 frequently used as the ion source in proteomic studies. Mass spectrometers serve as indispensable
95 analytical tools for determining molecular mass, a critical factor for protein identification,
96 characterization of chemical modifications, and structural analysis. Protein identification via MS

97 techniques can be achieved through two primary methods: bottom-up and *de novo* sequencing analysis.
98 The more commonly used *bottom-up* strategy involves the classical tryptic in-gel digestion or enzymatic
99 digestion of proteins into peptides, which are then identified on the mass spectrometer. **PTM analysis**
100 **can largely be facilitated by PTM-specific protein and peptide enrichment methods, such as the use of**
101 **ZipTips pipette tips after the digestion step.**^{12,13,14} Subsequent MS and MS/MS analysis of peptides will
102 increase sensitivity and specificity, reveal the identity of proteins, and allow specific assignment of
103 modifications sites.¹⁵ While numerous studies have focused on monolith-based enzyme microreactors
104 for the detection and identification of digestion products using mass spectrometry, to our knowledge, no
105 literature has reported a comparison between the classical **in-gel digestion** method and μ -IMER, in
106 conjunction with the use of ZipTips pipette tips for peptide enrichment^{16,17}.

107 This study aimed to develop an efficient sample preparation method for identifying tryptic digest
108 peptides of two model proteins found in cow's milk: β -casein (β CN) and β -lactoglobulin (β LG). These
109 proteins were selected for their abundant nutrient content and functional attributes, notwithstanding their
110 structural and compositional differences. We employed two protein digestion approaches: the **traditional**
111 **in-gel protein digestion method** and enzymatic digestion using a flow-through microreactor (μ -IMER).
112 Furthermore, we evaluated ZipTip pipette tips containing a chromatographic stationary phase for their
113 impact on sequence coverage, peptide concentration, and purification. The activity of trypsin
114 immobilized in the microreactor was assessed using the commercially available substrate BAEE,
115 enabling the determination of optimal hydrolysis conditions. **This holistic methodology enabled an in-**
116 **depth analysis of peptides in β -casein and β -lactoglobulin, thereby enriching our knowledge of these**
117 **essential bovine milk proteins.**

118 **Materials and methods**

120 **Materials.** All chemicals used in this experiment were of analytical reagent grade or higher. β -casein
121 (β CN) and β -lactoglobulin (β LG) were purchased from Sigma-Aldrich (Steinheim, Germany).
122 Deionized water was obtained from the Mili-Q ultrapure water producing system (Millipore, Bedford,
123 MA, USA). Trypsin Gold, Mass Spectrometry Grade used for digestion in a solution were provided by
124 Promega (Madison, Wisconsin, USA). Fused-silica capillaries (150 μ m i.d. \times 375 μ m o.d.) were
125 purchased from CM Scientific Ltd. (Dublin, Ireland); 3-(trimethoxysilyl) propyl methacrylate (γ -
126 MAPS), glycidyl methacrylate (GMA), ethylene dimethacrylate (EDMA), azobisisobutyronitrile
127 (AIBN), 1-dodecanol, cyclohexanol, sodium bicarbonate, benzamidine, sodium cyanoborohydride, the
128 storage solution (containing sodium azide), N- α -benzoyl-L-arginine ethyl ester (BAEE), trypsin from
129 bovine pancreas, trifluoroacetic acid (TFA), acetonitrile (HPLC ultra-gradient grade), ammonium
130 bicarbonate, dichloromethane, methanol, sodium hydroxide were purchased from Sigma-Aldrich
131 (Steinheim, Germany); acetone and toluene were purchased from Chempur (Poland); 1,6-
132 hexanediamine, glutaraldehyde, sodium phosphate monobasic dihydrate were purchased from Alchem
133 (Poland). All the chemicals supplied for the MALDI-TOF MS analyses were at the highest commercially
134 available purity by Fluka Feinchemikalien (Neu-Ulm, Germany; a subsidiary of Sigma-Aldrich).

135
136 **Instrumentation.** Rheos 2000 HPLC pump (Flux Instruments, Reinach, Switzerland) was used to flush
137 the columns after monolith synthesis and for permeability measurements. A syringe pump NE-1002X
138 (New Era Pump Systems, Farmingdale, NY) was used to pass reagents during the modification and
139 trypsin immobilization and the substrate solution through the μ -IMER. The thermostat (Julabo, type
140 F25) connected to a specially designed heat exchanger was used for reactions performed at a constant
141 temperature. Chromatographic experiments were conducted in a nanoLC system consisting of a 1260
142 Capillary Pump (Agilent Technologies, Waldbronn, Germany), a 10-port nanoLC valve (model
143 C72MX-6690D Vici-Valco, Schenkon, Switzerland) and a Crystal 100 UV-Vis detector (Thermo

144 Separation Products, San Jose, CA, USA). The system was controlled using Clarity software (DataApex,
145 Prague, Czech Republic).

146 MALDI-TOF MS mass spectra were acquired using a Bruker UltrafleX-treme II mass
147 spectrometer operating at a repetition rate of 2 kHz in TOF mode and 1 kHz in TOF/TOF mode. A
148 modified Nd:YAG laser emitting at a wavelength of 355 nm was utilized for the analyses. The
149 experimental procedures and parameters followed in this study were in accordance with previously
150 published protocols, ensuring consistency and comparability with prior work¹⁸.

151
152 **Classical in-gel protein digestion method with trypsin.** *Polyacrylamide gel electrophoresis study:* To
153 analyze the standard solutions of β -casein (β CN) and β -lactoglobulin (β LG), one-dimensional sodium
154 dodecyl sulfate polyacrylamide gel electrophoresis (1D SDS-PAGE) was employed. The Bolt™ Mini
155 Gel Tank from Novex Life Technologies, located in Carlsbad, CA, USA, was utilized for this purpose.
156 SeeBlue™ Plus2 Pre-Stained Protein Standard, obtained from Novex Life Technologies in Europe,
157 specifically from Bleiswijk, Netherlands, served as the molecular weight marker during the gel
158 electrophoresis. **Prior to 1D SDS-PAGE, proteins were purified using Amicon® Ultra centrifugal filter
159 units (Merck, Poland)**

160 *Tryptic digestion in-gel:* The trypsin digestion in gel was performed following the established protocol
161 described by Shevchenko et al.¹⁹. This protocol consisted of five key steps: (I) decolorization of the gel
162 using 10 mM ammonium bicarbonate (NH_4HCO_3) with acetonitrile, (II) reduction of disulfide bonds
163 using 10 mM dithiothreitol (DTT) in 10 mM NH_4HCO_3 , (III) **alkylation** of thiols using 55 mM
164 iodoacetamide (IAA) in 10 mM NH_4HCO_3 , (IV) trypsin digestion carried out for 24 hours, (V) extraction
165 of peptides²⁰.

166 To target phosphorylation and enrich modified peptides, ZipTip pipette tips were employed.
167 After the peptide extraction step, selected samples were subjected to ZipTip pipette tip treatment,
168 utilizing a chromatographic bed of 0.6 μL of C18 resin. This step aimed to concentrate and purify
169 peptides containing modifications, thereby improving the sensitivity and resolution of MALDI-TOF MS
170 analysis. Optimal binding to the ZipTip pipette tip was achieved by incorporating 0.1% trifluoroacetic
171 acid (TFA), which facilitated ion pairing.

172
173 **Capillary enzyme reactors (CER).** *Conditions for preparation and modification of the capillary
174 surface:* First, the capillary (150 μm i.d. \times 375 μm o.d.) was flushed with acetone, dichloromethane, and
175 then dried by flushing with nitrogen. After that, the inner surface of the fused silica capillary was
176 modified by etching with 1 M sodium hydroxide solution at 100 °C for 3 h followed by silanization with
177 10% γ -MAPS solution in toluene at 23 °C for 2 h.

178 *Monolithic support synthesis:* Polymerization solutions for the synthesis of a monolithic capillary
179 column were prepared according to the procedure described in our previous work²¹. Namely, the
180 polymerization solution consisted of a mixture of the functional monomer GMA and the crosslinking
181 monomer EDMA in the presence of 1% initiator AIBN (relative to the weight of the monomers) and the
182 porogen solution in a ratio of 40:60 (w/w). The weight ratio of the monomers was kept constant and
183 equaled 3:2 (w/w), while the porogen solution consisted of 1-dodecanol and cyclohexanol in a ratio of
184 30:70 (w/w). In the next step, the polymerization mixtures were subjected to sonication, centrifugation,
185 purging with nitrogen (to remove oxygen), and then injected into the capillaries using a syringe. The
186 ends of the capillary were sealed with pieces of silicone rubber, after which the capillaries were placed
187 in a water bath. The polymerization was carried out at 80 °C for 24 h.

188 The permeability of the produced monoliths (K_F) was evaluated by measuring the flow rate of
189 acetonitrile through the capillaries at a given pressure. The following formula was used:

190
$$K_F = \frac{F\eta L}{\Delta P \pi r^2} [m^2] \quad (1)$$

191 where: F – flow rate [$\mu\text{l}/\text{min}$]; η – acetonitrile viscosity [Pa s]; L – the capillary length [dm], ΔP –
192 pressure [Pa]; r – the capillary radius [dm].

193 The obtained polymer was characterized by high permeability $K_p = 4.85 \times 10^{-14} \text{ m}^2$ and homogeneous
194 structure.

195 *Trypsin immobilization:* Immobilization of the enzyme was carried out in capillaries filled with
196 monolithic GMA-co-EDMA carrier using a four-step method based on (I) initial aminolysis of the
197 epoxide ring, (II) aldehyde attachment, (III) enzyme binding and (IV) final reduction of imine bonds.
198 The first step was the aminolysis of epoxide rings performed using a 10% buffer of 1,6-diaminohexane
199 at 80 °C for 2.5 h at a flow rate of $F = 1 \mu\text{l}/\text{min}$. The second step was the connection of glutaraldehyde
200 dissolved in a buffer solution of pH 8.5 and at 23 °C for 3 h with a flow rate of $1 \mu\text{l}/\text{min}$. Next,
201 immobilization of the enzyme at a concentration of 3.5 mg/mL was carried out in the presence of 50
202 mM benzamidine at 4 °C for 24 h and a flow rate of $F = 0.5 \mu\text{l}/\text{min}$. The final step was the reduction of
203 imine bonds using 0.1 M sodium cyanoborohydride solution (NaCNBH_3) at 23 °C for 2 h at $F = 1 \mu\text{l}/\text{min}$.
204 Solutions were circulated through the capillary bed using a syringe pump equipped with a system to
205 regulate the temperature of both the capillary and the liquid being injected.

206 *The efficiency of the μ -IMER produced:* The efficiency of the obtained microreactor was evaluated by
207 measuring the activity of trypsin using *N*- α -benzoyl-arginine ethyl ester (BAEE). To find the BAEE
208 peak, standard solutions of the substrate at the concentration range of 0.5–75 mM were passed through
209 the IMER at a syringe pump flow rate of $F = 1 \mu\text{l}/\text{min}$ at 23 °C (room temperature) and 37 °C
210 (physiological temperature). The IMER was connected on line to the injection loop of the nanoLC
211 system, which allowed to inject the IMER effluent (containing the substrate and its digestion product)
212 sequentially into the separation column. Separation was carried out using a nanoLC system equipped
213 with a homemade column packed with the octadecyl stationary phase (HALO C18, 2.7 μm , Advanced
214 Materials Technology, Wilmington, DE, USA). The mobile phase consisted of water and acetonitrile
215 (both with 0.1% trifluoroacetic acid (TFA) at a flow rate of $F = 5.0 \mu\text{l}/\text{min}$. The chromatographic process
216 was started with 20% acetonitrile (ACN) content in the mobile phase, and then the it was increased to a
217 final 40% ACN value. Detection was performed at $\lambda = 223 \text{ nm}$.

218 As the reaction product, *N*- α -benzoyl-L-arginine (BA) was separated from the substrate *N*- α -
219 benzoyl-L-arginine ethyl ester (BAEE) on the C18 column, the degree of hydrolysis (%H) could be
220 calculated from the peak area of the substrate from the difference in BAEE concentrations in solutions
221 before and after the reaction on the μ -IMER. The calibration curve and the following formula was used:

$$222 \quad \%H = \frac{C_{BAEE, st} - C_{BAEE}}{C_{BAEE, st}} \times 100\% \quad (2)$$

223 where: $C_{BAEE, st}$ – standard BAEE solution concentration before passing through a μ -IMER [mM], C_{BAEE}
224 – BAEE concentration in solution after passing the standard solution through a μ -IMER [mM].

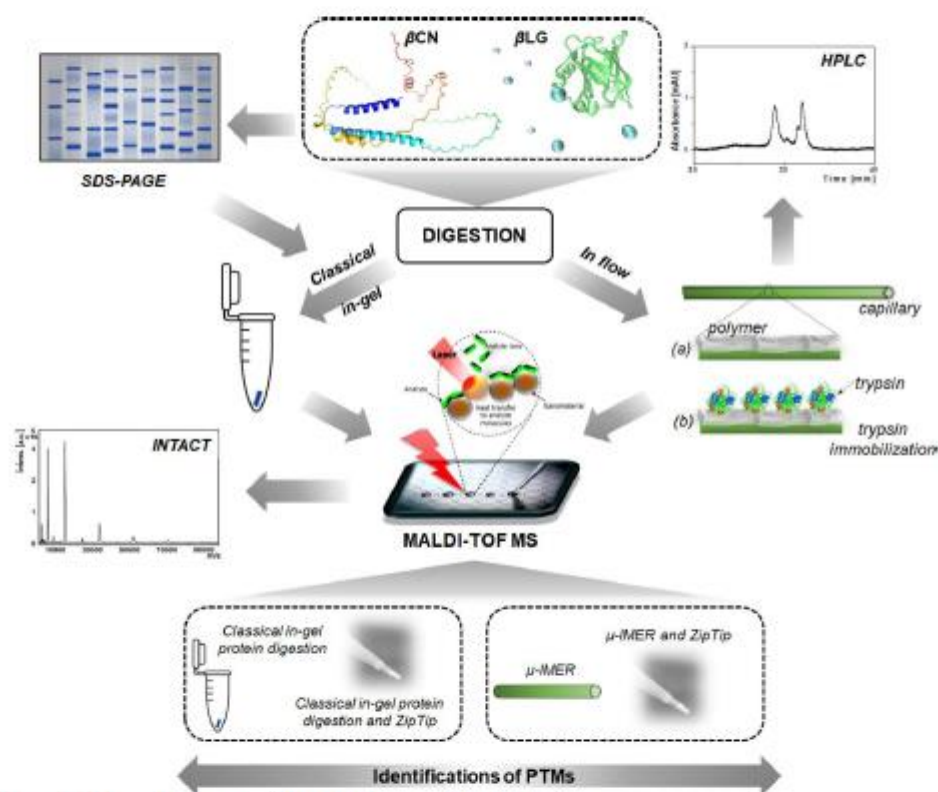
225 *Protein digestion in μ -IMER:* βCN and βLG at a concentration of 45 pm/ μl was dissolved in 50 mM
226 ammonium bicarbonate buffer (ABC), pH 8.05. Using a syringe pump, proteins were passed through
227 the μ -IMER at 37 °C and a flow rate of $F = 0.05 \mu\text{l}/\text{min}$. It corresponds to the residence time of 1653 s
228 $\approx 28 \text{ min}$ (capillary of 13.0 cm in length). The eluate was collected in a plastic vial and then analyzed
229 with MALDI-TOF MS. Similar to the classic in-gel protein digestion method, some of the samples were
230 subjected to an additional peptide enrichment step using ZipTips pipette tips.

231
232 *Spectrometric study.* Intact spectra were acquired using a positive ion linear mode, covering the m/z
233 range of 5000–10000. Sinapic acid (SA) served as the matrix for intact analyses, while Protein
234 Calibration Standard II was employed for calibration purposes. On the other hand, for the peptide mass
235 fingerprint (PMF) spectrum of trypsin-digested proteins, the positive reflectron mode was utilized,
236 spanning the m/z range of 500–3500. In this case, α -cyano-4-hydroxycinnamic acid (HCCA) and 2,5-
237 dihydroxybenzoic acid (DHB) were used as matrices, and Peptide Calibration Standard II served as the

238 calibrant. A mass tolerance of 0.3 Da was set for all spectra, and internal calibration was performed on
 239 immonium ions. The measurements were conducted at an accelerating voltage of 25 kV. To apply the
 240 samples onto a MALDI steel target (AnchorChip), the dried drop method was employed.

241 Software programs such as flexControl and flexAnalysis from Bruker Daltonik were utilized for
 242 acquiring and processing the mass spectra. Fragment spectra were collected using LIFT (Laser
 243 Ionization Fragmentation Technologies) in MS/MS mode to investigate both peptide sequences and their
 244 post-translational modifications, including phosphorylations, as well as oxidation. The resulting
 245 peptides generated from the trypsin digestion of β -lactoglobulin (β LG) and β -casein (β CN) were
 246 identified using the BioTools software (Bruker Daltonik). The sequence coverage reported was based
 247 on the average of three replicate analyses. The experimental procedure followed the scheme illustrated
 248 in Fig. 1.

249



250

251 **Figure 1.** Schematic representation of the experimental design.

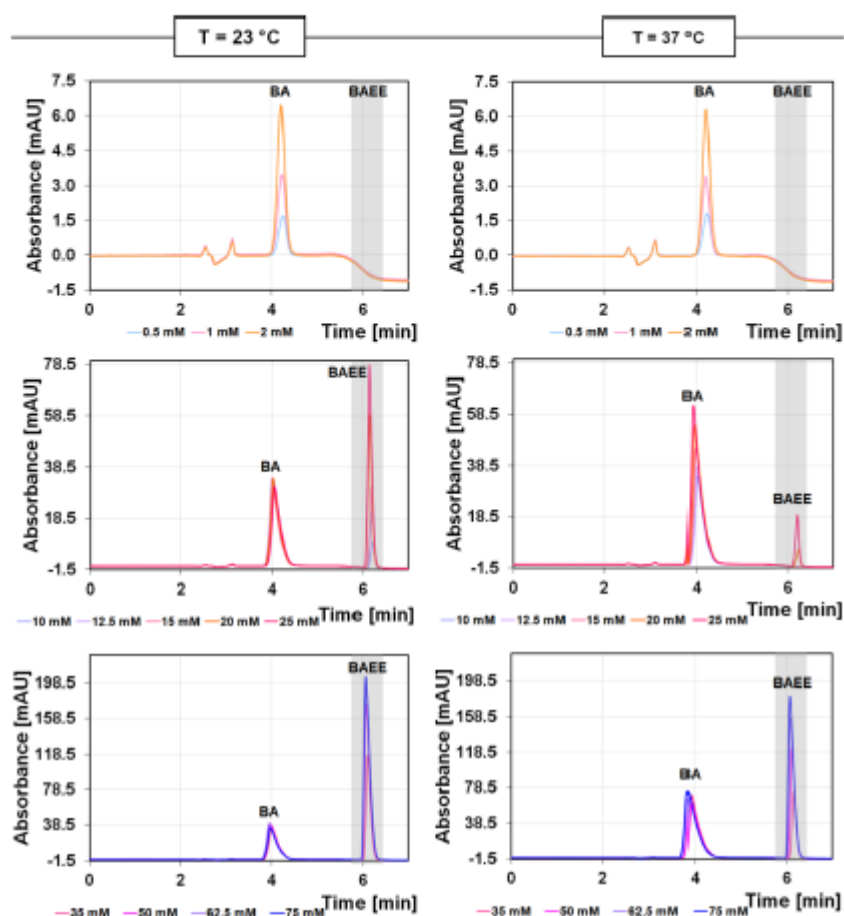
252 **Results and discussion**

253 **Classical in-gel protein digestion method with trypsin.** Gel electrophoresis is a widely used method
 254 for studying proteins, allowing for the separation of individual protein fractions based on differences in
 255 size, charge, or conformation. In the context of this study, gel electrophoresis was performed to analyze
 256 the proteins of interest, β -casein (β CN) and β -lactoglobulin (β LG). This technique provided information
 257 on the purity of the protein samples and offered a preliminary estimation of their molecular masses.
 258 Visual evaluation of the electrophoresis results (qualitative assessment) was conducted, as depicted in
 259 Fig. S1. The obtained bands indicated a mass of approximately 23 kDa for β CN and 18 kDa for β LG.

260 Following gel electrophoresis, protein bands were excised from the polyacrylamide gel, and an
261 in-gel digestion process was carried out. This process included washing the gel pieces, followed by
262 reduction and alkylation steps, in-gel digestion, and subsequent extraction of the resulting peptides, as
263 described in the experimental section. Prior to spectrometric analysis, the peptide samples underwent
264 purification and concentration using ZipTip pipette tips. This step was performed to assess whether this
265 particular sample preparation method could potentially improve the results obtained (Spectrometric
266 study).

267
268 **Capillary enzyme reactors (CER) – the efficiency of the μ -IMER produced.** Attachment of the
269 enzyme to the support structure is achieved by hydrophobic, electrostatic or covalent reaction
270 interactions. Choosing the correct support can be a real challenge because the enzyme loading, porosity
271 or pH stability must be taken into account. Many factors affect the effectiveness of digestion, these
272 include the choice of support, residence time as well as the dynamics of the flow supporting the
273 digestion. To allow enzyme-substrate interactions, a longer reaction (residence) time is usually required.
274 The residence time needs to be increased if reduced efficiency is observed in IMERs in comparison to
275 the free enzyme, or if reduced sequence coverage is observed by MS, particularly if no change in
276 substrate affinity is observed¹⁰.

277 The activity (efficiency) of the prepared microreactor was checked on the basis of the trypsin-
278 catalyzed hydrolysis reaction of *N*- α -benzoyl-arginine ethyl ester (BAEE), as by the action of trypsin,
279 BAEE is hydrolyzed to *N*- α -benzoyl-arginine (BA) and ethanol. Trypsin was chosen because it cleaves
280 the C-terminal of arginine and lysine, thus leaving positively charged amino acids on the newly formed
281 C-terminal, which promotes ionization and fragmentation²². For BAEE, the product (BA) of the reaction
282 was separated from the substrate (BAEE) by capillary liquid chromatography, while the yield of the
283 reaction was evaluated using the peak area of the substrate. Due to the similar absorption of radiation
284 by both the substrate and the product, the detection was carried out at $\lambda = 223$ nm. Initially, isocratic
285 elution with 40% acetonitrile (ACN) in the presence of 0.1% trifluoroacetic acid (TFA) was used, but
286 due to the long analysis time, gradient elution was applied. The chromatographic process was carried
287 out from 20% ACN content in the presence of TFA in the mobile phase, increasing it to 40%. TFA is
288 the agent most commonly used to separate peptides and proteins in chromatography and acts as an ion-
289 pairing agent. Fig. 2 shows the effect of substrate concentration (0.5–75 mM) and temperature (23 °C
290 and 37 °C) on the efficiency of the prepared microreactor at the applied flow rate $F = 1$ μ L/min.



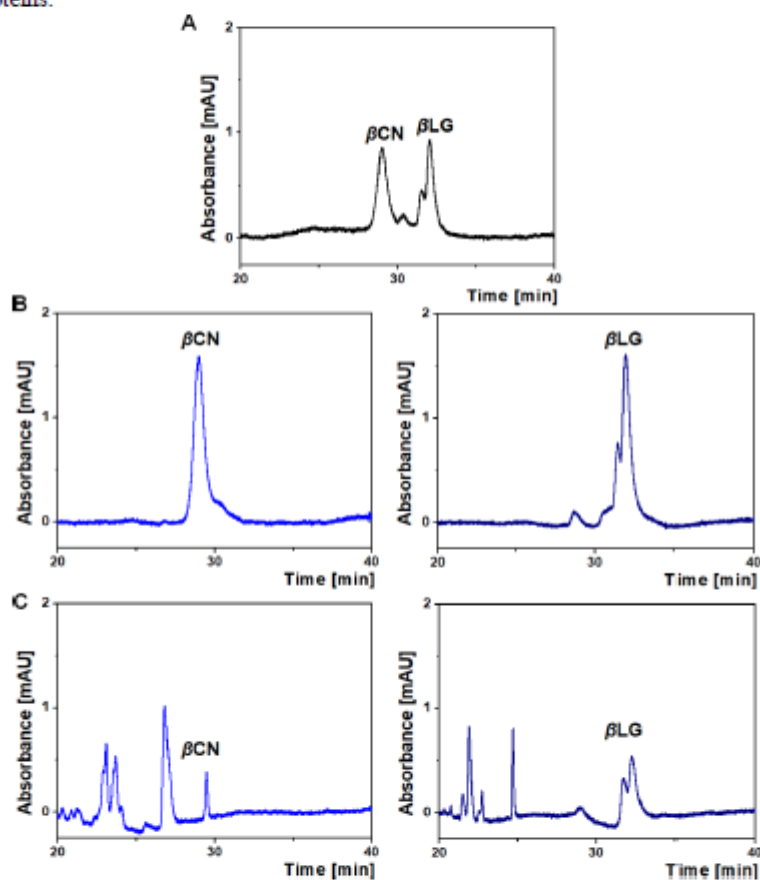
291
292 **Figure 2.** Effect of substrate concentration and temperature on the efficiency of the prepared
293 microreactor at the flow rate of $F = 1 \mu\text{L}/\text{min}$.

294 In our study, we explored the hydrolysis efficiency of BAEE (*N*- α -benzoyl-L-arginine ethyl
295 ester) using our immobilized enzyme microreactor (μ -IMER) under different conditions. For solutions
296 with low concentrations of BAEE (0.5 mM, 1 mM, and 2 mM) at room temperature (23 °C), we observed
297 complete hydrolysis, as evidenced by the absence of substrate signals in the eluate. This suggests that
298 the μ -IMER is highly effective at these concentrations. However, for higher concentrations ranging from
299 10 mM to 75 mM, the degree of hydrolysis varied between 91.23% and 27.74%. This incomplete
300 hydrolysis could be attributed to the presence of unreacted ester in the eluate, possibly due to insufficient
301 contact time between the enzyme and substrate or the saturation of enzymatic sites. It's worth noting
302 that BAEE can undergo spontaneous hydrolysis. According to literature, approximately 4% of BAEE is
303 spontaneously hydrolyzed within 24 hours when left at room temperature, while the solution remains
304 stable for at least 14 days when stored at 4°C²³. Therefore, the observed hydrolysis in our study is likely
305 enzymatic rather than spontaneous, especially at lower concentrations. When the temperature was
306 increased to 37 °C, which is closer to the optimal temperature for trypsin activity, complete hydrolysis
307 was again observed for low concentrations (0.5 mM, 1 mM, and 2 mM) as well as for some higher
308 concentrations (10 mM, 12.5 mM, and 15 mM)²⁴. For concentrations ranging from 20 mM to 75 mM,
309 the degree of hydrolysis was between 98.60% and 36.24%. Given that 37 °C is the optimal temperature

310 for trypsin, we chose this temperature for further studies involving proteins β -casein (β CN) and β -
311 lactoglobulin (β LG). This comprehensive analysis underscores the importance of optimizing both
312 substrate concentration and reaction temperature to achieve efficient hydrolysis, particularly when using
313 μ -IMERs for complex biological samples²⁴.
314

315 **Capillary enzyme reactors (CER) – protein digestion in μ -IMER.** The use of liquid chromatography
316 allowed the separation of milk proteins β CN and β LG. Considering that protein digestion requires longer
317 contact time with trypsin compared to the model BAEE ester, a lower flow rate of $F = 0.05 \mu\text{L}/\text{min}$ was
318 used.

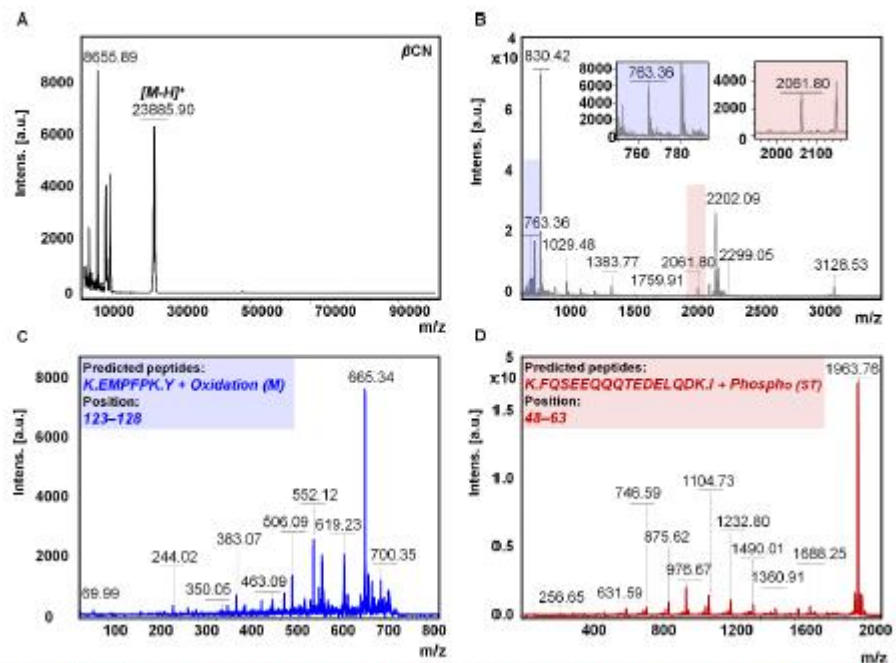
319 The chromatogram (Fig. 3) showed very good quality separation and clear signals from the
320 studied proteins.



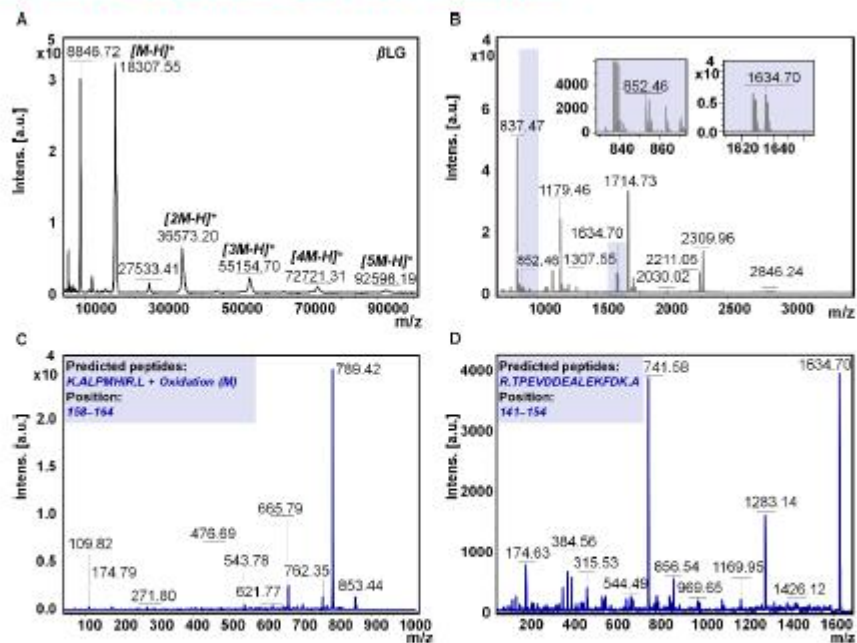
321 Figure 3. Chromatographic profile of a mixture of β CN and β LG – A, native proteins – B, and proteins
322 passed through a microreactor – C.
323

324 The first eluted protein in the mixture was β CN, then β LG. The retention times of the eluted
325 signals coincided with those of β CN and β LG included in the standards. In addition, two signals were
326 observed for β LG, which are derived from its genetic variants. A quick and easy way to prepare the
327 sample for the HPLC procedure was developed. Proteins that passed through a microreactor were
328 subjected to analogous tests. It was observed that the intensity of signals for both β CN and β LG
329 decreased compared to the native form of both proteins and additionally new signals appeared. The
330 results indicate the activity of the microreactor against the proteins studied.

331
332 **Spectrometric study.** Proteomic research heavily relies on mass spectrometry (MS) coupled with
333 various sample preparation techniques and separation methods. However, the complexity of proteomic
334 samples poses significant challenges in developing fast and efficient sample preparation methods for
335 subsequent MS analysis²⁵. In our study, we conducted a detailed characterization of the primary structure
336 of two proteins, β -casein (β CN) and β -lactoglobulin (β LG). Through careful analysis, we determined
337 the molecular weights of intact β CN (Fig. 4A) and β LG (Fig. 5A) to be approximately $23,885.90 \pm 0.216$
338 Da and $18,307.55 \pm 0.145$ Da, respectively. Additionally, besides the monomeric forms of the proteins,
339 the presence of dimers, trimers, and in the case of β LG, even tetramers and pentamers, was observed.
340 Interestingly, in the case of β LG, we also observed the presence of dimers $[2M-H]^+$ and various
341 oligomers such as trimers $[3M-H]^+$, tetramers $[4M-H]^+$, and pentamers $[5M-H]^+$ (Fig. 5A). These
342 findings align with the information provided in our previous research³ provides valuable insights into
343 oligomeric forms study of β LG.
344 To gain further insights, the proteins underwent extensive analysis with a focus its peptides
345 modifications. Tryptic digestion was performed, and the resulting peptides were subjected to PMF
346 analysis in positive mode (Fig. 4 B, Fig. 5 B). Peptides were identified using BioTools software,
347 employing non-standard cysteine searches modified to account for carbamidomethylation, oxidation,
348 and phosphorylation. Tables 1S and 2S present the individual masses of the detected peptides, their
349 sequences, the sites of oxidation and phosphorylation, and the sequence coverage considering the two
350 different sample preparation methods: with and without the use of ZipTip pipette tips. The
351 phosphorylation was observed specifically on serine residues. The mass spectra of the identified protein
352 peptides are shown in Fig. 4 C, D and Fig. 5 C, D.
353 The in-depth analysis provided valuable information regarding the peptide sequences, and their
354 modifications, contributing to a comprehensive understanding of the proteins β CN and β LG in this
355 study.
356



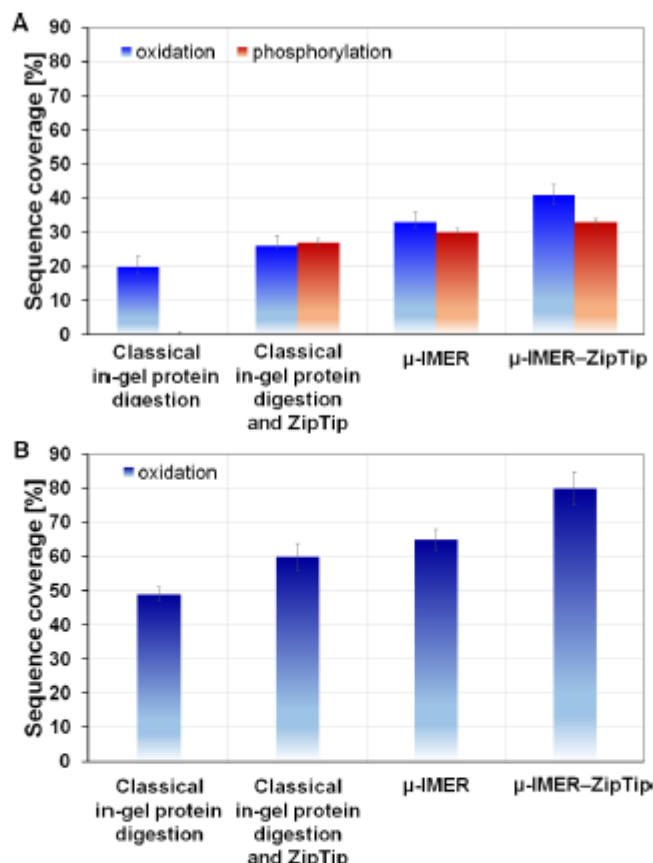
357
 358 **Figure 4.** Schematic diagram illustrating the distinct signal patterns of β -casein (β CN) as captured in
 359 MALDI MS analysis. The mass spectra in MALDI-TOF MS mode display the components of β CN in
 360 their intact state (Panel A); the spectrum obtained following trypsin digestion of β CN (Panel B); the
 361 fragmentation of the signal at $m/z = 763.36$ (Panel C); and the fragmentation of the signal at $m/z =$
 362 2061.80 (Panel D), all acquired using LIFT-TOF/TOF MS mode.



363
 364 **Figure 5.** Schematic diagram illustrating the distinct signal patterns of β -lactoglobulin (β LG) as
 365 observed in MALDI MS analysis. The mass spectra in MALDI-TOF MS mode showcase the

366 components of β LG in their intact state (Panel A); the tryptic digestion spectrum recorded for β LG
 367 (Panel B); the fragmentation of the signal at $m/z = 852.46$ (Panel C); and the fragmentation of the signal
 368 at $m/z = 1634.70$ (Panel D), all captured using LIFT-TOF/TOF MS mode.

369 To identify the proteins β -casein (β CN) and β -lactoglobulin (β LG), enzymatic digestion was
 370 performed using two different methods: the classical **in-gel protein digestion method** and the μ -IMER
 371 method. The aim was to determine the sample preparation method that would provide the highest degree
 372 of sequence coverage, allowing for more accurate protein identification (Fig. 6). In the classical method,
 373 the proteins were digested **in-gel** following the established protocol. For the μ -IMER method, the
 374 proteins were subjected to digestion within the flow-through microreactor, which offers advantages such
 375 as shorter digestion times and improved mass transfer. Additionally, to assess the impact of ZipTip
 376 pipette tips on sequence coverage, some samples underwent peptide enrichment using the
 377 chromatographic bed of the tips. By comparing the results obtained from the different digestion methods
 378 and sample preparation techniques, the most optimal approach for achieving the highest sequence
 379 coverage was determined. This selection is crucial for accurate protein identification, enabling a
 380 comprehensive understanding of the β CN and β LG proteins. The evaluation of the various methods and
 381 techniques allowed for the identification of the most suitable sample preparation method for subsequent
 382 analyses.



383 **Figure 6.** Sequence coverage using different sample preparation methods for analysis to β CN – A and
 384 β LG – B.
 385

386 The findings reveal that the sequence coverage for the protein β -casein (β CN), when subjected
387 to classical **in-gel protein digestion** was $20\pm 2\%$, indicating that a fifth of the protein's sequence was
388 analyzed and identified. This is specifically referring to the presence of oxidized molecules in the
389 protein's structure. However, when the ZipTip pipette tips were used in conjunction with classical
390 digestion, there was an improvement in the sequence coverage by 6%, increasing it to $26\pm 1\%$. These
391 ZipTip pipette tips, therefore, appear to enhance the detection and analysis capabilities of the sequence
392 coverage process. The use of a flow-through microreactor, also known as a μ -IMER, further boosted the
393 sequence coverage, bringing it to $33\pm 1.5\%$. This shows that the μ -IMER provides a more efficient
394 environment for protein digestion, leading to an increased understanding of the protein's sequence. This
395 value was further enhanced to $41\pm 3\%$, when the ZipTip pipette tips were applied post-digestion in the
396 μ -IMER, meaning the combination of the μ -IMER and ZipTip was particularly effective in improving
397 sequence coverage. This method, in fact, provided double the sequence coverage compared to the
398 classical digestion method alone. The researchers also tested a second protein, β -lactoglobulin (β LG).
399 Here, the classical digestion method offered significantly higher sequence coverage – $49\pm 2\%$, without
400 ZipTip and $60\pm 4\%$, with ZipTip. Again, using the μ -IMER led to an increase in sequence coverage, in
401 this case to $65\pm 3\%$. With the additional use of ZipTip, sequence coverage reached $80\pm 5\%$, which is
402 notably higher than the results achieved with the β CN protein. **In our study, we utilized laser ionization**
403 **fragmentation technologies in MS/MS mode (LIFT TOF/TOF MS) to explore phosphorylations.**
404 **Metastable fragmentation of selected ions was achieved using laser ionization, eliminating the need for**
405 **additional collision gas²⁶. Interestingly, no phosphorylation was detected in β CN when analyzed**
406 **directly. However, the incorporation of ZipTip pipette tips after classical digestion led to a marked**
407 **increase in the sequence coverage for phosphorylated β CN sequences, reaching $27\pm 4\%$. This coverage**
408 **was further enhanced to $30\pm 2\%$ and $33\pm 1\%$ when ZipTip was used in conjunction with μ -IMER and μ -**
409 **IMER-ZipTip, respectively. For β LG, the use of ZipTip enabled the detection of a significantly higher**
410 **proportion of modified peptides in both classical digestion ($79\pm 2\%$) and μ -IMER ($79\pm 4\%$). These**
411 **findings underscore the utility of ZipTip in enhancing the detection of oxidized molecules and**
412 **phosphorylations, particularly in the context of β CN, with similar improvements observed for β LG. The**
413 **data suggest that the combined use of ZipTip and μ -IMER offers a more effective strategy for achieving**
414 **comprehensive protein sequence coverage and post-translational modification analysis. Additionally,**
415 **our μ -IMER method revealed the presence of new peptides that were not identified using the classical**
416 **method, such as those with m/z values of approximately 763 and 3109 for β CN, and approximately**
417 **2706, 2722, and 2312 for β LG. Similarly, the use of ZipTip led to the identification of new peptides**
418 **when compared to both the classical method and μ -IMER, with m/z values of approximately 645, 763,**
419 **and 871 for β CN, and approximately 902 and 2312 for β LG in the classical method, and approximately**
420 **2235 for β CN and approximately 902 and 1248 for β LG in μ -IMER.**

421 The concept of utilizing ZipTip pipette tips is akin to the traditional solid-phase extraction (SPE)
422 technique. The primary purpose of these methods is to augment the concentration of the analytes
423 (components of interest) within the sample and, if required, to purify the sample by eliminating
424 unwanted substances. Both these processes can enhance sequence coverage, which is achieved by
425 amplifying the number of analyte molecules that undergo the Matrix-Assisted Laser
426 Desorption/Ionization (MALDI) process. Additionally, the removal of potential contaminants
427 contributes to a more accurate and unobstructed analysis^{27,28,29}. However, it's important to note that while
428 these processes increase the concentration of the analytes, they might also inadvertently concentrate
429 unwanted impurities²⁸. Hence, one should remain cautious about this possibility during such operations.
430 In the study under discussion, it's clear that the application of ZipTip amplified the degree of sequence
431 coverage in the case of oxidized β -casein (β CN) and β -lactoglobulin (β LG), and also enhanced the
432 detection of phosphorylated β CN in both the classical **in-gel protein digestion** and μ -IMER methods.

433 Nevertheless, it is observable that the sequence coverage was superior when the μ -IMER method was
434 used compared to the classical **in-gel protein digestion**. In particular, the use of the combined μ -IMER-
435 ZipTips methodology yielded the best results for β CN. These results emphasize the μ -IMER's potential
436 for preparing samples swiftly for MALDI-Time of Flight (TOF) Mass Spectrometry (MS) analysis. This
437 revelation highlights the immense potential of using the μ -IMER method to swiftly prepare samples for
438 MALDI-TOF MS analysis. As such, it's an encouraging prospect for advancing the field of proteomics,
439 which involves the large-scale study of proteins, their structures, and functions. By enhancing the
440 sequence coverage and improving the detection of post-translational modifications like oxidation and
441 phosphorylation, these methods could significantly improve the quality and depth of proteomic studies.

442 A key type of PTM is phosphorylation, which is essentially the addition of a phosphate group
443 to a protein. Phosphorylations have an instrumental role in a wide range of cellular activities^{30,31}.
444 Moreover, they are linked to the development of various health conditions. For instance, abnormalities
445 in phosphorylation processes are associated with the development of cancer and neurodegenerative
446 disorders^{32,33,34}. This makes the analysis of phosphorylation and other PTMs an essential component of
447 disease research and potential therapeutic intervention strategies. However, the analysis of PTMs
448 presents several challenges, particularly in the context of Mass Spectrometry (MS) and Tandem Mass
449 Spectrometry (MS/MS), which are widely used analytical techniques in proteomics^{22,35,36}. Some PTMs
450 are unstable during these analyses and may break down or change, making their identification and
451 characterization difficult. Furthermore, several modifications result in the formation of hydrophilic
452 (water-attracting) products. These products can make the handling and purification of PTM samples
453 prior to MS analysis more complex, as they may not interact favorably with the commonly used
454 techniques that are designed for hydrophobic (water-repelling) molecules¹⁵. PTMs can also affect the
455 efficiency of proteases, such as trypsin, which are enzymes used to break down proteins into smaller
456 peptides for easier analysis. PTMs can lead to unusual cleavage patterns or larger-than-expected peptide
457 products, complicating the interpretation of results¹⁵. Additionally, the presence of certain PTMs can
458 reduce the ionization and detection efficiency in MS. Ionization is a crucial step in MS where molecules
459 are charged so they can be moved and measured by an electric or magnetic field. Reduced ionization
460 can lead to lower detection levels, potentially obscuring significant findings. Lastly, when a protein has
461 multiple PTMs, the resulting MS and MS/MS data sets can be incredibly complex and difficult to
462 interpret. Each modification can affect the protein's behavior in the MS, leading to a wide array of
463 potential products and signals to be interpreted¹⁵. Overall, while the analysis of PTMs can offer critical
464 insights into protein function and disease development, it also presents various challenges that require
465 sophisticated techniques and careful interpretation of the generated data.

466 In proteomic analyses, enzyme autolysis stands as a significant factor that can introduce
467 complexity and potential inaccuracies in the identification and quantification of target peptides.
468 Traditional in-gel digestion methods, while generally effective, often yield a complex polypeptide
469 mixture. This mixture comprises fragments from both the target protein and the protease, complicating
470 subsequent analyses. In our study, we observed trypsin autolysis signals in the in-gel digestion of β -
471 casein (β CN) at specific m/z values (~842 and ~1045) with corresponding intensities of 3682 and 1375.
472 Additional signals were also noted at m/z values of 3092 and 2299, albeit with much lower intensities
473 (~350). These findings align with existing literature that discusses the implications of trypsin autolysis
474 in in-gel digestion methods³⁷. In the case of β -lactoglobulin (β LG), we detected multiple autolysis
475 signals at various m/z values (732; 842; 870; 1045; 1178), but these signals exhibited low intensities
476 (ranging from 300 to 900). This suggests that the impact of autolysis may be less significant for β LG
477 under our experimental conditions. Importantly, we utilized a specialized form of trypsin in which lysine
478 residues have been modified by reductive methylation. This modification yields a trypsin molecule that
479 is both highly active and extremely resistant to autolytic digestion, thereby potentially mitigating the
480 issue of autolysis. Remarkably, our μ -IMER method showed no evidence of trypsin autolysis. This

481 absence could be attributed to the enzyme's immobilization on the microreactor, which may confer
482 stability and reduce its susceptibility to autolysis³⁷. This finding not only highlights the utility of μ -
483 IMER in proteomic analyses but also warrants further studies to explore the stability and reusability of
484 immobilized trypsin in such systems.

485 This additional layer of complexity complicates the composition of the polypeptide mixture and
486 makes subsequent analysis of the Mass Spectrometry (MS) spectra more challenging. Autolysis peaks
487 can suppress peptide signals in the MS spectra, thereby reducing the sensitivity of the method. In simple
488 terms, the self-digested enzyme fragments can interfere with the detection of the actual target protein
489 fragments, making it harder to identify and analyze these components. To address these issues, one
490 strategy is the immobilization of enzymes on solid supports or other carriers. By fixing the enzymes
491 onto a solid structure, autolysis can be minimized while maintaining a high enzyme-to-substrate ratio,
492 which is crucial for efficient protein digestion³⁸. A particularly effective method in this regard is the use
493 of a flow-through microreactor, also known as μ -IMER. This technique offers several notable
494 advantages over traditional *in-gel* protein digestion. First, it greatly accelerates the digestion process,
495 enabling higher throughput than common protocols used in classical methods, such as those involving
496 gel preparation. Furthermore, the μ -IMER method reduces the complications associated with sample
497 handling and processing. For example, it can minimize concerns related to pipette transfer, which is a
498 common source of error and variability in traditional laboratory protocols³⁹. By streamlining and
499 improving the digestion process, the μ -IMER method can enhance the reliability and efficiency of
500 proteomic analyses. The majority of the literature focuses on off-line microreactors, which although
501 easier to implement, do not offer the real-time analysis capabilities of on-line systems³⁹. The challenge
502 in achieving on-line coupling, particularly with Mass Spectrometry (MS), lies in the difficulty of
503 harmonizing the experimental conditions across different units in the workflow. This is a significant
504 hurdle that our work aims to address. While some studies have managed to achieve on-line coupling
505 through Liquid Chromatography (LC) or Capillary Electrophoresis (CE)³⁹, our system is designed to be
506 more versatile and robust, capable of on-line coupling with MS. In terms of efficiency and time, the
507 study by Villegas et al. demonstrated that on-line digestion, separation, and characterization of proteins
508 could be achieved in less than 30 minutes using commercial cellulose resin particles with immobilized
509 trypsin³⁹. Our system, while also aiming for high efficiency, has a unique focus on robustness and
510 longevity. The unique monolithic support and capillary surface modifications contribute to its extended
511 lifespan, making it a cost-effective option. Another study showed that an efficient IMER could
512 significantly reduce the analysis time by approximately 15 hours compared to classical solution
513 digestion⁴⁰. Our IMER not only aims to shorten the analysis time but also provides comparable or
514 superior protein sequence coverage. This is achieved through the unique monolithic support that
515 enhances enzyme stability. Our system employs a Capillary Enzyme Reactor (CER) with a meticulously
516 prepared capillary surface. The capillary undergoes a series of chemical treatments, including etching
517 with sodium hydroxide and silanization with γ -MAPS, to create optimal conditions for enzyme
518 immobilization. This sets our system apart in terms of both efficiency and robustness. The monolithic
519 support in our system is synthesized using a specialized polymerization solution, which consists of a
520 mixture of the functional monomer GMA and the crosslinking monomer EDM²¹. This unique monolithic
521 support offers a robust and efficient platform for enzyme immobilization, contributing to the reactor's
522 longevity and performance.

523 Given the pivotal role of protein modifications, including post-translational modifications
524 (PTMs), in determining the structure, function, and biological interactions of proteins and peptides, their
525 detection and characterization are of paramount importance. PTMs can modify amino acid side chains
526 post-biosynthesis, thereby influencing their overall behavior and properties. This insight is particularly
527 valuable for the development of functional foods and dietary supplements, such as protein hydrolysates.
528 In this context, the methodology introduced in this study shows considerable promise. The enhanced

529 sequence coverage achieved through the use of μ -IMER and ZipTip, especially for proteins with
530 complex PTMs, underscores the potential of these techniques to make significant contributions to
531 protein research. Additionally, the speed and accuracy offered by these methods make them highly
532 applicable in various fields that require rapid and precise protein analysis, including the development of
533 functional foods and dietary supplements.

534

535 Conclusions

536 This study offers a comprehensive comparison of proteomic methodologies, focusing on classical in-gel
537 protein digestion, the use of a flow-through enzymatic microreactor (μ -IMER), and the application of
538 ZipTip pipette tips. All methods were followed by Matrix-Assisted Laser Desorption/Ionization-Time
539 of Flight Mass Spectrometry (MALDI-TOF MS) for analysis. We centered our research on two bovine
540 milk proteins, β -casein (β CN) and β -lactoglobulin (β LG), which are characterized by their unique
541 structural and molecular weight attributes. Our findings underscore the distinct advantages of using μ -
542 IMER, which yielded superior sequence coverage of $33\pm 1.5\%$ for β CN and $65\pm 3\%$ for β LG, thereby
543 promoting a more streamlined digestion process compared to classical in-gel digestion, which yielded
544 $20\pm 2\%$ for β CN and $49\pm 2\%$ for β LG. The incorporation of ZipTip pipette tips into both methods
545 significantly enhanced sequence coverage, reaching $26\pm 1\%$ for β CN and $60\pm 4\%$ for β LG in classical
546 in-gel digestion, and $41\pm 3\%$ for β CN and $80\pm 5\%$ for β LG in μ -IMER. It's important to note that
547 sequence coverage was sensitive to variations in protein structure. Specifically, β LG, the smaller of the
548 two proteins, demonstrated higher sequence coverage results. For oxidized β LG, sequence coverage
549 increased steadily, peaking when both μ -IMER and ZipTip techniques were employed. In the case of
550 β CN, the use of ZipTip in classical digestion enhanced sequence coverage to $27\pm 4\%$, and further
551 increased to $30\pm 2\%$ and $33\pm 1\%$ when μ -IMER and μ -IMER–ZipTip were used, respectively.
552 Additionally, ZipTip allowed for the detection of a higher percentage of modified peptides in both
553 classical digestion ($79\pm 2\%$) and μ -IMER ($79\pm 4\%$) for β LG.

554 By fusing the digestion efficiency of the μ -IMER method with the enhanced sensitivity and
555 sequence coverage offered by ZipTip, alongside a shorter analysis time, this technique could be
556 instrumental in elevating analytical capabilities across various scientific domains, including food
557 science. Our study suggests an innovative pathway to protein analysis by amalgamating classical in-gel
558 digestion, μ -IMER, and ZipTip techniques. It sheds light on the pros and cons of these methods when
559 dealing with diverse proteins, underscoring the impactful role of protein structure in the final outcomes.

560 Looking ahead, it would be worthwhile to test these methodologies on a wider variety of proteins
561 to gain further insights into the impact of different protein structures on sequence coverage and overall
562 analytical results. Exploring the use of additional proteases or combinations thereof could potentially
563 enhance digestion efficiency. Through ongoing research and development, we can aspire to broaden and
564 deepen our understanding of protein biology and its manifold applications.

565

566 References

- 567 1. Mills, S., Ross, R. P., Hill, C., Fitzgerald, G. F. & Stanton, C. Milk intelligence: Mining milk for
568 bioactive substances associated with human health. *International Dairy Journal* **21**, 377–401
569 (2011).
- 570 2. Kontopidis, G., Holt, C. & Sawyer, L. Invited Review: β -Lactoglobulin: Binding Properties,
571 Structure, and Function. *Journal of Dairy science* **87**, 785–796 (2004).
- 572 3. Gołębiowski, A. *et al.* Isolation and self-association studies of beta-lactoglobulin. *International*
573 *Journal of Molecular Sciences* **21**, 1–21 (2020).
- 574 4. Hohmann, L. G. *et al.* Comparative Effects of Milk Containing A1 versus A2 β -Casein on Health,
575 Growth and β -Casomorphin-7 Level in Plasma of Neonatal Dairy Calves. *Animals* **11**, 55 (2021).

- 576 5. Dullius, A., Goettert, M. I., Fernanda, C. & Souza, V. De. Whey protein hydrolysates as a source
577 of bioactive peptides for functional foods – Biotechnological facilitation of industrial scale-up.
578 *Journal of Functional Foods* **42**, 58–74 (2018).
- 579 6. Manninen, A. H. Protein hydrolysates in sports and exercise: A brief review. *Journal of Sports*
580 *Science and Medicine* **3**, 60–63 (2004).
- 581 7. Hou, Y., Wu, Z., Dai, Z., Wang, G. & Wu, G. Protein hydrolysates in animal nutrition: Industrial
582 production, bioactive peptides, and functional significance. *Journal of Animal Science and*
583 *Biotechnology* **8**, 1–13 (2017).
- 584 8. Liu, H. *et al.* An anticoagulant peptide from beta-casein: identification, structure and molecular
585 mechanism. *Food and Function* **10**, 886–892 (2019).
- 586 9. Sitehy, M., Chobert, J. M. & Haertlé, T. Phosphorylation of β -Lactoglobulin under Mild
587 Conditions. *Journal of Agricultural and Food Chemistry* **43**, 59–62 (1995).
- 588 10. Wouters, B., Currivan, S. A., Abdhussain, N., Hankemeier, T. & Schoenmakers, P. J.
589 Immobilized-enzyme reactors integrated into analytical platforms: Recent advances and
590 challenges. *TrAC - Trends in Analytical Chemistry* **144**, 1–9 (2021).
- 591 11. Parker, C. E., Warren, M. R. & Mocanu, V. Mass Spectrometry for Proteomics. in
592 *Neuroproteomics* 1–36 (Taylor and Francis Group, LLC, 2010).
- 593 12. Nika, H., Nieves, E., Hawke, D. H. & Angeletti, R. H. C-terminal protein characterization by
594 mass spectrometry using combined micro scale liquid and solid-phase derivatization. *Journal of*
595 *Biomolecular Techniques* **24**, 17–31 (2013).
- 596 13. Schmelter, C. *et al.* Comparison of two solid-phase extraction (SPE) methods for the
597 identification and quantification of porcine retinal protein markers by LC-MS/MS. *International*
598 *Journal of Molecular Sciences* **19**, (2018).
- 599 14. Schmelter, C. *et al.* Peptides of the variable IgG domain as potential biomarker candidates in
600 primary open-angle glaucoma (POAG). *Human Molecular Genetics* **26**, 4451–4464 (2017).
- 601 15. Larsen, M. R., Trelle, M. B., Thingholm, T. E. & Jensen, O. N. Analysis of posttranslational
602 modifications of proteins by tandem mass spectrometry. *BioTechniques* **40**, 790–798 (2006).
- 603 16. Han, X., Xie, Y., Wu, Q. & Wu, S. The Effect of Monolith Properties on the Digestion
604 Performance of Monolith-Based Immobilized Enzyme Microreactor. *Journal of*
605 *Chromatographic Science* **57**, 116–121 (2019).
- 606 17. Sabarudin, A., Shu, S., Yamamoto, K. & Umemura, T. Preparation of metal-immobilized
607 methacrylate-based monolithic columns for flow-through cross-coupling reactions. *Molecules*
608 **26**, 1–13 (2021).
- 609 18. Meller, K., Pomastowski, P., Grzywiński, D., Szumski, M. & Buszewski, B. Preparation and
610 evaluation of dual-enzyme microreactor with co-immobilized trypsin and chymotrypsin. *Journal*
611 *of Chromatography A* **1440**, 45–54 (2016).
- 612 19. Shevchenko, A., Wilm, M., Vorm, O. & Mann, M. Mass spectrometric sequencing of proteins
613 from silver-stained polyacrylamide gels. *Analytical Chemistry* **68**, 850–858 (1996).
- 614 20. Shevchenko, A., Tomas, H., Havliš, J., Olsen, J. V. & Mann, M. In-gel digestion for mass
615 spectrometric characterization of proteins and proteomes. *Nature Protocols* **1**, 2856–2860
616 (2007).
- 617 21. Meller, K., Pomastowski, P., Grzywiński, D., Szumski, M. & Buszewski, B. Preparation and

- 618 evaluation of dual-enzyme microreactor with co-immobilized trypsin and chymotrypsin. *Journal*
619 *of Chromatography A* **1440**, 45–54 (2016).
- 620 22. Sinha, A. & Mann, M. *A beginner's guide to mass spectrometry - based proteomics. The*
621 *Biochemist* vol. 42 (2020).
- 622 23. Bergmeyer, H. U. *Methods of Enzymatic Analysis*. (Verlag Chemie, GmbH, 1965).
- 623 24. Chelulei Cheison, S., Brand, J., Leeb, E. & Kulozik, U. Analysis of the effect of temperature
624 changes combined with different alkaline pH on the β -lactoglobulin trypsin hydrolysis pattern
625 using MALDI-TOF-MS/MS. *Journal of Agricultural and Food Chemistry* **59**, 1572–1581
626 (2011).
- 627 25. Jiang, S., Zhang, Z. & Li, L. A One-Step Preparation Method of Monolithic Enzyme Reactor for
628 Highly Efficient Sample Preparation Coupled to Mass Spectrometry-Based Proteomics Studies.
629 *Journal of Chromatography A* **1412**, 75–81 (2015).
- 630 26. Neubert, H., Halket, J. M., Ocaña, M. F. & Patel, R. K. P. MALDI post-source decay and LIFT-
631 TOF/TOF investigation of α -cyano-4-hydroxycinnamic acid cluster interferences. *Journal of the*
632 *American Society for Mass Spectrometry* **15**, 336–343 (2004).
- 633 27. Ekström, S., Wallman, L., Hök, D., Marko-Varga, G. & Laurell, T. Miniaturized solid-phase
634 extraction and sample preparation for MALDI MS using a microfabricated integrated selective
635 enrichment target. *Journal of Proteome Research* **5**, 1071–1081 (2006).
- 636 28. Zwir-Ferenc, A. & Biziuk, M. Solid phase extraction technique - Trends, opportunities and
637 applications. *Polish Journal of Environmental Studies* **15**, 677–690 (2006).
- 638 29. Bugyi, F., Turiák, L., Drahos, L. & Tóth, G. Optimization of reversed-phase solid-phase
639 extraction for shotgun proteomics analysis. *Journal of Mass Spectrometry* **58**, 1–14 (2023).
- 640 30. Qausain, S., Srinivasan, H., Jamal, S., Nasiruddin, M. & Khan, M. K. A. *Protein Modificomics.*
641 *Phosphorylation and Acetylation of Proteins as Posttranslational Modification: Implications in*
642 *Human Health and Associated Diseases* (Elsevier Inc., 2019). doi:10.1016/B978-0-12-811913-
643 6.00003-5.
- 644 31. Ramazi, S. & Zahiri, J. Post-translational modifications in proteins: resources, tools and
645 prediction methods. *Database* **2021**, 1–20 (2021).
- 646 32. Ramesh, M., Gopinath, P. & Govindaraju, T. Role of Posttranslational Modifications in
647 Alzheimer's Disease. *ChemBioChem* **21**, 1052–1079 (2019).
- 648 33. Junqueira, S. C., Centeno, E. G. Z., Wilkinson, K. A. & Cimarosti, H. Post-translational
649 modifications of Parkinson's disease-related proteins: Phosphorylation, SUMOylation and
650 Ubiquitination. *Biochimica et Biophysica Acta - Molecular Basis of Disease* **1865**, 2001–2007
651 (2019).
- 652 34. Leeming, D. J. *et al.* Post-translational modifications of the extracellular matrix are key events
653 in cancer progression: Opportunities for biochemical marker development. *Biomarkers* **16**, 193–
654 205 (2011).
- 655 35. Biemann, K. Mass spectrometry of peptides and proteins. *Annual Review of Biochemistry* **61**,
656 977–1010 (1992).
- 657 36. Silva, A. M. N., Vitorino, R., Domingues, M. R. M., Spickett, C. M. & Domingues, P. Post-
658 translational modifications and mass spectrometry detection. *Free Radical Biology and Medicine*
659 **65**, 925–941 (2013).

- 660 37. Rice, R. H., Means, G. E. & Brown, W. D. Stabilization of bovine trypsin by reductive
661 methylation. *Biochimica et Biophysica Acta* **492**, 316–321 (1977).
- 662 38. Meller, K., Szumski, M. & Buszewski, B. Microfluidic reactors with immobilized enzymes—
663 Characterization, dividing, perspectives. *Sensors and Actuators, B: Chemical* **244**, 84–106
664 (2017).
- 665 39. Nagy, C., Szabo, R. & Gaspar, A. Microfluidic Immobilized Enzymatic Reactors for Proteomic
666 Analyses—Recent Developments and Trends (2017–2021). *Micromachines* **13**, 1–19 (2022).
- 667 40. Moore, S., Hess, S. & Jorgenson, J. Characterization of an immobilized enzyme reactor for on-
668 line protein digestion. *Journal of Chromatography A* **1476**, 1–8 (2016).

669

670 **Acknowledgements**

671 This work was financially supported by the National Science Centre within the framework of Preludium
672 19 project No. 2020/37/N/ST4/04082 (2021–2023). Viorica Railean is member of Emerging Fields
673 “One Health – antimicrobial stewardship in human and veterinary medicine” operating under Excellence
674 Initiative-Research University. Paweł Pomastowski is a member of Toruń Center of Excellence
675 “Towards Personalized Medicine” operating under Excellence Initiative-Research University. Michał
676 Szumski is a member of Emerging Field “Conservation and Restoration of the Cultural Heritage”.

677

678 **Author contributions**

679 A.R.: Conceptualization, Methodology, Investigation, Writing – Original Draft, Visualization, Data
680 curation, Funding acquisition, Project administration. V.R.: Writing – Review & Editing, Visualization.
681 P.P.: Conceptualization, Review & Editing, Technical support. B.B.: Conceptualization, Supervision.
682 M.Sz.: Methodology, Investigation, Writing – Review & Editing.

683

684 **Competing interests**

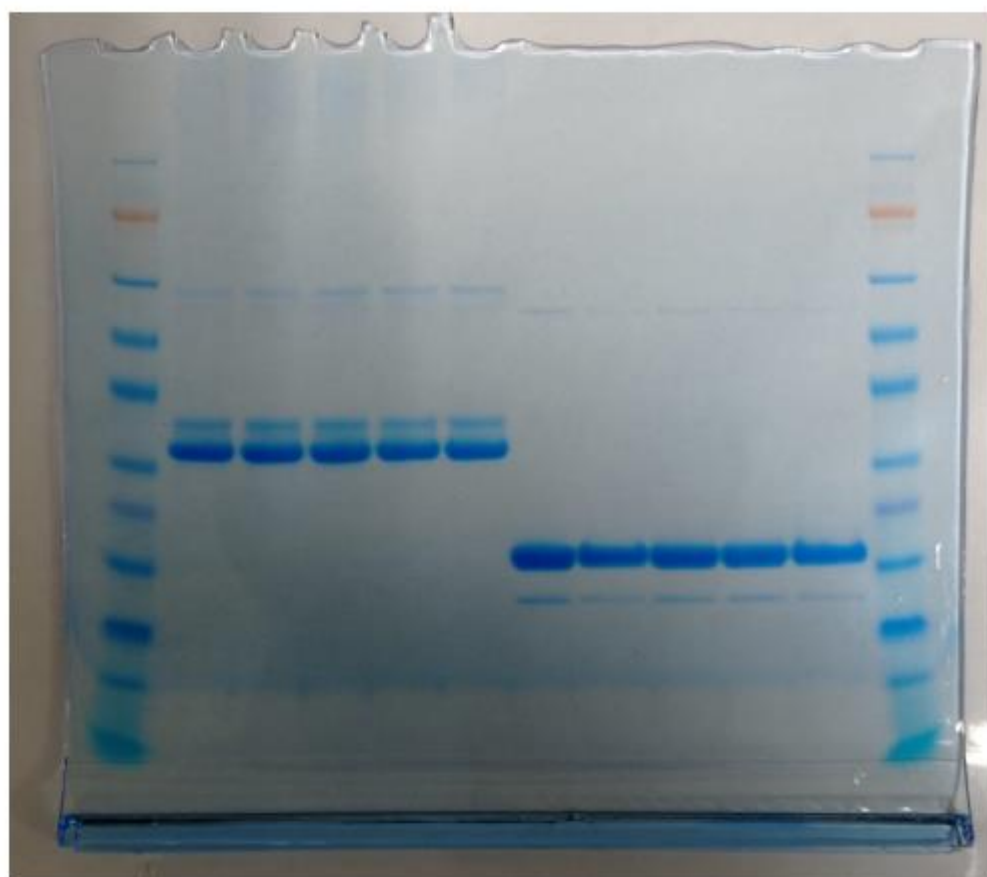
685 The authors declare no competing interests.

686

687 **Data availability**

688 All data generated or analysed during this study are included in this published article [and its
689 supplementary information files].

690



18

19 Fig. S1a. Original image of SDS-PAGE electropherogram for β CN and β LG in a non-reduced mode.

20

21

22 Table S1

23 The individual masses of detected peptides, their sequences, and the degree of sequence coverage considering the
24 two methods of sample preparation with and without ZipTip pipette tips for β CN.

Sample preparation	Mass [Da]		Sequence coverage [%]	Sequence range	Sequence
	Theoretical	Measured			
A Classical in-gel protein digestion	747.38	747.36	20	123–128	K.EMPFPK.Y
	779.50	779.49		185–191	K.VLPVPQK.A
	829.47	829.44		192–198	K.AVPYPQR.D
	2185.13	2185.16		199–217	R.DMPIQAFLLYQEPVLPVLR.G
	2201.08	2201.16		199–217	R.DMPIQAFLLYQEPVLPVLR.G + Oxidation (M)
	741.44	741.44		218–224	R.GPFPPIV.-
B	871.45	871.55	26	41–47	R.DNKKIEK.F
	645.18	645.32		115–120	K.EAMAPK.H
	747.32	747.36		123–128	K.EMPFPK.Y

Classical in-gel protein digestion and ZipTip	763.36	763.36		123-128	K.EMPFPK.Y + Oxidation (M)
	779.47	779.49		185-191	K.VLPVPQK.A
	829.43	829.44		192-198	K.AVPYPQR.D
	2185.22	2185.16		199-217	R.DMPIQAFLLYQEPVLPVLR.G
	2201.21	2201.16		199-217	R.DMPIQAFLLYQEPVLPVLR.G + Oxidation (M)
	741.45	741.44		218-224	R.GPFPPIV.-
	2061.80	2060.82	27	48-63	K.FQSEEQQTEDELQDK.I + Phospho (ST)
748.39	747.36		123-128	K.EMPFPK.Y	
780.51	779.49		185-191	K.VLPVPQK.A	
830.48	829.44		192-198	K.AVPYPQR.D	
2186.14	2185.16		199-217	R.DMPIQAFLLYQEPVLPVLR.G	
742.45	741.44		218-224	R.GPFPPIV.-	
C μ -IMER	3109.41	3109.57	33	17-44	R.ELEELNVPGEIVESLSSSEESITHINKK.I
	747.33	747.36		123-128	K.EMPFPK.Y
	763.38	763.36		123-128	K.EMPFPK.Y + Oxidation (M)
	779.46	779.49		185-191	K.VLPVPQK.A
	829.42	829.44		192-198	K.AVPYPQR.D
	2185.04	2185.16		199-217	R.DMPIQAFLLYQEPVLPVLR.G
	2201.02	2201.16		199-217	R.DMPIQAFLLYQEPVLPVLR.G + Oxidation (M)
	741.41	741.44		218-224	R.GPFPPIV.-
	871.41	871.55	30	41-47	R.INKKIEK.F
	2060.69	2060.82		48-63	K.FQSEEQQTEDELQDK.I + Phospho (ST)
747.33	747.36		123-128	K.EMPFPK.Y	
779.46	779.49		185-191	K.VLPVPQK.A	
829.41	829.44		192-198	K.AVPYPQR.D	
2185.04	2185.16		199-217	R.DMPIQAFLLYQEPVLPVLR.G	
741.41	741.44		218-224	R.GPFPPIV.-	
D μ -IMER and ZipTip	3109.77	3109.57	41	17-44	R.ELEELNVPGEIVESLSSSEESITHINKK.I
	2235.99	2236.20		64-83	K.IHPFAQTQSLVYFPFGPIPK.S
	747.20	747.36		123-128	K.EMPFPK.Y
	763.29	763.36		123-128	K.EMPFPK.Y + Oxidation (M)
	779.28	779.49		185-191	K.VLPVPQK.A
	829.33	829.44		192-198	K.AVPYPQR.D
	2185.11	2185.16		199-217	R.DMPIQAFLLYQEPVLPVLR.G
	2201.12	2201.16		199-217	R.DMPIQAFLLYQEPVLPVLR.G + Oxidation (M)
	741.32	741.44		218-224	R.GPFPPIV.-
	2060.80	2060.82	33	48-63	K.FQSEEQQTEDELQDK.I + Phospho (ST)
747.40	747.36		123-128	K.EMPFPK.Y	

2262.09	2262.03	129–147	K.YPVEPFTESSQLSLITDVEK.L + Phospho (ST)
779.53	779.49	185–191	K.VLPVPQK.A
2185.08	2185.16	197–215	R.DMPIQAFLLYQEPVLGPVR.G
2185.32	2185.16	197–215	R.DMPIQAFLLYQEPVLGPVR.G
741.49	741.44	216–222	R.GPFPILV.-

25

26 Table S2

27 The individual masses of detected peptides, their sequences, and the degree of sequence coverage considering the
28 two methods of sample preparation with and without ZipTip pipette tips for β LG.

Sample preparation	Mass [Da]		Sequence coverage [%]	Sequence range	Sequence
	Theoretical	Measured			
A Classical in-gel protein digestion	1120.45	1120.46	49	77–85	K.WENGECAQK.K
	915.46	915.47		100–107	K.IDALNENK.V
	1064.56	1064.58		108–116	K.VLVLDTDYK.K
	1192.66	1192.67		108–117	K.VLVLDTDYKK.Y
	2817.23	2817.26		118–140	K.YLLFCMENS AEPEQSLACQLVR.T
	2833.21	2833.25		118–140	K.YLLFCMENS AEPEQSLACQLVR.T + Oxidation (M)
	1244.57	1244.58		141–151	R.TPEVDDEALEK.F
	1634.76	1634.77		141–154	R.TPEVDDEALEKFDK.A
	2845.26	2845.47		155–178	K.ALKALPMHIRLSFNPTQLEEQCHI.-
	2861.26	2861.47		155–178	K.ALKALPMHIRLSFNPTQLEEQCHI.- + Oxidation (M)
	836.46	836.47		158–164	K.ALPMHIR.L
852.46	852.46	158–164	K.ALPMHIR.L + Oxidation (M)		
1714.79	1714.80	165–178	R.LSFNPTQLEEQCHI.-		
B Classical in-gel protein digestion and ZipTip	2312.20	2312.25	60	57–76	R.VYVEELKPTPEGDLEILLQK.W
	1120.44	1120.46		77–85	K.WENGECAQK.K
	902.55	902.56		92–99	K.TKIPAVFKI
	1064.56	1064.58		108–116	K.VLVLDTDYK.K
	1192.66	1192.67		108–117	K.VLVLDTDYKK.Y
	2817.21	2817.26		118–140	K.YLLFCMENS AEPEQSLACQLVR.T
	2833.18	2833.25		118–140	K.YLLFCMENS AEPEQSLACQLVR.T + Oxidation (M)
	1244.56	1244.58		141–151	R.TPEVDDEALEK.F
	1634.74	1634.77		141–154	R.TPEVDDEALEKFDK.A
	2845.24	2845.47		155–178	K.ALKALPMHIRLSFNPTQLEEQCHI.-
	2861.22	2861.47		155–178	K.ALKALPMHIRLSFNPTQLEEQCHI.- + Oxidation (M)
836.46	836.47	158–164	K.ALPMHIR.L		
852.46	852.46	158–164	K.ALPMHIR.L + Oxidation (M)		
1714.77	1714.80	165–178	R.LSFNPTQLEEQCHI.-		

C μ -DIMER	2706.23	2706.37	65	31-56	K.VAGTWYSLAMAAASDISLLDAQSAPLR.V
	2722.23	2722.36		31-56	K.VAGTWYSLAMAAASDISLLDAQSAPLR.V + Oxidation (M)
	2312.14	2312.25		57-76	R.VYVEELKPTPEGDLEILLQK.W
	1192.60	1192.67		108-117	K.VLVLDTDYKK.Y
	2817.13	2817.26		118-140	K.YLLFCMENSAPPEQSLACQCLVR.T
	1634.70	1634.77		141-154	R.TPEVDDEALEKFDK.A
	2845.18	2845.47		155-178	K.ALKALPMHIRLSFNPTQLEEQCHI.-
	2861.18	2861.47		155-178	K.ALKALPMHIRLSFNPTQLEEQCHI.- + Oxidation (M)
	836.36	836.47		158-164	K.ALPMHIR.L
1714.72	1714.80	165-178	R.LSFNPTQLEEQCHI.-		
D μ -DIMER and ZipTip	2706.39	2706.37	80	31-56	K.VAGTWYSLAMAAASDISLLDAQSAPLR.V
	2312.27	2312.25		57-76	R.VYVEELKPTPEGDLEILLQK.W
	1120.52	1120.46		77-85	K.WENGECAQK.K
	1248.60	1248.56		77-86	K.WENGECAQKK.I
	902.61	902.56		92-99	K.TKIPAVFK.I
	915.53	915.47		100-107	K.IDALNENK.V
	1192.73	1192.67		108-117	K.VLVLDTDYKK.Y
	2817.29	2817.26		118-140	K.YLLFCMENSAPPEQSLACQCLVR.T
	1244.63	1244.58		141-151	R.TPEVDDEALEK.F
	1634.80	1634.77		141-154	R.TPEVDDEALEKFDK.A
	2845.33	2845.47		155-178	K.ALKALPMHIRLSFNPTQLEEQCHI.-
	836.53	836.47		158-164	K.ALPMHIR.L
	852.53	852.46		158-164	K.ALPMHIR.L + Oxidation (M)
1714.83	1714.80	165-178	R.LSFNPTQLEEQCHI.-		

29

30 Data availability

31 All data generated or analysed during this study are included in this published article [and its
32 supplementary information files].

4.6. Study on silver ions binding to β -lactoglobulin

[P6] **A. Rodzik**, V. Railean, P. Pomastowski, P. Žuvela, M. W. Wong, M. Sprynskyy, B. Buszewski *Study on silver ions binding to β -lactoglobulin*, *Biophysical Chemistry*, 2022, 291, doi: 10.1016/j.bpc.2022.106897.



Study on silver ions binding to β -lactoglobulin

Agnieszka Rodzik^{a,b}, Viorica Railean^{a,c}, Paweł Pomastowski^{a,*}, Petar Žuvela^d, Ming Wah Wong^d, Myroslav Sprynskyy^b, Bogusław Buszewski^{a,b}

^a Centre for Modern Interdisciplinary Technologies, Nicolaus Copernicus University in Toruń, Wileńska 4, 87-100 Toruń, Poland

^b Department of Environmental Chemistry and Bioanalysis, Faculty of Chemistry, Nicolaus Copernicus University in Toruń, Gagarina 7, 87-100 Toruń, Poland

^c Department of Public Health Protection and Animal Welfare, Faculty of Biological and Veterinary Sciences, Nicolaus Copernicus University in Toruń, Gagarina 7, 87-100 Toruń, Poland

^d Department of Chemistry, National University of Singapore, 3 Science Drive 3, 117543, Singapore

ARTICLE INFO

Keywords:
Silver ions
 β -Lactoglobulin
Nanocomposites
Active functional groups
Molecular dynamics
Mechanism formation

ABSTRACT

The drug-resistant pathogen phenomenon, resulting in infections and deaths that are increasingly difficult to treat, requires research into searching new potential antimicrobial agents. The presented study is focused on the investigation of impact of silver ions (Ag^+ ions) to β -lactoglobulin (β LG) structure and mechanism formation of silver- β -lactoglobulin nanocomposites, that could find potential applications in medicine. To determine the physicochemical characteristics of silver ion binding, kinetics and isothermal models were used. The presence of functional groups involved in the binding process was investigated by spectroscopic methods (FTIR-ATR, Raman spectroscopy). The binding ability and nanocomplexes formation was determined by instrumental analyses (SEM, TEM, EDX). Based on the obtained results, the binding of Ag^+ ions to β LG were heterogeneous in nature consisting of three main steps: rapid sorption of Ag^+ ions on the β LG surface, intramolecular diffusion of Ag^+ ions, and chemical equilibrium. Microscopic studies showed a change in the surface morphology of β LG and the appearance of silver nanoparticles. Spectroscopic studies indicated that acidic (Glu^- , Asp^-) and Lys, Tyr, Met amino groups play a key role in the formation of the Ag/β LG nanocomplex. Finally, molecular dynamics (MD) and density functional theory (DFT) calculated studies as a comparative and complementary method have proven contribution of respective amino acids in the binding process.

1. Introduction

In the last few years, an increase of antimicrobial resistance has occurred. There is an active search for new effective treatment and drug delivery methods for resistant pathogens [1]. Currently, many different metals have been used as antimicrobial agents, including zinc, titanium [2], gold [3] and silver. However, among these, silver in the form of silver nanoparticles (AgNPs) is the most significant. Among methods of fighting the problem of drug resistance is the study of metal-protein interactions. As a result of such interactions, we can obtain metalloproteins, metallocomplexes, nanoparticles and nanocomposites (combinations of metallocomplex and nanoparticles). Interactions of metal ions with proteins play an important role because many proteins use metal for their proper or better activity, finding application in, among others, the treatment of various diseases [4].

AgNP are found to be the most effective agents owing to their unique large area-to-volume ratio, which gives them unique properties in

comparison to molecules and to the bulk of the same material [5]. Currently there is a huge amount of research using silver compounds for various clinical studies [6,7]. Hazarika et al. [8] studied the effects of AgNPs on the structure and function of bovine serum albumin (BSA) with the aim of using NPs for drug delivery in appropriate amounts and a specific site. The silver ion (Ag^+ ion) is used due to its soft acceptor properties and its relatively flexible coordination sphere. This allows the ion to coordinate with a variety of ligands with multiple geometries and heteroatoms. The variety of coordination geometries of silver (I) can be explained by the lack of stereochemical directionality associated with the d10 configuration [9]. Ag^+ ions exhibit strong antibacterial properties [10]. It plays an important role in killing bacteria as it easily adsorbs to most biomolecules such as DNA, membrane proteins, enzymes or intracellular cofactors found in bacteria, inactivating their functions [11]. Recently, our group performed experimental and computational studies on the mechanism of metallocomplex formation due to the binding of zinc ions to ovalbumin (OVA) along with the simultaneous

* Corresponding author.

E-mail address: p.pomastowski@umk.pl (P. Pomastowski).

<https://doi.org/10.1016/j.bpc.2022.106897>

Received 28 April 2022; Received in revised form 13 September 2022; Accepted 22 September 2022

Available online 26 September 2022

0301-4622/© 2022 The Authors. Published by Elsevier B.V. This is an open access article under the CC BY license (<http://creativecommons.org/licenses/by/4.0/>).

formation of zinc oxide nanoparticles. Moreover, additionally, antimicrobial studies conducted indicated inhibitory activity against clinical strains [12].

Due to the bioactive content, relatively high amount of branched-chain amino acids, and low cost, whey proteins may be applied as nutraceuticals [13]. It has been proven that whey protein can prevent diabetes type II and diseases associated with fat accumulation [14]. Their high nutritional, biological and technological values are widely used also in many food applications [15]. Whey protein supplementation is prevalent in anticancer therapy due to its higher leucine presence and ability to modulate insulin-like growth factor (IGF-1) levels [16,17]. They also exhibit antibacterial activity against a wide range of Gram-positive and Gram-negative bacteria [18]. The major whey protein among ruminants is β -lactoglobulin (β LG). It is a small globular protein of the lipocalin family, containing 162 amino acid residues with about 18,300 Da [19]. The β LG structure is dominated by a β -sheet comprising nine β -strands and one major α -helix at the C-terminal end of the molecule. Additionally, it contains two disulfide bonds (Cys66-Cys160 and Cys106-Cys119) and a free thiol (Cys121) [20]. Due to the significant presence of cysteine, tryptophan and branched-chain amino acids, the potential to bind various hydrophobic ligands (vitamin A, fatty acids) and bioactive peptides β LG has excellent nutritional properties [19,21,22] and therefore was chosen as a model protein in the present study.

The amino acid side chains of proteins provide a wide range of interactions (hydrophobic, hydrophilic, ionic, covalent bonds). In the present study, it is undertaken to investigate the modification of proteins with metal ions, which can lead to an extension of their functionality that would not be possible without them [23], attracting attention and thus opening the way to new applications in medicine [24] as new antibacterial agents, or in nanotechnology [25], among others.

Therefore, the present study focused on the immobilization of Ag^+ ions to β -lactoglobulin (β LG) structure and mechanism of formation of silver- β -lactoglobulin nanocomplexes and silver nanoparticles- β -lactoglobulin to understand the metal-protein binding process and physico-chemical characterization of the obtained nanocomposites. In this regard, kinetic and isothermal sorption experiments as well as instrumental analyses such as spectroscopy and electron microscopy were performed. In addition, an important complement to the obtained results was molecular dynamics (MD) allowing to model the structures of $\text{Ag}\beta$ LG nanocomplexes and density functional theory (DFT) calculation indicating the binding sites and the reduction process of silver ions.

2. Experimental

2.1. Synthesis/immobilisation of Ag^+ ions to β LG

At this step, the stock solutions of the protein ($C = 5000 \text{ mg/L}$) have been prepared by suspending the β LG in distilled water (Millipore Intertech, Bedford, MA, USA) and mixed with silver nitrate (V) (Ag^+ ion) at a ratio of 1:1 (v/v). The protein mixture was prepared at $\text{pH} = \text{pI} = 4.6$. Such isoelectric point (pI) was selected based on our previous studies [26]. The obtained solutions were vortexed and sonicated. Next, the protein suspension and silver nitrate(V) solutions were incubated at room temperature (RT). For the kinetic study, 60 mg/L of silver ion concentration was used and investigated at certain period of time (from 2 min to 2880 min) while for isothermal studies several concentrations of silver ions have been prepared (from 1 to 700 mg/L) and monitored during 1440 min period of time.

Then, after incubation, the obtained solutions were centrifuged 10 min (4°C , 12,000 rpm.) and the supernatant was mineralized in aqua regia and diluted to 1% nitric acid(V) (Sigma Aldrich, Poland) and Ag^+ ions concentration was determined by Inductively Coupled Plasma-Mass Spectrometry (ICP-MS) (7900 ICP-MS, Agilent Technologies) while remained precipitate was subjected to further instrumental analyses.

2.2. Kinetic study of Ag^+ ions immobilisation to β LG

The experimental data were submitted to kinetic and isothermal models, and the degree of model fit was determined by the correlation coefficient (R) and standard error (S). Zero-order, pseudo-first-order, pseudo-second-order kinetic models and the Weber-Morris intraparticle diffusion models were used to evaluate the experimental results. Additionally, the distribution coefficient (K_d) of Ag^+ ions sorption by β LG and Gibbs' free energy for silver adsorption were calculated.

Kinetic models, the distribution coefficient (K_d) and Gibbs' free energy were determined using the equation presented in our previous study [26].

Kinetic models were determined using the following formulas:

- The zero-order kinetics model:

$$C = C_0 - k_0 t \quad (1)$$

where: C – the concentration of Ag^+ ions in aqueous solution for a certain period of time [mg/L], C_0 – the initial concentration of Ag^+ ions in aqueous solution [mg/L], k_0 – the adsorption rate constant [(mg/L)/min], t – the adsorption duration [min].

- The pseudo-first order kinetics model

$$q = q_1 (1 - e^{-k_1 t}) \quad (2)$$

where: q_1 – the amount of Ag^+ ions sorbed for a certain period of time [mg/g], q_e – the amount of Ag^+ sorbed at equilibrium [mg/g], k_1 – the rate constant of pseudo-first order sorption kinetics [1/min].

- The pseudo-second order kinetics model

$$q = \frac{q_2^2 k_2 t}{1 + q_2 k_2 t} \quad (3)$$

where: k_2 – the rate constant of pseudo-second order sorption kinetics [(g/mg)/min].

- The Weber-Morris intraparticle diffusion model

$$q = A + K_p t^{0.5} \quad (4)$$

where: A – a constant indicating the thickness of the boundary layer diffusion or external surface adsorption [mg/g], K_p – the intraparticle diffusion rate constant [(mg/g)/min^{0.5}].

The amount of silver sorption by β LG from an aqueous solution (for experimental data) was determined as follows:

$$q = (C_0 - C) \frac{V}{m} \quad (5)$$

where: V – the volume of solution from which sorption occurs [L], m – the sorbent mass [g].

Additionally, the distribution coefficient (K_d) of Ag^+ ions sorption by β LG and Gibbs' free energy for silver adsorption were calculated.

The following equations were used:

$$K_d = \frac{q_e}{C_e} \quad (6)$$

where: q_e – the amount of silver sorbed by β LG isoforms at equilibrium time [mg/g], C_e – the equilibrium concentrations of silver in solution [mg/L].

$$\Delta G^0 = -RT \ln K_d \quad (7)$$

where: ΔG^0 – the energy of adsorption [kJ/mol], R – the gas constant (8.314 J/mol·K), T – the adsorption absolute temperature (295 K), K_d – the distribution coefficient.

2.3. Isothermal study of Ag^+ ions binding to β LG

The obtained experimental results were examined using Freundlich isotherm, Langmuir isotherm, Henry isotherm and isotherm as a function of C_e/C_0 (C_e – the equilibrium concentrations of silver in solution [mg/L], C_0 – the initial concentration of Ag^+ ions in aqueous solution [mg/L]) to investigate the mechanism of silver ion sorption by β LG based on the model formulas presented in our previous publication described in detailed by [26].

- *The Freundlich isotherm*

$$q = K_F C_e^n \quad (8)$$

where: K_F – constant division (L/g), n – an empirical constant, characterized by the heterogeneity of the adsorption process. This model is generally used to describe the sorption process on the surface of heterogeneous hydrocolloids.

- *The Langmuir isotherm*

$$q = \frac{q_m K_L C_e}{1 + K_L C_e} \quad (9)$$

where: q_m – maximum amount of silver adsorbed in monolayer (mg/g), K_L – constant Langmuir division (L/mg). This model assumes that on the surface of adsorbent forms a monolayer of molecules which interact with adsorption sites, and do not interact with each other, and that there is no possibility to create a multilayer as well as that the adsorption energy is constant [27].

- *The Henry isotherm*

$$q = K_H C_e \quad (10)$$

where: K_H – equilibrium constant of Henry's adsorption [L/g].

The degree of model matching to experimental isothermal data was determined using the Pearson correlation coefficient (R) and standard error (S).

2.4. Fourier transform infrared spectroscopic with attenuated total reflectance (FTIR-ATR) and Raman spectroscopy (Raman) analysis

FTIR-ATR and Raman spectra were recorded for β LG modified by Ag^+ ions and native β LG to verify silver binding with β LG. Origin Pro/2016 software (OriginLab Corporation) was used for data processing.

The infrared spectrum was recorded in the range 400–4000 cm^{-1} using an FTIR-ATR spectrophotometer from Bruker (Billerica, Massachusetts, USA). About 1 mg of control β LG powder and nanocomplexes were used for spectral analysis by applying them to a platinum ATR with a durable monolithic diamond measurement interface.

Raman analysis was performed using a Raman spectrometer (Senterra, Bruker Optik). All Raman spectra were recorded at room temperature in the range of 400–4000 cm^{-1} at the wavelength equal to $\lambda = 532$ nm as excitation light, with power of approximately 20 mW and the counting time spectrum at 2×30 s with an accumulation of 10 fM. Sample preparation was performed by dropping the samples onto ZnSe lens with Focal length 50.8 mm, 12 mm, and 2.4 mm (IUVO-LASER, Poland), drying at room temperature for 24 h, and analyzing.

2.5. Scanning and transmission electron microscopy (SEM, TEM) with energy dispersive X-ray (EDX) analysis

Using scanning electron microscopy (SEM, LEO model 1430 VP) coupled with energy dispersive X-ray (EDX) detector (XFlash 4010, Bruker AXS, Berlin, Germany) and transmission electron microscopy (TEM, model G2 P20X-Twin 200 kV, FEI) in combination with an energy dispersive X-ray detector (EDX, Energy Dispersive X-ray, RTEM SN9577,

134 eV, Edax), the occurring changes in the surface morphology and the silver nanoparticles formation were analyzed. In addition, quantitative elemental analysis was performed.

For SEM studies, samples were applied on the microscopic slide as a solution of native protein and nanocomplexes. In order to perform TEM analysis, the samples were layered to a carbon-coated grind (Lacey type Cu 400 mesh, Plano).

2.6. Molecular dynamics (MD) simulations

To perform molecular dynamics (MD) simulations, the initial β LG structure (PDB ID: 3BLO) was obtained from the Protein Data Bank (PDB). Structure was originally characterized using X-ray crystallography at 2.56 Angstrom resolution [28]. System was solvated using a TIP3P water octahedral solvation box with a variable side length based on the estimated size of the protein and the silver ions concentrations. Silver ions (in three concentrations: 6, 60 and 600 mg/L corresponding to 5, 50 and 500 ions; computed with a fixed volume and upcaled) were placed randomly into the system, by replacing the water molecules with silver ions [29]. Three side-lengths of 34, 34, and 39 Angstrom were used for solvation boxes for systems with 5, 50, and 500 ions, respectively. Subsequently, the systems were electrostatically neutralized using Na^+ and Cl^- ions. AMBER ff99-GB-ILDN force field [30] was employed for the MD simulations. Parameters of Ag^+ ($R_{min}/2 = 1.443$, $\epsilon = 0.00818431$, $\sigma = 0.230939$) to account for non-bonded interactions have been obtained from the literature [31]. Interactions/contacts of silver with key amino acids (Glu⁻, Asp⁻, Cys, His, Try, Trp, Phe, Met, Arg, Lys) were analysed. Generally, a threshold of -4.0–6.0 Angstrom is considered for interactions of silver nanoparticles and proteins [8,32]. Here, as we have built protein-ion systems, a more restrictive threshold of 3.5 Angstrom has been employed instead. Energy minimization was employed to remove bad contacts and structural clashes; followed by fast heating to 290.15 K at a constant volume. Subsequently, density of all the systems were equilibrated subjecting systems to constant pressure (1 bar) and temperature (290.15 K) – NPT ensemble. Production MD simulations in the NVT ensemble were conducted in GROMACS 5.1.2 software. Visualization and analysis of the large-scale data were done using Visual Molecular Dynamics (VMD) 1.9.3 [33] and Python 3.9, respectively.

2.7. Density functional theory (DFT) calculations

To shed light on the interaction of silver ion (Ag^+) with the β LG protein, density functional theory (DFT) calculations, using Gaussian 16 Programs (Frisch et al., 2016), were performed for five modelled 1:1 Ag^+ -AA complexes (AA = Asp⁻, Glu⁻, Tyr, Lys and Met) using M06-2x functional [34]. The basis sets used for geometry optimizations correspond to the smaller 6-31G⁺ basis set for non-silver atoms and Def2-SVPD [35] basis set for silver atoms. For the larger basis set for single-point energy calculations, the 6-311 + G(2d,p) basis set is used for non-silver atoms and Def2-TZVPD [36] for silver atoms. It is worth noting that the D2SVP and Def2-TZVPD basis sets for Ag contain an effective core potential (ECP). Implicit solvation model GMD [37] was employed to model the solvent effect of aqueous medium ($\epsilon = 78.4$) for both geometry optimizations and single-point energy calculations.

3. Results and discussion

3.1. Kinetics and isothermal studies

Kinetic studies provide information allowing us understand the time dependence of the binding process rate of β LG binding with Ag^+ ions. Therefore, the experimental kinetic data were submitted to zero, pseudo-first, pseudo-second order kinetic models and Weber-Morris intraparticle diffusion model. Matching the experimental kinetic data to the models allowed to explain the rate of Ag^+ ions binding with β LG,

but also to determine the degree of adsorption of Ag^+ ions in protein adsorbent. The kinetics of the Ag^+ ions sorption process expressed as a plot of concentration of Ag^+ ions in solution per unit of time are presented in the Fig. 1A.

The obtained results, indicate that the Ag^+ ion adsorption process for βLG is not linear and three separate steps can be noticed. It was found that step I is associated with rapid initial sorption, while step II is a gradual slow sorption. Then, the sorption equilibrium was observed. In order to calculate the rate constants of sorption kinetics of Ag^+ ions for linear segments of the obtained steps, a zero-order kinetics model was used, which describes in detail the successive steps of sorption. The values of the rate constants for step I was 3.36 (mg/L)/min while for step II 0.017 (mg/L)/min . The values of the rate constants are summarized in Table 1, which also shows correlation coefficient (R) and standard error (S).

The fast sorption step (step I) occurs during the first 2 min of the process, in which $16.13\% \pm 1.36$ of Ag^+ ions were binding with βLG and the protein sorption capacity was $2.69 \pm 0.23 \text{ mg/g}$. The sorption process in step II is much slower and ends after 720 min. The sorption effectiveness of Ag^+ ions for this step were effectively increased to $45.84\% \pm 9.49$ and the sorption capacity increased to $7.65 \pm 1.58 \text{ mg/g}$. The maximum sorption capacity and sorption effectiveness were $48.24 \pm 3.73\%$ and $8.05 \pm 0.62 \text{ mg/g}$ respectively. In order to better explain the processes, the experimental data were submitted to a

Table 1
Kinetic model parameters for the Ag^+ ions sorption by βLG .

Kinetic models			
Zero order kinetic model	Pseudo-first order kinetic model	Pseudo-second order kinetic model	The Weber-Morris intraparticle diffusion model
I $k_0 = 3.36 \text{ (mg/L)/min}$	$k_1 = 0.016 \text{ [1/min]}$	$k_2 = 0.0038 \text{ [1/min]}$	$A = 0.20 \text{ [mg/g]}$
II $k_0 = 0.017 \text{ (mg/L)/min}$			$K_0 = 2.67 \text{ [mg/g min}^{0.5}]$
	$S = 1.58$ $R = 0.76$	$S = 1.22$ $R = 0.86$	$S = 0.32$ $R = 0.98$

pseudo-first and pseudo-second order models (Fig. 1B). In turn, matching the experimental kinetic data with the Weber-Morris intraparticle diffusion model (Fig. 1C) showed two steps. Step I was assigned the external sorption, the boundary layer diffusion effect and the process of reducing Ag^+ ion concentration. In turn, step II was assigned a gradual sorption with a limited mechanism of Weber-Morris intraparticle diffusion, ending in sorption equilibrium. The intersection point of the y-axis of the second-degree line is a measure of the thickness (volume) of external surface sorption and its slope determines the value of the

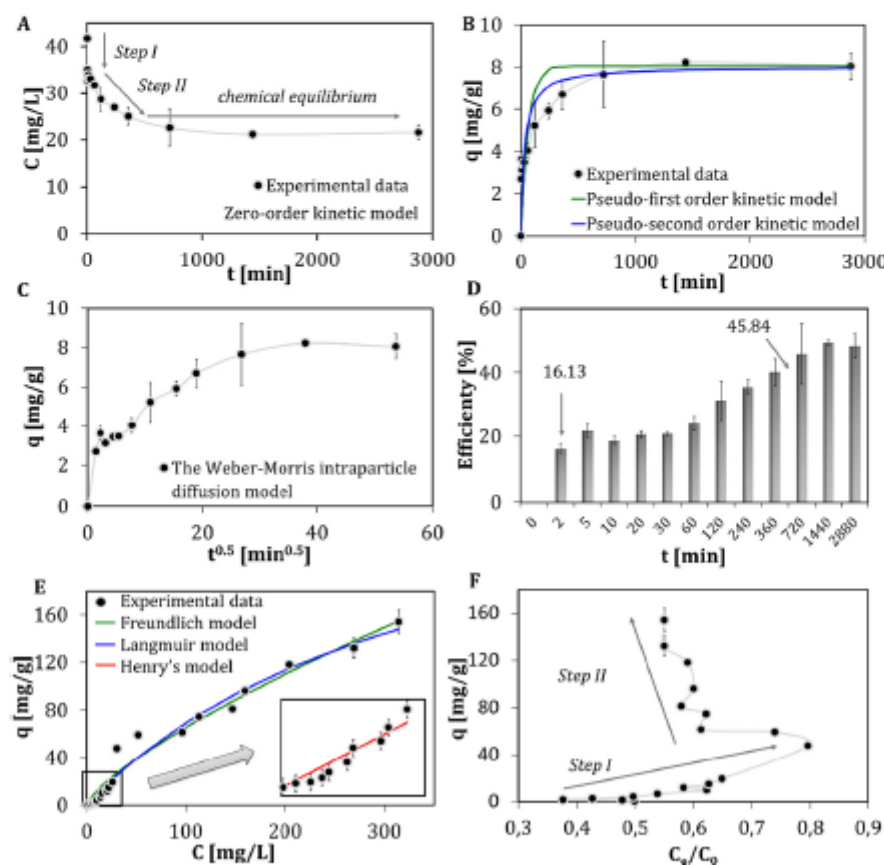


Fig. 1. The kinetic steps of the Ag^+ ions sorption onto βLG using the zero-order kinetic model (A), experimental data and fitted pseudo-first- and pseudo-second order kinetics models of the Ag^+ sorption by βLG (B), the Weber-Morris intraparticle diffusion model (C), $\text{Ag}\beta\text{LG}$ complex sorption effectiveness (D), isotherm of Ag^+ ions sorption onto βLG and fitting of the Freundlich, Langmuir and Henry's isotherm models (E), sorption isotherm of Ag^+ ions as a function of C_4/C_0 (F).

intraparticle diffusion coefficient for the sorption of Ag^+ ions by βLG , as shown in the Table 1. Analyzing the Weber-Morris intraparticle diffusion model, it can be concluded that the sorption of Ag^+ ions is mainly regulated by the sorption on the external βLG surface. Then, in step II, gradual sorption indicates the absorption of Ag^+ ions within the βLG structure. The mentioned sorption effectiveness per unit time is shown in Fig. 1D.

Moreover, the values of change Gibbs' free energy (ΔG^0) and the distribution coefficient (K_d) of sorption of Ag^+ ions to βLG were calculated, which were -14.52 kJ/mol and 372.78 respectively. The negative value of Gibbs' free energy results from the spontaneous nature of the sorption processes for the bond of Ag^+ ions to βLG . In the kinetic study of the silver-casein complex, the calculated value of ΔG^0 was -18.42 kJ/mol and the distribution coefficient was 1826 [38]. Similarly, for silver-lactoferrin complex, the value of distribution coefficient and Gibbs free energy were 699.83 and -16.06 kJ/mol, respectively [39]. Comparison of the thermodynamic parameters obtained in the present work for $\text{Ag}/\beta\text{LG}$ nanocomplex with casein (CN) and lactoferrin (LTF) complexes indicates that silver is more readily adsorbed by CN due to the highest K_d value. Nevertheless, these differences may be due to the structure of the proteins themselves. Casein exhibits a very complex structure that forms micelles [40], whereas both LTF and βLG are globular proteins. Following this, the protein masses are 18.6 kDa (βLG), 76.5 kDa (LTF) and about 90 kDa for caseins considering its four fractions: α_{s1} , α_{s2} , β and κ , respectively [41]. When translating this into the amino acid amounts of the individual milk proteins, we obtain the following: 162 (βLG), 689 (LTF), >784 (CN). Thus, it can be concluded that the process of metal binding to protein is highly dependent on the protein structure, mass and amount of amino acids.

To further study related to the mechanisms involved in the binding of Ag^+ ions by βLG , the adsorption isotherm was investigated. Fig. 1E illustrates the obtained isotherm of the Ag^+ ion sorption process for the experimental results as a plot of the change in sorption capacity versus the solution's equilibrium concentration. In addition, Henry, Langmuir and Freundlich isotherm models were fitted to the obtained experimental results. The characteristic parameters of the applied isotherm models are summarized in Table 2.

Henry's adsorption isotherm model was carried out for initial low concentrations of silver ions. This model has the simplest equation in which the amount of surface adsorbate (Ag^+ ions) is proportional to the equilibrium concentration of adsorbate (Ag^+ ions). In turn, the shape curve for the obtained Langmuir isotherm shows that the more sites in the βLG substrate are filled by Ag^+ ions, the more difficult it is for the binding Ag^+ ions to find free sites. The Langmuir isotherm curve indicates that Ag^+ ions adsorb uniformly on the βLG surface.

The rate constants of the Freundlich and Langmuir models used are 2.06 L/g and 0.0028 mL/g, respectively, thus it can be concluded that the Freundlich model provides a better fit for the experimental data obtained. Therefore, the binding process of Ag^+ ions to βLG is surface-based.

In turn, the experimental results for the isotherm as a C_e/C_0 show a more complex nature of the process (Fig. 1F). Namely, the use of this relationship makes it possible to indicate two steps of Ag^+ ion sorption. The first step indicates a small sorption capacity and a monolayer of Ag^+ ions on the βLG surface. Subsequently, in the second step, the

application of higher concentrations of Ag^+ ions about 150–700 mg/L causes the relaxation of βLG structure due to structured changes of silver βLG system caused by Ag^+ -Asp⁻ and Ag^+ -Glu⁻ bind [42]. Gradual penetration inside the structure also influences on relaxation effect. In the next step, the reduction of Ag^+ ions up to a concentration of $C_e/C_0 > 0.79$ and the release of metallic silver (Ag^0) to form nanoparticles was observed.

The obtained data indicate that at low concentrations (1–75 mg/L) the sorption processes is achieved. The use of higher concentrations of silver ions indicates that the use of isothermal models is incorrect due to the formation of silver nanoparticles. The lack of sense fitting of isothermal models is due to the formation of nanoparticles described in classical theories as nucleation of crystalline grains. The first step, and therefore nucleation, occurs by the reduction of silver ions (Ag^+) to metallic silver (Ag^0) [43]. The resulting particles, which most likely have poor stability, then undergo coalescence processes leading to a reduction in particle number. If the concentration increases sufficiently, the dissolved silver binds with the result that a stable surface is formed. When the particles reach a certain size, known as the critical radius the particles become energetically favorable thereby stabilizing enough to continue to grow. The resulting nucleus subsequently becomes in the system and grows when more silver atoms diffuse through the solution and attach to the surface [44,45]. If the concentration of dissolved atomic silver decreases, there is no way for enough atoms to bond together to form a stable nucleus. Then, at this nucleation step, new nanoparticles stop forming while the remaining dissolved silver is absorbed through diffusion into the growing nanoparticles in solution [46]. Moreover, βLG is a small globular protein, and globular proteins are characterized by a specific secondary structure in the native state, namely, they have a certain number of α -helix, β -helix and disordered peptide chain conformations. Due to the compact structure of βLG , it is difficult for silver ions to get inside the protein structure [47].

Based on the obtained isothermal studies, silver ions concentration of 6, 60 and 600 mg/L (3, 30 and 300 mg/L concentration of silver ions in nanocomplexes) were selected for further studies.

3.2. Spectroscopic studies

Kinetic and isothermal studies indicated that silver binds to βLG molecules. In turn, to observe changes in the structure of βLG and to answer the question, which active functional groups of βLG are responsible for the binding process, FTIR-ATR and Raman spectroscopic studies were performed.

In the case of FTIR-ATR analysis, Ag^+ ions lead to a decrease in the intensity of the signals recorded in the entire spectral range 400–4000 cm^{-1} compared to the control (native βLG), especially for $\text{Ag}/\beta\text{LG}30$ and $\text{Ag}/\beta\text{LG}300$ nanocomplexes (Fig. 2A). On the other hand, the binding of βLG to Ag^+ ions lead to the disappearance of 3274, 3078 and 1240 cm^{-1} signals for $\text{Ag}/\beta\text{LG}30$, $\text{Ag}/\beta\text{LG}300$ nanocomplexes; 1311 cm^{-1} for $\text{Ag}/\beta\text{LG}3$, $\text{Ag}/\beta\text{LG}30$, $\text{Ag}/\beta\text{LG}300$ nanocomplexes and disappearance of 1514 cm^{-1} band only for $\text{Ag}/\beta\text{LG}300$ nanocomplex. The observed changes are the result of silver interference in the protein structure. The changes registered at 3274, 3078 cm^{-1} originate from N–H stretching vibrations in the amide band A and B [48]. Bands at 1240 cm^{-1} and 1311 cm^{-1} representing a combination of N–H bending phase and C–N stretching vibrations with small in-plane C–O bending and C–C stretching vibrations originate from amide III (1220–1400 cm^{-1}) [49].

The 1240 cm^{-1} band also originates from the in-plane bending vibration of N–H and C–H, and the C–N stretching vibration of His [48] and the 1311 cm^{-1} band is derived from C–C and C–N stretching vibrations and C–H in-plane bending vibrations of Trp [50]. Band 1514 cm^{-1} is from amide II as a consequence of an out-of-phase combination of N–H in-plane bending vibrations and C–N stretching vibrations with less in-plane C–O bending vibrations and C–C and N–C stretching vibrations [48,49]. Structural changes resulting from the presence of amides may depend on the interaction of reduced silver ions with βLG

Table 2
Henry, Langmuir and Freundlich parameters approximation mathematical models of adsorption isotherms to the experimental data.

Isothermal models		
Henry	Langmuir	Freundlich
$K_H = 0.62$ [L/g]	$K_L = 0.0028$ [L/mg]	$K_F = 2.06$ [L/g]
	$q_m = 317.26$ [mg/g]	$n = 0.75$
$S = 2.02$	$S = 8.57$	$S = 8.89$
$R = 0.95$	$R = 0.98$	$R = 0.98$

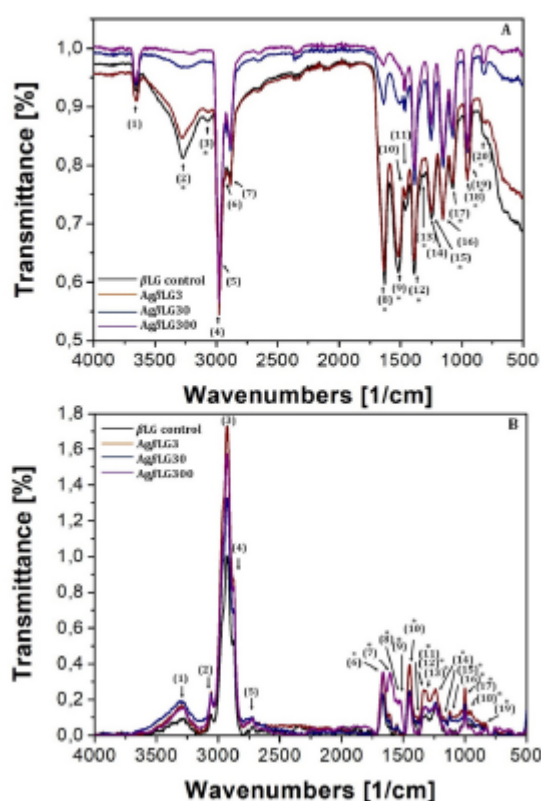


Fig. 2. FTIR-ATR (A) and Raman (B) spectra for control β LG and Ag/ β LG nanocomplexes. Peak bands in cm^{-1} for FTIR-ATR and Raman, respectively: (1) 3654, 3284; (2) 3274, 3059; (3) 3078, 2933; (4) 2980, 2874; (5) 2971, 2728; (6) 2931, 1666; (7) 2888, 1611; (8) 1627, 1582; (9) 1514, 1553; (10) 1472, 1449; (11) 1461, 1398; (12) 1386, 1340; (13) 1311, 1318; (14) 1250, 1241; (15) 1240, 1173; (16) 1154, 1123; (17) 1073, 1002; (18) 964, 958; (19) 954, 829; (20) 814.

structure. Band at 1514 cm^{-1} signal may also originate from the stretching mode of C—C and C—OH vibrations plane bending vibrations occurring in Tyr [50].

Moreover, the addition of Ag^+ ions also resulted in a new signal recorded at 814 cm^{-1} for the nanocomplexes Ag/ β LG3, Ag/ β LG30, Ag/ β LG300, which originates from π - π interaction of rings of Tyr and Phe residues with silver ions [51]. The appearance of new bands indicates a change in β LG structure after the addition of silver ions.

The 1306 cm^{-1} signal recorded in case of both control β LG and Ag/ β LG nanocomplexes, with various signal intensities, may originate from the C—OH deformation of aspartic (Asp^-) and glutamic (Glu^-) acids [51] responsible for Ag^+ ion binding to β LG structure. On the other hand, the signal at 1073 cm^{-1} can be associated with C—N stretching of Trp involved in Ag^+ ions binding [51], and the signals at 964 cm^{-1} and 954 cm^{-1} were assigned to band of C—H of Met involved in the binding process. Whereas bands 1472 cm^{-1} and 1461 cm^{-1} may be associated with amino acid side chains in peptide and protein structures, excited by asymmetric and symmetric CH_3 bending vibrations [52]. Band 1472 cm^{-1} may correspond to the scissors modes found in Arg, which has a relatively long CH_2 chain [51], while for band 1461 cm^{-1} , the CH_2 deformation modes appearing in Cys were assigned [51]. The signals at 1250 cm^{-1} and 1154 cm^{-1} may be the results of C—C and C—O

stretching vibrations and in-plane bending vibrations C—OH of Tyr residues [50]. The 1250 cm^{-1} and 1306 cm^{-1} signals are derived also from N—H bending and C—N stretching of amide III [49]. The 1627 cm^{-1} signal recorded in both control β LG and Ag/ β LG3, Ag/ β LG30, Ag/ β LG300 nanocomplexes is assigned to C = O stretching vibrations with a small contribution from out-of-phase C—N stretching CN deformation and NH plane bending in the amide I region (1600 – 1650 cm^{-1}) [49]. This band can be assigned also to the asymmetric and symmetric deformation vibration of the NH_3^+ group derived from Lys [50].

Additionally, the FTIR technique monitors changes in the secondary structure of proteins such as β -sheet (1620 – 1630 cm^{-1}) [47]. The recorded spectrum also shows a 3654 cm^{-1} signal from NH stretching vibrations in the amide band A [48]. In contrast, the signals 2900 , 2971 , 2931 , 2888 cm^{-1} are dominated by the absorption of hydrophobic hydrocarbon residues [53].

Raman spectroscopy (Fig. 2B) was also used to explain the binding mechanism of Ag^+ ions to β LG, which indicated the site of active functional groups of β LG structure in the binding process by Ag^+ ions. The registered Raman spectra confirm the phenomenon recorded in the FTIR spectra regarding the appearance of new bands. However, for Raman analysis in the registered spectral range of 700 – 4000 cm^{-1} , indicate the increasing of the all spectral signals after addition of Ag^+ ions compared to the control β LG, where the silver ions were not present.

Received Raman spectra suggested the presence of 1666 cm^{-1} and 1611 cm^{-1} bands derived from C=O peptide in-plane stretching vibrations and on-plane N—H bending vibrations corresponding to amide I in the region of 1600 – 1690 cm^{-1} [54–56]. The band 1611 cm^{-1} may also attributed to out-of-plane deformation of Tyr [55]. Bands registered at 1502 cm^{-1} and 1553 cm^{-1} originate from an out-of-phase combination of C—N stretching and N—H bending motions from amide II, whereas signals 1340 , 1318 and 1241 cm^{-1} are due to C—N stretching and N—H bending corresponding to amide III (1200 – 1340 cm^{-1}) [54,56]. The respective observations in the respective regions are the result of conformational changes in the protein. The increase of intensity in the wavelength range 1500 – 1300 cm^{-1} for Ag/ β LG300 nanocomplex is related to the binding of nanoparticles with amino acids contained in proteins which changes their structure [57]. Moreover, signals at 1340 cm^{-1} and 1318 cm^{-1} derived from indole ring vibrations of Trp. Bands at 1553 , 1398 and 958 cm^{-1} may also originate from Trp [56,58,59]. The registered Trp signals indicates an essential role in the binding of β LG to Ag^+ ions. For band 1553 cm^{-1} , an imidazole ring derived from the histidine residue (His) can be assigned [55]. Only the spectra for the Ag/ β LG300 nanocomplex showed a band at 1553 cm^{-1} . The two bands 1318 cm^{-1} and 1173 cm^{-1} are assigned to Arg [60]. The mentioned signal at 1340 cm^{-1} can be attributed to the presence of CH_2 wagging and C—H in-plane deformation of Met or through CH_2 in-plane bending of Lys [60].

Raman signals at 3284 , 3059 and 2728 cm^{-1} were assigned to CH (CH_2 , CH_3), —C—H or = C—H stretching bonds [58]. For bands 2874 cm^{-1} and 2933 cm^{-1} , C—H stretching vibration bands of aliphatic side chains were observed [61]. The signal recorded at 1449 cm^{-1} and 1002 cm^{-1} represent ionized COO^- derived Glu^- and the band at 1123 cm^{-1} correspond to ionized COO^- derived Asp^- [60]. The presence of these bands suggests that these β LG functional groups (Glu^- , Asp^-) play an important role in the binding of Ag^+ ions to β LG and also in formation of silver nanoparticles. The intense band at 1002 cm^{-1} is typical for phenyl ring of Phe [58,59] and the signals noticed at 1241 , 1173 , 1123 and 829 cm^{-1} are associated with the presence of C—OH plane bending vibrations Tyr involved in the binding process [58,59]. FTIR spectroscopy is based on absorption phenomenon of functional group and Raman spectroscopy is complementary technique based on a light scattering effect. Both FTIR and Raman spectroscopy have provided information about the vibrations of molecules that promote the binding of silver to β LG.

3.3. Scanning and transmission electron microscopy (SEM, TEM) with energy dispersive X-ray (EDX) and X-ray diffraction (XRD) analysis

The synthesized Ag/βLG nanocomplexes were also characterized using microscopic methods. Among these methods, three different techniques were used: EDX, SEM and TEM. EDX allowed us to determine the elements in the sample and also to obtain elemental maps. SEM permitted scanning the surface of the sample giving information about the surface topography and TEM was used to determine the size of the formed nanosystem.

The EDX analysis shown in Fig. 3 was performed for both native (control) βLG and Ag/βLG nanocomplexes. For the Ag/βLG nanocomplexes, the analysis confirmed the presence of metal silver with signals around 3 keV, compared to the control. Moreover, it was observed that with increasing Ag⁺ ion concentration, stronger Ag⁺ ion signals appear corresponding to percentage masses of 0.67% (Ag/βLG3), 1.72% (Ag/βLG30) and 3.65% (Ag/βLG300). In the resulting spectra, carbon, nitrogen and oxygen play a dominant role. In addition, small amounts of sodium, phosphorus, sulfur, copper and aluminium are also observed. The presence of sodium, phosphorus and sulfur is due to the structure of βLG itself, while copper and aluminium are due to the apparatus background. Additionally, mapping images show the homogeneous dispersion of silver on the surface of all nanocomplexes (Fig. 3).

SEM study (Fig. 4) was used to analyze the morphology changes of proteins before and after the binding process.

In addition, a comparison has been made between the images of the

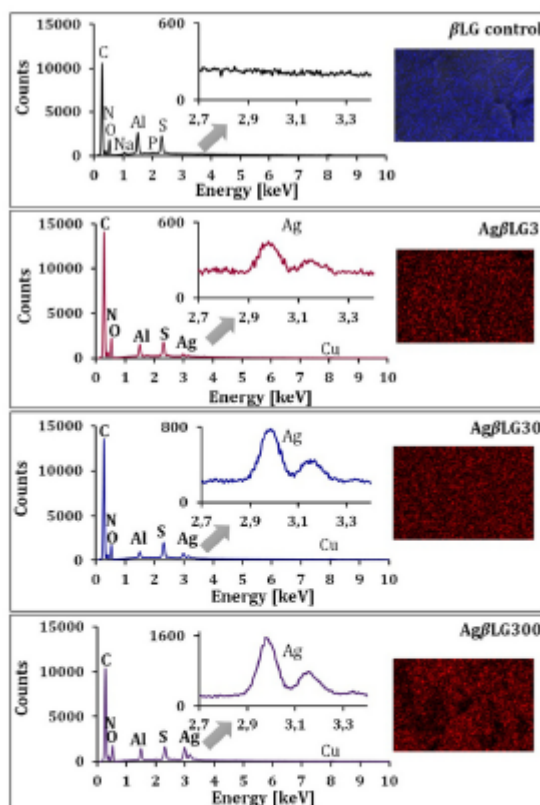


Fig. 3. EDX analysis and elemental mapping analysis for control βLG and Ag/βLG nanocomplexes.

nanocomplexes and the native βLG. These changes were found to be dependent on the Ag⁺ ion concentration. Homogeneous structures of the obtained Ag/βLG nanocomplexes were observed. However, as the Ag⁺ ion concentration increases, the surface morphology becomes more porous indicating that more Ag⁺ ions are bound under higher concentration. Modification of the protein surface with silver ions and more specifically with higher silver ion content, the specific surface area of the protein increased significantly. The presence of silver nanoparticles was noticed using TEM analysis for highest concentration of silver. Moreover, the size, shape and crystallinity of the prepared Ag/βLG nanocomplexes were determined. The obtained results confirm the SEM results that as the Ag⁺ ion concentration increases, the structure of the nanocomplexes is more dense and more porous. On the other hand, after addition of Ag⁺ ions at higher concentration the TEM results (Fig. 4) show the formation of spherical silver nanoparticles (about 5 nm) homogeneously dispersed and also aggregates (about 1300 nm) fixed into the protein structure.

The formation of silver nanoparticles as a result of metal-protein interaction during microscopic analyses, confirms the observations obtained from the isotherm as a function of C₀/C₀ by the reduction of Ag⁺ ions to Ag⁰, coalescence and nanocrystallization [43].

However, there are also places where aggregations form between silver nanoparticles. The high-resolution TEM (HRTEM) image and selected area electron diffraction (SAED) pattern for the Ag/βLG nanocomplex at a concentration of 300 (mg/L) is shown in Fig. 4. The characteristic HRTEM image with distinct lattice fringes with 0.23 nm spacing shows that the growth of silver nanoparticles occurs mainly in the plane (111). The interplanar distance of the Ag plane (111) is consistent with the (111) d-spacing of bulk Ag (0.2355 nm). SAED with bright circular rings relating to the (111), (220), (222), (331) planes of one of the spherical particles indicate that they have a highly crystalline structure. Similar results were obtained for silver nanoparticles by AgNPs synthesis using *Lactobacillus paracasei* LPC20 bacterial strains isolated from whey [62].

3.4. Molecular dynamics (MD) simulations and quantum mechanics (QM) calculations – binding affinity of amino acids towards Ag⁺ ions

In order to clarify further the interaction mechanism between silver ions and βLG, pointing out the sites responsible for binding and complementing the results obtained so far, molecular modeling (MD) and quantum chemistry calculations were additionally carried out using density functional theory (DFT). Initial structures with three concentrations of Ag⁺ ions used for MD simulations are depicted in Fig. 5A. Stability of control βLG and Ag/βLG nanocomplexes was evaluated at three different concentrations. As a metric, the root mean square error of deviation (RMSD) relative to the energy minimized structure was used. All complexes (Ag/βLG3, Ag/βLG30, Ag/βLG300) were found to be stable with average RMSDs of −1.25–1.50 Angstroms (Fig. 5B). Hence, it was concluded that the molecular dynamics simulations converged well. In turn, the flexibility patterns were analyzed using the root mean square error of fluctuations (RMSF). Four Ag⁺ ions show no significant change in the flexibility of βLG, while the flexibility of four key regions decreases with increasing silver concentration (Fig. 5C). Subsequently, the distances between ten amino acids (AAs): Glu⁻, Asp⁻, Cys, His, Tyr, Trp, Phe, Met, Arg, Lys and Ag⁺ ions were analyzed throughout the MD simulation with a threshold of 0.35 nm as shown in Table S1.

Among the twenty AAs, the aforementioned AAs are the strongest binders of Ag⁺ ions and were selected for molecular dynamics (MD) analysis [63]. Number of binding sites (n(binding sites)) refers to the total number of binding sites detected in a defined sampling range (40–140 ns) of the MD trajectories where the simulations were deemed converged (stable RMSD), consistently. Percentage of binding sites (%) in Table S1 refers to the ratio between the total number of binding sites per amino-acid over the total number of binding sites across the amino-acids (i.e., sum of all binding sites). Excellent correlation between the

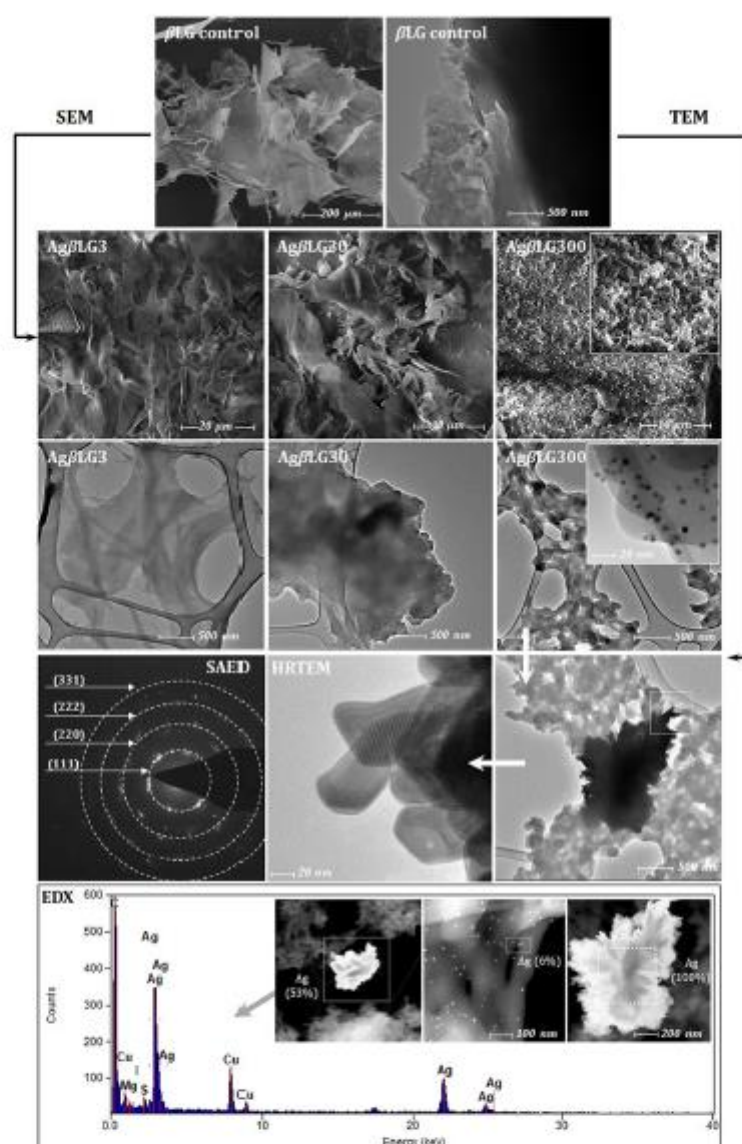


Fig. 4. SEM and TEM image for control β LG and Ag β LG nanocomplexes at concentrations of 3, 30, and 300 mg/L; energy dispersive X-ray spectrum, selected-area electron diffraction image, and high-resolution TEM image for Ag β LG300.

concentration of ions in the systems and the total number of binding sites ($R^2 > 0.9$) per amino-acid has been observed. Model structure of Ag β LO nanocomplexes as proposed based on the computational results is depicted in Fig. 6. Based on chemical properties, amino acids can be divided into four groups: (I) acidic, (II) polar/hydrophilic, (III) non-polar/hydrophobic, (IV) basic. According to the selected AAs for molecular modeling, group (I) includes Asp and Glu, group (II) consists of Cys and Tyr, group (III) is composed of Trp, Phe, Met and among group (IV) we can distinguish His, Arg and Lys. The strongest binding sites of silver ions for each group were observed for Asp and Glu, Tyr, Met, Lys, respectively. In addition, it was observed that the binding sites of silver ions with the mentioned amino acids are increased with increasing silver

ions concentration. In view of this to quantify the binding of silver ion with amino acid (AA) residues, DFT calculations were performed for five 1:1 Ag $^+$ -AA complexes, AA = Asp $^-$, Glu $^-$, Tyr, Lys and Met as shown in Fig. 6. The AAs were modelled with one amide unit and capped with methyl groups. Solvation effect in aqueous environment was modelled using the implicit GMD solvation model.

The optimized geometries and binding free energies ($\text{Ag}^+ + \text{AA} \rightarrow \text{Ag}^+-\text{AA}$, ΔG_{298}) of the lowest-energy conformations of the five complexes are given in Fig. 6. Due to the strong affinity of nitrogen towards Ag $^+$ ion, interaction of Ag $^+$ with the side chain, via Ag $^+ \cdots \text{N}$ coordination interaction, is observed in all complexes. As a result, Ag(I) forms a bidentate or tridentate Ag $^+$ -AA complex. The second attachment site is

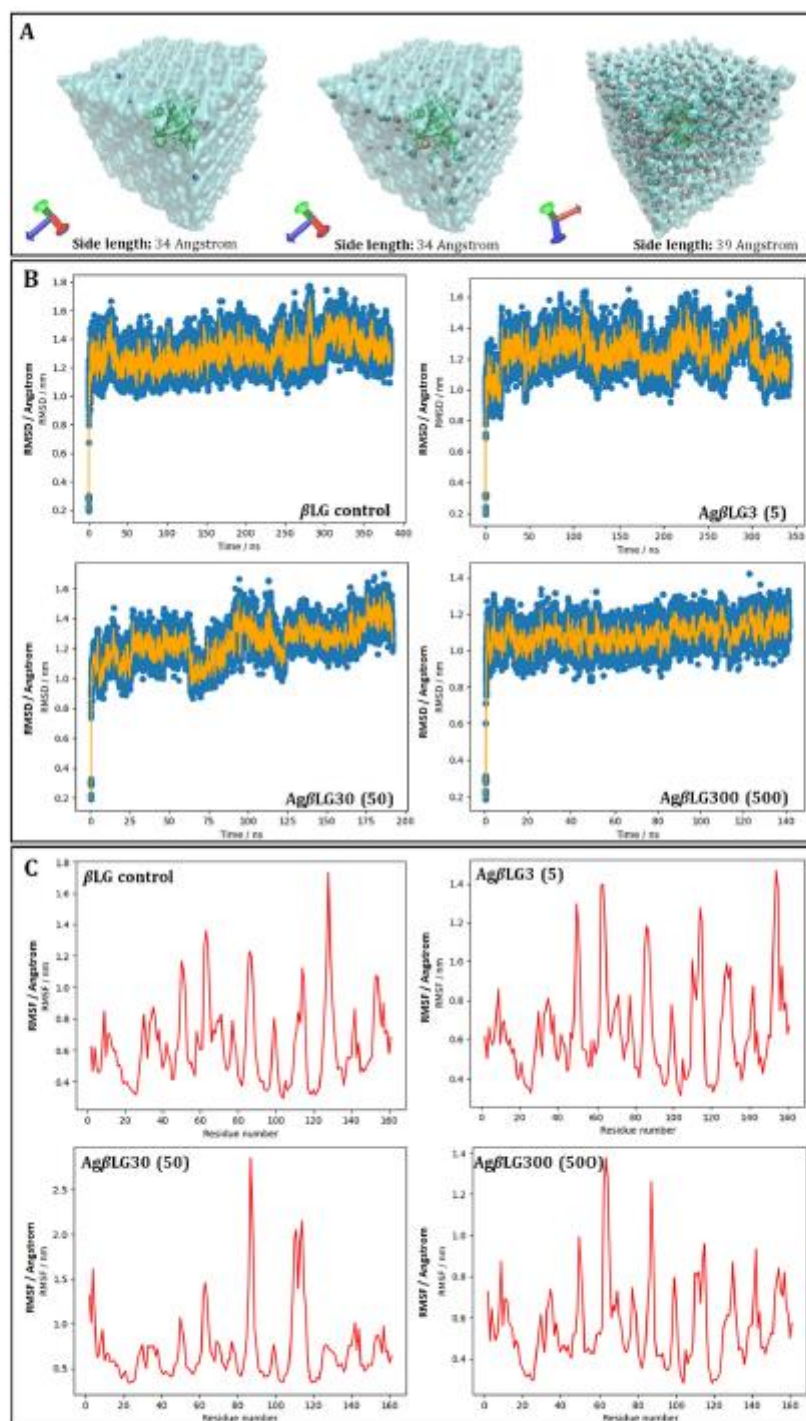


Fig. 5. Initial structures of Ag β LG nanocomplexes at three different concentrations (A) – concentrations: 5, 50 and 500 Ag⁺ ions per 1 β LG molecule, respectively; root mean square error of deviation – RMSD (B) and root mean square error of flexibility – RMSF (C) patterns for systems with: native β LG and its three complexes with 5, 50 and 500 Ag⁺ ions.

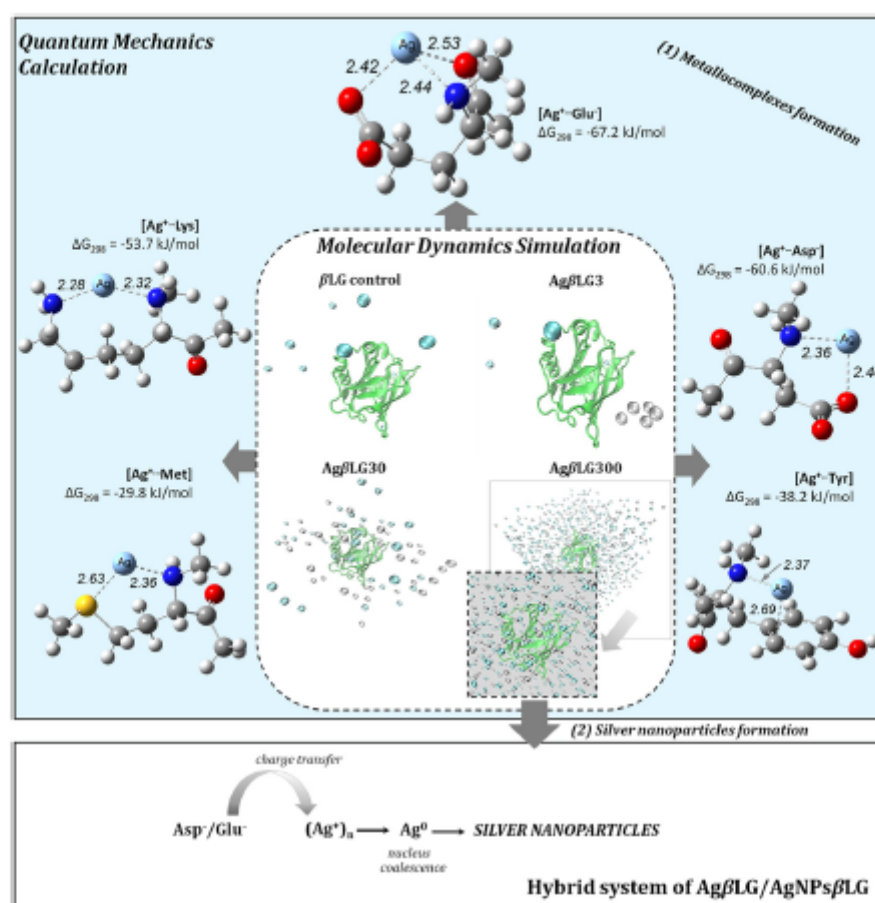


Fig. 6. Schematic illustration of the β LG (control) and Ag β LG nanocomplexes structures; Optimized geometries of modelled Ag⁺-AA complexes; Proposed mechanism of silver nanoparticles formation of Ag β LG300 nanocomposites by interaction of Ag β LG nanocomplex with Asp⁻ and Glu⁻.

different for different amino acids. For the aromatic AA (Tyr), the second site is one of carbon of the six-membered ring, via cation- π interaction [64,65]. Lys and Met coordinate Ag⁺ to the nitrogen and sulfur atoms, respectively, which function as lone pair donors. In the cases of Ag⁺-Asp⁻ and Ag⁺-Glu⁻ complexes, interaction between the carboxyl group (OOO⁻) and Ag⁺ is monodentate so that multiple interactions with Ag⁺ is optimized. Thus, a tridentate complex is formed for Ag⁺-Glu⁻ complex, with a more flexible Glu⁻ side chain.

From the spectroscopic results, it was found that Ag⁺ ions bind to the carboxyl groups of Asp⁻ and Glu⁻ due to the obtained high signal intensities. Similarly, high intensity band was observed for Lys and Tyr. The presence of Met, Arg, His, Cys, Trp was observed to a lower degree. The potential binding sites obtained from FTIR-ATR and Raman studies were complementary. On the other hand, molecular modeling studies are characterized by higher accuracy of the simulations performed. The MD analysis performed enriches the results obtained from FTIR-ATR and Raman analysis, indicating the most significant role in the interaction of Asp⁻ and Glu⁻ with silver ions. Pomastowski et al. [39] in their study of the interaction of silver ions with lactoferrin also indicated a dominant role for aspartic acid and glutamic acid. The MD studies were also complemented the FTIR-ATR measurements in which Lys was observed in the 1627 cm⁻¹ region on the spectrum, which also played a key role in binding. In addition, MD analysis indicated binding of silver cations to

aromatics, more to Tyr and less to Trp and Phe, complementing the spectroscopic results in which intensity changes occurred depending on silver ion concentration (6, 60, and 600 mg/L). Attention was also drawn to the binding of silver to sulfur present in Met, especially at higher silver concentrations, which is also observed on the FTIR-ATR spectrum.

The process of reduction initiated is due to electron transfer from the amino acid residues of β LG to the adsorbed silver cations resulting in the formation of atomic silver (Ag⁰). Subsequently, the reduced silver (Ag⁰) acts as nucleation sites on which, through an electrochemical process, silver cations (Ag⁺) are reduced to atomic silver, leading to the formation of silver nanoclusters (Ag⁰). These nanoclusters coalesce to form nanoparticles stabilized by protein molecules [39]. Based on the isotherm results and the TEM study performed, the presence of silver nanoparticles of about 5 nm was additionally observed in the case of Ag β LG300 nanocomplex, the one with the highest concentration of silver ions. Silver nanoparticles were formed as an additional element as a result of the formation of the Ag β LG complex at the highest concentration of the Ag β LG300 complex. The proposed scheme of the mechanism is shown in Fig. 6.

Moreover, based on the molecular dynamic simulation and quantum mechanics calculation approach the proposed mechanism of the silver ions binding and silver nanoparticles formation was proposed (Fig. 6).

Silver interacting with β LG at lower silver ions concentrations (6, 60 mg/L) leads to the formation of metallocomplexes. On the other hand, using higher concentration of silver ions (600 mg/L) a difference is observed, namely the formation of metallocomplexes but also the formation of silver nanoparticles forming $Ag\beta$ LG/AgNP β LG hybrid system. This is due to the strong affinity of Glu⁻ and Asp⁻ at higher silver concentration (600 mg/L) per mole of β LG (20 silver ions/ β LG molecule).

For all five complexes, the calculated binding free energy is exothermic, suggesting that the formation of the Ag⁺-AA complex is an energetically favorable process. As expected, the largest interaction energies are predicted for Ag⁺-Asp⁻ and Ag⁺-Glu⁻ complexes ($\Delta G_{298} = -60.6$ and -67.2 kJ/mol, respectively), which attributed to the strong electrostatic interaction of the negatively charged carboxyl ion (COO⁻) and Ag⁺ cation. This result readily confirms the strong affinity of Glu⁻ and Asp⁻ residues towards aqueous Ag⁺ ion in the MD simulations. The exothermic process indicates that the formation of silver nanoparticles is not determined by the addition of a reducing agent, but by the presence of the protein itself. The calculated trend of complexation free energies of the five Ag⁺-AA complexes (Glu⁻ > Asp⁻ > Lys > Tyr > Met) is also in good accord with the MD simulation finding (Table S1).

4. Conclusions

In the present work, we report for the first time the characterization of binding mechanism of Ag⁺ ions with whey protein such as β LG, resulting in the formation of nanocomplexes; means from one site immobilization of the silver ions to protein structure and from another site the formation of the silver nanoparticles. Based on the obtained results, Ag⁺ ions were found to be efficiently immobilized by native β LG protein. The kinetic studies performed on the binding of Ag⁺ ions to β LG showed a heterogeneous kinetic process occurring in three steps. The first step was rapid sorption occurring after only two minutes, the second step in turn was associated with moderate sorption, and the third step was the gradual achievement of sorption equilibrium. Applying the Weber-Morris model, the experimental data show two sorption steps ending in a sorption equilibrium step. The first step is related to adsorption on the external surface of β LG, while the second step is related to the intramolecular diffusion of Ag⁺ ions. In addition, isothermal studies identify two dominant steps in the sorption of Ag⁺ ions. During the first step, a monolayer of Ag⁺ ions is formed on the surface of β LG, followed by relaxation of the β LG structure and penetration (step II). Scanning and transmission electron microscopy indicates that Ag⁺ ion concentration changes the surface morphology of β LG while a using of higher concentration of Ag⁺ ions lead to the more porous structure and also silver nanoparticles formation. Spectroscopic studies and molecular modeling determined the major roles of silver ion interaction with Glu⁻, Asp⁻, Lys, Tyr and Met. Moreover, quantum mechanical calculations based on DFT simulations indicated the reduction of silver and the presence of nanoparticles, due to the binding of silver ions with Asp⁻ and Glu⁻; therefore, for the first time the silver ions immobilization and silver nanoparticles formation mechanism (formation of $Ag\beta$ LG/AgNP β LG hybrid system) was proposed.

The performed physicochemical studies and molecular modeling of the interaction of silver with β LG lead us to conduct further studies on the antibacterial properties of the obtained nanocomposites to meet the challenge of developing new low-cost potential antibacterial agents.

CRedit authorship contribution statement

Agnieszka Rodzika Conceptualization, Methodology, Investigation, Writing – original draft, Visualization, Data curation. Viorela Raileanu Methodology, Investigation, Writing – review & editing, Visualization. Pawel Pomastowski Conceptualization, Funding acquisition, Project administration. Petar Žuvelec Investigation, Data curation, Writing – original draft, Visualization, Software, Data curation. Ming Wah Wong

Investigation, Software, Writing – review & editing, Data curation, Resources. Myroslav Sprynskyy Writing – review & editing. Bogusław Buszewski Conceptualization, Supervision, Resources.

Declaration of Competing Interest

The authors declare that they have no known competing financial interests or personal relationships that could have appeared to influence the work reported in this paper.

Acknowledgements

This work was financially supported by the National Science Centre within the framework of Opus 14 project No. 2017/27/B/ST4/02628 (2018-2021). Bogusław Buszewski, Paweł Pomastowski and Agnieszka Rodzika are members of Toruń Center of Excellence "Towards Personalized Medicine" operating under Excellence Initiative-Research University.

Appendix A. Supplementary data

Supplementary data to this article can be found online at <https://doi.org/10.1016/j.bpc.2022.106897>.

References

- [1] A.F. Santos, D.F. Brotto, L.R.V. Favarin, N.A. Cabeza, G.R. Andrade, M. Batistote, A. A. Cavalleiro, A. Neves, D.C.M. Rodrigues, A. dos Anjos, Study of the antimicrobial activity of metal complexes and their ligands through bioassays applied to plant extracts, *Revista Brasileira de Farmacognosia*. 24 (2014) 309–315, <https://doi.org/10.1016/j.bj.2014.07.008>.
- [2] F.Y. Ahmed, U.F. Aly, R.M. Abd El-Baky, N.G.F.M. Waly, Comparative study of antibacterial effects of titanium dioxide nanoparticles alone and in combination with antibiotics on MDR *Pseudomonas aeruginosa* strains, *Int. J. Nanomedicine* 15 (2020) 3393–3404, <https://doi.org/10.2147/IJN.S246310>.
- [3] X. Li, S.M. Robinson, A. Gupta, K. Saha, Z. Jiang, D.F. Moyano, A. Sahar, M. A. Riley, V.M. Rotello, Functional gold nanoparticles as potent antimicrobial agents against multi-drug-resistant bacteria, *ACS Nano* 8 (2014) 10682–10686, <https://doi.org/10.1021/nm504262s>.
- [4] A. Rodzik, P. Pomastowski, G.N. Sagandykova, B. Buszewski, Interactions of whey proteins with metal ions, *Int. J. Mol. Sci.* 21 (2020) 1–26, <https://doi.org/10.3390/ijms21062156>.
- [5] S.U. Khan, T.A. Saleh, A. Wahab, M.H.U. Khan, D. Khan, W.U. Khan, A. Rahim, S. Kamal, F.U. Khan, S. Falhad, Nanosilver: new ageless and versatile biomedical therapeutic scaffold, *Int. J. Nanomedicine* 13 (2018) 733–762, <https://doi.org/10.2147/IJN.S153167>.
- [6] M. Claudel, J.V. Schwarte, K.M. Fromm, New antimicrobial strategies based on metal complexes, *Chemistry*. 2 (2020) 849–899, <https://doi.org/10.3390/chemistry2040056>.
- [7] J. Alexander, Wesley, history of the medical use of silver, *Surg. Infect.* 10 (2009) 289–294.
- [8] Z. Hazarika, A.N. Jha, Computational analysis of the silver nanoparticle-human serum albumin complex, *ACS Omega* 5 (2020) 170–178, <https://doi.org/10.1021/acsomega.9b02340>.
- [9] M. Abul Haj, C.B. Aakeröy, J. Desper, Silver (I) coordination chemistry: from 1-D chains to molecular rectangles, *New J. Chem.* 37 (2013) 204–211, <https://doi.org/10.1039/c3n00000a>.
- [10] V. Demchenko, S. Riabov, S. Kobylynskiy, L. Goncharenko, N. Rybalchenko, A. Kruk, O. Moskaleiko, M. Shut, Effect of the type of reducing agents of silver ions in interpolyelectrolyte-metal complexes on the structure, morphology and properties of silver-containing nanocomposites, *Sci. Rep.* 10 (2020) 1–9, <https://doi.org/10.1038/s41598-020-64079-0>.
- [11] Z. Xu, C. Zhang, X. Wang, D. Liu, Release strategies of silver ions from materials for bacterial killing, *ACS Appl. Bio Mater.* 4 (2021) 3985–3999, <https://doi.org/10.1021/acsalbm.0c01485>.
- [12] B. Buszewski, P. Žuvelec, A. Król-Górcniak, V. Raileanu-Flugaru, A. Rogowska, M. W. Wong, M. Yi, A. Rodzik, M. Sprynskyy, P. Pomastowski, Interactions of zinc aqua complexes with ovalbumin at the forefront of the Zn²⁺/ZnO-OVO hybrid complex formation mechanism, *Appl. Surf. Sci.* 542 (2021), 148641, <https://doi.org/10.1016/j.apsusc.2020.148641>.
- [13] E. Ha, M.B. Zemel, Functional properties of whey, whey components, and essential amino acids: mechanisms underlying health benefits for active people (Review), *J. Nutr. Biochem.* 14 (2003) 251–258, [https://doi.org/10.1016/S0955-2863\(03\)00030-5](https://doi.org/10.1016/S0955-2863(03)00030-5).
- [14] F. Alimoradi, E. Hojaji, H. Jooyandeh, S.A. Hossain, Z. Moghadam, J. Mohadi, Whey proteins: health benefits and food applications, *J. Int. Res. Med. Pharm. Sci.* 9 (2016) 63–73.

- [15] F. Guyonvarc'h, M.H. Famelart, G. Henry, M. Gulzar, J. Leonil, P. Hamon, S. Bouhallab, T. Croguennec, Current ways to modify the structure of whey proteins for specific functionalities—a review, *Dairy Sci. Technol.* 95 (2015) 795–814, <https://doi.org/10.1007/s13594-014-0190-5>.
- [16] F.J. Teixeira, H.O. Santos, S.L. Howell, G.D. Pimentel, Whey protein in cancer therapy: a narrative review, *Pharmacol. Res.* 144 (2019) 245–256, <https://doi.org/10.1016/j.phrs.2019.04.019>.
- [17] F. Mazzuca, M. Roberto, G. Arrivi, E. Sarfati, F.M. Schipilliti, E. Crimini, A. Bortocelli, M. Di Girolamo, M. Muscaritoli, P. Marchetti, Clinical impact of highly purified, whey proteins in patients affected with colorectal Cancer undergoing chemotherapy: preliminary results of a placebo-controlled study, *Integr. Cancer Ther.* 18 (2019) 1–11, <https://doi.org/10.1177/1534735419866920>.
- [18] D. Brumini, A. Criscone, S. Bordonaro, G.E. Vegarud, D. Marletta, Whey proteins and their antimicrobial properties in donkey milk: a brief review, *Dairy Sci. Technol.* 96 (2016) 1–14, <https://doi.org/10.1007/s13594-015-0246-1>.
- [19] S. Le Mau, S. Bouhallab, L. Giblin, A. Brodtkorb, T. Croguennec, Bovine β -lactoglobulin/fatty acid complexes binding, structural, and biological properties, *Dairy Sci. Technol.* 94 (2014) 409–426, <https://doi.org/10.1007/s13594-014-0160-y>.
- [20] K. Sakai, K. Sakurai, M. Sakai, M. Hoshino, Y. Goto, Conformation and stability of thiol-modified bovine β -lactoglobulin, *Protein Sci.* 9 (2000) 1719–1729.
- [21] M.D. Pérez, M. Calvo, Interaction of β -lactoglobulin with retinol and fatty acids and its role as a possible biological function for this protein: a review, *J. Dairy Sci.* 78 (1995) 978–988, [https://doi.org/10.3168/jds.S0022-0302\(95\)76713-3](https://doi.org/10.3168/jds.S0022-0302(95)76713-3).
- [22] A. Mensi, Y. Choiset, H. Rabesona, T. Haertlé, P. Borel, J.M. Chobert, Interactions of β -lactoglobulin variants A and B with vitamin A: a competitive binding of retinoids and carotenoids, *J. Agric. Food Chem.* 61 (2013) 4114–4119, <https://doi.org/10.1021/jf400711d>.
- [23] A.M. Smith, Interaction of metal ions with proteins as a source of inspiration for biomimetic materials, in: *Functional Metallo-supramolecular Materials*, 2015, pp. 1–31.
- [24] R.F.S. Lee, I. Menin, I. Patiny, D. Ortiz, P.J. Dyson, Versatile tool for the analysis of metal-protein interactions reveals the promiscuity of Metallo-drug-protein interactions, *Anal. Chem.* 89 (2017) 11985–11989, <https://doi.org/10.1021/acs.analchem.7b02211>.
- [25] S.R. Saptarshi, A. Dusch, A.L. Lopata, Interaction of nanoparticles with proteins relation to bio-reactivity of the nanoparticle, *J. Nanobiotechnol.* 11 (2013) 1–12, <https://doi.org/10.1186/1477-3155-11-26>.
- [26] B. Buszewski, A. Rodař, V. Railean-Plugaru, M. Sprynskyy, P. Pomastowski, A study of zinc ions immobilization by β -lactoglobulin, *Colloids Surf. A Physicochem. Eng. Asp.* 591 (2020), 124443, <https://doi.org/10.1016/j.colsurfa.2020.124443>.
- [27] B.E. Reed, M.R. Matsumoto, Modeling cadmium adsorption by activated carbon using the Langmuir and Freundlich isotherm expressions, *Sep. Sci. Technol.* 28 (1993) 2179–2195, <https://doi.org/10.1080/01496399308016742>.
- [28] B.Y. Qin, M.C. Bewley, L.K. Creamer, H.M. Baker, E.N. Baker, G.B. Jameson, Structural basis of the Tanford transition of bovine β -lactoglobulin, *Biochemistry*, 37 (1998) 14014–14023, <https://doi.org/10.1021/bi981016t>.
- [29] P. Mark, L. Nilsson, Structure and dynamics of the TIP3P, SPC, and SPC/E water models at 298 K, *J. Phys. Chem. A* 105 (2001) 9954–9960, <https://doi.org/10.1021/jp003020w>.
- [30] K. Lindorff-Larsen, S. Piana, K. Palmo, P. Maragakis, J.L. Klepeis, R.O. Dror, D. E. Shaw, Improved side-chain torsion potentials for the Amber ff99SB protein force field, *Protein: structure, Funct. Bioinforma.* 78 (2010) 1950–1958, <https://doi.org/10.1002/proc.22711>.
- [31] P. Li, L.F. Song, K.M. Merz, Systematic parameterization of monovalent ions employing the nonbonded model, *J. Chem. Theory Comput.* 11 (2015) 1645–1657, <https://doi.org/10.1021/ct500918t>.
- [32] P.S. Nayak, S.M. Borah, H. Gogoi, S. Asthana, R. Bhatnagar, A.N. Jha, S. Jha, Lactoferrin adsorption onto silver nanoparticle interface: implications of corona on protein conformation, nanoparticle cytotoxicity and the formulation adjuvanticity, *Chem. Eng. J.* 361 (2019) 470–484, <https://doi.org/10.1016/j.cej.2018.12.084>.
- [33] W. Humphrey, A. Dalke, K. Schulten, VMD: visual molecular dynamics, *J. Mol. Graph.* 14 (1996) 33–38, <https://doi.org/10.1016/j.cmb.2017.07.012>.
- [34] Y. Zhao, D.G. Truhlar, The M06 suite of density functionals for main group thermochemistry, thermochemical kinetics, noncovalent interactions, excited states, and transition elements: two new functionals and systematic testing of four M06-class functionals and 12 other functionals, *Theor. Chem. Accounts* 120 (2008) 215–241, <https://doi.org/10.1007/s00214-007-0310-x>.
- [35] F. Weigend, A. Baltes, Segmented contracted basis sets for one- and two-component Dirac-Fock effective core potentials, *J. Chem. Phys.* 133 (2010), <https://doi.org/10.1063/1.3495681>.
- [36] D. Rappoport, F. Furche, Property-optimized Gaussian basis sets for molecular response calculations, *J. Chem. Phys.* 133 (2010), <https://doi.org/10.1063/1.3484283>.
- [37] A.V. Marenich, C.J. Cramer, D.G. Truhlar, Universal solvation model based on solute electron density and on a continuum model of the solvent defined by the bulk dielectric constant and atomic surface tensions, *J. Phys. Chem. B* 113 (2009) 6378–6396, <https://doi.org/10.1021/jp810292a>.
- [38] B. Buszewski, V. Railean-Plugaru, P. Pomastowski, A. Sidorenko, Silver nanoparticles: synthesis, characteristics, and application, in: *Research Anthology on Synthesis, Characterization, and Applications of Nanomaterials*, 2021, pp. 440–457, <https://doi.org/10.4018/978-1-7998-8591-7.ch021>.
- [39] P. Pomastowski, M. Sprynskyy, P. Žuvela, K. Rafińska, M. Milanowski, J.J. Liu, M. Yi, B. Buszewski, Silver-Lactoferrin Nanocomplexes as a potent antimicrobial agent, *J. Am. Chem. Soc.* 138 (2016) 7899–7909, <https://doi.org/10.1021/jacs.6b02699>.
- [40] T. Huppertz, P.F. Fox, A.L. Kelly, *Proteins in Food Processing: Second Edition*, Elsevier Ltd., 2018, <https://doi.org/10.1016/B978-0-08-100722-8.00004-8>.
- [41] J.E. Kinsella, D.M. Whitehead, Proteins in whey: chemical, physical, and functional properties, advances in food and nutrition, *Research*, 33 (1989) 343–438, [https://doi.org/10.1016/S1043-4526\(08\)60130-8](https://doi.org/10.1016/S1043-4526(08)60130-8).
- [42] A. Sharma, K.S. Ghosh, Studies on molecular interactions between bovine β -lactoglobulin and silver nanoparticles, *Protein Pept. Lett.* 27 (2020) 793–800, <https://pubmed.ncbi.nlm.nih.gov/32003652/>.
- [43] J. Polte, Fundamental growth principles of colloidal metal nanoparticles - a new perspective, *CrystEngComm*, 17 (2015) 6809–6830, <https://doi.org/10.1039/c5ce01014d>.
- [44] P.G. Vekilov, Nucleation, *Cryst. Growth Des.* 10 (2010) 5007–5019, <https://doi.org/10.1021/eg1011633>.
- [45] M. Takase, T. Tomura, M. Yamada, K. Hata, S. Kuwamoto, T. Yonezawa, Size of elementary clusters and process period in silver nanoparticle formation, *J. Am. Chem. Soc.* 133 (2011) 14164–14167, <https://doi.org/10.1021/ja202815y>.
- [46] R. Anderson, R. Buscall, R. Eldridge, P. Mulvaney, P. Scales, Concentrated synthesis of metal nanoparticles in water, *RSC Adv.* 4 (2014) 31914–31925, <https://doi.org/10.1039/c4ra04223a>.
- [47] G.M. Kavanagh, A.H. Clark, S.B. Ross-Murphy, Heat-induced gelation of globular proteins: part 3. Molecular studies on low pH β -lactoglobulin gels, *Int. J. Biol. Macromol.* 28 (2000) 41–50, [https://doi.org/10.1016/S0141-8130\(00\)00144-6](https://doi.org/10.1016/S0141-8130(00)00144-6).
- [48] A. Barth, Infrared spectroscopy of proteins, *Biochim. Biophys. Acta* 1767 (2007) 1073–1101, <https://doi.org/10.1016/j.bbabin.2007.06.004>.
- [49] T. Kruzić, N.S. Obradović, M.B. Rakin, Application of whey protein and whey protein hydrolysate as protein based carrier for probiotic starter culture, *Food Chem.* 293 (2019) 74–82, <https://doi.org/10.1016/j.foodchem.2019.04.062>.
- [50] A. Barth, The infrared absorption of amino acid side chains, *Prog. Biophys. Mol. Biol.* 74 (2000) 141–173, [https://doi.org/10.1016/S0079-6107\(00\)00021-3](https://doi.org/10.1016/S0079-6107(00)00021-3).
- [51] M. Wolpert, P. Hellwig, Infrared spectra and molar absorption coefficients of the 20 alpha amino acids in aqueous solutions in the spectral range from 1800 to 500 cm⁻¹, *Spectrochim. Acta A: Mol. Biomol. Spectrosc.* 64 (2006) 987–1001, <https://doi.org/10.1016/j.saa.2005.08.025>.
- [52] M. Crestelli Guidi, C. Mirri, E. Fratini, V. Licursi, R. Negri, A. Marcelli, R. Amendola, In vivo skin leptin modulation after 14 MeV neutron irradiation: a molecular and FT-IR spectroscopic study, *Anal. Bioanal. Chem.* 404 (2012) 1317–1326, <https://doi.org/10.1007/s00216-012-5018-3>.
- [53] D. Ami, F. Lavatelli, P. Rognoni, G. Palladini, S. Raimondi, S. Giorgetti, I. Monti, S. M. Doglia, A. Natalello, G. Merlino, In situ characterization of protein aggregates in human tissues affected by light chain amyloidosis: a FTIR microspectroscopy study, *Sci. Rep.* 6 (2016) 1–12, <https://doi.org/10.1038/srep29096>.
- [54] D. Kuroukci, R.P. Van Duyne, L.K. Lednev, Exploring the structure and formation mechanism of amyloid fibrils by Raman spectroscopy: a review, *Analyst*, 140 (2015) 4967–4980, <https://doi.org/10.1039/c5an00342c>.
- [55] E. Li-Chan, S. Nakai, M. Hirotsuka, Raman spectroscopy as a probe of protein structure in food systems, in: *Protein Structure-Function Relationships in Foods*, 1994, pp. 163–197, https://doi.org/10.1007/978-1-4615-2670-4_8.
- [56] A. Ryguła, K. Majzner, K.M. Marzec, A. Kacior, M. Pilarczyk, M. Baranska, Raman spectroscopy of proteins: a review, *Journal Raman, Spectroscopy*, 44 (2013) 1061–1076, <https://doi.org/10.1002/jrs.4335>.
- [57] F. Faghilzadeh, N.M. Anaya, L.A. Schifano, V. Oyanedel-Craver, Fourier transform infrared spectroscopy to assess molecular-level changes in microorganisms exposed to nanoparticles, *Nanotechnol. Environ. Eng.* 1 (2016) 1–16, <https://doi.org/10.1007/s41204-016-0001-8>.
- [58] E.C.Y. Li-Chan, Vibrational spectroscopy applied to the study of milk proteins, *Dairy Sci. Technol.* 87 (2007) 443–458, <https://doi.org/10.1051/dst/2007023>.
- [59] Z.-Q. Wen, Raman spectroscopy of protein pharmaceuticals, *J. Pharm. Sci.* 96 (2007) 2861–2878, <https://doi.org/10.1002/jps>.
- [60] G. Zhu, X. Zhu, Q. Fan, X. Wan, Raman spectra of amino acids and their aqueous solutions, *Spectrochim. Acta A Mol. Biomol. Spectrosc.* 78 (2011) 1187–1195, <https://doi.org/10.1016/j.saa.2010.12.079>.
- [61] R.P. Kengue-Momo, P. Daniel, F. Lagarde, Y.L. Jeyachandran, J.F. Pilard, M. J. Durand-Thouand, G. Thouand, Protein interactions investigated by the Raman spectroscopy for biosensor applications, *Int. J. Spectrosc.* (2012) 1–7, <https://doi.org/10.1155/2012/462901>.
- [62] V. Railean-Plugaru, P. Pomastowski, B. Buszewski, Use of lactobacillus paracasei isolated from whey for silver nanocomposite synthesis: antimicrobial and antimicrobial properties against selected pathogens, *J. Dairy Sci.* 104 (2021) 2480–2498, <https://doi.org/10.3168/jds.2020-19049>.
- [63] A.A. Buglak, R.R. Ramazanov, A.I. Kononov, Silver cluster–amino acid interactions: a quantum-chemical study, *Amino Acids* (2019), <https://doi.org/10.1007/s00726-019-02728-z>.
- [64] D. Corinti, A. Marcelli, B. Chiavarino, M. Schütz, A. Boschet, O. Dopfer, M. E. Crestoni, S. Fornarini, Cation- π interactions between a Noble Metal and a polyfunctional aromatic ligand: Ag⁺ (benzylamine), *Chem. Eur. J.* 28 (2022) 1–11, <https://doi.org/10.1002/chem.202200300>.
- [65] J.C. Ma, D.A. Dougherty, The cation- π interaction, *Chem. Rev.* 97 (1997) 1303–1324, <https://doi.org/10.1021/cr9603744>.

Study on silver ions binding to β -lactoglobulin

Agnieszka Rodzik^{a,b}, Viorica Railean^{a,c}, Paweł Pomastowski^{a*}, Petar Žuvela^d, Ming Wah Wong^d,
Myroslav Sprynskyy^b, Bogusław Buszewski^{a,b}

^a Centre for Modern Interdisciplinary Technologies, Nicolaus Copernicus University in Toruń,
Wileńska 4, 87-100, Toruń, Poland

^b Department of Environmental Chemistry and Bioanalysis, Faculty of Chemistry, Nicolaus
Copernicus University in Toruń, Gagarina 7, 87-100 Toruń, Poland

^c Department of Public Health Protection and Animal Welfare, Faculty of Biological and Veterinary
Sciences, Nicolaus Copernicus University in Toruń, Gagarina 7, 87-100 Toruń, Poland

^d Department of Chemistry, National University of Singapore, 3 Science Drive 3, 117543, Singapore

*Corresponding author: Paweł Pomastowski (p.pomastowski@umk.pl)

Table S1. Interaction's analysis of Ag⁺ ions with β LG.

AA	Ag β LG3 n(bind.sites)	Ag β LG3 %(bind.sites)	Ag β LG30 n(bind.sites)	Ag β LG30 %(bind.sites)	Ag β LG300 n(bind.sites)	Ag β LG300 %(bind.sites)
Glu ⁻	42532	67.016	119147	57.910	148081	48.812
Asp ⁻	16860	26.566	69971	34.009	94501	31.150
Cys	0	0.000	7	0.003	65	0.021
His	0	0.000	0	0.000	0	0.000
Tyr	295	0.465	2915	1.417	6336	2.089
Trp	3	0.005	38	0.018	855	0.282
Phe	0	0.000	91	0.044	74	0.024
Met	0	0.000	561	0.273	777	0.256
Arg	19	0.030	947	0.460	4994	1.646
Lys	3756	5.918	12067	5.865	47687	15.719
	63465		205744		303370	

4.7. The influence of zinc ions concentration on β -lactoglobulin structure – physicochemical properties of Zn- β -lactoglobulin complexes

[P7] **A. Rodzik**, V. Railean, P. Pomastowski, P. Žuvela, M. W. Wong, B. Buszewski, *The influence of zinc ions concentration on β -lactoglobulin structure – physicochemical properties of Zn- β -lactoglobulin complexes*, Journal of Molecular Structure, 2022, 1268, 1-10, doi: 10.1016/j.molstruc.2022.133745.



The influence of zinc ions concentration on β -lactoglobulin structure – physicochemical properties of Zn- β -lactoglobulin complexes



Agnieszka Rodzik^{a,b}, Viorica Railean^{b,c}, Paweł Pomastowski^{b,*}, Petar Žuvela^d,
Ming Wah Wong^d, Bogusław Buszewski^{a,b,*}

^a Department of Environmental Chemistry and Bioanalysis, Faculty of Chemistry, Nicolaus Copernicus University in Toruń, Gagarina 7, 87-100 Toruń, Poland

^b Centre for Modern Interdisciplinary Technologies, Nicolaus Copernicus University in Toruń, Wileńska 4, 87-100 Toruń, Poland

^c Department of Public Health Protection and Animal Welfare, Faculty of Biological and Veterinary Sciences, Nicolaus Copernicus University in Toruń, Gagarina 7, 87-100 Toruń, Poland

^d Department of Chemistry, National University of Singapore, 3 Science Drive 3, 117543, Singapore

ARTICLE INFO

Article history:

Received 5 April 2022

Revised 15 July 2022

Accepted 17 July 2022

Available online xxx

Keywords:

Zinc ions

β -lactoglobulin

FTIR-ATR

Raman

Molecular dynamics

Density functional theory

ABSTRACT

The study of metal-ions binding to whey proteins is the first step for their application in nutraceuticals. This study is focused on the investigation of the zinc ions concentration (6, 60 and 600 mg/L) effect on the metallocomplexes formation (Zn β LG3, Zn β LG30, Zn β LG300) with the β -lactoglobulin and their characterization by a series of instrumental and computational techniques. Detailed surface morphology of the metallocomplexes was investigated by transmission and scanning electron microscopy combined with energy dispersive X-ray analysis, and X-ray diffraction. Moreover, metallocomplex formation was monitored by attenuated total reflectance infrared spectroscopy and Raman spectroscopy. Experimental results were complemented by molecular dynamics (MD) studies indicating the precise binding sites of β LG to Zn²⁺(aq) ions and quantum mechanics (QM) simulation combined with density functional theory (DFT). Electron microscopy studies indicated that with increasing concentrations of Zn²⁺(aq) ions, the surface morphology of β LG changes, and the formed metallocomplexes exhibit higher porosity. Meanwhile, spectroscopic studies indicated the formation of metallocomplexes through the binding of Zn²⁺(aq) ions to amino acids (AAs) such as glutamic acid (Glu), aspartic acid (Asp), tryptophan (Trp), tyrosine (Tyr), and phenylalanine (Phe). Strong positive correlations between the increasing concentration of Zn²⁺(aq) ions and the number of binding sites were determined based on the MD results. DFT calculations confirm the strong binding affinity of Asp⁻ and Glu⁻ to Zn²⁺(aq) ions.

© 2022 Elsevier B.V. All rights reserved.

1. Introduction

Metal ions play a crucial role in most biochemical processes fundamental to life [1]. Many proteins bind one or more metal ions to properly perform their function by stabilizing their tertiary and quaternary structures. Metal ions also participate in the catalytic mechanism of enzymes (e.g., Fe³⁺ in lactoferrin, Zn²⁺ in carbonic anhydrases; hemoglobin containing Fe³⁺ ions that cause oxygen transport from the lungs to body tissues [2,3]. Such proteins are termed metalloproteins. An important metal is zinc, which is one of the most abundant transition metals in living organisms, right after iron [4]. Zinc ions play an important role in stabilizing proteins as well as in facilitating the folding of their subunits

[3]. It is an essential trace element for the growth, development and integrity of the immune system, which means that it influences major immune factors such as enzymes, thymic peptides and cytokines and thus regulates the activation of lymphoid cell proliferation and apoptosis [5]. It participates in bone mineralization and in the effective wound healing process [6]. The effects of zinc deficiency include skin lesions, stunted growth, decreased immunity, and impaired wound healing [6]. Zinc coordination chemistry in proteins and peptides involves N, O and S donors of histidine (His), glutamic acid (Glu), aspartic acid (Asp) and/or cysteine (Cys) side chains with any permutation of these ligands and with several protein ligands from three to six. The limited number of ligand donors and their geometry induces proteins to control and adjust their affinity for Zn²⁺ depending on physiological functions dependent on, among other things, the structural properties of the Zn²⁺-binding sites (the second coordination sphere involving hydrogen bonding to ligands) [7]. Unique complexes from a chemical and biological point of view are the zinc finger domains. These

* Corresponding author.

E-mail addresses: p.pomastowski@umk.pl (P. Pomastowski), bbusz@umk.pl (B. Buszewski).

are Zn(II) complexes with Cys- and His-containing peptides whose structure is highly ordered during metal complexation [8]. Often, water molecules are also involved in the binding of metals, providing them with stability in a particular conformation [9]. Unlike other transition metals in biology, zinc does not undergo redox reactions due to its d-filled shell. Although zinc has no redox activity and is considered nontoxic, studies report that free zinc cations contribute to neuronal and glia degradation [10]. However, zinc cations exhibit Lewis acid properties and ease of forming stable complexes with proteins thus eliminating their toxic properties. Performed studies binding of zinc ions to bioactive ligands e.g. casein [11], ovalbumin [12], eliminate toxic properties of free zinc ions and contribute to its assimilation. Therefore, it is important to further elucidate the occurring processes and mechanisms of zinc binding to proteins. Obtaining stable metallocomplexes is essential for their potential application in industry.

High-value proteins are whey proteins obtained as a by-product of cheese production. The main whey protein in cow's milk is β -lactoglobulin (β LG). It comprises 162 amino acid residues containing two disulfide bonds (Cys66-Cys160 and Cys106-Cys119) and one free thiol (Cys121). Secondary structure of the β LG macromolecule consists of nine antiparallel β strands and one α helix [13]. It is a source of essential branched-chain amino acids such as leucine (Leu), isoleucine (Ile) and valine (Val). β LG can bind and transport hydrophobic ligands and is able to bind vitamins A and D as well as metals such as Zn^{2+} [14]. As a result the synthesis of a metal-protein system can produce an artificial arrangement through weak electrostatic interactions, hydrogen bonds, Van der Waals forces or acceptor-donor bonds, termed a metallocomplex [15]. Buszewski et al. have been demonstrated two types of bond of metal-protein interactions for the obtained Zn^{2+}/ZnO -OVA hybrid complex: (i) one-to-one Zn^{2+} -Asp binding; (ii) one-to-more Zn^{2+} -Asp/Glu binding where the amino-acids (AAs) originate from one more OVA monomers (i.e., forming interface bonds) [12]. Tang et al. have proven the endothermic nature of zinc ions uptake by β -lactoglobulin and α -lactalbumin structure via interactions with His, Asp and Glu AAs [16]. Studies of antibacterial activity of several metallocomplexes such as silver-lactoferrin (Ag-LTF) – protein found naturally in milk [17] and zinc ions/zinc oxide-ovalbumin (Zn^{2+}/ZnO -OVA) – protein isolated from egg white [12] indicate their application in medicine and food industry as innovative antibacterial agents. Metallocomplexes containing whey proteins can also be used to encapsulate active ingredients of foods and drugs, thus increasing their solubility, transport, dispersibility or bioavailability [18]. Fourier transform infrared spectroscopy (FTIR) and Raman spectroscopy studies of the interaction of Zn^{2+} with individual casein isoforms (α_1 CN, β CN and κ CN) reported previously by our group [19] indicated the major role of binding due to the phosphate and carboxylic groups of Asp and Glu, and the aromatic amino acids such as tyrosine (Tyr), tryptophan (Trp) and phenylalanine (Phe). In order to determine the specific binding sites of metals (e.g. Zn^{2+}) to protein and, evaluate thermodynamic and kinetic parameters of the processes involved, and reliably assign functional groups to experimental FTIR/Raman spectra, molecular dynamics (MD) simulations/analysis and quantum mechanical (QM) calculations can be carried out [12]. Understanding the connections between metals and biomolecules as protein, offers infinite opportunities to influence the properties, speciation, reactivity, and ultimately the biological effect of metals in specific medical contexts [20].

Not only metal ions themselves, but also their appropriate concentration of metals, are essential for maintaining the biological activity of proteins. Removal or ion exchange is often associated with a loss or reduction in the biological activity of metalloproteins. Knowing the type and number of amino acid residues that coordinate the metal ion is crucial for clarifying how specific they

are for the presence of a particular metal and for understanding their possible relationship to protein function [21,22].

Therefore, this work focuses on the immobilization of $Zn^{2+}(aq)$ ions by β LG at different $Zn^{2+}(aq)$ ion concentrations with the aim of detailed understanding of the mechanism and nature of the formation of Zn β LG metallocomplexes. For this purpose, microscopic and spectroscopic were carried out complemented by MD and QM calculations, indicating the precise Zn β LG binding sites (with an emphasis on the impact of concentration) taking into account the oxidation processes occurring during metal-protein formation.

2. Experimental

2.1. Preparation and physicochemical characteristics of Zn β LG3, Zn β LG3 and Zn β LG30 complexes

Metallocomplexes were prepared by suspending β LG in 0.09% sodium chloride at pH = pI = 4.6 (pI; isoelectric point). At the respective pH, the total charge of the protein molecule is equal with zero; the protein has no electrophoretic mobility. For the respective experiments zinc nitrate (V) solutions (Sigma-Aldrich, Poland, Warsaw, Poland) were prepared in three different concentrations of $Zn^{2+}(aq)$ ions: 6 ($\sim 1 \times 10^{-4}$ mol/L), 60 ($\sim 1 \times 10^{-3}$ mol/L), and 600 ($\sim 1 \times 10^{-2}$ mol/L) mg/L. Subsequently, β LG solution (5000 mg/L = $\sim 3 \times 10^{-4}$ mol/L) was mixed with $Zn^{2+}(aq)$ ions concentrations in a ratio of 1:1 (v/v) and incubated at room temperature (RT) for 24 h.

$Zn^{2+}(aq)$ ion concentrations were measured by Inductively Coupled Plasma-Mass Spectrometry (ICP-MS) (7900 ICP-MS, Agilent Technologies, Warsaw) for both the supernatant and the precipitate after mineralization of the samples in aqua regia diluting them to 1% HNO₃ (Sigma-Aldrich, Poland).

For the preparation of spectroscopic data Origin Pro/2016 software (OriginLab Corporation) was used.

Instrumental analyses were performed for the native (control) β LG and Zn β LG complexes (Zn β LG3, Zn β LG30 and Zn β LG300). The choice of three concentrations was determined based on our previous work [23] where the binding efficiency of $Zn^{2+}(aq)$ ions (60 mg/L) to β LG was found to be about 69%. Moreover, it has been observed that the efficiency increases with the increases of the concentrations. Therefore, in this work three different concentrations (low, medium and high) have been chosen for a comparative study.

2.1.1. Scanning and transmission electron microscopy (SEM, TEM), energy dispersive X-ray (EDX) and X-ray diffraction (XRD) analysis

The observation of changes in the surface morphology of native protein and metallocomplexes as well as quantitative analysis of elements was carried out using scanning electron microscopy (SEM, LEO model 1430 VP) in combination with energy dispersive X-ray (EDX) detector (XFlash 4010, Bruker AXS, Berlin, Germany) and transmission electron microscopy (TEM, model G2 F20X-Twin 200 kV, FEI) in combination with energy dispersive X-ray detector (EDX, Energy Dispersive X-ray, RTEM SN9577, 134 eV, Edax). For SEM analysis samples were prepared by applying powder of native protein and metallocomplexes on the grid, whereas for TEM analysis, the samples were layered to a carbon-coated grid (Lacey type Cu 400 mesh, Plano).

In order to characterize the form and nature of the obtained metallocomplexes, the X-ray diffractometer (X'Pert Pro-Analytical Phillips) equipped with Ni filter and CuK α radiation source ($\lambda = 1.54056$ Å) was used. The registered XRD pattern was processed using XRD Malvern Panalytical software. The samples were applied on a microscope slide, dried and then, analyzed.

2.1.2. Fourier transform infrared spectroscopic with attenuated total reflectance (FTIR-ATR) and Raman Spectroscopy (Raman) analysis

The presence of active functional groups occurring in Zn β LG3, Zn β LG30 and Zn β LG300 complexes for confirmation of metal-protein binding was studied by Fourier Transform Infrared Spectroscopic with Attenuated Total Reflectance (FTIR-ATR) and Raman Spectroscopy (Raman) method.

FTIR-ATR spectra were collected in MIR 400 – 4000 cm⁻¹ range by coadded 15 scans at 4 cm⁻¹ resolution using FTIR-ATR from Bruker (Billerica, Massachusetts, USA). Approximately 1 mg of native β LG powder and metallocomplexes were used for spectral analysis by applying them to a platinum-ATR with a durable monolithic diamond measurement interface.

Raman spectra in the range 400 – 4000 cm⁻¹ at the wavelength equal to $\lambda = 532$ nm as excitation light, with power of approximately 20 mW and the counting time spectrum at 2×30 s with an accumulation of 10 fM were measured using the Raman spectrometer (Senterra, Bruker Optik). The samples were prepared by dropping of the samples on ZnSe lens, focal length 50.8 mm, 12 mm, 2.4 mm (IUVOLASER, Poland), drying at room temperature for 24 h and analyzed.

2.2. The mechanism of Zn β LG3, Zn β LG3 and Zn β LG30 complexes formation

2.2.1. Molecular dynamics simulations

For Molecular Dynamic (MD) simulations, the initial β LG structure (PDB ID: 3BLG) was obtained from the Protein Data Bank (PDB). Originally, the structure was characterized by X-ray crystallography with a resolution of 2.56 Angstrom [24]. Zinc ions at three concentrations: 6, 60, and 600 mg/L were randomly introduced into the system, then solvated using a TIP3P water box with variable side length depending on the size of the protein/zinc ions [25]. Then, the systems were electrostatically neutralized with Na⁺ and Cl⁻ ions. MD simulations were performed using the AMBER ff99-SB-ILDN force field [26]. The MD simulations were performed according to the protocol developed and refined in our previous works described in Pomastowski et al., 2016; Buszewski et al., 2021 [12,17]. To remove bad contacts and structural clashes, energy minimization was applied followed by fast heating to 298.15 K at constant volume. In turn, the density of all systems were equilibrated by subjecting them to constant pressure (1 bar) and temperature (298.15 K) – NPT ensemble. The production of MD simulations in the NVT ensemble was conducted in GROMACS 5.1.2 software. Visualization and large-scale data analysis in Visual Molecular Dynamics (VMD) 1.9.3 [27] software, and Python 3.9.

2.2.2. Quantum mechanics calculations

To further clarify the interaction mechanism between Zn²⁺(aq) ions and β LG, density functional theory (DFT) calculations, using Gaussian 16 Programs [28] were performed for four modeled Zn-AA (AA = Asp, Glu, Tyr and Cys) complexes. These complexes were optimized using the M06-2X functional [29] together with the 6-31+G⁺⁺ basis set. Higher level relative binding free energies (ΔG_{298}) were obtained at M06-2X/6-311++G(3df,2p) level.

3. Results and discussion

3.1. Determination of zinc ion (Zn²⁺(aq) ions) concentration by inductively coupled plasma-mass spectrometry (ICP-MS)

The binding process of Zn²⁺(aq) ions at concentrations 6, 60, 600 mg/L to β LG has been investigated by ICP-MS. The application of ICP-MS method allowed to quantitatively measure the content of zinc ions in metallocomplexes. The study was carried out for

both, obtained supernatant and precipitate derived from the synthesis. For the supernatant, the amount of Zn²⁺(aq) ions adsorbed in 1 g β LG was found to be 0.30 ± 0.10 mg/g (~ 1 mol), 9.78 ± 0.58 mg/g (~3 mole) and 110.6 ± 1.59 mg/g (~31 mole) for 3, 30 and 300 mg/L, respectively. For the precipitate in the same concentrations, the following values were obtained 1.46 ± 0.01 mg/g (~ 1 mol), 19.36 ± 0.11 mg/g (~ 5 mole) and 102.97 ± 0.00 mg/g (~ 29 mole) respectively. Results indicate that the sorption capacity of metallocomplexes increases with increasing Zn²⁺(aq) ion concentration.

In addition, the values of the change in Gibbs free energy (ΔG_{298}) and distribution coefficient (K_d) of Zn²⁺(aq) ion sorption at concentrations of 6, 60 and 600 mg/L to β LG were calculated. For the supernatant, these values were -9.91 and 56.92, -13.78 and 275.11, -14.31 and 342.27 kJ/mol, respectively, and for the precipitate, -14.90 and 434.78, -16.71 and 909.09, -16.92 and 990.10 kJ/mol, respectively. The negative ΔG_{298} values confirm that the binding process of Zn²⁺(aq) ions to β LG is spontaneous and, more energetically favourable with increasing Zn²⁺(aq) ion concentration. In previous studies of the interaction of zinc cations at a concentration of 50 mg/L to individual casein fractions (CNs) of α_{S1} -, β -, κ CN performed by our group, the calculated Gibbs energy and distribution coefficient were -15.52 and 559.49 kJ/mol (Zn α_{S1} CN), -14.80 and 417.25 kJ/mol (Zn β CN), -16.52 and 842.62 kJ/mol (Zn κ CN) for the complexes, respectively [19]. The calculated values of ΔG_{298} for Zn β LG complexes are similar to those of ZnCN complexes. On the other hand, based on the K_d coefficient, it can be assumed that zinc ions are more readily adsorbed by β LG due to its highest value. This may be an effect of the fact that β LG is a globular and smaller protein than CN, which forms a micelle from its individual fractions. Considering the results obtained, the structure and size of the protein as well as the metal concentration play an important role in metal-protein interactions.

3.2. Microscopic and X-ray diffraction analysis

In order to analyze the protein morphology before and after the binding process, electron microscopy was employed. Fig. 1 shows the surface morphological changes of Zn β LG metallocomplexes at different concentrations (6, 60, 600 mg/L) of Zn²⁺(aq) ions. The images of the metallocomplexes were compared with the control sample (native β LG).

As shown in Fig. 1A, differences between surface morphologies protein have been observed. It was observed that the respective changes are Zn²⁺(aq) ion concentration dependent. With the increase in the Zn²⁺(aq) ions concentration, more tailored, dense and rough morphologies were observed. The metallocomplexes Zn β LG3 and Zn β LG30 have a rather rough and irregular surface compared to the surface of the metallocomplex Zn β LG300, which is more regular and structured. In addition, transmission electron microscope (TEM) analysis was performed for the control β LG, and Zn β LG metallocomplexes and the results are shown in Fig. 1B. Through TEM analysis, it is possible to obtain information on the structure, size and morphology of the metal-protein particles. The obtained TEM micrographs of the metallocomplexes indicate that with increasing Zn²⁺(aq) ion concentration, the structure of the complexes is denser and more porous which indicates that more Zn²⁺(aq) ions are bound in case of higher concentration. The physical properties of the protein surface play an important role. Paulson et al. [22] in their study explain that the effect of metal ions on protein aggregation depends on several factors, e.g. pH, protein concentration and the concentration of metals that contribute to inhibiting or accelerating aggregation. These studies play an important role in all kinds of pathologies in medicine. It was concluded that as the concentration of metal ions in the brain increases, a

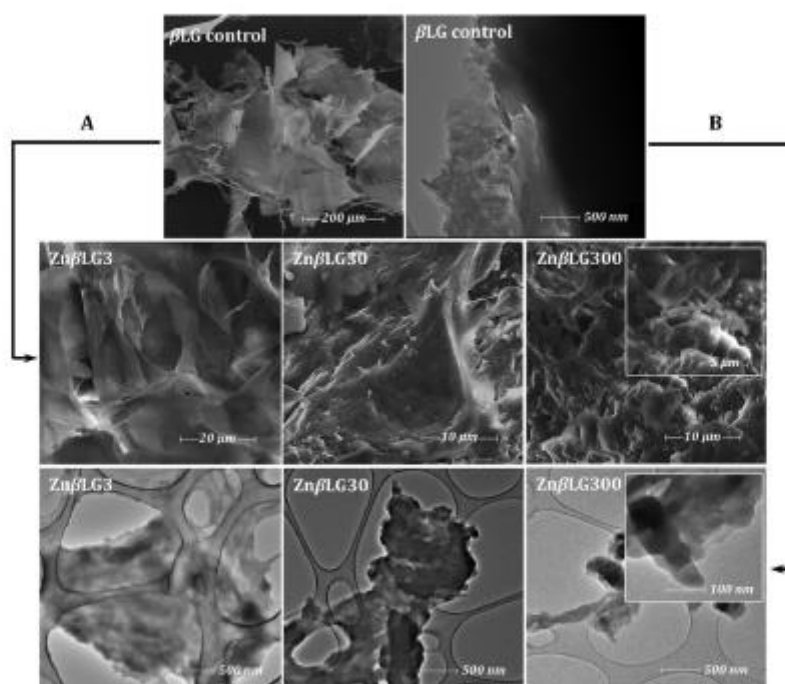


Fig. 1. SEM (A) and TEM (B) images of β LG control and Zn β LG complexes.

more significant aggregation of proteins promotes the progression of Alzheimer's disease. We presume that using different concentrations of d-electrons metal ions such as zinc ions and their action on the protein could influence the biological properties and applications of the obtained metallocomplexes.

Moreover, confirmation of $Zn^{2+}(aq)$ ion adsorption was provided by elemental EDX chemical analysis, which determines the elemental composition of the studied metallocomplexes. The obtained EDX spectra are shown in Fig. 2.

EDX analysis for the control β LG as well as the metallocomplexes showed carbon, nitrogen, and oxygen were predominantly present. Additionally, small amounts of sodium, phosphorus, sulfur, copper, aluminum and chlorine were found in the samples. Sodium, phosphorus and sulfur originate from the protein structure while chlorine from sodium chloride in the prepared complex solution. In turn, copper and aluminum come from the apparatus background. Furthermore, additional signals indicating the presence of $Zn^{2+}(aq)$ ions involved in binding with β LG were revealed for metallocomplexes. EDX analysis for the metallocomplexes showed that with increasing concentration of $Zn^{2+}(aq)$ ions, more intense signals of $Zn^{2+}(aq)$ ions appear, whose percentage masses are 0.47% for Zn β LG3, 0.91% for Zn β LG30 and 1.06% for Zn β LG300.

Furthermore, SEM-EDX analysis enabled mapping of the elemental distribution in the sample. The SEM-EDX mapping images represent the homogeneous dispersion of $Zn^{2+}(aq)$ ions on the surface of all metallocomplexes. Additionally, the obtained X-ray diffraction image for the metallocomplexes is characterized by a single broad signal at $20\text{--}30^\circ 2\theta$ ($CuK\alpha$), indicating the amorphous nature of the metallocomplexes. These results are shown in Fig. 3.

The results are in contrast to previous work published by Buszewski et al., 2021, where the Zn^{2+}/ZnO -OVA hybrid complexes,

registered four additional peaks, characteristic for the crystalline structure of ZnO nanoparticles [12].

3.3. Spectroscopic analysis

The binding of metal ions with proteins is an important process affecting their catalytic activity, structural stability as well as functional regulation. Generally, the coordination of zinc by proteins is mediated by functional groups of the protein side chain, which include histidine (His), methionine (Met), cysteine (Cys), tyrosine (Tyr), aspartic acid (Asp) and glutamic acid (Glu) [30]. In order to confirm the formation of Zn β LG3, Zn β LG30 and Zn β LG300 metallocomplexes, we used FTIR-ATR from which the active groups involved in the binding process were identified (Fig. 4A).

The observed changes in the FTIR-ATR spectra indicated potential binding sites. After the addition of the $Zn^{2+}(aq)$ ions, the intensity of the metallocomplexes spectral signals decreased compared to the control (native β LG). The binding of the β LG to $Zn^{2+}(aq)$ ions caused the disappearance of 3078 cm^{-1} and 1311 cm^{-1} signals in metallocomplexes formulations (Zn β LG3, Zn β LG30, Zn β LG300). The respective changes originate from NH stretching vibrations in the amide band A and B, [31] and from amide III ($1220\text{--}1400\text{ cm}^{-1}$), which is a combination of NH bending phase and CN stretching vibrations with small CO in-plane bending and CC stretching vibrations [32]. Moreover, the sorption of $Zn^{2+}(aq)$ ions caused also the appearance of a new signal registered at 817 cm^{-1} , which originates from Tyr and Phe residues [33]. Sorption of the $Zn^{2+}(aq)$ ions additionally induced the decrease in the signal intensity registered in the $400\text{--}4000\text{ cm}^{-1}$ spectral range compared to the control. The signals observed at 1386 cm^{-1} for the obtained Zn β LG metallocomplexes and control β LG with different signal intensities can be attributed to binding of zinc ions to β LG

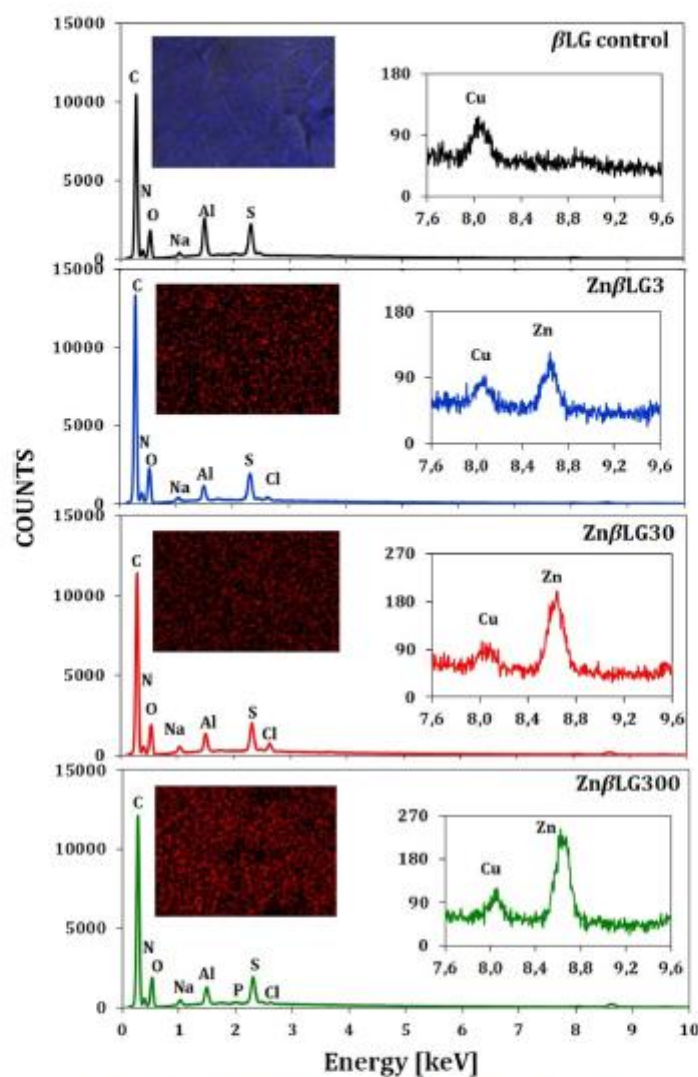


Fig. 2. SEM-EDX spectrum and mapping analysis of β LG control and Zn β LG complexes.

to Asp and Glu [31,33]. In contrast, the 1073 cm^{-1} signal indicates the presence of Trp involved in $\text{Zn}^{2+}(\text{aq})$ ions binding [31]. Signal observed at 1514 cm^{-1} is characteristic for amide II as a consequence of an out-of-phase combination of the NH in-plane bending and CN stretching vibrations with a smaller contribution from the CO in-plane bending and CC and NC stretching vibrations [31,32]; in addition, the described signal can also be attributed to Tyr originating from the stretching mode of the CC and C-O vibrations and the COH in-plane bending vibrations [34]. According to Barth, 2000, the signals at 1250 cm^{-1} and 1154 cm^{-1} can also correspond to the Tyr residues [34]. The 1250 cm^{-1} signal, as well as the 1311 cm^{-1} and 1386 cm^{-1} signal, correspond to amide III [31,32]. The 1627 cm^{-1} signal recorded in both control β LG and metallocomplexes is due to C=O stretching vibrations with minor contributions from the out-of-phase CN stretching vibrations, CCN deformation and NH in-plane bending in the amide I region

($1600 - 1650\text{ cm}^{-1}$) [31]. In contrast, weaker signals at around 1472 cm^{-1} and 1461 cm^{-1} are from amino acid side chains in peptide and protein structures, induced by asymmetric and symmetric CH_2 bending vibrations [35]. The signals at 964 and 954 cm^{-1} are associated with the presence of methionine (Met) involved in the binding process [33]. The 3657 , 3274 , and 3078 cm^{-1} signals from NH stretching vibrations in the amide A band were also noticed on the recorded spectrum [31]. In contrast, the signals 2980 , 2971 , 2931 and 2888 cm^{-1} are dominated by the absorption of hydrophobic hydrocarbon residues [36].

Further, Raman spectroscopy (Fig. 4B) was used to shed light on the binding mechanism of $\text{Zn}^{2+}(\text{aq})$ ions to β LG, which indicated the location of the active chemical groups of β LG in the binding process by $\text{Zn}^{2+}(\text{aq})$ ions. The recorded spectra by Raman spectroscopy were able to verify appearance the bands established by FTIR-ATR method. But for Raman analysis in the entire $700 -$

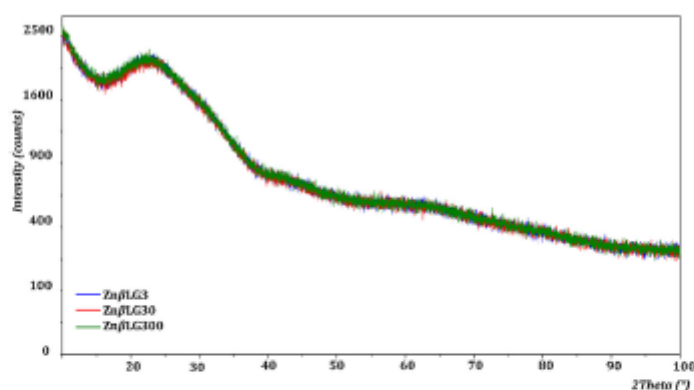


Fig. 3. X-ray diffraction of ZnβLG complexes.

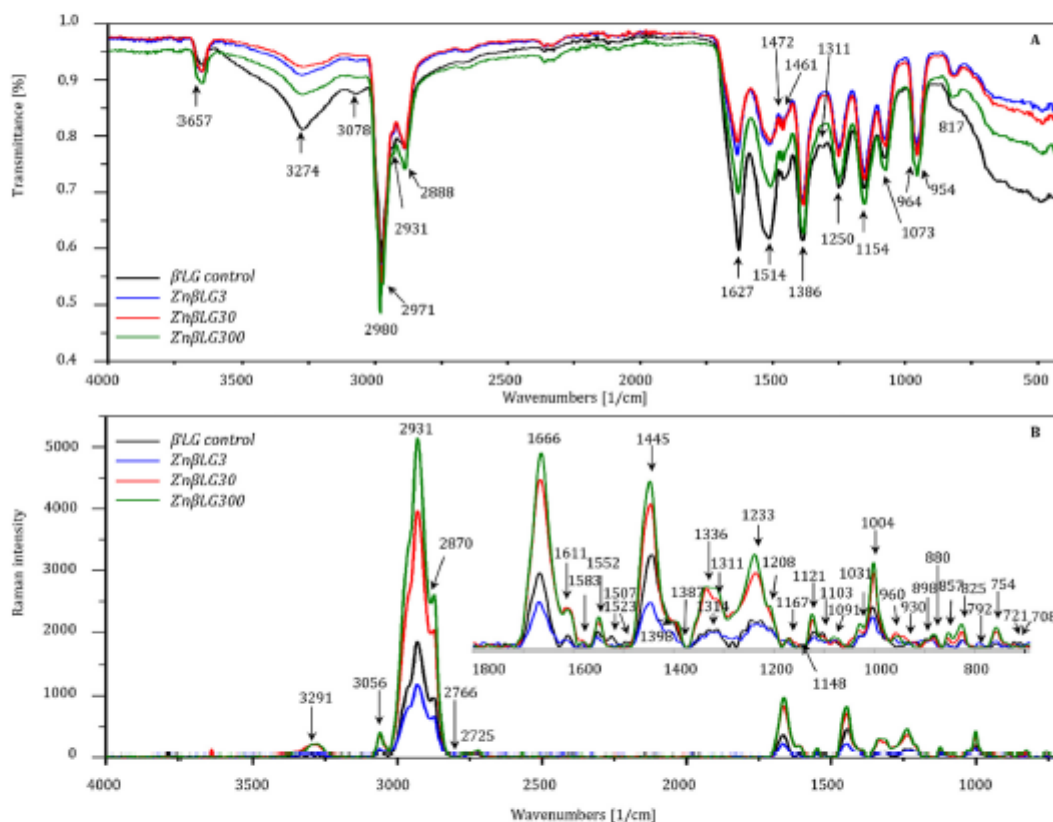


Fig. 4. FTIR-ATR (A) and Raman (B) spectrum of βLG control and ZnβLG complexes.

4000 cm^{-1} spectral range, the addition of $\text{Zn}^{2+}(\text{aq})$ ions to βLG showed an increase in the intensity of all spectral signals in comparison with the control βLG.

The obtained Raman spectra indicated the presence of 1666 and 1611 cm^{-1} bands originating from in-plane stretching vibrations of the c peptide and from on-plane N-H bending vibrations equivalent to amide I in the range 1600 – 1690 cm^{-1} [37,38,39]. Signals 1583, 1552, 1523, and 1507 cm^{-1} are from amide II in

the 1480 – 1585 cm^{-1} region and result from an out-of-phase C-N stretching and N-H bending motion combination, while signals 1336, 1314, 1311, 1233, and 1208 cm^{-1} represent amide III (~1200 – 1340 cm^{-1}) and arise from C-N stretching and N-H bending [37,39].

In addition, signals 1336 and 1311 cm^{-1} represent new signals indicating the presence of Trp for ZnβLG30, ZnβLG300 metallocomplexes and in case of signal 1583 cm^{-1} , a new Trp band

additionally appears for the metalcomplex Zn β LG3. The presence of new Trp signals indicates an important role in the binding of β LG with Zn $^{2+}$ (aq) ions. Trp has also been assigned to bands 1552, 1398, 1387, 1233, 1103, 960, 930, 898, 880, 792 and 754 cm $^{-1}$ [39,40,41]. New bands were also observed for all metalcomplexes for the bands at 1387 and 1031 cm $^{-1}$ and for the band at 1091 cm $^{-1}$ for Zn β LG3. Only the control β LG and the Zn β LG3 metalcomplex showed bands at 1523, 1314 cm $^{-1}$. Whereas at 721 and 708 cm $^{-1}$ there are C-S stretching bands from Met [38].

Raman signals at 3291, 3056, 2766 and 2725 cm $^{-1}$ have been assigned to CH (CH $_2$, CH $_3$), -C-H or =C-H stretching bonds [40], with the 3291 and 2725 cm $^{-1}$ bands appearing only for Zn β LG30, Zn β LG300 metalcomplexes and the 2766 cm $^{-1}$ band occurring for Zn β LG300 metalcomplex.

This indicates that higher concentrations of Zn $^{2+}$ (aq) ions interfere more strongly in the protein structure. In the range of 2860 – 2940 cm $^{-1}$ (2870, 2931 cm $^{-1}$), C-H stretching vibration bands of aliphatic side chains were observed [42]. The bands around 1445, 1004 and 754 cm $^{-1}$ correspond to ionized COO $^-$ group derived from Glu and the bands at around 1121 and 1091 cm $^{-1}$ to ionized COO $^-$ group derived from Asp [43]. The presence of these shifts bands suggests that these β LG functional groups (Glu, Asp) play an essential role in the binding of Zn $^{2+}$ (aq) ions to β LG. Intense bands at 1004 cm $^{-1}$ and 1031 cm $^{-1}$ are characteristic of Phe [40,41], and bands 1507, 1233, 1208, 1167, 1148, 857 and 825 cm $^{-1}$ are related with the presence of Tyr [40,41]. For all Zn β LG metalcomplexes, the disappearance of signals indicative of Zn $^{2+}$ (aq) ion interference in the protein structure is observed at 1148 cm $^{-1}$, and the 1167 and 708 cm $^{-1}$ bands disappeared for Zn β LG3, the 930 cm $^{-1}$ band disappeared for Zn β LG3 and Zn β LG30, and the 721 cm $^{-1}$ band disappeared for Zn β LG3 and Zn β LG300 complexes. Table 1 shows the total signals found by FTIR-ATR and Raman spectroscopy.

Both FTIR-ATR and Raman spectra are rich in bands originating from proteins as well as interference from zinc ions, nevertheless, the obtained signals may overlap, which makes them difficult to interpret.

3.4. Molecular dynamics and quantum mechanics analysis

The ab initio MD method for predicting protein structure and dynamics enabled a tighter complement of FTIR-ATR and Raman experimental data. In view of this, the stability of control β LG and Zn β LG complexes was evaluated at three different concentrations. Root mean square error of deviation (RMSD) w. r. t. energy minimized structure was used as a metric. All the complexes are shown to be stable with an average RMSD of ~1.25 – 1.50 Angstrom. Molecular dynamics simulations are well converged. Flexibility patterns analyzed via the root mean square error of fluctuation (RMSF). Four Zn $^{2+}$ (aq) ions do not exhibit a notable change in the flexibility of control β LG, whereas the flexibility of the four key regions decreases with the increase of Zn $^{2+}$ (aq) ions concentration. Sampled MD range for Zn $^{2+}$ (aq) ions- β LG interactions comprised 50 – 150 ns. Fig. 5A presents the model of the obtained β LG structure by molecular dynamics simulation and the effect of different zinc ion concentrations on the β LG structure. The optimized geometries of the 4 Zn-AA complexes are depicted in Fig. 5B. Interactions between Zn $^{2+}$ (aq) ions and Glu, Asp, Cys, His, Tyr, Trp, Phe, Met, Arg, and Lys were analyzed with a distance threshold of 0.35 nm (Fig. 5C).

According to literature data, the most common zinc-binding sites are those containing several types of amino acids, among which Cys, His, Glu and Asp account for 96% of all zinc-binding sites [44]. Our results indicate the strong correlation between concentration and number of binding sites Glu/Asp dominating amino acids interacting with Zn $^{2+}$ (aq) ions. Glu accounts for 65 – 85% of all the interactions. The non-polar amino acids Trp, Phe, Met are

Table 1
Wavenumber of FTIR-ATR and Raman bands and assignments for side-chain vibrations of β LG.

Wavenumber (cm $^{-1}$)	Band assignment	Ref.
FTIR-ATR		
3657, 3274, 3078	Amide A and B	[31]
2980, 2971, 2931, 2888	Absorption of hydrophobic hydrocarbon residues	[36]
1627	Amide I	[31]
1514	Amide II	[31,32]
1472, 1461	Amino acid side chains in peptide and protein structures, induced by asymmetric and symmetric CH $_3$ bending vibrations	[35]
1386, 1311, 1250	Amide III	[31,32]
1386	Asp, Glu	[31,33]
1514, 1233, 1154, 817	Tyr	[33,34]
1073	Trp	[31]
964, 954	Met	[33]
817	Phe	[33]
Raman spectroscopy		
3291, 3056, 2766, 2725	CH (CH $_2$, CH $_3$), -C-H or =C-H stretching bond	[40]
2931, 2870	C-H stretching vibration bands of aliphatic side chains	[42]
1666, 1611	Amide I	[37,38,39]
1583, 1552, 1523, 1507	Amide II	[39,40]
1583, 1552, 1398, 1387, 1336, 1311, 1233, 1103, 960, 930, 898, 880, 792, 754	Trp	[39,40,41]
1507, 1208, 1167, 1148, 857, 825	Tyr	[40] [41]
1445, 1004	Glu	[38]
1336, 1314, 1311, 1233, 1208	Amide III	[37,39]
1121, 1091	Asp	[43]
1031, 1004	Phe	[40] [41]
721, 708	Met	[38]

not involved in the interaction with zinc ions due to their high pKa values around 9.0. A similar situation exists for the basic amino acids His, Arg and Lys [45]. Although Zn-Lys active sites appear for Lys at higher concentrations, the pKa value of about 8.95 for Lys under the conditions of the analysis performed at pH 4.6 indicates that it cannot interact with zinc cations. Similar observations were observed for polar amino acids, whose high values of pKa constants indicate that, like non-polar or basic amino acids, they cannot interact with zinc ions, for Cys due to the presence of a thiol group, whose pKa value is 8.18, and Tyr, for which the pKa is 9.11 [45]. As an additional confirmation, in order to quantify the

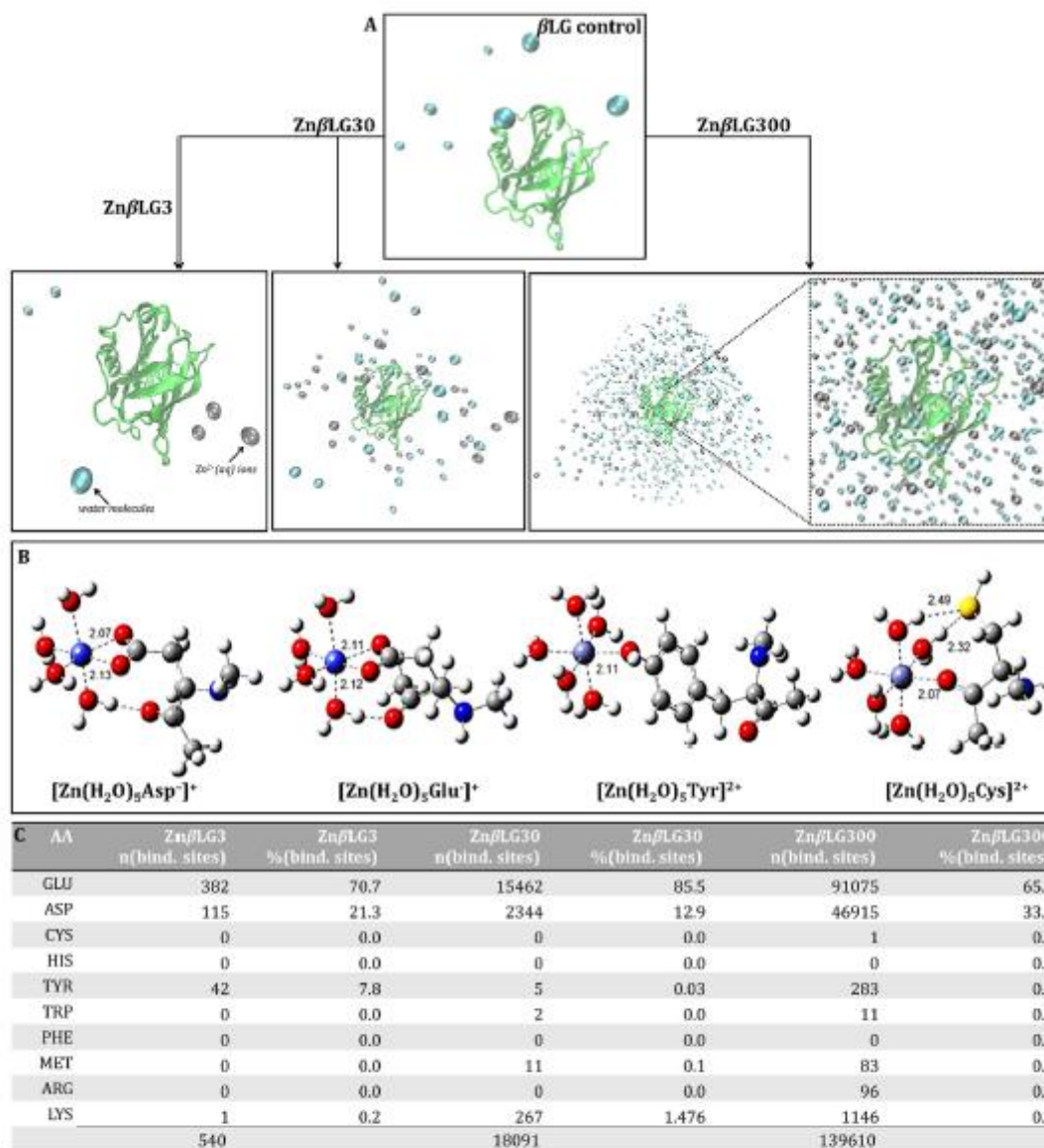


Fig. 5. The structures of β LG control and Zn β LG complexes (A); Optimized geometries (M06-2X/6-31+G(d,p)) of 4 modelled Zn-AA complexes. Interaction distances are in Å (B). Interaction analysis between Zn²⁺(aq) ions and AAs (C).

binding affinity of amino acid (AA) residues to Zn²⁺(aq) ion, model complexation reactions of four AAs, namely Glu, Asp (strong interaction) and Tyr and Cys (weak interaction), were calculated with respect to aqua Zn²⁺ complex, [Zn(H₂O)₆]²⁺ (in octahedral geometry).

The AAs were modelled with one amide unit and capped with methyl groups. The complexation free energies (ΔG_{298}) of the four Zn-AA complexes were computed at M06-2X/6-311++G(3df,2p)/M06-2X/6-31+G(d,p) level of theory (in aqueous solvent).





Strong complexes with bidentate interaction between the carboxyl group and Zn^{2+} were obtained for the Zn-Glu and Zn-Asp complexes. In both cases, the calculated binding Gibbs free energy is exergonic, suggesting that the displacement of 2 water molecules to form the six-coordinated Zn-AA complex is an energetically favourable process. The strong Zn-AA interaction is readily attributed to the strong electrostatic interaction of the negatively charged carboxyl ion (COO^-) and Zn^{2+} cation. This result readily confirms the strong affinity of Glu and Asp residues towards aqueous Zn^{2+} ion in the MD simulations. FTIR-ATR and Raman analyses indicate structural changes due to the presence of amides visible in the spectra thus affecting the conformational changes of the protein. The spatial structure in the MD studies performed may change due to conformational changes. These results complement/confirm the experimental spectral results in which the intense 1386 cm^{-1} signal from FTIR-ATR analysis indicates the binding of $\text{Zn}^{2+}(\text{aq})$ ions to Asp and Glu and the 1445 cm^{-1} and 1004 cm^{-1} signals correspond to Glu and 1121 cm^{-1} and 1091 cm^{-1} Asp in Raman spectroscopy. For the Zn-Tyr and Zn-Cys complexes, the complexation process is unfavorable (positive binding free energy). Only one water molecule is displaced in these Zn-AA complexes. For the Zn-Tyr complex, the OH group of Tyr coordinates with Zn^{2+} ion. In the case of the Zn-Cys complex, the thiol group is not competitive compared to the carbonyl group for Zn^{2+} binding. As a result, the carbonyl O coordinates to the Zn^{2+} ion in $[\text{Zn}(\text{H}_2\text{O})_5\text{Cys}]^{2+}$ and the SH group stabilizes the complex via bidentate hydrogen bonds. Overall, the calculated trend of complexation free energies of the four Zn-AA complexes (Glu > Asp >> Tyr > Cys) is in good accord with the MD simulation finding.

4. Conclusions

In-depth physicochemical study on metal complexes demonstrated that the concentration of $\text{Zn}^{2+}(\text{aq})$ ions notably influences the process of binding to whey protein - β -lactoglobulin (β LG). Scanning electron microscopy showed that the surface morphology of β LG changes depending on the applied $\text{Zn}^{2+}(\text{aq})$ ions concentration of 6, 60 and 600 mg/L. For metal complexes in the concentrations of 3 and 30 mg/L, the differences in surface morphology are similar in character, but the concentration of 300 mg/L affects the surface morphological changes to a greater extent. The formation of metal complexes monitored by transmission electron microscopy indicates that with increasing $\text{Zn}^{2+}(\text{aq})$ ions concentration the obtained metal complexes are characterized by a more porous structure. The energy dispersive X-ray (EDX) analysis performed confirmed the adsorption of $\text{Zn}^{2+}(\text{aq})$ ions. The spectroscopic analysis performed showed that aspartic acid (Asp) and glutamic acid (Glu), as well as the aromatic rings of tyrosine (Tyr), tryptophan (Trp) and phenylalanine (Phe), play a key role in the binding of $\text{Zn}^{2+}(\text{aq})$ ions to carboxyl groups. Density functional theory (DFT) calculated trend of complexation free energies of the four Zn-AA complexes (Glu > Asp >> Tyr > Cys) is in good accord with the molecular dynamic (MD) simulation findings. These results suggest that the obtaining of the protein metal complexes can be the first step in the development of new therapeutic agents used in medicine, but also in the food industry as a potential dietary supplement.

Declaration of competing interest

There are no conflicts of interest regarding this paper.

CRediT authorship contribution statement

Agnieszka Rodzik: Conceptualization, Methodology, Investigation, Visualization, Data curation, Writing - original draft. **Viviana Railean:** Methodology, Investigation, Writing - review & editing, Visualization. **Pawel Pomastowski:** Conceptualization, Funding acquisition, Project administration. **Petar Žuvela:** Investigation, Data curation, Writing - original draft, Visualization, Software, Data curation. **Ming Wah Wong:** Investigation, Software, Writing - review & editing, Data curation, Resources. **Bogusław Buszewski:** Conceptualization, Supervision, Resources.

Data availability

No data was used for the research described in the article.

Acknowledgements

This work was financially supported by the National Science Centre within the framework of Opus 14 project No. 2017/27/B/ST4/02628 (2018 - 2021). Bogusław Buszewski, Pawel Pomastowski and Agnieszka Rodzik are members of Toruń Center of Excellence "Towards Personalized Medicine" operating under Excellence Initiative-Research University.

References

- [1] M. Moustakas, The role of metal ions in biology, biochemistry and medicine, *Materials* 14 (2021) 1-4, doi:10.3390/ma14030549.
- [2] J.S. Garcia, C.S. De Magalhães, M.A.Z. Arruda, Trends in metal-binding and metalloprotein analysis, *Talanta* 69 (2006) 1-15, doi:10.1016/j.talanta.2005.08.041.
- [3] C. Andreini, L. Banci, I. Bertini, A. Rosato, Counting the zinc-proteins encoded in the human genome, *J. Proteome Res.* 5 (2006) 196-201, doi:10.1021/pr050361j.
- [4] G. Porcheron, A. Garénaux, J. Proulx, M. Sabri, C.M. Dozois, Iron, copper, zinc, and manganese transport and regulation in pathogenic Enterobacteria: correlations between strains, site of infection and the relative importance of the different metal transport systems for virulence, *Front. Cell Infect. Microbiol.* 3 (2013) 1-24, doi:10.3389/fcimb.2013.00090.
- [5] M. Dardenne, Zinc and immune function, *Eur. J. Clin. Nutr.* 56 (2002) S20-S23, doi:10.1038/sj.ejcn.1601479.
- [6] P.H. Lin, M. Sermersheim, H. Li, P.H.U. Lee, S.M. Steinberg, J. Ma, Zinc in wound healing modulation, *Nutrients* 10 (2018) 1-20, doi:10.3390/nu10010016.
- [7] A. Krężel, W. Maret, The biological inorganic chemistry of zinc ions, *Arch. Biochem. Biophys.* 611 (2016) 3-19, doi:10.1016/j.abb.2016.04.010.
- [8] K. Kluska, J. Adamczyk, A. Krężel, Metal binding properties, stability and reactivity of zinc fingers, *Coord. Chem. Rev.* 367 (2018) 18-64, doi:10.1016/j.ccr.2018.04.009.
- [9] S. Barber-Zucker, B. Shaanan, R. Zarivach, Transition metal binding selectivity in proteins and its correlation with the phylogenomic classification of the cation diffusion facilitator protein family, *Sci. Rep.* 7 (2017) 1-12, doi:10.1038/s41598-017-16777-5.
- [10] C.J. Frederickson, J.Y. Koh, A.I. Bush, The neurobiology of zinc in health and disease, *Nat. Rev. Neurosci.* 6 (2005) 449-462, doi:10.1038/nrn1671.
- [11] P. Pomastowski, M. Sprynskyy, B. Buszewski, The study of zinc ions binding to casein, *Colloids Surf. B* 120 (2014) 21-27, doi:10.1016/j.colsurfb.2014.03.009.
- [12] B. Buszewski, P. Žuvela, A. Król-Górniak, V. Railean-Plugaru, A. Rogowska, M.W. Wong, M. Yi, A. Rodzik, M. Sprynskyy, P. Pomastowski, Interactions of zinc aqua complexes with ovalbumin at the forefront of the $\text{Zn}^{2+}/\text{ZnO}$ -OVO hybrid complex formation mechanism, *Appl. Surf. Sci.* 542 (2021) 148641, doi:10.1016/j.apsusc.2020.148641.
- [13] J. Chamani, Comparison of the conformational stability of the non-native α -helical intermediate of thiol-modified β -lactoglobulin upon interaction with sodium n-allyl sulfates at two different pH, *J. Colloid Interface Sci.* 299 (2006) 636-646, doi:10.1016/j.jcis.2006.02.049.
- [14] K. Marshall, Therapeutic applications of whey protein, *Altern. Med. Rev.* 9 (2004) 136-156.
- [15] A. Rodzik, P. Pomastowski, G.N. Sagandykova, B. Buszewski, Interactions of whey proteins with metal ions, *Int. J. Mol. Sci.* 21 (2020) 1-26, doi:10.3390/ijms21062156.
- [16] N. Tang, L.H. Skibsted, Zinc bioavailability from whey. Enthalpy-entropy compensation in protein binding, *Food Res. Int.* 89 (2016) 749-755, doi:10.1016/j.foodres.2016.10.002.
- [17] P. Pomastowski, M. Sprynskyy, P. Žuvela, K. Rafińska, M. Milanowski, J.J. Liu, M. Yi, B. Buszewski, Silver-Lactoferrin Nanocomplexes as a Potent Antimicrobial Agent, *J. Am. Chem. Soc.* 138 (2016) 7899-7909, doi:10.1021/jacs.6b02699.
- [18] H.M. Baker, E.N. Baker, Lactoferrin and Iron: structural and dynamic aspects of binding and release, *Biomaterials* 17 (2004) 209-216, doi:10.1023/B:BIOM.0000027694.40260.70.

- [19] A. Rodzik, P. Pomastowski, V. Railean-Plugaru, M. Sprynsky, B. Buszewski, The study of zinc ions binding to α S1-, β - and κ -casein, *Int. J. Mol. Sci.* 21 (2020) 1–18, doi:10.3390/ijms21218096.
- [20] K.J. Franz, N. Metzler-Nolte, Introduction: metals in Medicine, *Chem. Rev.* 119 (2019) 727–729, doi:10.1021/acs.chemrev.8b00685.
- [21] I. Dokmanić, M. Šikić, S. Tomić, Metals in proteins: correlation between the metal-ion type, coordination number and the amino-acid residues involved in the coordination, *Acta Crystallogr. Sect. D Biol. Crystallogr.* 64 (2008) 257–263, doi:10.1107/S090744490706595X.
- [22] B.G. Poulson, K. Szczepski, J.J. Lachowicz, L. Jaremko, A.H. Enwas, M. Jaremko, Aggregation of biologically important peptides and proteins: inhibition or acceleration depending on protein and metal ion concentrations, *RSC Adv.* 10 (2020) 215–227, doi:10.1039/c9ra09350h.
- [23] B. Buszewski, A. Rodzik, V. Railean-Plugaru, M. Sprynsky, P. Pomastowski, A study of zinc ions immobilization by β -lactoglobulin, *Colloids Surf. A* 591 (2020) 124443, doi:10.1016/j.colsurfa.2020.124443.
- [24] B.Y. Qin, M.C. Bewley, L.K. Creamer, H.M. Baker, E.N. Baker, G.B. Jameson, Structural basis of the Tanford transition of Bovine β -Lactoglobulin, *Biochemistry* 37 (1998) 14014–14023, doi:10.1021/bi981016a.
- [25] P. Mark, L. Nilsson, Structure and dynamics of the TIP3P, SPC, and SPC/E water models at 298 K, *J. Phys. Chem. A* 105 (2001) 9954–9960, doi:10.1021/jp003020w.
- [26] K. Lindorff-Larsen, S. Piana, K. Palmo, P. Maragakis, J.L. Klepeis, R.O. Dror, D.E. Shaw, Improved side-chain torsion potentials for the Amber ff99SB protein force field, *Proteins: Struct. Funct. Bioinf.* 78 (2010) 1950–1958, doi:10.1002/prot.22711.
- [27] W. Humphrey, A. Dalke, K. Schulten, VMD: visual molecular dynamics, *J. Mol. Graph.* 14 (1996) 33–38, doi:10.1016/j.carbon.2017.07.012.
- [28] M. Frisch, G. Trucks, H. Schlegel, G. Scuseria, M. Robb, J. Cheeseman, G. Scalmani, V. Barone, G. Petersson, H. Nakatsuji, X. Li, M. Caricato, A. Marenich, J. Bloino, B. Janesko, R. Gomperts, B. Mennucci, H. Hratchian, J. Ortiz, A. Izmaylov, J. Sonnenberg, Gaussian 16, Revision A, Gaussian Inc., Wallingford CT, 2016 <http://gaussian.com/ROAhttp://gaussian.com/>.
- [29] Y. Zhao, D.G. Truhlar, The M06 suite of density functionals for main group thermochemistry, thermochemical kinetics, noncovalent interactions, excited states, and transition elements: two new functionals and systematic testing of four M06-class functionals and 12 other function, *Theor. Chem. Acc.* 120 (2008) 215–241, doi:10.1007/s00214-007-0310-x.
- [30] F. Bou-Abdallah, T. Giffune, The thermodynamics of proteins interactions with essential first row transition metals Fadi, *Biochim. Biophys. Acta* 1860 (2016) 879–891, doi:10.1016/j.bbagen.2015.11.005.The.
- [31] A. Barth, Infrared spectroscopy of proteins, *Biochim. Biophys. Acta* 1767 (2007) 1073–1101, doi:10.1016/j.bbabin.2007.06.004.
- [32] T. Krnić, N.S. Obradović, M.B. Rakin, Application of whey protein and whey protein hydrolysate as protein based carrier for probiotic starter culture, *Food Chem.* 293 (2019) 74–82, doi:10.1016/j.foodchem.2019.04.062.
- [33] M. Wolpert, P. Helwig, Infrared spectra and molar absorption coefficients of the 20 alpha amino acids in aqueous solutions in the spectral range from 1800 to 500 cm⁻¹, *Spectrochim. Acta - Part A: Mole. Biomol. Spectrosc.* 64 (2006) 987–1001, doi:10.1016/j.saa.2005.08.025.
- [34] A. Barth, The infrared absorption of amino acid side chains, *Prog. Biophys. Mol. Biol.* 74 (2000) 141–173, doi:10.1016/S0079-6107(00)00021-3.
- [35] M. Cestelli Guidi, C. Mirri, E. Fratini, V. Licursi, R. Negri, A. Marcelli, R. Amendola, In vivo skin leptin modulation after 14 MeV neutron irradiation: a molecular and FT-IR spectroscopic study, *Anal. Bioanal. Chem.* 404 (2012) 1317–1326, doi:10.1007/s00216-012-6018-3.
- [36] D. Ami, F. Lavatelli, P. Rognoni, G. Palladini, S. Raimondi, S. Giorgetti, L. Monti, S.M. Doglia, A. Natalello, G. Merlini, In situ characterization of protein aggregates in human tissues affected by light chain amyloidosis: a FTIR microspectroscopy study, *Sci. Rep.* 6 (2016) 1–12, doi:10.1038/srep29096.
- [37] D. Kuruski, R.P. Van Duyn, L.K. Lednev, Exploring the structure and formation mechanism of amyloid fibrils by Raman spectroscopy: a review, *Analyst* 140 (2015) 4967–4980, doi:10.1039/c5an0342c.
- [38] E. Li-Chan, S. Nakai, M. Hirotsuka, Raman spectroscopy as a probe of protein structure in food systems, in: *Protein Structure-Function Relationships in Foods*, 1994, pp. 163–197, doi:10.1007/978-1-4615-2670-4_8.
- [39] A. Rygula, K. Majzner, K.M. Marzec, A. Kaczor, M. Pilarczyk, M. Baranska, Raman spectroscopy of proteins: a review, *J. Raman Spectrosc.* 44 (2013) 1061–1076, doi:10.1002/jrs.4335.
- [40] E.C.Y. Li-Chan, Vibrational spectroscopy applied to the study of milk proteins, *Dairy Sci Technol* 87 (2007) 443–458, doi:10.1051/lait:2007023.
- [41] Z.-Q. Wen, Raman Spectroscopy of protein pharmaceuticals, *J. Pharm. Sci.* 96 (2007) 2861–2878, doi:10.1002/jps.
- [42] R.P. Kengne-Momo, P. Daniel, F. Lagarde, Y.L. Jeyachandran, J.F. Pilard, M.J. Durand-Thouand, G. Thouand, Protein interactions investigated by the Raman spectroscopy for biosensor applications, *Int J Spectrosc.* (2012) 1–7, doi:10.1155/2012/462901.
- [43] G. Zhu, X. Zhu, Q. Fan, X. Wan, Raman spectra of amino acids and their aqueous solutions, *Spectrochim. Acta Part A* 78 (2011) 1187–1195, doi:10.1016/j.saa.2010.12.079.
- [44] Z. Chen, Y. Wang, Y.F. Zhai, J. Song, Z. Zhang, ZincExplorer: an accurate hybrid method to improve the prediction of zinc-binding sites from protein sequences, *Mol. Biosyst.* 9 (2013) 2213–2222, doi:10.1039/c3mb70100j.
- [45] R.J. Ouellette, J.D. Rawo, Amino Acids, Peptides, and Proteins, in: *Organic Chemistry Study Guide*, 2015, pp. 569–586, doi:10.1016/b978-0-12-801889-7.00027-3.

4.8. Metal-protein action for the wound healing process using murine model C57BL/6J mouse

[P8] A. Rodzik, P. Pomastowski, M. Buszewska-Forajta, V. Railean, A. Gołębiowski, B. Buszewski, K. Niedojadło, K. Rafińska, *Metal-protein action for the wound healing process using murine model C57BL/6J mouse*, Scientific Reports, Submission ID 15404681-edaf-4c74-885f-ae8688b6dbd7.

1 **Metal-protein action for the wound healing process using**
2 **murine model C57BL/6J**

3 Agnieszka Rodzik^{1,2}, Paweł Pomastowski¹, Magdalena Buszewska-Forajta^{3,4}, Viorica Railean^{5,1},
4 Adrian Gołębiowski^{1,2}, Bogusław Buszewski^{1,2}, Katarzyna Niedojadło⁶, Katarzyna Rafińska^{2*}

5
6 ¹ Centre for Modern Interdisciplinary Technologies, Nicolaus Copernicus University in Toruń, Wileńska
7 4, 87-100, Toruń, Poland

8 ² Department of Environmental Chemistry and Bioanalysis, Faculty of Chemistry, Nicolaus Copernicus
9 University in Toruń, Gagarina 7, 87-100 Toruń, Poland

10 ³ Institute of Veterinary Medicine, Faculty of Biological and Veterinary Sciences, Nicolaus Copernicus
11 University in Toruń, Lwowska 1, 87-100 Toruń, Poland

12 ⁴ Department of Plant Physiology, Genetics, and Biotechnology, University of Warmia and Mazury in
13 Olsztyn, 10-229 Olsztyn, Poland

14 ⁵ Department of Infectious, Invasive Diseases and Veterinary Administration, Institute of Veterinary
15 Medicine, Nicolaus Copernicus University in Toruń, Gagarina 7, 87-100 Toruń, Poland

16 ⁶ Department of Cellular and Molecular Biology, Faculty of Biological and Veterinary Sciences,
17 Nicolaus Copernicus University in Toruń, Lwowska 1, 87-100 Toruń, Poland

18 *Corresponding author: Katarzyna Rafińska (katraf@umk.pl)

19
20 **GRAPHICAL ABSTRACT**

21 **ABSTRACT**

22 The present study investigated the effect of zinc and silver nanocomposites based on whey protein (β -
23 lactoglobulin) on wound healing using the C57BL/6J mouse model. Indirectly, a study was conducted
24 to determine the antimicrobial properties of the nanocomposites by determining the minimum inhibitory
25 concentration (MIC) and performing a colony forming unit (CFU) test. The process of wound closure
26 was monitored using a stereoscopic microscope. The Inductively Coupled Plasma-Mass Spectrometer
27 (ICP-MS) was used to analyze the distribution of zinc and silver in the blood and liver to evaluate the
28 process of metal ion absorption through the wound and to estimate potential toxic effects on the body.
29 Transmission electron microscopy (TEM) analysis showed that tested zinc and silver nanocomposites
30 enhances collagen deposition during wound healing. At the same time, only one change observed in
31 hepatocytes after treatment with silver and zinc dressings was the drop in the level of glycogen. Obtained
32 results have given insight into the actions of zinc and silver complexes and have provided a novel
33 direction to study the role of metal ions in hard-to-heal wound regeneration as well the carriers for their
34 releasing.

35

36 **Keywords:** wound healing, zinc, silver, nanocomposites, model C57BL/6J mouse, collagen fibrils,
37 toxicity

38

39 1. INTRODUCTION

40 Regeneration of hard-to-heal wounds is a major therapeutic problem due to the complexity of
41 the process and the lack of effective drugs. Wounds that do not heal are prone to infection and left
42 unresolved; an infected wound can cause amputation or even death. For this reason, scientific efforts are
43 directed toward the search for new compounds with natural origins that could be used as drugs or
44 evaluated for subsequent drug design ¹. For many years, the participation of many metal ions in wound
45 healing has been confirmed, as they play crucial roles in various biological processes, including
46 inflammation, cellular proliferation, and tissue remodeling. One of the key metal ions involved in wound
47 healing is zinc (Zn^{2+}) which is an essential trace element that plays a crucial role in immune function,
48 protein synthesis (extracellular proteins, such as collagen and keratin), and cell division. It is involved
49 in the synthesis and stabilization of the extracellular matrix, as well as in the regulation of enzymes,
50 including metalloproteinases, which are important for wound healing. Silver ions (Ag^+) also have been
51 known to play a role in wound healing, particularly due to their antimicrobial properties. Bacteria
52 occurring in wounds can adversely affect the healing process, hence the increase in multi-resistant
53 strains of bacteria is a cause for concern in the field of wound care. Silver is a useful tool in the treatment
54 of infected wounds; however, the effectiveness of silver-based products depends on the form of silver
55 used and the mechanism of delivery ². It is important to note that the use of zinc or silver ions in wound
56 healing should be carefully considered and monitored, as excessive exposure can be toxic. Therefore,
57 the use of protein-ion complexes that will control the level of metal ions in the wound may be a good
58 solution.

59 In our previous studies we have developed the methods for synthesis metal ions – protein
60 complexes which exhibit different biological activities. Buszewski et al. in their work indicated the
61 inhibitory effect of Zn^{2+}/ZnO -OVA hybrid complex based on egg white ovalbumin (OVA) against yeast
62 strain *Candida albicans ATCC10231* and bacteria *Acetivobacter baumannii ATCC1605*, *Klebsiella*
63 *pneumonia ATCC10031*³. The results obtained by Pomastowski et al. also demonstrate that the
64 synthesized silver-lactoferrin hybrid complex can be used as an economical and environmentally
65 friendly antimicrobial agent ⁴. So far, we have focused on the immobilization of zinc (Zn^{2+}) ⁵ and silver
66 (Ag^+) ⁶ ions on β -lactoglobulin (β LG), which is a small globular protein present in whey (a waste product
67 of milk production). Zn^{2+} adsorption on β LG was aimed at obtaining metal complexes ($Zn\beta$ LG). In turn,
68 as a result of the Ag^+ ion adsorption, reduction process was taking place and apart from the $Ag\beta$ LG
69 metal complex, silver nanoparticles (Ag NPs) were obtained, creating a hybrid system
70 ($Ag\beta$ LG/ Ag NPs β LG). It turns out that depending on the structure of the protein itself as well as on the
71 type of metal, its oxidation state, coordination numbers, and geometry, an infinite number of structures

72 and conformations can be obtained, which have an impact on further properties of the particular
73 complex/hybrid system ⁷.

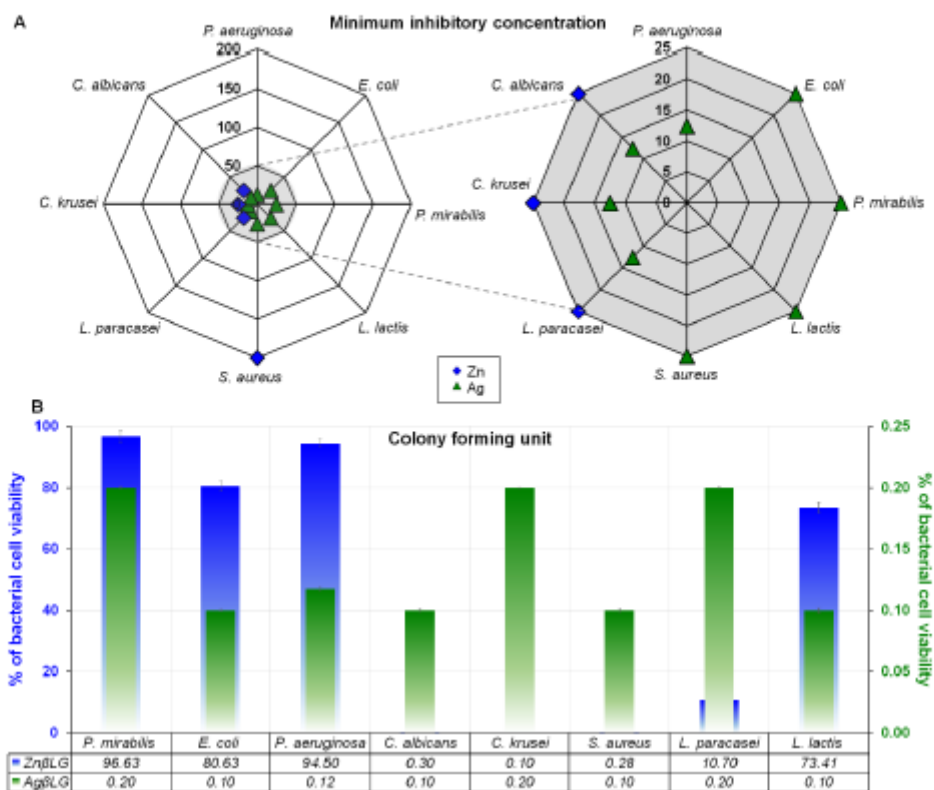
74 The present work is focused on determining the effect of synthesized metal-protein complexes:
75 Zn- β -lactoglobulin (Zn β LG) and Ag- β -lactoglobulin (Ag β LG) as potential antimicrobial agents on the
76 wound healing process based on an animal model (C57BL/6J mice). The antimicrobial properties of the
77 tested nanocomposites against microorganisms isolated from bedsores, diabetic foot and they were
78 studied by determining minimum inhibitory concentration (MIC) and colony-forming unit (CFU) test.
79 In addition, the degree of zinc and silver accumulation in blood and liver was determined which allowed
80 indirectly to estimate the toxicity of used composites. We also studied the effect of the complexes on
81 wound healing and liver function at the ultrastructural level.

82 2. RESULTS

83 2.1. Antimicrobial potential of nanocomposites

84 For the study, four pathogens isolated from the bedsores, that are the cause of delayed healing
85 and infections occurring in acute and chronic wounds were selected, such as *Staphylococcus aureus*,
86 *Pseudomonas aeruginosa*, *Proteus mirabilis*, and *Escherichia coli*. Successively, isolated from chronic
87 wounds were fungi including *Candida albicans* and *Candida krusei*, which cause fungal infections in
88 immunocompromised patients⁸. Also, two probiotic lactic acid bacteria (LAB) *Lactococcus paracasei*,
89 *Lactococcus lactis*, producing lactic acid, which is the end product of carbohydrate fermentation. They
90 have health-promoting properties and also inhibit the growth of pathogenic microorganisms by showing
91 strong antibacterial properties⁹. For the Zn β LG complex, after 24 h incubation, for two fungal strains
92 (*C. krusei*, *C. albicans*) and the probiotic strain *L. paracasei*, the MIC value was 25 μ g/mL. Specific
93 activity was noted for *S. aureus* whose MIC was 200 μ g/mL isolated from the bedsores (Fig. 1A). On
94 the other hand, MIC of Ag β LG for pathogens such as *E. coli*, *P. mirabilis*, *L. lactis* and *S. aureus* was
95 25 μ g/mL. Ag β LG complexes also presented greater inhibitory activity against *L. paracasei*, *C. krusei*,
96 *C. albicans* and *P. aeruginosa* with MIC 12.5 μ g/mL (Fig. 1A).

97

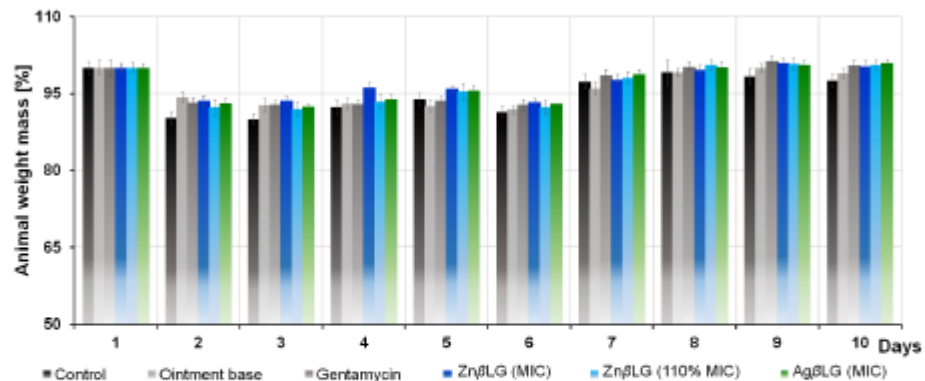


98
99 **Fig. 1.** Radar charts showing the full profile of the tested microorganisms treated with the synthesized zinc
100 complexes –ZnβLG and silver complexes –AgβLG: Minimum Inhibitory Concentration expressed in µg/mL (A),
101 expressed as colony forming unit [%] (B).

102 Furthermore, the experimental MIC values agreed with the CFU/mL values for each strain
103 treated with the zinc and silver complexes (Fig. 1B). In the case of ZnβLG complex, the inhibition did
104 not even reach 50%. However, for AgβLG complexes, inhibition occurred in 99% against all
105 microorganisms.

106 2.2. Animal behavior and body weight of mice

107 During the observation period of the wound closure process, uncommon behavior of the mice
108 was observed in the first four days. The animals showed lack of appetite, anemic behavior, and no desire
109 to integrate. The mice's integration behavior, willingness to play, acclimatization and scratching at the
110 bandage areas occurred in the second half of the experiment starting on the fifth day. Importantly, on all
111 days of the experiment, the mice's behavior was correlated with their body weight characterized by
112 weight loss up to the sixth day of the experiment (Fig. 2).



113

114 **Fig. 2.** Body weights of animals represented in % depending on the day and the type of preparation used.

115

116

117

118

119

120

121

122

123

124

125

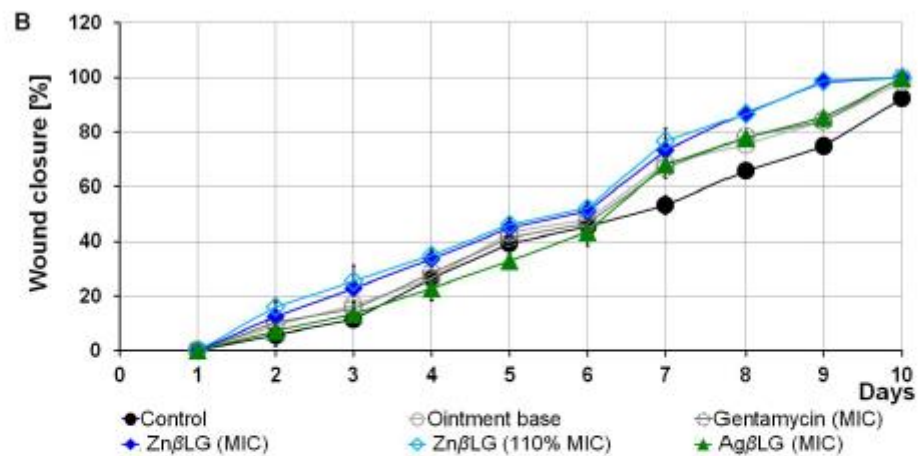
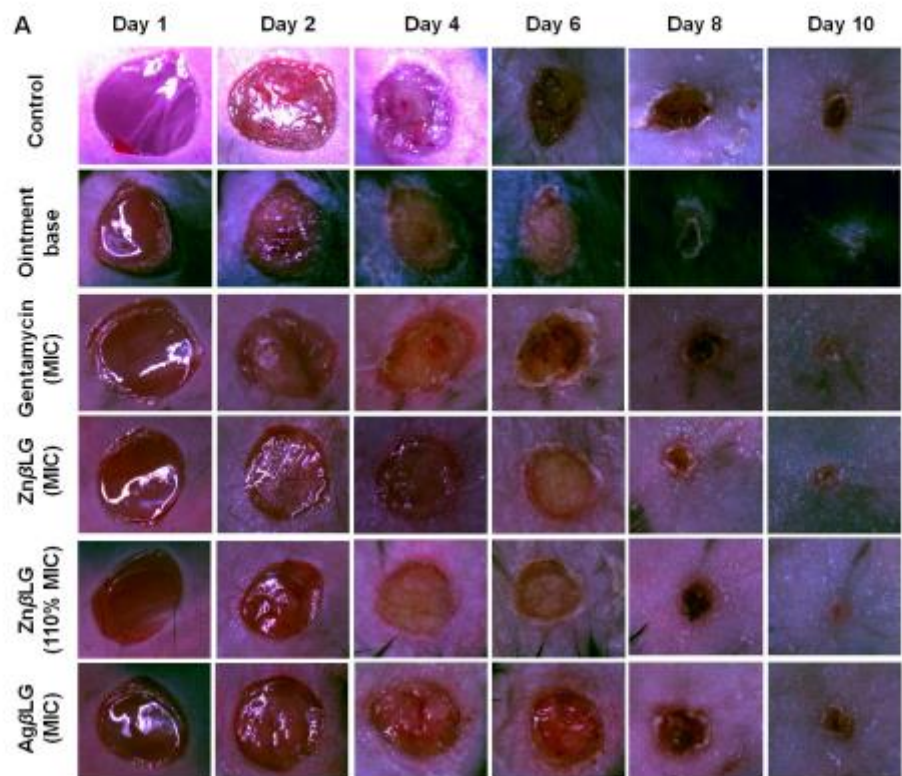
126

127

From the sixth day of observation, the animals' body weight began to increase, which was associated with gradual regeneration. The rodents reached their initial body weight on the eighth day of observation. In the case of the applied nanocomposites, the regeneration process occurred faster compared to the control. The change in weight and unnatural behavior of the mice in the present experiment may be the result of limited physical movement and discomfort after dressing application and itching of the wound site. The application of nanocomposites to wounds allowed observation of hair regrowth in contrast to controls. The nanocomposites showed a similar effect (hair regrowth) to gentamicin. This suggests that nanocomposites could be considered potential agents for treating hard-to-heal wounds.

2.3. Effect of nanocomposites on wound healing process, ANOVA analysis

On each day of observation, three independent measurements were taken of wound surface volume, which are presented as the mean \pm SD. Fig. 3 shows the process of wound closure. The ANOVA test showed no statistically significant differences in all study groups ($p = 0.591$).



128

129 *Fig. 3.* Wound closure in relation to the applied preparation (A), and wound volume as a percentage of closure
 130 area in reference to the wound size on the first day of the experiment (B).

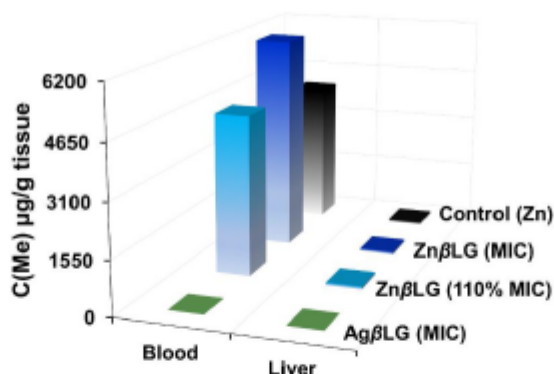
131

The results indicate a gradual process of wound closure. An increased regeneration effect of
 132 about 30% occurred as early as the fourth day. For mice treated with zinc complexes of both ZnβLG
 133 (MIC) and ZnβLG (110% MIC), wound closure took place at about 50% on the sixth day already. For

134 the same day, the Ag β LG complex (MIC) had a slightly weaker effect, with a wound healing rate of
 135 about 40% and an effect worse than the control (45%). From day seven, for all complex's, significantly
 136 faster wound closure was observed at about 73% for Zn β LG (MIC) and 77% for Zn β LG (110% MIC),
 137 so Zn β LG (110% MIC) showed a better effect. In contrast, wound closure was about 68% for Ag β LG
 138 (MIC) complex. Similar observations were noted for gentamicin, which is an antibiotic often used to
 139 treat hard-to-heal wounds. The above values (day seven) indicate that the complexes performed much
 140 better in contrast to the control, for which the wound remained slightly open. Complete wound closure
 141 (approximately 100%) for the zinc and silver complexes occurred on the tenth day compared to the
 142 control, for which the wound remained open. The results indicate that a period of ten days is sufficient
 143 for diabetic wounds to heal.

144 2.4. Distribution of zinc and silver in tissues

145 The distribution of metals (Zn, Ag) in organs after treatment with Zn β LG (MIC), Zn β LG (110%
 146 MIC), and Ag β LG (MIC) nanocomposites was assessed by ICP-MS (Fig. 4). The use of a zinc dressing
 147 Zn β LG (MIC) and Zn β LG (110% MIC) increased the level of this element in the blood compared to the
 148 level in control tissue. However, the level of zinc in the liver was comparable to the level in the liver of
 149 control mice. In presented study, the level of silver after treatment with Ag β LG (MIC) in both blood
 150 and liver were at similar very low level.



151

152

Fig. 4. Zinc and silver concentrations in liver and blood samples.

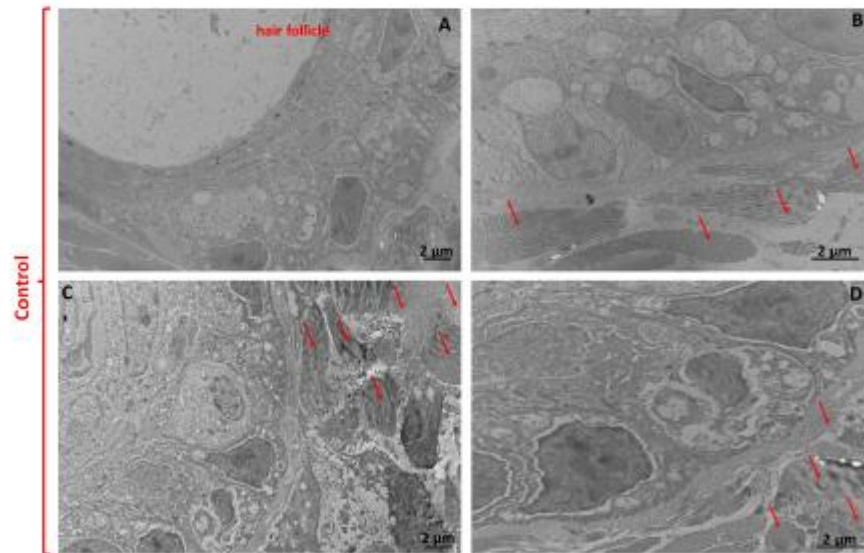
153

2.5. Microscopic studies

154

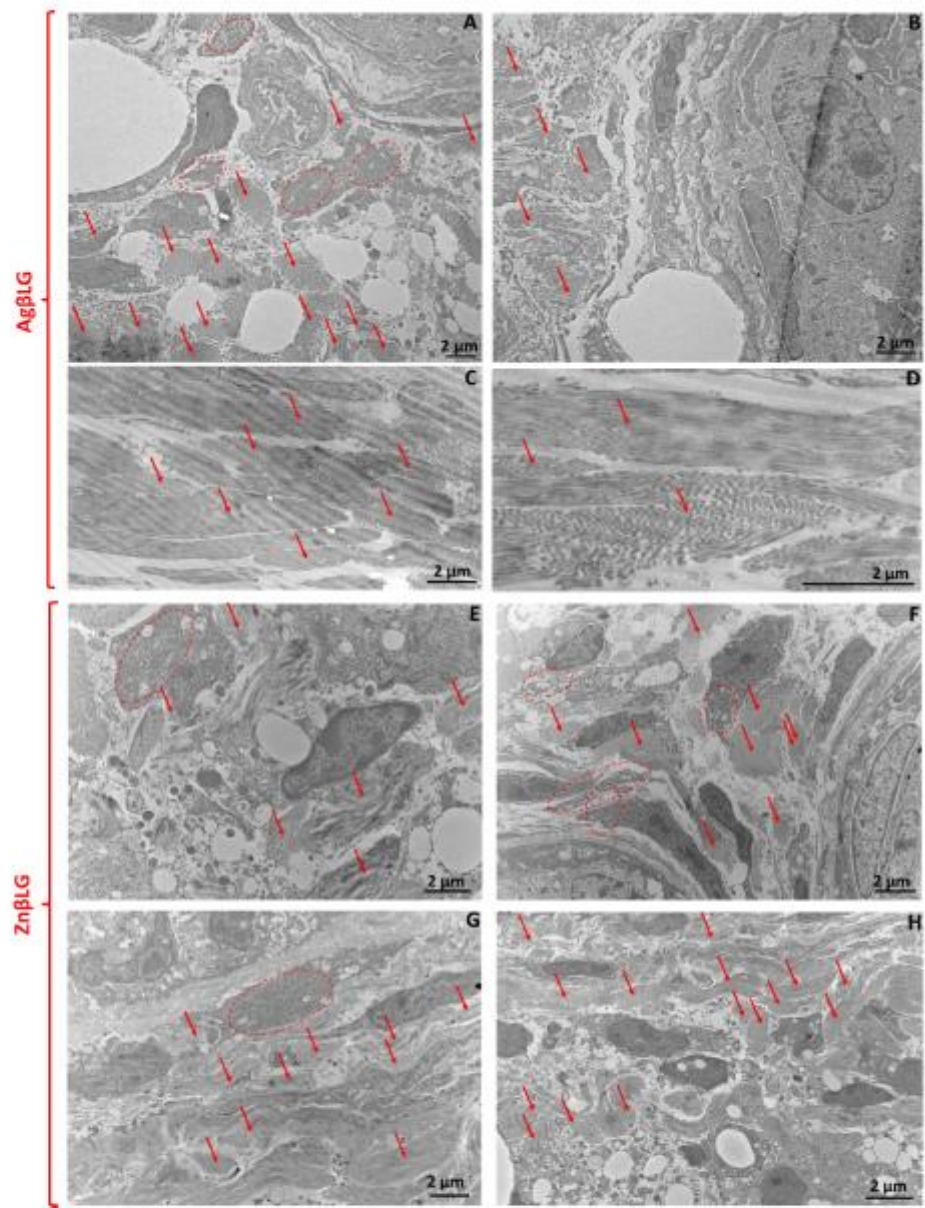
The aim of microscopic observations was to check the effect of the applied composites on the
 155 structure of the scar. Under histological evaluation, healed wounds from all tested groups were similar
 156 with almost normal hair follicles. Micrograph of a section of a 10-day wound show organization of
 157 collagen fibrils. In the control sections of the skin, small clusters of collagen fibers are visible. Cells that
 158 make up the hair follicle have the correct structure (Fig. 5 A-D). In the skin in which healing was
 159 supported by Ag β LG, the amount of collagen fibrils was higher. Similarly, their clusters were also larger
 160 and the arrangement more compact (Fig. 6 A-D). A similar structure was visible in skin sections, the

161 healing of which was supported by ZnβLG. In this group, fibroblasts with a large amount of rough
162 endoplasmic reticulum were also visible, which may indicate still very active synthesis of extracellular
163 matrix proteins for the progressing healing process (Fig. 6 E-H).
164



165
166
167
168
169
170
171
172
173
174
175
176

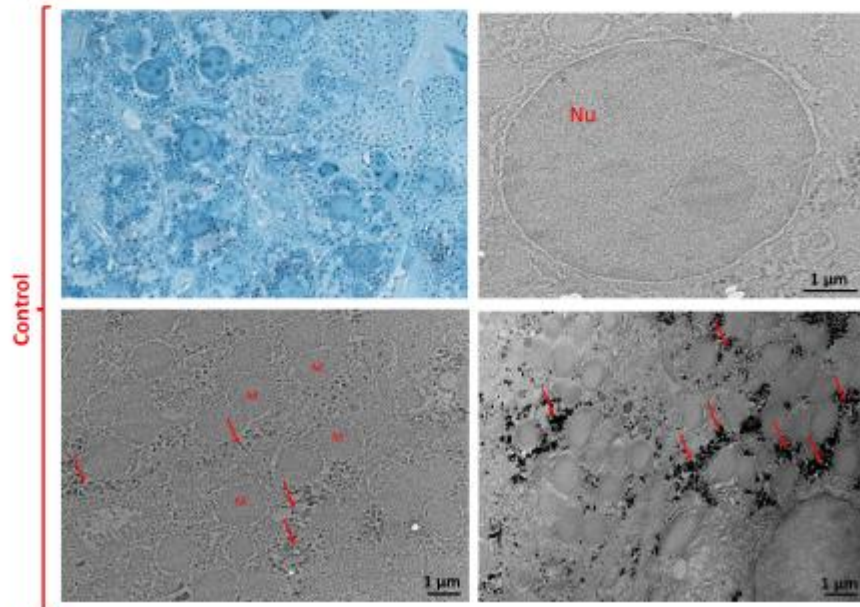
Fig. 5. Micrograph of a section of a 10-day control wound without treatment with ZnβLG and AgβLG. A – normal hair follicle; B, C, D – collagen fibrils marked with arrows.



177
 178
 179
 180
 181
 182
 183

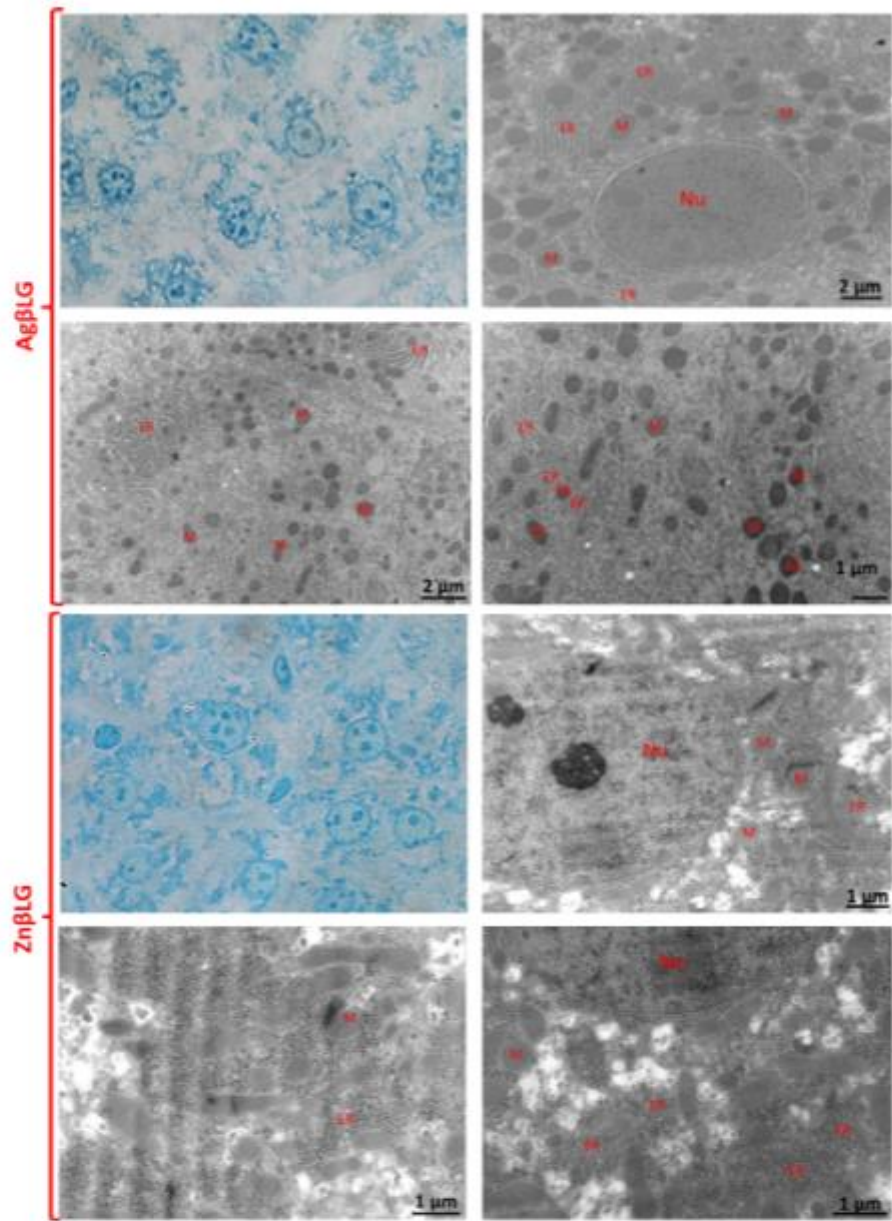
Fig. 6. Micrograph of a section of a 10-day wound treated with AgβLG (A-D) and ZnβLG (E-H). Area of intensive collagen fibrils synthesis is marked with a red border. Collagen fibrils are marked with arrows.

184 Sections of liver taken from control animals showed normal hepatocytes with smooth and rounded
185 nucleus in which uniform euchromatin as well as nucleolus is present (*Fig. 7*). Glycogen deposits are
186 visible in the cytoplasm, near the smooth endoplasmic reticulum (SER). Mitochondria are also
187 interspersed in this area.



188
189 *Fig. 7.* Micrograph of a section of liver from control mice Glycogen aggregates are marked with arrows,
190 Nu – nucleus, M – mitochondrium.

191
192 In liver section from mouse treated with Zn β LG and Ag β LG, only minor changes were registered.
193 Nuclei still had regular round shape and inside the main fraction of chromatin is euchromatin. Many
194 mitochondria were located between endoplasmic reticulum membranes. The only significant difference
195 was the lack of glycogen deposits (*Fig. 8*).
196



197

198

199

200

201

202

203

Fig. 8. Micrograph of a section of a liver in mice with 10-day wound treated with AgβLG and ZnβLG. Area of intensive collagen fibrils synthesis is marked with a red border. Nu – nucleus, M – mitochondrium, ER – endoplasmic reticulum.

204 3. Discussion

205 Wound dressings have been conventionally used to protect the wound from external
206 contamination, but they can also be functionalized with a variety of therapeutic complexes that are
207 delivered to the wound site. Most traditional dressings (cotton bandages, cotton wool) have no active
208 function in the healing process, but sophisticated dressings can be developed to participate in this process
209 by incorporating active ingredients. Integrated complexes should play a vigorous role in the wound
210 healing process by aiding in the removal of necrotic tissue, preventing or treating infection, or both.
211 Therefore, dressings have the potential to be functionalized with multiple classes of antibiotics or other
212 compounds that display antimicrobial properties (metal-protein complexes)¹⁰. Overuse of antibiotics
213 has caused them to lose their effectiveness in treating serious bacterial infections. Infection of chronic
214 wounds with antibiotic-resistant bacterial pathogens results in slower wound healing, therefore the use
215 of effective antibiotic therapy or the search for new therapeutic agents with antimicrobial properties is
216 recommended as part of treatment strategies¹¹. The exposed subcutaneous tissue is a favorable substrate
217 for a wide range of microorganisms to grow and colonize in it.

218 It is challenging to compare the obtained results to published data. To the best of our knowledge,
219 this research is pioneering and there is still a lack of wide knowledge regarding the biological effect of
220 nanocomposites, composed of protein and metal. To date, two major preparations which are applied for
221 the healing process are zinc oxide nanoparticles (ZnONPs) and silver nanoparticles (AgNPs)^{12, 13}.

222 The biological action of silver nanoparticles is complex, involving secondary oxidation and
223 interaction with bacterial proteins, causing destabilization and cell organelle disintegration.
224 Nanocomplexes function similarly, but exhibit lower cytotoxicity towards eukaryotic cells¹³. When
225 metals bind to proteins, they reduce toxicity to eukaryotic cells while maintaining antibacterial effects.
226 Zinc oxide has demonstrated antibacterial, antioxidant, and anti-inflammatory properties, promoting cell
227 migration, angiogenesis, and re-epithelialization - all crucial for wound healing. Studies indicate that
228 cellulose-zinc oxide nanocomposites and collagen and zinc oxide dressings can enhance wound healing
229 and demonstrate no toxicological effects on human cells^{14, 15}. PLGA/silk fibroin-based membranes
230 loaded with ZnO nanoparticles further improve wound healing in animal models by boosting re-
231 epithelialization, granulation tissue formation, collagen deposition, and angiogenesis¹⁶.

232 Silver nanoparticles are widely used in biomedical applications such as wounds healing with
233 different etiology, especially in burn wounds^{13,17,18}, diabetic wounds¹⁹, topical creams and antiseptic
234 sprays¹³ as an antibacterial, antifungal and antiviral agent preparation with an anti-inflammatory effect
235 or therapeutics for cancer⁴. However, there is still a lack of publication regarding the use of
236 metalocomposites as preparations with potential therapeutic effects, there are some papers regarding the
237 fixation of AgNPs with alginate or nicotinamide¹⁹.

238 In our study, we have proved that especially AgβLG shows antibacterial effect against clinical
239 bacterial strains isolated from bedsores *S. aureus*, *P. aeruginosa*, *P. mirabilis*, and *E. coli* as well against
240 fungi isolated from chronic wounds *C. albicans* and *C. krusei*. Moreover, the level of silver after

241 treatment with Ag β LG (MIC) in both blood and liver were at similar very low level. The concentrations
242 of silver found in human tissues are extremely low²⁰. In our earlier work, insignificant traces of silver
243 were registered in both blood and liver samples, which were 9.3 $\mu\text{g/g}$ and 0.022 $\mu\text{g/g}$, respectively²¹. In
244 a study of the viability of peripheral blood mononuclear cells (PBMCs) following treatment of a mouse
245 model with an external preparation of LBPC-AgNCs, cell viability was estimated to be very high >97%
246 despite the fact that small amounts of silver were recorded in the blood and liver.

247 Our studies confirmed that Ag β LG can positively affect the organization of collagen fibrils
248 during wound healing. This is still a small scope of research concerning the effect of silver on collagen
249 fibrils deposition and should be expanded in the future, taking into account such factors differentiating
250 silver nanoparticles and nanocomplexes as their size, charge, coverage and stability. It is also important
251 to correlate the progress in wound healing with the level of released silver ions and potential
252 cytotoxicity. Earlier, studies by Tian et al. also evidenced that AgNPs are involved in regulation of
253 collagen deposition which results in excellent alignment in the wound healing process¹⁸. The conducted
254 research shows that the presence of metal nanoparticles may have a positive effect on wound healing
255 not only by preventing bacterial infections but also by stimulating collagen synthesis. However, further
256 experiments are needed to confirm this effect. Limited research so far indicate that AgNPs suppresses
257 the proliferation of fibroblasts but they can induce their differentiation and maturation. Studies by Liu
258 et al. indicated that AgNPs can enhance differentiation of fibroblasts into myofibroblasts that are
259 involved in collagen fibers production²². Birk and Trelstadh postulate that procollagen is secreted and
260 gained in vesicles on the exterior of the cell and then transformed into collagen fibrils²³. Detailed studies
261 by Kwan et al. showed that in wounds treated with AgNPs better spatial distribution of collagen can be
262 observed which is connected with mechanical properties of healed skin²⁴. Also You et al. also showed
263 that silver nanoparticles in collagen/chitosan scaffolds promote fibroblast migration²⁵.

264 In our study similar effect as for Ag β LG was visible for wound healed with Zn β LG. In these
265 tissue sections, a large number of fibroblasts with an extensive membrane system was visible, which
266 may indicate an intensive synthesis of extracellular matrix components. This is one of the first evidence
267 of the impact of Zn on collagen organization. Up to now only Khan et al. showed by Masson's trichrome
268 staining that wounds treated with PLGA/silk fibroin based electrospun membrane loaded with zinc oxide
269 nanoparticles exhibited a higher quantity of collagen with the better organization¹⁶. Zinc can play a
270 multifaceted role in collagen fibril organization in wounds through its involvement in enzyme function,
271 gene expression, direct interactions with collagen, and antioxidant properties. Zinc ions can directly
272 interact with collagen molecules, stabilizing their triple-helical structure and promoting the formation
273 of collagen fibrils. This interaction may contribute to the organization of collagen fibrils within the
274 extracellular matrix. Adequate zinc levels are vital for maintaining the structural integrity and function
275 of connective tissues in the body. However, more studies are needed to confirm the effect of zinc on
276 fibroblast viability, their differentiation and organization of collagen fibrils.

277 The correct morphology of liver cells from mice treated with Ag β LG and Zn β LG indicate that
278 applied concentrations of nanocomposites are not very toxic. However, the hepatocytes of these
279 animals were characterized by the lack of glycogen deposits in the cytoplasm. Similar effect was
280 observed in mice with elevated levels of heavy metals such as lead, cadmium or zinc²⁶. It indicates that
281 even low levels of silver ions or elevated level of zinc ions in the liver can lead to changes at the
282 molecular level which have impact on different metabolic pathways for example through pathway
283 involving Glycogen synthase kinase 3 (GSK-3).

284 4. Methods

285 Antimicrobial potential of nanocomposites

286 Antimicrobial properties were studied by minimum inhibitory concentration (MIC) and by
287 performing colony forming unit (CFU) assay. All investigated nanocomposites in present study have
288 been previously synthesized, characterized and described by our group in 5, 6. The synthesized zinc
289 (Zn β LG) and silver (Ag β LG) complexes based on whey protein β -lactoglobulin (β LG) were subjected
290 to kinetic and isothermal studies to understand the mechanism and nature of complex formation. An
291 important difference is that in the case of the Ag β LG complex, a metallocomplex was obtained with the
292 formation of silver nanoparticles (AgNPs) due to the spontaneous reduction of silver ions – this
293 contributed to the formation of the Ag β LG/AgNPs β LG hybrid, which was not observed in the case of
294 immobilization of Zn²⁺ ions into the protein. The formed spherical AgNPs of 5 nm size were
295 characterized by homogeneous dispersion.

296 In the present investigation, zinc and silver complexes based on whey proteins: Zn- β -
297 lactoglobulin (Zn β LG) and Ag- β -lactoglobulin (Ag β LG) were tested against different microorganisms
298 from the collection of the Centre for Modern Interdisciplinary Technologies (Nicolaus Copernicus
299 University, Toruń: (I) *Proteus mirabilis* PX 220 86112 MLD, (II) *Escherichia coli* MB 11464 1 CHB,
300 (III) *Pseudomonas aeruginosa* DSM 5007717 HAM, (IV) *Staphylococcus aureus* ATCC 33591 THL –
301 isolated from the bedsores, (V) *Candida albicans* ATCC 10231 THL, (VI) *Candida krusei* CBS 2107
302 CBS – isolated from the diabetic foot, (VII) *Lactobacillus paracasei* DSM 2649 DSM, (VIII)
303 *Lactococcus lactis* ATCC 10231 – isolated from whey.

304 The study was performed in Miller Hilton (MH) broth medium according to Clinical and
305 Laboratory Standards Institute (CLSI) procedures (with appropriate modifications) and by microdilution
306 in 96-well plates using resazurin. In the first step, bacterial cells were inoculated in MH broth medium
307 and incubated for 24 h at 37°C. Zinc and silver complexes were also prepared in MH medium by serial
308 dilution method in the concentration range of 200–6.25 μ g/mL. Subsequently, the cultured bacterial
309 strain (1×10^6 CFU/mL) and different concentrations of complexes were introduced into 96-well plates
310 (Sigma Aldrich, Poznań, Poland) in a 1:1 ratio. After mixing, 12 μ l of the redox indicator resazurin
311 (Sigma-Aldrich, St. Louis, MO, USA) was added to each well. All samples were prepared in triplicate.
312 The samples thus prepared were incubated for 24 h at 37°C. The MIC value was visually determined by

313 the color change of resazurin from blue to pink. The lowest concentration at which no color change was
314 observed was considered as the MIC value.

315 The CFU assay procedure was similar to the MIC assay, except that after the incubation period,
316 various dilutions of the bacterial suspension were prepared and then 100 μ l of each sample was
317 transferred to TSA tryptone-soy agar plates incubated at 37°C for 24 h and then the colonies were
318 counted manually.

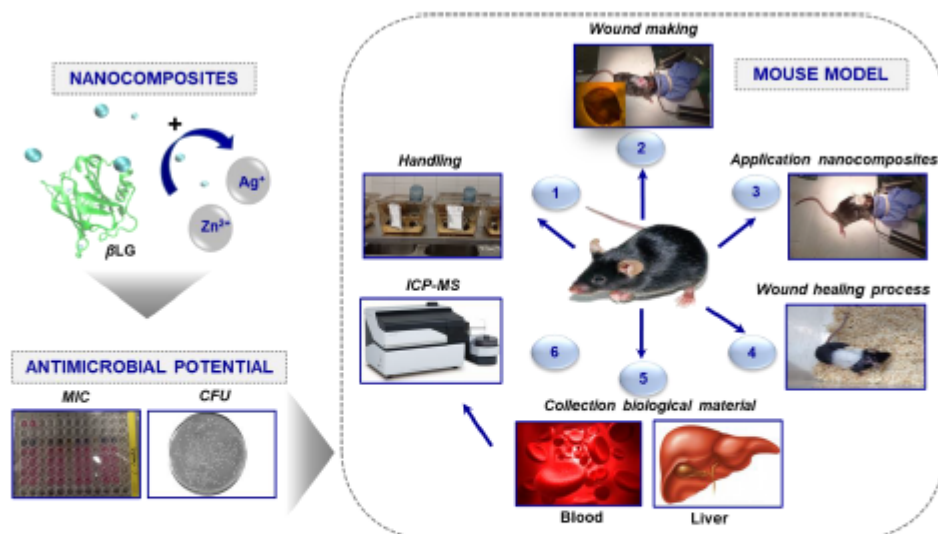
319 Animal model

320 In the present study, C57BL/6J mice aged 7–8 weeks were obtained from the Tri-City Academic
321 Animal Laboratory and Service Center at the Medical University of Gdansk and divided into 8 animals
322 in each group with an average weight of 21.53 ± 1.59 g. Groups were observed for ten days. All the
323 experimental procedures were approved by the Local Animal Care and Use Committee in Bydgoszcz
324 (BYD 21/2021, 26.04. 2021).

325 Wound healing process – determination of acclimatization and body weight of mice,
326 ANOVA analysis, wound formation, liver and blood organ collection

327 The procedure of the conducted experiment was carried out in six steps: (I) handling (adaptation
328 for the laboratory condition in a period of 2 weeks), (II) wound formation, (III) application of an agent
329 with potential therapeutic properties, (IV) observation of the wound healing process, (V) collection of
330 biological material and euthanasia, (VI) analysis of zinc and silver distribution in tissues. The steps have
331 been shown in Fig. 9.

332



333

334 Fig. 9. Schematic representation of the experimental design.

335 First step of experiment covered the acclimatization of animals to the laboratory conditions. For
336 this purpose, the animals were placed in cages according to the minimum living area for a single

337 individual and kept under controlled environmental conditions with air temperature of 20–24°C,
338 humidity of $55 \pm 10\%$, rate of air exchange in the room of 15–20 changes/1h; an automated light cycle
339 with a sequence of 12h light/12h darkness. Animals had provided access to food and water ad libitum.
340 In the second step of the study, mice were given anesthesia with isoflurane (5%) by inhalation (flow rate
341 of 3.5 l/min) (Combi-Vet Anesthesia Machine Rothacher-Medical GmbH, Bern, Switzerland). The state
342 of anesthesia was maintained by continuous inhalation of isoflurane at a concentration of 3%. To create
343 a wound, the skin on the back of the mouse was shaved and then disinfected with 70% ethanol. Round
344 wounds (6 mm) were created by cutting the skin with surgical scissors. Each wound was measured and
345 inspected at 10-day follow-up. In addition, photographic documentation was performed using a cold-
346 light stereoscopic microscope (100 W-MST 132 Lab, Optika microscopes, Italy). During the third step,
347 synthesized zinc and silver complexes were applied to the wounds once a day. The formulation was
348 prepared according to the previous study 13 considering the minimum inhibitory concentration (MIC)
349 – gentamicin 30 $\mu\text{g}/\text{mL}$ (according to our previous studies 14), Ag β LG 25 $\mu\text{g}/\text{mL}$ and Zn β LG 200
350 $\mu\text{g}/\text{mL}$. For zinc complexes, both 100% MIC and 110% MIC were tested. After application, the wound
351 was covered with a sterile plaster to reduce the risk of wound infection. In the fourth step, the effect of
352 the applied complexes was monitored by measuring the weight and assessing wound closure using a
353 stereoscopic microscope connected to a cold light source (100 W-MST 132 Lab, Optika microscopes
354 Italy, Italy). Percentage of wound closing was calculated in accordance to the equation: $V [\%] =$
355 $(V_{\text{day},n}/V_{\text{day},1}) * 100\%$. A free-to-access platform ([https://goodcalculators.com/one-way-anova-](https://goodcalculators.com/one-way-anova-calculator/)
356 [calculator/](https://goodcalculators.com/one-way-anova-calculator/)[%20accessed%2017.10.2022](https://goodcalculators.com/one-way-anova-calculator/)) was used to show changes. The fifth step involved the
357 collection of biological material (blood, liver) for ICP-MS analysis. The collected liver samples were
358 frozen and stored at -80 °C to deactivate the enzymatic reaction. Blood, in turn, was collected into a tube
359 with the anticoagulant sodium citrate (3.2%). At the end of observation, the animals were euthanized by
360 intraperitoneal injection of 18% sodium pentobarbital (200 mg/ml), at a dose of 200 mg/kg. Finally (step
361 six), the amount of zinc and silver in the collected samples was determined.

362 **Ethics statement**

363 All procedures complied with the regulations covering animal experimentation within EU
364 (European Communities Council DIRECTIVE 2010/63/EU), reported in accordance with ARRIVE
365 guidelines and were approved by the Local Animal Care and Use Committee in Bydgoszcz (BYD
366 21/2021, 26.04. 2021).

367 368 **Accumulation of zinc and silver in liver tissue and blood samples – Inductively Coupled 369 Plasma-Mass Spectrometry (ICP-MS)**

370 In order to quantify the concentration of zinc and silver ions in liver and blood tissue samples, an
371 ICP-MS technique (Shimadzu ICP-MS 2030, Shimadzu, Kyoto, Japan) with a collision cell with a
372 helium flow rate of 6 mL/min was used. Both liver and blood were preheated for 4 h at 80°C using a
373 thermomixer (Thermomixer comfort, Eppendorf SE, Hamburg, Germany) in 150 μL HNO₃ (1%)

374 (Merck Suprapure, Merck, Darmstadt, Germany). Determinations were made for $^{66,67}\text{Zn}$ and ^{45}Sc ,
375 ^{107}Ag and ^{103}Rh , as an internal standard, using the external calibration method in three repetitions.

376 Microscopic analysis

377 The experimental material was fixed in 2% paraformaldehyde and 2.5% glutaraldehyde in 0.1 M
378 phosphate (pH 7.4) for 2 hours, washed in buffer and then dehydrated in an ethanol series: 30, 50, 70,
379 90, 96 and 100% in each for 10 minutes. The step of post-fixation in OsO_4 was omitted due to the
380 possibility of measuring the silver or zinc content by EDS. The tissues were then embedded in LR White
381 resin according to standard protocol and sectioned on an ultramicrotome (Leica Ultracut UC7). Finally,
382 ultrathin sections were stained with 2.5% uranyl acetate and 0.4% lead citrate solutions, and examined
383 on a JEOL 1010 transmission electron microscope at 80 kV.

384 Data availability

385 The datasets used and analysed during the current study available from the corresponding author
386 on reasonable request.

387 CONCLUSION

388 The obtained complexes with antibacterial properties can be counted as an inexpensive method
389 for the treatment of hard-to-heal wounds. The wounds were reduced and healed in a relatively fast time
390 for the tested mice. Especially valuable is observation that $\text{Ag}\beta\text{LG}$ and $\text{Zn}\beta\text{LG}$ may have a positive
391 effect on the organization of collagen fibrils, and at the same time they do not show toxic properties in
392 relation to tissues. The obtained results are promising and may illustrate the potential therapeutic
393 properties of the preparations.

394

395 Credit authorship contribution statement

396 A.R.: Conceptualization, Methodology, Investigation – obtaining $\text{Zn}\beta\text{LG}$ and $\text{Ag}\beta\text{LG}$ complexes,
397 testing the antimicrobial properties of the complexes by MIC and CFU, carrying out studies of the
398 wound healing process, Writing – Original Draft, Visualization, Data curation. P.P.: Conceptualization,
399 Funding acquisition, Project administration, Writing – Review & Editing. M.B.F.: Investigation –
400 carrying out studies of the wound healing process, Writing – Original Draft. V.R.: Methodology,
401 Investigation – testing the antimicrobial properties of the complexes by MIC and CFU, Writing –
402 Review & Editing, Visualization. A.G.: Investigation – quantify the concentration of zinc and silver
403 ions in liver and blood tissue samples (ICP-MS) B.B.: Supervision, Resources. K.N.: Investigation –
404 microscopic study. K.R.: Investigation – microscopic study, Writing – Original Draft (microscopic
405 study).

406 Acknowledgements

407 This work was financially supported by the National Science Centre within the framework of Opus 14
408 project No. 2017/27/B/ST4/02628 (2018-2021). K.R., P.P. and B.B. are members of Toruń Center of
409 Excellence “Towards Personalized Medicine” operating under Excellence Initiative-Research
410 University and V.R., M.B.F. are member of Emerging Fields “One Health – antimicrobial stewardship

411 in human and veterinary medicine” operating under Excellence Initiative-Research University.

412

413 Conflict of interest

414 There are no conflicts of interest regarding this paper.

415

416 References

- 417 1. Santos, A. F. et al. Study of the antimicrobial activity of metal complexes and their ligands
418 through bioassays applied to plant extracts. *Revista Brasileira de Farmacognosia* 24, 309–315 (2014).
- 419 2. Graham, C. The role of silver in wound healing. *British Journal of Nursing* 14, 22–28 (2005).
- 420 3. Buszewski, B. et al. Interactions of zinc aqua complexes with ovalbumin at the forefront of the
421 Zn²⁺/ZnO-OVO hybrid complex formation mechanism. *Applied Surface Science* 542, 148641 (2021).
- 422 4. Pomastowski, P. et al. Silver-Lactoferrin Nanocomplexes as a Potent Antimicrobial Agent.
423 *Journal of the American Chemical Society* 138, 7899–7909 (2016).
- 424 5. Rodzik, A. et al. The influence of zinc ions concentration on β -lactoglobulin structure -
425 physicochemical properties of Zn- β -lactoglobulin complexes. *Journal of Molecular Structure* 1268, 1–
426 10 (2022).
- 427 6. Rodzik, A. et al. Study on silver ions binding to β -lactoglobulin. *Biophysical Chemistry* 291, 1–
428 12 (2022).
- 429 7. Claudel, M., Schwarte, J. V. & Fromm, K. M. New Antimicrobial Strategies Based on Metal
430 Complexes. *Chemistry* 2, 849–899 (2020).
- 431 8. Jud, P. et al. Invasive *Candida krusei* infection and *Candida* vasculitis of a leg ulcer in an
432 immunocompetent patient: A case report. *International Journal of Infectious Diseases* 55, 96–98 (2017).
- 433 9. Yerlikaya, O. Probiotic potential and biochemical and technological properties of *Lactococcus*
434 *lactis* ssp. *lactis* strains isolated from raw milk and kefir grains. *Journal of Dairy Science* 102, 124–134
435 (2019).
- 436 10. Negut, I., Grumezescu, V. & Grumezescu, A. M. Treatment strategies for infected wounds.
437 *Molecules* 23, 1–23 (2018).
- 438 11. Khalim, W., Mwesigye, J., Tungotoyo, M. & Twinomujuni, S. S. Resistance pattern of infected
439 chronic wound isolates and factors associated with bacterial resistance to third generation
440 cephalosporins at Mbarara Regional Referral Hospital, Uganda. *PLoS ONE* 16, 1–12 (2021).
- 441 12. Zhai, M., Xu, Y., Zhou, B. & Jing, W. Keratin-chitosan/n-ZnO nanocomposite hydrogel for
442 antimicrobial treatment of burn wound healing: Characterization and biomedical application. *Journal of*
443 *Photochemistry and Photobiology B: Biology* 180, 253–258 (2018).
- 444 13. Rahimi, M. et al. Carbohydrate polymer-based silver nanocomposites: Recent progress in the
445 antimicrobial wound dressings. *Carbohydrate Polymers* 231, 115696 (2020).
- 446 14. Khalid, A., Khan, R., Ul-Islam, M., Khan, T. & Wahid, F. Bacterial cellulose-zinc oxide
447 nanocomposites as a novel dressing system for burn wounds. *Carbohydrate Polymers* 164, 214–221
448 (2017).
- 449 15. Balaure, P. C. et al. In vitro and in vivo studies of novel fabricated bioactive dressings based on
450 collagen and zinc oxide 3D scaffolds. *International Journal of Pharmaceutics* 557, 199–207 (2019).

- 451 16. Khan, A. ur R. et al. Exploration of the antibacterial and wound healing potential of a PLGA/silk
452 fibroin based electrospun membrane loaded with zinc oxide nanoparticles. *Journal of Materials*
453 *Chemistry B* 9, 1452–1465 (2021).
- 454 17. Wasef, L. G. et al. Effects of Silver Nanoparticles on Burn Wound Healing in a Mouse Model.
455 *Biological Trace Element Research* 193, 456–465 (2020).
- 456 18. Tian, J. et al. Topical delivery of silver nanoparticles promotes wound healing. *ChemMedChem*
457 2, 129–136 (2007).
- 458 19. Montaser, A. S. et al. Preparation and characterization of alginate/silver/nicotinamide
459 nanocomposites for treating diabetic wounds. *International Journal of Biological Macromolecules* 92,
460 739–747 (2016).
- 461 20. Drake, P. L. & Hazelwood, K. J. Exposure-related health effects of silver and silver compounds:
462 A review. *Annals of Occupational Hygiene* 49, 575–585 (2005).
- 463 21. Railean, V. et al. In Vivo Efficacy of Wound Healing under External (Bio)AgNCs Treatment:
464 Localization Case Study in Liver and Blood Tissue. *International Journal of Molecular Sciences* 24, 1–
465 11 (2023).
- 466 22. Liu, X. et al. Silver nanoparticles mediate differential responses in keratinocytes and fibroblasts
467 during skin wound healing. *ChemMedChem* 5, 468–475 (2010).
- 468 23. Birk, D. E. & Trelstad, R. L. Extracellular Compartments in Tendon Morphogenesis: Collagen
469 Fibril, Bundle, and Macroaggregate Formation. *The Journal of Cell Biology* 103, 231–240 (1986).
- 470 24. Kwan, K. H. L. et al. Modulation of collagen alignment by silver nanoparticles results in better
471 mechanical properties in wound healing. *Nanomedicine: Nanotechnology, Biology, and Medicine* 7,
472 497–504 (2011).
- 473 25. You, C. et al. Silver nanoparticle loaded collagen/chitosan scaffolds promote wound healing via
474 regulating fibroblast migration and macrophage activation. *Scientific Reports* 7, 1–11 (2017).
- 475 26. Damek-Poprawa, M. & Sawicka-Kapusta, K. Damage to the liver, kidney, and testis with
476 reference to burden of heavy metals in yellow-necked mice from areas around steelworks and zinc
477 smelters in Poland. *Toxicology* 186, 1–10 (2003).
- 478
- 479

5. Podsumowanie i wnioski

Przedstawione w niniejszej rozprawie doktorskiej badania pozwalają na sformułowanie następujących głównych wniosków.

1. Immobilizacja jonów cynku i srebra z β -laktoglobuliną oraz jonów cynku z poszczególnymi frakcjami kazeiny (α_{S1} -, β -, κ -CN) jest procesem heterogenicznym składającym się z trzech etapów.
2. Analiza spektroskopowa wykazała, że kluczową rolę w procesie wiązania metali do białek odgrywają grupy karboksylowe kwasu glutaminowego i asparaginowego oraz grupy fosforanowe w przypadku kazein.
3. Mikroskopia elektronowa wykazała, że morfologia powierzchni badanych białek zmienia się w zależności od zastosowanego do modyfikacji jonu metalu oraz jego stężenia.
4. Mechanizm formowania się nanokompozytów uzupełniony metodami molekularnymi i obliczeniowymi wskazał potencjalne miejsca wiązania dla kwasu glutaminowego i kwasu asparaginowego, które były zgodne z wynikami eksperymentalnymi. W przypadku jonów srebra oddziałujących z β LG oprócz powstania metalokompleksów, zaobserwowano tworzenie się nanocząstek srebra tworzących układ hybrydowy Ag β LG/AgNPs β LG.
5. Zsyntetyzowane kompleksy wykazują działanie zarówno przeciwbakteryjne jak i przeciwgrzybiczne wobec szczepów klinicznych oraz bakterii powszechnie uznanych za bezpieczne (LAB), a także mogą być potencjalnymi antyseptykami w regeneracji trudno gojących się ran, odleżyn.

Charakter wiązania jonów metali z wielowymiarową strukturą biokoloidów (białek) jest złożony i czasami niespodziewany. Mechanizmy, dzięki którym jon metalu jest wybrany przez białko, a następnie reguluje jego funkcję, nie są na ogół dobrze poznane. Z tego powodu naukowcy poszukują obecnie nowych sposobów badania mechanizmu, za pomocą którego cząsteczki lub jony metali wiążą się z białkami, aby np. wyeliminować toksyczność wolnych jonów metali. Dlatego ważne jest zrozumienie mechanizmu, za pomocą którego jony metali wiążą się z białkami i jak te oddziaływania przyczyniają się do określenia specyficzności wiązania. Wykonanie widm FTIR, Ramana, UV-Vis, fluorescencji, NMR dla badanych białek i ich kompleksów pozwala na wskazanie przesunięć chemicznych czy drgań, które przypisane są odpowiednio grupom aminowym/hydroksylowym, karboksylowym czy fosforanowym. Ponadto techniki te pozwalają na analizę porównawczą widm przed i po modyfikacji

powierzchni białka (np. procesem wiązania metali), objawiającej się pojawieniem nowego sygnału i/lub przesunięciem pierwotnego drgania. Do zrozumienia zachowania biologicznych makrocząsteczek takich jak białka w oddziaływaniu z jonami metali użyteczną metodą są symulacje modelowania molekularnego wraz z obliczeniami kwantowo-mechanicznymi.

W niniejszej pracy po raz pierwszy został opisany mechanizm formowania się nanokompozytów na bazie β LG z jonami cynku oraz srebra. Zbadana została natura oraz wpływ stężenia jonów metali na proces wiązania z białkiem. Dodatkowo, wskazano na redukcję srebra i obecność nanocząstek srebra wynikającą z wiązania jonów srebra z kwasem asparaginowym i kwasem glutaminowym tworząc układ hybrydowy metalokompleks/nanocząstka srebra ($\text{Ag}\beta\text{LG}/\text{AgNPs}\beta\text{LG}$).

Istotnym wyzwaniem naukowym podjętym w pracy doktorskiej było opisanie mechanizmu wiązania jonów cynku do poszczególnych frakcji kazeinowych ($\text{Zn}\alpha_1\text{CN}$ -, $\text{Zn}\beta\text{CN}$, $\text{Zn}\kappa\text{CN}$) wskazując na udział poszczególnych frakcji w wiązaniu oraz na wpływ stężenia stosowanego metalu. Stwierdzono, że zróżnicowany sposób przebiegu procesu wiązania poszczególnych kompleksów ZnCN ściśle zależy od ich wielkości, sekwencji aminokwasowej oraz hydrofobowości.

W celu dogłębnego wyjaśnienia mechanizmu oddziaływania pomiędzy jonami cynku/srebra, a β LG i izoformami kazein, wskazania miejsc odpowiedzialnych za wiązanie, interpretacji reakcji utleniania-redukcji oraz uzupełnienia dotychczasowych wyników, niezbędne było wykorzystanie modelowania/dokowania molekularnego oraz obliczeń z zakresu chemii kwantowej z wykorzystaniem teorii funkcjonałów gęstości.

Otrzymanie kompleksów jonów metali na bazie białek mleka oraz białek serwatkowych stanowi obiecujące rozwiązanie rosnącego problemu lekooporności ze względu na silne działanie antybakteryjne przeciwko lekoopornym szczepom. Rezultaty, które udało się uzyskać, niosą ze sobą kolosalne implikacje dla wielu dziedzin nauki, a zwłaszcza dla chemii analitycznej. Są one również znaczące dla ewentualnej aplikacji wyników tych badań w praktyce, gdzie opracowane nanokompozyty mogą znaleźć zastosowanie w farmacji czy medycynie. Szczególnie wartościowe mogą się okazać w kontekście walki z trudno gojącymi się ranami czy odleżynami. To podejście ma potencjał do transformacji sposobu, w jaki leczymy i zarządzamy tymi trudnymi do leczenia stanami zdrowia, umożliwiając opracowanie skuteczniejszych i bezpieczniejszych terapii. Nanokompozyty mogą zrewolucjonizować leczenie oferując nie tylko potencjalne rozwiązania w celu przyspieszenia gojenia się ran, ale również jako alternatywa dla tradycyjnych metod leczenia odleżyn.

Przeprowadzone badania były fundamentem pracy doktorskiej, którą cechowało unikalne interdyscyplinarne podejście. W jego centrum było połączenie różnych dziedzin nauki, w tym chemii, biochemii, biotechnologii i nanotechnologii. To holistyczne spojrzenie pozwoliło na skuteczne zrozumienie procesów na poziomie molekularnym oraz umożliwiło projektowanie i tworzenie nanokompozytów z wykorzystaniem najnowszych technologii. Całość badania miała na celu nie tylko odkrycie nowych perspektyw naukowych, ale także praktyczne zastosowanie tych wyników w medycynie i farmacji. Jest to przykład na to jak nowoczesne, interdyscyplinarne badania naukowe mogą przyczynić się do postępu w dziedzinie opieki zdrowotnej oferując potencjalnie transformatywne rozwiązania dla trudnych do leczenia stanów zdrowotnych. Osiągnięte wyniki mają nie tylko potencjalne zastosowania w dziedzinach medycyny i farmacji, ale także mogą przynieść znaczne korzyści dla przemysłu spożywczego, a szczególnie sektora mleczarskiego. Użycie kompleksów jonów cynku i kazeiny, które są składnikami nanokompozytów, może zrewolucjonizować produkcję i przetwórstwo mleka, wprowadzając innowacyjne metody i techniki. Kompleksy jonów cynku i kazeiny mogą mieć kilka zastosowań. Po pierwsze jako antyoksydanty mogą pomóc w przedłużaniu trwałości produktów mleczarskich, co ma kluczowe znaczenie dla ich jakości i bezpieczeństwa. Po drugie, mogą pełnić funkcję strukturalną wpływając na teksturę i konsystencję produktów mleczarskich, co przekłada się na ich atrakcyjność sensoryczną. Wreszcie mogą także służyć jako naturalne konserwanty, zwiększając trwałość produktów i wpływając na ich walory smakowe. Wykorzystanie tych kompleksów w przemyśle spożywczym, szczególnie w mleczarstwie, może prowadzić do znacznej poprawy jakości i bezpieczeństwa produktów, a także do zwiększenia wydajności i efektywności produkcji. Wydaje się, że wkrótce nanokompozyty mogą stać się integralnym elementem przemysłu spożywczego, od przetwórstwa po pakowanie i dystrybucję. Należy jednak podkreślić, że wdrażanie tych technologii wymaga dalszych badań i regulacji prawnych, aby zapewnić, że są one nie tylko skuteczne, ale również bezpieczne dla zdrowia konsumentów i środowiska. Ale wyniki tych badań już teraz pokazują ogromny potencjał nanokompozytów w przemyśle spożywczym, a szczególnie w mleczarstwie.

6. Streszczenie

W niniejszej rozprawie doktorskiej przeprowadzona została immobilizacja jonów cynku i srebra do białka serwatkowego (β -laktoglobuliny) oraz jonów cynku do poszczególnych frakcji kazeinowych (α_{S1} -, β -, κ -CN). Zbadane zostały mechanizmy wiązania i zdolności sorpcyjne białek (biokoloidów) za pomocą badań kinetycznych i izotermicznych oraz metod modelowania/dokowania molekularnego i obliczeń kwantowych. Otrzymane nanokompozyty poddane zostały fizykochemicznej charakterystyce za pomocą całego spektrum technik instrumentalnych takich jak metody spektrometryczne, spektroskopowe, mikroskopowe oraz dyfrakcyjne, które wzajemnie się uzupełniały. Kolejnym aspektem prowadzonych badań z uwagi na pojawiający się problem lekooporności oraz poszukiwanie nowych antyseptyków, wykonane zostały badania aplikacyjne określające potencjał przeciwdrobnoustrojowy syntetyzowanych nanokompozytów. Zwieńczeniem badań i niezwykle istotną kwestią podjętą w rozprawie doktorskiej było wykorzystanie modelu zwierzęcego (myszy) celem określenia wpływu uzyskanych nanokompozytów na proces gojenia się ran jak również dystrybucję cynku i srebra w narządach (wątroba, krew).

Wstępny etap badań polegał na scharakteryzowaniu białek biorących udział w procesie wiązania za pomocą metody MALDI-TOF MS oraz wyznaczeniu ich punktów izoelektrycznych poprzez pomiar potencjału zeta i określeniu ich stabilności. Porównane zostały również wyniki metod proteomicznych opartych na klasycznym trawieniu białek w roztworze z przepływowym mikroreaktorem enzymatycznym przy zastosowaniu końcówek pipety ZipTip. Następnie przeprowadzono syntezę jonów metali z badanymi białkami przeprowadzając klasyczne badania kinetyczne i izotermiczne, które pozwoliły zrozumieć skomplikowane i wieloetapowe mechanizmy powstawania kompleksów. Otrzymane dane eksperymentalne porównano z wybranymi modelami kinetycznymi (zerowego-, pierwszego-, pseudo-pierwszego-, pseudo drugiego-rzędu, modelem wewnątrzcząsteczkowej dyfuzji Webera-Morrisa) oraz modelami izotermicznymi (Henry'ego, Freundlicha, Langmuira). Cała gama technik instrumentalnych wykazująca dużą komplementarność między sobą pozwoliła na identyfikację powierzchniowych grup funkcyjnych białek uczestniczących w procesie wiązania, określenie morfologii powierzchni i stabilności, również z naciskiem na wpływ stężenia metalu. Ważnym etapem pracy była konfrontacja wyników eksperymentalnych z modelowaniem/dokowaniem molekularnym oraz obliczeniami kwantowo-mechanicznymi. Uzyskana wysoka zgodność między wynikami eksperymentalnymi oraz teoretycznymi pozwoliła stwierdzić, iż w przypadku oddziaływań jonów cynku z białkami mamy do czynienia

tylko i wyłącznie z układami typu metalokompleks. Z kolei w przypadku oddziaływań jonów srebra z β LG tworzy się układ hybrydowy – metalokompleks wraz z tworzeniem się nanocząstek srebra ($\text{Ag}\beta\text{LG}/\text{AgNPs}\beta\text{LG}$). Ponadto, wykazano działanie przeciwdrobnoustrojowe nanokompozytów $\text{Zn}/\text{Ag}\beta\text{LG}$, $\text{Zn}\alpha\text{SI}\text{CN}$, $\text{Zn}\beta\text{CN}$, $\text{Zn}\kappa\text{CN}$ wobec patogenów o znaczeniu klinicznym. Przeprowadzone badania aplikacyjne *in vivo* na modelu zwierzęcym (myszy) wskazują na obserwowalny wzrost masy ciała gryzoni po dziesięciodniowych obserwacjach, stopniową regenerację organizmu zwierząt, pojawienie się strupa oraz odrastające włosy. W pracy wykazano, iż oddziaływania typu metal-białko o właściwościach przeciwdrobnoustrojowych mogą przyczynić się do rozwiązania problemu lekooporności oraz stać się potencjalnym kandydatem jako preparat stosowany do leczenia trudno gojących się ran.

7. Abstract

In this doctoral dissertation, immobilization of zinc and silver ions to whey protein (β -lactoglobulin) and zinc ions to individual casein fractions (α_{SI} -, β -, κ -CN) was carried out. Mechanisms of binding and sorption capacities of proteins (biocolloids) were investigated using kinetic and isothermal studies, as well as molecular modeling/docking methods and quantum calculations. The obtained nanocomposites were subjected to physicochemical characterization using the whole spectrum of instrumental techniques such as spectrometric, spectroscopic, microscopic and diffraction methods, which complemented each other. Another aspect of the studies, due to the emerging problem of drug resistance and the search for new antiseptics, application studies were performed to determine the antimicrobial potential of the synthesized nanocomposites. The culmination of the research and an extremely important issue undertaken in the dissertation was the use of an animal model (mice) to determine the effect of the obtained nanocomposites on the process of wound healing as well as the distribution of zinc and silver in organs (liver, blood).

The initial stage of the study consisted of characterizing the proteins involved in the binding process using MALDI-TOF MS and determining their isoelectric points by measuring the zeta potential and determining their stability. Furthermore, the results of proteomic methods based on classical protein digestion in solution were compared with microfluidic immobilized enzyme reactor (μ -IMER) using ZipTip pipette tips. Subsequently, the synthesis of metal ions with the studied proteins was carried out by performing classical kinetic and isothermal studies, which allowed us to understand the complex and multistep mechanisms of complex formation. The obtained experimental data were compared with selected kinetic models (zero-order, first-order, pseudo-first-order, pseudo-second-order, intraparticle diffusion Weber-Morris model) and isothermal models (Henry, Freundlich, Langmuir). A whole range of instrumental techniques showing high complementarity among themselves allowed the identification of surface functional groups of proteins involved in the binding process, determination of surface morphology and stability, also with emphasis on the effect of metal concentration. An important step in the work was the confrontation of experimental results with molecular modeling/docking and quantum mechanical calculations. The high agreement obtained between experimental and theoretical results allowed us to conclude that in the case of interactions of zinc ions with proteins we are dealing only with metallocomplex type systems. In contrast, in the case of interactions of silver ions with β LG, a hybrid system is formed – a metallocomplex with the formation of silver nanoparticles ($\text{Ag}\beta\text{LG}/\text{AgNPs}\beta\text{LG}$). In addition, antimicrobial

activity of Zn/Ag β LG, Zn α_5 CN, Zn β CN, Zn κ CN nanocomposites against clinically relevant pathogens was demonstrated. *In vivo* application studies conducted on an animal model (mice) indicate an observable increase in the body weight of rodents after ten-day observation, gradual regeneration of the animal body, the appearance of scab and regrowth of hair. The study shows that metal-protein interactions with antimicrobial properties can contribute to solving the problem of drug resistance and become a potential candidate as a preparation used to treat hard-to-heal wounds.

8. Dorobek naukowy

Publikacje naukowe:

1. **A. Rodzik**, V. Railean, P. Pomastowski, B. Buszewski, M. Szumski, *Immobilized enzyme microreactors for efficient analysis of tryptic peptides in β -casein and β -lactoglobulin*, Scientific Reports, Submission ID 5d953fac-cd31-4150-9da3-e4e688f203eb. (**IF = 4,996; PM = 140**)
2. **A. Rodzik**, P. Pomastowski, M. Buszewska-Forajta, V. Railean, A. Gołębiowski, B. Buszewski, K. Niedojadło, K. Rafińska, *Metal-protein action for the wound healing process using murine model C57BL/6J mouse*, Scientific Reports, Submission ID 15404681-edaf-4c74-885f-ae8688b6dbd7. (**IF = 4,996; PM = 140**)
3. **A. Rodzik**, A. Król-Górniak, V. Railean, M. Sugajski, A. Gołębiowski, D. S. Horne, B. Michalke, M. Sprynskyy, P. Pomastowski, B. Buszewski, *Study on zinc ions binding to the individual casein fractions α_{S1} -, β - and κ -casein*, Journal of Molecular Structure, 2023, 1272, doi: 10.1016/j.molstruc.2022.134251. (**IF = 3,841; PM = 70**)
4. V. Railean, M. Buszewska-Forajta, **A. Rodzik**, A. Gołębiowski, P. Pomastowski, B. Buszewski, *In vivo efficacy of the wound healing under external (Bio)AgNCs treatment and localization case study in liver and blood tissue*, International Journal of Molecular Sciences, 2023, 24 (1), doi: org/10.3390/ijms24010434. (**IF = 6,208; PM = 140**)
5. **A. Rodzik**, V. Railean, P. Pomastowski, P. Žuvela, M. W. Wong, M. Sprynskyy, B. Buszewski *Study on silver ions binding to β -lactoglobulin*, Biophysical Chemistry, 2022, 291, doi: 10.1016/j.bpc.2022.106897. (**IF = 3,628; PM = 70**)
6. **A. Rodzik**, V. Railean, P. Pomastowski, P. Žuvela, M. W. Wong, B. Buszewski, *The influence of zinc ions concentration on β -lactoglobulin structure – physicochemical properties of Zn- β -lactoglobulin complexes*, Journal of Molecular Structure, 2022, 1268, 1-10, doi: 10.1016/j.molstruc.2022.133745. (**IF = 3,841; PM = 70**)
7. A. Gołębiowski, P. Pomastowski, **A. Rodzik**, A. Król-Górniak, T. Kowalkowski, M. Górecki, B. Buszewski, *Isolation and self-association studies of beta-lactoglobulin*, International Journal of Molecular Sciences, 2020, 21(24), 1-21, doi: 10.3390/ijms21249711. (**IF = 5,924; PM = 140**)
8. B. Buszewski, P. Žuvela, A. Król-Górniak, V. Railean-Plugaru, A. Rogowska, M. W. Wong, M. Yi, **A. Rodzik**, M. Sprynskyy, P. Pomastowski, *Interactions of zinc aqua*

complexes with ovalbumin at the forefront of the Zn²⁺/ZnO-OVO hybrid complex formation mechanism, Applied Surface Science, 2021, 542, 1-12, doi: 10.1016/j.apsusc.2020.148641. (IF = 6,707; PM = 140)

9. A. Rodzik, P. Pomastowski, V. Railean-Plugaru, M. Sprynskyy, B. Buszewski, *The study of zinc ions binding to α S1-, β -, κ -casein*, International Journal of Molecular Sciences, 2020, 21(21), 1-18, doi: 10.3390/ijms21218096. (IF = 6,208; PM = 140)
10. M. Złoch, A. Rodzik, O. Pryshchepa, K. Pauter, M. Szultka-Młyńska, A. Rogowska, W. Kupczyk, P. Pomastowski, B. Buszewski, *Problems with identifying and distinguishing salivary streptococci: a multi-instrumental approach*, Future Microbiology, 2020, 15(12), 1157-1171, doi: 10.2217/fmb-2020-0036. (IF = 3,165; PM = 100)
11. A. Rodzik, P. Pomastowski, G. N. Sagandykova, B. Buszewski, *Interactions of whey proteins with metal ions*, International Journal of Molecular Sciences, 2020, 21(6), 1-26, doi: 10.3390/ijms21062156. (IF = 5,924; PM = 140)
12. B. Buszewski, A. Rodzik, V. Railean-Plugaru, M. Sprynskyy, P. Pomastowski, *A study of zinc ions immobilization by β -lactoglobulin*, Colloids and Surfaces A, 2020, 591, 1-13, doi: 10.1016/j.colsurfa.2020.124443. (IF = 5,518; PM = 70)
13. O. Pryshchepa, G. N. Sagandykova, P. Pomastowski, V. Railean-Plugaru, A. Król, A. Rogowska, A. Rodzik, M. Sprynskyy, B. Buszewski, *A new approach for spontaneous silver ions immobilization onto casein*, International Journal of Molecular Sciences, 2019, 20(16), 1-18, doi:10.3390/ijms20163864. (IF = 6,208; PM = 140)
14. P. Pomastowski, M. Złoch, A. Rodzik, M. Ligor, M. Kostrzewa, B. Buszewski, *Analysis of bacteria associated with honeys of different geographical and botanical origin using two different identification approaches: MALDI-TOF MS and 16S rDNA PCR techniques*, PLoS ONE, 2019, 14(5), 1-20, doi: 10.1371/journal.pone.0217078. (IF = 2,740; PM = 100)

Rozdziały w monografiach:

1. O. Pryshchepa, M. Złoch, P. Pomastowski, V. Railean-Plugaru, A. Rodzik, M. Szultka-Młyńska, B. Buszewski, *Modern Approaches for Microorganisms' Identification*. In: Buszewski B., Baranowska I. (eds) Handbook of Bioanalytics. Springer Nature, 2022, 833-861.

2. B. Buszewski, P. Pomastowski, A. Król-Górniak, A. Rogowska, **A. Rodzik**, G. Sagandykova, V. Railean-Plugaru, *Spectroscopic Techniques in Research of Biocolloids*, In: Buszewski B., Baranowska I. (eds) Handbook of Bioanalytics, Springer Nature, 2022, 805-832.
3. **A. Rodzik**, P. Pomastowski, V. Railean-Plugaru, B. Buszewski, *Hybrydowe układy metal-białko w ujęciu serwatkowym*, *Analityka: nauka i praktyka*, 2021, 2, 4-12. (**PM= 20**)
4. P. Pomastowski, A. Król, A. Rogowska, **A. Rodzik**, G. Sagandykova, V. Railean-Plugaru, B. Buszewski, *Zastosowanie technik spektroskopowych w analizie biokolooidów*, w: I. Baranowska, B. Buszewski, *Bioanalityka w nauce i życiu; Tom 2 Nowe strategie analityczne i rozwiązania aparaturowe, część C: Nowe rozwiązania metodyczne i aparaturowe w bioanalityce*, Wydawnictwo Naukowe PWN, Warszawa, 2020, 565-588 (**PM = 20**).
5. O. Pryshchepa, M. Złoch, P. Pomastowski, V. Railean-Plugaru, **A. Rodzik**, M. Szultka-Młyńska, B. Buszewski, *Nowoczesne metody identyfikacji mikroorganizmów* w: I. Baranowska, B. Buszewski, *Bioanalityka w nauce i życiu; Tom 2 Nowe strategie analityczne i rozwiązania aparaturowe*, Wydawnictwo Naukowe PWN, Warszawa, 2020, 589-611, (**PM = 20**).

Konferencje naukowe:

1. **A. Rodzik**, V. Railean-Plugaru, P. Pomastowski, B. Buszewski, 26th International Symposium on Separation Sciences, Ljubljana (Słowenia), *Proteomic analysis of milk by MALDI-TOF MS*, (28.06–01.07.2022 r.) – poster.
2. **A. Rodzik**, V. Railean-Plugaru, P. Pomastowski, B. Buszewski, XI Polska Konferencja Chemii Analitycznej, PoKoChA, Łódź (Polska), *Badanie modyfikacji potranslacyjnych białek za pomocą technik spektrometrycznych*, (19-23.06.2022 r.) – poster.
3. M. Buszewska-Forajta, **A. Rodzik**, V. Railean-Plugaru, A. Gołębiowski, P. Pomastowski, B. Buszewski, XI Polska Konferencja Chemii Analitycznej, PoKoChA, Łódź (Polska), *Nanokompozyty – nadzieja dla trudnogojących się ran?* (19-23.06.2022 r.) – wykład.
4. M. Buszewska-Forajta, P. Pomastowski, **A. Rodzik**, V. Railean-Plugaru, B. Buszewski, 45. Seminarium Naukowo – Techniczne „Chemistry for Agriculture” w Karpaczu (Polska), *Nanokompozyty typu metal-białko jako nowe leki dla trudno gojących się ran*, (21-24.11. 2021r.) – wykład.

5. **A. Rodzik**, V. Railean-Plugaru, P. Pomastowski, M. Sprynskyy, B. Buszewski, 35th Conference of The European Colloid & Interface Society, Ateny (Grecja), *Nutrition potential of zinc- β -lactoglobulin complexes*, (05-10.09.2021 r.) – poster.
6. A. Gołębiowski, T. Kowalkowski, **A. Rodzik**, P. Pomastowski, B. Buszewski, 35th Conference of The European Colloid & Interface Society, Ateny (Grecja), *Characteristics of beta-lactoglobulin from whey protein isolate*, (05-10.09.2021 r.) – poster.
7. **A. Rodzik**, P. Pomastowski, V. Railean-Plugaru, M. Sprynskyy, B. Buszewski, QUO VADIS Life Sciences, Opole (Polska), *Immobilization of zinc ions onto β -lactoglobulin*, (23-27.06.2021 r.) – komunikat ustny
8. A. Gołębiowski, P. Pomastowski, **A. Rodzik**, A. Król-Górniak, T. Kowalkowski, M. Górecki, B. Buszewski, QUO VADIS Life Sciences, Opole (Polska), *Isolation and multi aspects characteristic of beta-lactoglobulin from whey protein isolate*, (23-27.06.2021 r.) – komunikat ustny.
9. A. Król-Górniak, **A. Rodzik**, P. Pomastowski, V. Railean-Plugaru, B. Buszewski, QUO VADIS Life Sciences, Opole (Polska), *Zinc ions binding to α -, β -, κ -casein*, (23-27.06.2021 r.) – poster.
10. **A. Rodzik**, P. Pomastowski, V. Railean-Plugaru, B. Buszewski, 15th International Scientific Conference „The Vital Nature Sign”, Kaunas (Litwa), *New approaches in functionalization of cow's milk proteins*, (20-21.05.2021 r.) – e-poster.
11. **A. Rodzik**, V. Railean-Plugaru, K. Rafińska, T. Kowalkowski, P. Pomastowski, B. Buszewski, 15th International Students Conference ‘Modern Analytical Chemistry’, Praga (Czechy), *Zinc ions binding to β -lactoglobulin: proteomic study and physicochemical characteristic*, (19-20.09.2019 r.) – komunikat ustny.
12. **A. Rodzik**, V. Railean-Plugaru, T. Kowalkowski, K. Rafińska, P. Pomastowski, B. Buszewski, 25th International Symposium on Separation Sciences, Łódź (Polska), *Binding of zinc ions to β -lactoglobulin*, (15-18.09.2019 r.) – komunikat ustny.
13. **A. Rodzik**, A. Rogowska, A. Król, V. Railean-Plugaru, G. Sagandykova, M. Sprynskyy, P. Pomastowski, B. Buszewski, 11. Kongres Societas Humboldtiana Polonorum, Szczecin (Polska), *Immobilization of silver ions onto casein*, (12-15.09.2019 r.) – komunikat ustny.

14. P. Pomastowski, **A. Rodzik**, B. Buszewski, Fourth International Symposium on Dielectric Materials and Applications, Jordan, *Immobilization of metal ions onto proteins*, (02-04.05.2019 r.) – komunikat ustny.
15. **A. Rodzik**, P. Pomastowski, B. Buszewski, 5th Scientific Conference Metabolomics Circle 2018, Przysiek k/Torunia (Polska), *Proteomic analysis of selected whey proteins by MALDI-TOF MS approach*, (26-28.10.2018 r.) – e-poster.
16. P. Pomastowski, **A. Rodzik**, B. Buszewski, 5th Scientific Conference Metabolomics Circle 2018, Przysiek k/Torunia (Polska), *Immobilization of metal ions onto whey proteins*, (26-28.10.2018 r.) – komunikat ustny.

Granty:

1. Grant Preludium 19 finansowany przez Narodowe Centrum Nauki, nr 2020/37/N/ST4/04082, pt.: *Wykorzystanie technik laserowej desorpcji/ionizacji wspomaganą matrycą oraz nanostrukturami w analizie hydrolizatów białkowych ze szczególnym uwzględnieniem modyfikacji potranslacyjnych* (01.02.2021 r. – 30.06.2023 r.), Kierownik: mgr Agnieszka Rodzik; Wykonawca: dr Viorica Railean.
2. Grant Opus 14 finansowany przez Narodowe Centrum Nauki, nr 2016/21/B/ST4/02130, pt.: *Synteza kompleksowych związków srebra i cynku na bazie kazein i białek serwatki oraz nanocząstek srebra i tlenku cynku przez probiotyczne bakterie kwasu mlekowego* (01.10.2018 r. – 31.05.2021 r.), Kierownik: dr hab. Paweł Pomastowski, prof. UMK; Wykonawca: mgr Agnieszka Rodzik.
3. Grant Młodych Wydziału Chemii, nr PDB/granty wydziałowe, pt.: *Badanie aktywności biologicznej modyfikowanych frakcji kazeiny* (22.04.2021 r. – 30.11.2021 r.), Kierownik: mgr Agnieszka Rodzik.
4. Grant Młodych Wydziału Chemii, nr 492/2020, pt.: *Badania aktywności biologicznej kompleksu Zn-β-laktoglobulina* (03.03.2020 r. – 14.01.2021 r.), Kierownik: mgr Agnieszka Rodzik.
5. Grant Młodych Wydziału Chemii, nr 2092/2019, pt.: *Badanie mechanizmów wiązania metali do białek przy wykorzystaniu nowoczesnych technik instrumentalnych* (18.10.2019 r. – 14.01.2020 r.), Kierownik: mgr Agnieszka Rodzik.

Nagrody i osiągnięcia:

1. Laureat II naboru projektu PROM – międzynarodowej wymiany stypendialnej doktorantów i kadry akademickiej na UMK (2021 r.).
2. Zespołowa nagroda JM Rektora Uniwersytetu Mikołaja Kopernika w Toruniu za osiągnięcia uzyskane w dziedzinie naukowej w 2020 roku.
3. Zespołowe wyróżnienie JM Rektora Uniwersytetu Mikołaja Kopernika w Toruniu za osiągnięcia uzyskane w dziedzinie naukowej w 2020 roku.
4. Stypendium Rektora Uniwersytetu Mikołaja Kopernika w Toruniu dla wysoko ocenianej publikacji (2020 r.)

Udział w innych projektach oraz towarzystwach naukowych:

1. Członek Priorytetowego Zespołu Badawczego uczelni wspieranego w ramach ID-UB (Inicjatywa Doskonałości – uczelnia badawcza) w latach 2020-2022.
2. Prowadzenie warsztatów w ramach XIX Toruńskiego Festiwalu Nauki i Sztuki pt.: *Oblicza komunikacji* (24-28.04.2019 r.).
3. Współorganizowanie 5-tej Konferencji Naukowej Metabolomics Circle 2018, Przysiek k/Torunia (Polska) (26-28.10.2018 r.).

Szkolenia:

1. Uczestnictwo w szkoleniu Szkoła Cytometrii *Cytometria przepływowa – podstawowe narzędzie badawcze* (Bydgoszcz, 14.02–18.02.2022 r.)
2. Warsztaty szkoleniowe Metabolomics Workflow. Using High-Resolution LC-MS Mass Profiler Professional software for data mining and identification of metabolites, (24.05–26.05.2018 r.)
3. Warsztaty szkoleniowe Practical application of Gilson GX-271 ASPEC automatic extractor for SPE automated liquid handling – preparation of purified samples for HPLC-MS, GC-MS and other applications, (24.05–26.05.2018 r.)

9. Oświadczenia

Toruń, 09.08.2023 r.

Mgr Agnieszka Rodzik
Interdyscyplinarne Centrum Nowoczesnych Technologii
Katedra Chemii Środowiska i Bioanalitiky
Wydział Chemii, Uniwersytet Mikołaja Kopernika
Ul. Gagarina 7, 87-100

OŚWIADCZENIE

Niniejszym oświadczam, że jako Współautor następujących publikacji:

1. A. Rodzik, P. Pomastowski, V. Railean-Plugaru, B. Buszewski, *Hybrydowe układy metal-białko w ujęciu serwatkowym*, *Analityka: nauka i praktyka*, 2021, 2, 4-12.
2. B. Buszewski, A. Rodzik, V. Railean-Plugaru, M. Sprynskyy, P. Pomastowski, *A study of zinc ions immobilization by β -lactoglobulin*, *Colloids and Surfaces A*, 2020, 591, 1-13, doi: 10.1016/j.colsurfa.2020.124443.
3. A. Rodzik, P. Pomastowski, V. Railean-Plugaru, M. Sprynskyy, B. Buszewski, *The study of zinc ions binding to α_{S1} -, β -, κ -casein*, *International Journal of Molecular Sciences*, 2020, 21(21), 1-18, doi: 10.3390/ijms21218096.
4. A. Rodzik, A. Król-Górniak, V. Railean-Plugaru, M. Sugajski, A. Gołębiowski, D. S. Horne, B. Michalke, M. Sprynskyy, P. Pomastowski, B. Buszewski, *Study on zinc ions binding to the individual casein fractions α_{S1} -, β - and κ -casein*, *Journal of Molecular Structure*, 2022, 1272, doi: 10.1016/j.molstruc.2022.134251.
5. A. Rodzik, V. Railean, P. Pomastowski, B. Buszewski, M. Szumski, *Immobilized enzyme microreactors for efficient analysis of tryptic peptides in β -casein and β -lactoglobulin*, *Scientific Reports*, Submission ID 5d953fac-cd31-4150-9da3-e4e688f203eb.
6. A. Rodzik, V. Railean, P. Pomastowski, P. Žuvela, M. W. Wong, M. Sprynskyy, B. Buszewski, *Study on silver ions binding to β -lactoglobulin*, *Biophysical Chemistry*, 2022, 291, doi: 10.1016/j.bpc.2022.106897.
7. A. Rodzik, V. Railean, P. Pomastowski, P. Žuvela, M. W. Wong, B. Buszewski, *The influence of zinc ions concentration on β -lactoglobulin structure – physicochemical properties of Zn- β -lactoglobulin complexes*, *Journal of Molecular Structure*, 2022, 1268, 1-10, doi: 10.1016/j.molstruc.2022.133745.
8. A. Rodzik, P. Pomastowski, M. Buszewska-Forajta, V. Railean, A. Gołębiowski, B. Buszewski, K. Niedojadło, K. Rafińska, *Metal-protein action for the wound healing process using murine model C57BL/6J mouse*, *Scientific Reports*, Submission ID 15404681-edaf-4c74-885f-ae8688b6dbd7.

wchodzących w skład mojej rozprawy doktorskiej, oświadczam, że mój wkład polegał na dyskusji ogólnej koncepcji pracy, zaplanowaniu i realizacji doświadczeń, analizie i interpretacji wyników, przygotowaniu wstępnych wersji manuskryptów.

..Agnieszka Rodzik.....



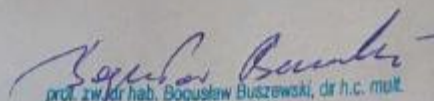
Toruń, 09.08.2023 r.

OŚWIADCZENIE

Niniejszym oświadczam, że jako Współautor następujących publikacji:

1. A. Rodzik, P. Pomastowski, V. Railean-Plugaru, B. Buszewski, *Hybrydowe układy metal-białko w ujęciu serwatkowym*, *Analityka: nauka i praktyka*, 2021, 2, 4-12.
2. B. Buszewski, A. Rodzik, V. Railean-Plugaru, M. Sprynskyy, P. Pomastowski, *A study of zinc ions immobilization by β -lactoglobulin*, *Colloids and Surfaces A*, 2020, 591, 1-13, doi: 10.1016/j.colsurfa.2020.124443.
3. A. Rodzik, P. Pomastowski, V. Railean-Plugaru, M. Sprynskyy, B. Buszewski, *The study of zinc ions binding to α_{S1} , β -, κ -casein*, *International Journal of Molecular Sciences*, 2020, 21(21), 1-18, doi: 10.3390/ijms21218096.
4. A. Rodzik, A. Król-Górniak, V. Railean-Plugaru, M. Sugajski, A. Gołębiowski, D. S. Horne, B. Michalke, M. Sprynskyy, P. Pomastowski, B. Buszewski, *Study on zinc ions binding to the individual casein fractions α_{S1} , β - and κ -casein*, *Journal of Molecular Structure*, 2022, 1272, doi: 10.1016/j.molstruc.2022.134251.
5. A. Rodzik, V. Railean, P. Pomastowski, B. Buszewski, M. Szumski, *Immobilized enzyme microreactors for efficient analysis of tryptic peptides in β -casein and β -lactoglobulin*, *Scientific Reports*, Submission ID 5d953fac-cd31-4150-9da3-e4e688f203eb.
6. A. Rodzik, V. Railean, P. Pomastowski, P. Žuvela, M. W. Wong, M. Sprynskyy, B. Buszewski *Study on silver ions binding to β -lactoglobulin*, *Biophysical Chemistry*, 2022, 291, doi: 10.1016/j.bpc.2022.106897.
7. A. Rodzik, V. Railean, P. Pomastowski, P. Žuvela, M. W. Wong, B. Buszewski, *The influence of zinc ions concentration on β -lactoglobulin structure – physicochemical properties of Zn- β -lactoglobulin complexes*, *Journal of Molecular Structure*, 2022, 1268, 1-10, doi: 10.1016/j.molstruc.2022.133745.
8. A. Rodzik, P. Pomastowski, M. Buszewska-Forajta, V. Railean, A. Gołębiowski, B. Buszewski, K. Niedojadło, K. Rafińska, *Metal-protein action for the wound healing process using murine model C57BL/6J mouse*, *Scientific Reports*, Submission ID 15404681-edaf-4c74-885f-ae8688b6dbd7.

wchodzących w skład rozprawy doktorskiej mgr Agnieszki Rodzik, oświadczam, że mój wkład polegał na współudziale przy opracowaniu koncepcji harmonogramu badań i manuskryptów, interpretacji wyników a także korekcie manuskryptów i pełnieniu nadzoru merytorycznego.


prof. zw. dr hab. Bogusław Buszewski, dr h.c. mult.

Toruń, 23.08.2023 r.

dr hab. Paweł Piotr Pomastowski, prof. UMK
Interdyscyplinarne Centrum Nowoczesnych Technologii
ul. Wileńska 4, 87-100 Toruń

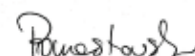
OŚWIADCZENIE

Jako współautor następujących publikacji:

1. A. Rodzik, P. Pomastowski, V. Railean-Plugaru, B. Buszewski, *Hybrydowe układy metal-białko w ujęciu serwatkowym*, *Analityka: nauka i praktyka*, 2021, 2, 4-12.
2. B. Buszewski, A. Rodzik, V. Railean-Plugaru, M. Sprynskyy, P. Pomastowski, *A study of zinc ions immobilization by β -lactoglobulin*, *Colloids and Surfaces A*, 2020, 591, 1-13, doi: 10.1016/j.colsurfa.2020.124443.
3. A. Rodzik, P. Pomastowski, V. Railean-Plugaru, M. Sprynskyy, B. Buszewski, *The study of zinc ions binding to α_{S1} -, β -, κ -casein*, *International Journal of Molecular Sciences*, 2020, 21(21), 1-18, doi: 10.3390/ijms21218096.
4. A. Rodzik, A. Król-Gómiak, V. Railean-Plugaru, M. Sugajski, A. Gołębiowski, D. S. Horne, B. Michalke, M. Sprynskyy, P. Pomastowski, B. Buszewski, *Study on zinc ions binding to the individual casein fractions α_{S1} -, β - and κ -casein*, *Journal of Molecular Structure*, 2022, 1272, doi: 10.1016/j.molstruc.2022.134251.
5. A. Rodzik, V. Railean, P. Pomastowski, P. Žuvela, M. W. Wong, M. Sprynskyy, B. Buszewski *Study on silver ions binding to β -lactoglobulin*, *Biophysical Chemistry*, 2022, 291, doi: 10.1016/j.bpc.2022.106897.
6. A. Rodzik, V. Railean, P. Pomastowski, P. Žuvela, M. W. Wong, B. Buszewski, *The influence of zinc ions concentration on β -lactoglobulin structure – physicochemical properties of Zn- β -lactoglobulin complexes*, *Journal of Molecular Structure*, 2022, 1268, 1-10, doi: 10.1016/j.molstruc.2022.133745.
7. A. Rodzik, P. Pomastowski, M. Buszewska-Forajta, V. Railean, A. Gołębiowski, B. Buszewski, K. Niedojadło, K. Rafińska, *Metal-protein action for the wound healing process using murine model C57BL/6J mouse*, *Scientific Reports*, Submission ID 15404681-edaf-4c74-885f-ae8688b6dbd7.
8. A. Rodzik, V. Railean, P. Pomastowski, B. Buszewski, M. Szumski, *Immobilized enzyme microreactors for efficient analysis of tryptic peptides in β -casein and β -lactoglobulin*, *Scientific Reports*, Submission ID 5d953fac-cd31-4150-9da3-e4e688f203eb

wchodzących w skład rozprawy doktorskiej Pani mgr Agnieszki Rodzik,

oświadczam, że mój wkład polegał na współudziale w opracowywaniu koncepcji, planowaniu eksperymentów, dyskusji nad wynikami badań, sprawowaniu nadzoru nad realizacją badań, korektach manuskryptów oraz pozyskiwaniu środków na realizację badań (prace 1-7). Uzyskane wyniki (prace 1-7) są rezultatem bezpośrednim w ramach kierowanego przeze mnie projektu pt. „*Synteza kompleksowych związków srebra i cynku na bazie kazeiny i białek serwatki oraz nanocząstek srebra i tlenku cynku przez probiotyczne bakterie kwasu mlekowego*”, finansowanego przez Narodowe Centrum Nauki w ramach programu Opus 14 nr 2017/27/B/ST4/02628.



Toruń, August 16, 2023

Dr. Viorica Railean

Faculty of Biological and Veterinary Sciences
Institute of Veterinary Medicine
Department of Infectious, Invasive Diseases and Veterinary Administration,
ul. Lwowska 1, 87-100 Toruń
Interdisciplinary Center of Modern Technologies
Nicolaus Copernicus University in Toruń
ul. Wileńska 4, 87-100 Toruń

STATEMENT

As a co-author of the following publications:

1. A. Rodzik, P. Pomastowski, V. Railean-Plugaru, B. Buszewski, *Hybrydowe układy metal-białko w ujęciu serwatkowym*, *Analityka: nauka i praktyka*, 2021, 2, 4-12.
2. B. Buszewski, A. Rodzik, V. Railean-Plugaru, M. Sprynskyy, P. Pomastowski, *A study of zinc ions immobilization by β -lactoglobulin*, *Colloids and Surfaces A*, 2020, 591, 1-13, doi: 10.1016/j.colsurfa.2020.124443.
3. A. Rodzik, P. Pomastowski, V. Railean-Plugaru, M. Sprynskyy, B. Buszewski, *The study of zinc ions binding to α_{SI} -, β -, κ -casein*, *International Journal of Molecular Sciences*, 2020, 21(21), 1-18, doi: 10.3390/ijms21218096.
4. A. Rodzik, A. Król-Górniak, V. Railean-Plugaru, M. Sugajski, A. Gołębiowski, D. S. Horne, B. Michalke, M. Sprynskyy, P. Pomastowski, B. Buszewski, *Study on zinc ions binding to the individual casein fractions α_{SI} -, β - and κ -casein*, *Journal of Molecular Structure*, 2022, 1272, doi: 10.1016/j.molstruc.2022.134251.
5. A. Rodzik, V. Railean, P. Pomastowski, B. Buszewski, M. Szumski, *Immobilized enzyme microreactors for efficient analysis of tryptic peptides in β -casein and β -lactoglobulin*, *Scientific Reports*, Submission ID 5d953fac-cd31-4150-9da3-e4e688f203eb.
6. A. Rodzik, V. Railean, P. Pomastowski, P. Žuvela, M. W. Wong, M. Sprynskyy, B. Buszewski *Study on silver ions binding to β -lactoglobulin*, *Biophysical Chemistry*, 2022, 291, doi: 10.1016/j.bpc.2022.106897.
7. A. Rodzik, V. Railean, P. Pomastowski, P. Žuvela, M. W. Wong, B. Buszewski, *The influence of zinc ions concentration on β -lactoglobulin structure – physicochemical properties of Zn- β -lactoglobulin complexes*, *Journal of Molecular Structure*, 2022, 1268, 1-10, doi: 10.1016/j.molstruc.2022.133745.

8. A. Rodzik, P. Pomastowski, M. Buszewska-Forajta, V. Railean, A. Gołębiowski, B. Buszewski, K. Niedojadlo, K. Rafińska, *Metal-protein action for the wound healing process using murine model C57BL/6J mouse*, Scientific Reports, Submission ID 15404681-edaf-4c74-885f-ae8688b6dbd7.

being part of the doctoral dissertation of MSc Agnieszki Rodzik, I declare that my contribution included cooperation in the field of methodology development, analysis (synthesis/characterization of nanocomposites, MIC and CFU), interpretation of the results and participation in the review&editing of the manuscripts.



.....


Dr hab. inż. Myroslav Sprynskyy, prof. UMK
Katedra Chemii Środowiska i Bioanalitiky
Wydział Chemii, Uniwersytet Mikołaja Kopernika
Ul. Gagarina 7, 87-100

OŚWIADCZENIE

Niniejszym oświadczam, że jako Współautor następujących publikacji:

1. B. Buszewski, A. Rodzik, V. Railean-Plugaru, M. Sprynskyy, P. Pomastowski, *A study of zinc ions immobilization by β -lactoglobulin*, Colloids and Surfaces A, 2020, 591, 1-13, doi: 10.1016/j.colsurfa.2020.124443.
2. A. Rodzik, P. Pomastowski, V. Railean-Plugaru, M. Sprynskyy, B. Buszewski, *The study of zinc ions binding to α_{S1} , β -, κ -casein*, International Journal of Molecular Sciences, 2020, 21(21), 1-18, doi: 10.3390/ijms21218096.
3. A. Rodzik, A. Król-Górniak, V. Railean-Plugaru, M. Sugajski, A. Gołębiowski, D. S. Horne, B. Michalke, M. Sprynskyy, P. Pomastowski, B. Buszewski, *Study on zinc ions binding to the individual casein fractions α_{S1} , β - and κ -casein*, Journal of Molecular Structure, 2022, 1272, doi: 10.1016/j.molstruc.2022.134251.
4. A. Rodzik, V. Railean, P. Pomastowski, P. Žuvela, M. W. Wong, M. Sprynskyy, B. Buszewski *Study on silver ions binding to β -lactoglobulin*, Biophysical Chemistry, 2022, 291, doi: 10.1016/j.bpc.2022.106897.

wchodzących w skład rozprawy doktorskiej mgr Agnieszki Rodzik, oświadczam, że mój wkład polegał na współpracy przy dyskusji badań kinetycznych i izotermicznych.


.....

Toruń, 01.02.2023 r.

Dr Anna Król-Górniak
Interdyscyplinarne Centrum Nowoczesnych Technologii
Katedra Chemii Środowiska i Bioanalitiky
Wydział Chemii, Uniwersytet Mikołaja Kopernika
Ul. Gagarina 7, 87-100

OŚWIADCZENIE

Niniejszym oświadczam, że jako Współautor następującej publikacji:

1. A. Rodzik, A. Król-Górniak, V. Railean-Plugaru, M. Sugajski, A. Gołębiowski, D. S. Home, B. Michalke, M. Sprynskyy, P. Pomastowski, B. Buszewski, *Study on zinc ions binding to the individual casein fractions α_{S1} , β - and κ -casein*, Journal of Molecular Structure, 2022, 1272, doi: 10.1016/j.molstruc.2022.134251.

wchodzącej w skład rozprawy doktorskiej mgr Agnieszki Rodzik, oświadczam, że mój wkład polegał na przeprowadzeniu badań elektroforezy kapilarniej oraz napisaniu części manuskryptu.

Anna Król-Górniak

.....

Toruń, 13.03.2023 r.

Mgr Mateusz Sugajski
Interdyscyplinarne Centrum Nowoczesnych Technologii
Katedra Chemii Środowiska i Bioanalitiky
Wydział Chemii, Uniwersytet Mikołaja Kopernika
Ul. Gagarina 7, 87-100

OŚWIADCZENIE

Niniejszym oświadczam, że jako Współautor następującej publikacji:

1. A. Rodzik, A. Król-Górniak, V. Railean-Plugaru, M. Sugajski, A. Gołębiowski, D. S. Horne, B. Michalke, M. Sprynskyy, P. Pomastowski, B. Buszewski, *Study on zincionsbinding to the individualcaseinfractions α_{S1} -, β - and κ -casein*, Journal of MolecularStructure, 2022, 1272, doi: 10.1016/j.molstruc.2022.134251.

wchodzącej w skład rozprawy doktorskiej mgr Agnieszki Rodzik, oświadczam, że mój wkład polegał na przeprowadzeniu badań dokowania molekularnego i napisaniu części manuskryptu.


.....



UNIwersYTET
MIKOŁAJA KOPERNIKA
W TORUNIU
Wydział Chemii

Toruń, 09.08.2023 r.

Mgr Adrian Gołębiowski
Interdyscyplinarne Centrum Nowoczesnych Technologii
Katedra Chemii Środowiska i Bioanalitiky
Wydział Chemii, Uniwersytet Mikołaja Kopernika
Ul. Gagarina 7, 87-100

OŚWIADCZENIE

Niniejszym oświadczam, że jako Współautor następujących publikacji:

1. A. Rodzik, A. Król-Górniak, V. Railean-Plugaru, M. Sugajski, A. Gołębiowski, D. S. Horne, B. Michalke, M. Sprynskyy, P. Pomastowski, B. Buszewski, *Study on zinc ions binding to the individual casein fractions α_{S1} -, β - and κ -casein*, Journal of Molecular Structure, 2022, 1272, doi: 10.1016/j.molstruc.2022.134251.
2. A. Rodzik, P. Pomastowski, M. Buszewska-Forajta, V. Railean, A. Gołębiowski, B. Buszewski, K. Niedojadło, K. Rafińska, *Metal-protein action for the wound healing process using murine model C57BL/6J mouse*, Scientific Reports, Submission ID 15404681-edaf-4c74-885f-ae8688b6dbd7.

wchodzącej w skład rozprawy doktorskiej mgr Agnieszki Rodzik, oświadczam, że mój wkład polegał na przeprowadzeniu badań ICP-MS.

.....
Gołębiowski

03.03.2023 r.

David S. Horne, BSc, PhD

Affiliate Address: Wisconsin Center for Dairy Research

University of Wisconsin—Madison, WI, United States

Home Address: 2 Bighall Farm Steadings

Bathgate, West Lothian

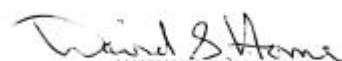
Scotland, EH48 1LQ

STATEMENT

I hereby declare that, as a Co-author of the following publication:

1. A. Rodzik, A. Król-Górniak, V. Railean-Plugaru, M. Sugajski, A. Gołębiowski, D. S. Horne, B. Michalke, M. Sprynskyy, P. Pomastowski, B. Buszewski, *Study on zinc ions binding to the individual casein fractions α_{S1} -, β - and κ -casein*, Journal of Molecular Structure, 2022, 1272, doi: 10.1016/j.molstruc.2022.134251.

being part of the doctoral dissertation of MSc Agnieszki Rodzik, I declare that my contribution was to participate on co-editing of the manuscript.



03.03.2023

Prof. Dr. Bernhard Michalke
Research Unit Analytical BioGeoChemistry
Helmholtz Center Munich-German Research Center for Environmental Health
Neuherberg 85764, Germany

STATEMENT

I hereby declare that, as a Co-author of the following publication:

1. A. Rodzik, A. Król-Gómiak, V. Railean-Plugaru, M. Sugajski, A. Gołębiowski, D. S. Home, B. Michalke, M. Sprynskyy, P. Pomastowski, B. Buszewski, *Study on zinc ions binding to the individual casein fractions α_{S1} , β - and κ -casein*, Journal of Molecular Structure, 2022, 1272, doi: 10.1016/j.molstruc.2022.134251.

being part of the doctoral dissertation of MSc Agnieszki Rodzik, I declare that my contribution was to participate on co-editing of the manuscript.



Prof. Dr. Bernhard Michalke



UNIwersYTET
MIKOŁAJA KOPERNIKA
W TORUNIU
Interdyscyplinarne Centrum
Nowoczesnych Technologii

Toruń, 9 sierpnia 2023 r.

dr hab. Michał Szumski, prof. UMK
Uniwersytet Mikołaja Kopernika w Toruniu
Interdyscyplinarne Centrum Nowoczesnych Technologii
ul. Wileńska 4, 87-100 Toruń

OŚWIADCZENIE

Niniejszym oświadczam, że jako współautor następującej publikacji:

1. A. Rodzik, V. Railean, P. Pomastowski, B. Buszewski, M. Szumski, *Immobilized enzyme microreactors for efficient analysis of tryptic peptides in β -casein and β -lactoglobulin*, Scientific Reports, Submission ID 5d953fac-cd31-4150-9da3-e4e688f203eb,

wchodzącej w skład rozprawy doktorskiej mgr Agnieszki Rodzik, oświadczam, że mój wkład polegał na współpracy przy dyskusji eksperymentów naukowych oraz korekcie manuskryptu.

Dr Petar Žuvela
Department of Chemistry
National University of Singapore
3 Science Drive 3, 117543, Singapore

STATEMENT

I hereby declare that, as a Co-author of the following publication:

1. A. Rodzik, V. Railean, P. Pomastowski, P. Žuvela, M. W. Wong, M. Sprynskyy, B. Buszewski *Study on silver ions binding to β -lactoglobulin*, Biophysical Chemistry, 2022, 291, doi: 10.1016/j.bpc.2022.106897.
2. A. Rodzik, V. Railean, P. Pomastowski, P. Žuvela, M. W. Wong, B. Buszewski, *The influence of zinc ions concentration on β -lactoglobulin structure – physicochemical properties of Zn- β -lactoglobulin complexes*, Journal of Molecular Structure, 2022, 1268, 1-10, doi: 10.1016/j.molstruc.2022.133745.

being part of the doctoral dissertation of MSc Agnieszki Rodzik, I declare that my contribution was participation in design, simulations and investigation (pertaining to the molecular dynamics and DFT calculations for this study), visualization and validation of data as well as writing and editing of the manuscripts.



Prof. Ming Wah WONG
Department of Chemistry
National University of Singapore
3 Science Drive 3, Singapore 117543
Email: chmwmw@nus.edu.sg
Tel: +65 68744320, Fax: +65 67791691
9th March 2023

Statement of Co-authorship

I hereby declare that, as a Co-author of the following publications:

1. A. Rodzik, V. Railean, P. Pomastowski, P. Žuvela, M. W. Wong, M. Sprynskyy, B. Buszewski *Study on silver ions binding to β -lactoglobulin*, Biophysical Chemistry, 2022, 291, doi: 10.1016/j.bpc.2022.106897.
2. A. Rodzik, V. Railean, P. Pomastowski, P. Žuvela, M. W. Wong, B. Buszewski, *The influence of zinc ions concentration on β -lactoglobulin structure – physicochemical properties of Zn- β -lactoglobulin complexes*, Journal of Molecular Structure, 2022, 1268, 1-10, doi: 10.1016/j.molstruc.2022.133745.

being part of the doctoral dissertation of M.Sc. candidate Agnieszki Rodzik, I declare that my contribution was the computational studies.

Yours sincerely,



M. W. Wong



UNIWERSYTET
MIKOŁAJA KOPERNIKA
W TORUNIU

Wydział Nauk Biologicznych
i Weterynaryjnych

Toruń, 09.08.2023 r.

Dr hab. inż. Magdalena Buszewska-Forajta
Instytut Medycyny Weterynaryjnej
Uniwersytet Mikołaja Kopernika w Toruniu

OŚWIADCZENIE

Niniejszym oświadczam, że jako Współautor następującej publikacji:

1. A. Rodzik, P. Pomastowski, M. Buszewska-Forajta, V. Railean, A. Gołębiowski, B. Buszewski, K. Niedojadło, K. Rafińska, *Metal-protein action for the wound healing process using murine model C57BL/6J mouse*, Scientific Reports, Submission ID 15404681-edaf-4c74-885f-ac8688b6dbd7.

wchodzącej w skład rozprawy doktorskiej mgr Agnieszki Rodzik, oświadczam, że mój wkład polegał na przeprowadzeniu badań nad procesem gojenia się ran i napisaniu części manuskryptu.

Buszewska-Forajta

Toruń, 09.08.2023 r.

Dr hab. Katarzyna Niedojadło, prof. UMK
Katedra Biologii Komórkowej i Molekularnej
Wydział Nauk Biologicznych i Weterynaryjnych
Uniwersytet Mikołaja Kopernika
ul. Lwowska 16, 87-100

OŚWIADCZENIE

Niniejszym oświadczam, że jako Współautor następującej publikacji:

1. A. Rodzik, P. Pomastowski, M. Buszewska-Forajta, V. Railean, A. Gołębiowski, B. Buszewski, K. Niedojadło, K. Rafińska, *Metal-protein action for the wound healing process using murine model C57BL/6J mouse*, Scientific Reports, Submission ID 15404681-edaf-4c74-885f-ae8688b6dbd7.

wchodzącej w skład rozprawy doktorskiej mgr Agnieszki Rodzik, oświadczam, że mój wkład polegał na przeprowadzeniu badań mikroskopowych.

Katarzyna Niedojadło

Toruń, 09.08.2023 r.


Dr hab. Katarzyna Rafińska, prof. UMK
Katedra Chemii Środowiska i Bioanalityki
Wydział Chemii, Uniwersytet Mikołaja Kopernika
Ul. Gagarina 7, 87-100

OŚWIADCZENIE

Niniejszym oświadczam, że jako Współautor następującej publikacji:

1. A. Rodzik, P. Pomastowski, M. Buszewska-Forajta, V. Railean, A. Gołębiowski, B. Buszewski, K. Niedojadło, K. Rafińska, *Metal-protein action for the wound healing process using murine model C57BL/6J mouse*, Scientific Reports, Submission ID 15404681-edaf-4c74-885f-ae8688b6dbd7.

wchodzącej w skład rozprawy doktorskiej mgr Agnieszki Rodzik, oświadczam, że mój wkład polegał na przeprowadzeniu badań mikroskopowych i napisaniu części manuskryptu.


.....